Kinetics and mechanisms of Ikaros-mediated transcriptional regulation

by

Ziwei Liang

A thesis submitted to Imperial College London

for the degree of Doctor of Philosophy

Lymphocyte Development Group

MRC Clinical Sciences Centre

Imperial College School of Medicine

October 2014

I, Ziwei Liang, declare that the work presented in this thesis is my own, and that any work carried out by others has been acknowledged and appropriately referenced in the text.

明珠不急光
慢慢养
多分寸
即无价

Abstract

The Ikaros family of zinc finger transcription factors is essential for B cell development, and frequently mutated in B cell malignancies. Our lab has previously identified Ikaros target genes in pre-B cells by combining Ikaros ChIP-seq binding data and gene expression profiling. To address the kinetics and mechanisms of Ikaros-mediated transcriptional regulation, I have used an inducible Ikaros system, which allows for the monitoring of cellular and molecular changes during Ikaros-mediated gene silencing at high temporal resolution. Within minutes of Ikaros induction, the Ikaros-regulated model loci *Igll1* and *Myc* showed decreased promoter accessibility and RNA polymerase II (RNAPII) occupancy. These early events were followed by changes in nucleosome composition, including an increased histone H2B/H3 ratio, the deposition of the histone variant H2A.Z, and decreased active histone acetylation marks. Histone deacetylation was not required to initiate down-regulation of *Igll1* and *Myc* transcription, since treatment with the histone deacetylase inhibitor Trichostatin A did not interfere with Ikaros-mediated gene silencing. I next elucidated the mechanistic relationship between the early events of decreased promoter accessibility and decreased RNAPII occupancy. Addition of Triptolide resulted in the removal of RNAPII from the *Igll1* and *Myc* promoters, but did not affect nucleosome occupancy and its regulation mediated by Ikaros. This suggested that Ikaros regulates nucleosome positioning and occupancy directly, and not through effects on RNAPII. Consistent with this hypothesis, Ikaros-mediated gene silencing was delayed by RNAi-mediated knockdown of chromatin remodeler Mi-2β (Chd4), the ATPase subunit of the Mi-2/NuRD complex. Hence, Ikaros-initiated chromatin remodelling was identified as one of the earliest events during Ikaros-mediated gene silencing, and was required for rapid transcriptional down-regulation of Ikaros target genes.

Acknowledgement

I would like to first sincerely thank Matthias for giving me this great opportunity to do my PhD, and for the great support, inspiration, guidance and understanding. Thank you for teaching me to be a scientist. I want to thank Mandy for her great support and suggestions, both in science and in watering the plants. Also, I am very grateful to my scholarships, UK-China scholarship for excellence and MRC studentship.

I need to extend my thanks to all the members in the lymphocyte development group, both past and present, thank you all for the friendly and lively atmosphere, the fun times, and your support and help. Particularly, I want to thank Isa for her time and patience, constant support and for being a dear friend. And Thais, for being such a great friend and an amazing person, for sharing the laughters and tears. I-Chun and Feng, thank you for the exclusive kindness, understanding and support. Amelie, thank you for being a brilliant lab manager and a close friend. I also want to thank Vlad for being the Sherlock Holmes when trouble shooting gets desperate, and kindly reading my thesis. Francesco, thank for being so sweet, sometimes mean, and so much fun. David and Jorge, thank you for all the fun chats, the serious ones and the critical ones. Yeye, Tien-Chi and Nashun, thank you for all the wonderful times. Ludovica, without you I wouldn't get the most beautiful bike. Also, I want to thank the surgeon who fixed my wisdom teeth, amazing.

I can't say enough about the support I get from Tommy. Thank you for being so wonderful, so unbelievably kind and patient and supportive, thank you for everything!

我要谢谢我最爱最爱的爸爸妈妈，谢谢你们对我的教育，给我无限的爱和支持。谢谢你们的包容和体贴。你们是世界上最开明最酷的爸爸妈妈。最爱你们!念博士是我至今做过的最艰难的事，但是很值得。我得说，太赞了！

Contents

List of figures

List of tables

Glossary

4OHT	4-hydroxytamoxifen
AA	Nucleosome with Homotypic Histone H2A
Ac	Acetylation
AF9	ALL1-fused Gene from Chromosome 9
APS	Ammonium Persulphate
AZ	Nucleosome with Heterotypic Histone H2A/H2A.Z
BCR	B Cell Receptor
BET	Bromodomain and Extraterminal
bHLH	Basic Helix-Loop-Helix
bp	Base Pair
CHD	Chromodomain, Helicase, DNA binding
ChIP	Chromatin Immunoprecipitation
CLP	Common Lymphoid Progenitors
CTD	Carboxy Terminal Domain
CYT	Cytoplasmic
DAPI	4',6-diamidino-2-phenylindole
DAXX	Death-associated Protein
DMSO	Dimethyl Sulfoxide
DRB	5,6-dichloro-1-β-D-ribofuranosylbenzimidazle
DSG	Disuccinimidyl Glutarate
DSIF	DRB Sensitivity-inducing Factor
EBF1	Early B-cell Factor 1
Ell	Eleven-nineteen Lysine-rich Leukaemia Gene
ENL	Eleven-nineteen Leukaemia
ERt2	Ligand-binding Domain of Estrogen Receoptor
ESC	Embryonic Stem Cell
EtOH	Ethanol
FACS	Fluorescent Activated Cell Sorting
Foxo1	Forkhead Box Protein O1
GFP	Green Fluorescent Protein
h	Hour(s)
HAT	Histone Acetyltransferease
HDAC	Histone Deacetylase
HEXIM	Hexamethylene Bisacetamide-inducible proteins
HIRA	Histone Regulator A
HSC	Haematopoietic Stem Cell
IF	Immunofluorescence
IgH	Immunoglobulin Heavy Chain

IgL	Immunoglobulin Light Chain
IK	Ikaros
INO80	Inositol Requiring 80
IRES	Internal Ribosome Entry Site
ISWI	Imitation Switch
K	Lysine
LARP7	La-related Protein
LB	Lysogeny Broth
Me	Methyaltion
MePCE	7SK Methyl Phosphate Capping Enzyme
mg	Milligram
min	Minute(s)
ml	Millilitre
MLL	Mix Lineage Leukaemia
MLP	Multi-lineage Progenitors
mRNA	Messenger RNA
MSCV	Murine Stem Cell Virus
NELF	negative elongation factor
NK	Natural Killer Cells
NL	Nuclear
NLS	Nuclear Localization Signal
nt	Nucleotide
NuRD	Nucleosome Remodelling and Deacetylation Complex
PAFc	Polymerase-associated Factor Complex
PBS	Phosphate-buffered Saline
PFA	Paraformaldehyde
PHD	Plant Homeo Domain
PI	Propidium Iodide
PIC	Pre-Initiation Complex
PRC	Polycomb Repression Complex
pre-BCR	Pre-B Cell Receptor
P-TEFb	Positive Transcription Elongation Factor
RNAPII	RNA Polymerase II
(RT-)qPCR	(Real Time) Quantitative Polymerse Chain Reaction
RPM	Reads per Million
s	Second(s)
S or Ser	Serine
SDS	Sodium Dodecyl Sulfate
SEC	Super Elongation Complex
shRNA	Short Hairpin RNA
SLC	Surrogate Light Chain
SWI/SNF	Switching Defective/Sucrose Nonfermenting
TPL	Triptolide
TSA	Trichostatin A

TSS	transcriptional Start Site
TTS	transcriptional Termination Site
WCL	Whole Cell Lysate
ZZ	Nucleosome with Homotypic Histone H2A.Z
µg	Microgram
µl	Microlitre

1 Introduction

1.1 Early B cell development and the Ikaros family of transcription factors

1.1.1 Early B cell development

Mammalian haematopoiesis is a hierarchical process. In this hierarchy, haematopoietic stem cells (HSCs) obtain a broad developmental potential, and are able to generate all cells of the immune system. As cells progress down into a specific lineage, they gradually restrict cell fate potentials and acquire specialised cellular functions. The orderly step-wise process of early B cell development is discussed here, with reference to the key transcription factors required for lineage specification (Cedar and Bergman, 2011) (Figure 1.1).

Murine HSCs initially give rise to multi-lineage progenitors (MLPs), which do not self-renew but have the potential to generate early progenitors of lymphoid and myeloid lineages (Morrison et al., 1995). Common lymphoid progenitors (CLPs) can further specify B cell lineages, or eventually differentiate into T lymphocytes or nature killer cells (NKs) (Kondo et al., 1997). The process of early B cell development is intimately connected to the rearrangement of immunoglobulin genes, a process also known as V(D)J recombination. Specification of the B cell lineage features the expression of the pan-B cell marker B220 in pre-pro-B cells (Hardy fraction A, Fr A) (Hardy et al., 1991; Matthias and Rolink, 2005). This is followed by the expression of CD19, and the recombination of diversity (D_H) and joining (J_H) segments of the immunoglobulin heavy chain (IgH) in pro-B cells (Hardy Fr B/C). The *IgH* locus then continues to rearrange its variable (V_H) segments to DJ_H. The product of the rearranged IgH is assembled with the surrogate light chain (SLC) to form a pre-B cell receptor (pre-BCR) on the surface of cycling pre-B cells (Hardy Fr C'). Following this, SLC is down-regulated and immunoglobulin light chain (IgL) genes are rearranged in resting pre-B cells (Hardy Fr D). The appearance of the assembled B cell receptor (BCR) on the cell surface defines the immature B cell (Hardy Fr E) stage (Hardy et al., 1991; Matthias and Rolink, 2005) (Figure 1.1).

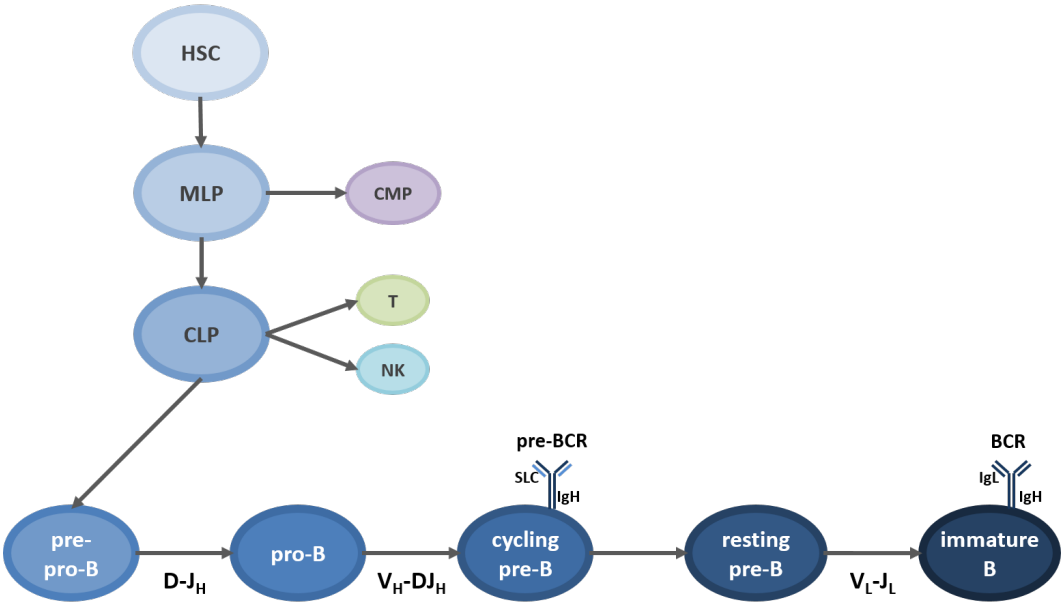

Figure 1.1 Schematic illustration of early B cell development in the bone marrow

B cell development from HSCs takes place in a highly ordered hierarchical manner. Murine HSCs initially give rise to MLPs, which can generate early progenitors of lymphoid and myeloid lineages. CLPs can eventually give rise to B cells, or T lymphocytes or NKs. After the entry of pre-pro-B cells, D_H-J_H rearrangement is initiated and finished in pro-B cells. This is followed by the rearrangement of V_H-DJ_H. The product of the rearranged IgH is then assembled with SLC to form pre-BCR on the cellular surface in cycling pre-B cells. Following this, SLC is down-regulated and the rearrangement of IgL is initiated in resting pre-B cells. The appearance of the assembled BCR on the cellular surface defines the immature B cell stage.

Loss of function studies using mouse models have identified key transcription factors for the specification of B cell lineage, including PU.1, Ikaros, E2A, EBF1, Pax5 and Foxo1. The expression of these transcription factors is temporally regulated. PU.1 and Ikaros are the earliest expressed transcription factors, even before the commitment to the lymphoid branch. PU.1-deficient mice die during embryonic development and show defective generation of both lymphoid and myeloid progenitors (Scott et al., 1994). The expression level of PU.1 helps to specify distinct cell fates in the haematopoietic system. Low expression of PU.1 induces B cell development; however, high expression of PU.1 suppresses the B cell fate and promotes the development of the myeloid lineages (DeKoter and Singh, 2000). Further investigation revealed that PU.1 binding to chromatin is cell-type specific, and is colocalised with lineage-determining transcription factors, such as E2A and EBF in B cells (Heinz et al.,

2010). This suggests that the B cell lineage is specified by a combination of key transcription factors. As with PU.1, the transcription factor Ikaros is also expressed very early during haematopoiesis. Ikaros-deficient mice lack B cell progenitors, and show defects in the development of other immune cell compartments (Georgopoulos et al., 1994; Wang et al., 1996; Yoshida et al., 2006). This will be further discussed in section 1.1.2.

E2A, another key transcription factor in B cell development, is encoded by *Tcf3* with two splice variants E12 and E47. In the absence of E2A, B cell development is blocked as early as the pre-pro-B stage, and *IgH* segments fail to undergo rearrangement (Bain et al., 1994; Zhuang et al., 1994). During pre-pro-B cell development, E2A is up-regulated concomitantly with the initiation of *IgH* rearrangement, and activates the expression of *Ebf1* (early B cell factor1) and *Foxo1* (forkhead box protein O1) (Lin et al., 2010b; Zhuang et al., 2004). Similar to E2A, ablation of EBF1 also leads to a very early block at the pre-pro-B stage in B cell development. EBF-deficient cells fail to rearrange D_H to J_H at the *IgH* locus (Lin and Grosschedl, 1995). However, ectopic expression of EBF1 rescues B cell development in $E2A^{-/-}$ mice (Seet et al., 2004), suggesting that EBF1 is a downstream target of E2A. E2A and EBF are important to activate B cell specific genes. For example, forced expression of E2A and EBF1 leads to the activation of the pre-BCR component λ5 in early B cell progenitor cells (Sigvardsson et al., 1997) and in non-lymphoid cells (Sigvardsson, 2000). In addition to E2A and EBF1, the transcription factor Pax5 is required for B cell lineage commitment. Induction of *Pax5* expression in pro-B cells requires the binding of EBF1 to the *Pax5* promoter, and the binding of PU.1, Foxo1, IRF4 and IRF8 to the *Pax5* enhancer (Decker et al., 2009; O'Riordan and Grosschedl, 1999). Pax5 is required for the expression of additional B cell specific genes contributing to further lineage commitment, and for the suppression of alternative lineage choices. The importance of Pax5 in specifying B cell lineage is highlighted in studies showing that targeted inactivation of the *Pax5* locus leads to a developmental block at pro-B cell stage (Nutt et al., 1999). Furthermore, $Pax5^{-/-}$ pro-B cells retain significant developmental plasticity, and are able to adopt alternative cell fates with the addition of appropriate signals (Nutt et al., 1999; Urbanek et al., 1994).

The pre-BCR is composed of an Ig heavy chain (Igμ) and the SLC consisting of λ5 (encoded by *Igll1*) and VpreB (encoded by *Vpreb1/2*). The deposition of the pre-BCR on the cell surface, alongside the signalling subunits Igα and Igβ, is an important checkpoint during early B cell development. Signals from the pre-BCR provide rapid feedback for the functionality of the recombined IgH. The importance of the pre-BCR has been revealed by a series of gene

disruption experiment. The *IgH* locus was targeted by homozygous deletion mutation in the transmembrane region of IgH (μ_{TM}), and a mouse stain that is unable to deposit the pre-BCR on the cell surface was generated. In these $\mu_{TM}^{-/-}$ mice, the transition from cycling pre-B stage to resting pre-B stage is blocked, and no further B cell development is observed (Kitamura et al., 1991). Similarly, $SLC^{-/-}$ mice show an impaired B cell development; however, the developmental block is incomplete, where a small number of immature B and mature B cells are still observed (Shimizu et al., 2002). This is possibly due to the prematurely expressed immunoglobulin light chain (Shimizu et al., 2002; Su et al., 2003). Therefore only signalling-competent pre-B cells can initiate a cascade of cellular responses and mature further. Pre-BCR first promotes a burst of cell proliferation, expanding the cells which have successfully rearranged Igμ (Jumaa et al., 2005; Yasuda et al., 2008). Pre-BCR then facilitates differentiation. Pre-BCR signalling results in elevated expression of the Ikaros family member Aiolos (Thompson et al., 2007). Ikaros and Aiolos cooperate to down-regulate λ5 and VpreB, and ensure the termination of pre-BCR expression (Thompson et al., 2007). The pre-BCR signalling also induces cell cycle arrest at G1 (Ma et al., 2010; van Loo et al., 2007), and initiates V_L to J_L rearrangement at the κ and λ light chain loci (Herzog et al., 2009). If inappropriately regulated, enhanced proliferation of cycling pre-B cells may lead to the accumulation of genetic lesions and the development of pre-B cell leukaemia (Jumaa et al., 2005).

1.1.2 The transcription factor Ikaros

The transcription factor Ikaros, encoded by *Ikzf1*, is expressed in haematopoietic stem cells, all lymphoid and some myeloid cells (Georgopoulos et al., 1992; Hahm et al., 1994; Lo et al., 1991). Structural analysis revealed that Ikaros is a zinc finger protein, with its zinc fingers organized into two separate clusters residing at the N- and C-terminus (Georgopoulos et al., 1992). Gel shift and DNaseI footprinting assays of Ikaros mutant-GST fusion proteins demonstrated that the N-terminal zinc fingers determine the DNA binding activity of Ikaros (Hahm et al., 1994). Later, the zinc fingers in the C-terminus were shown to be essential for dimerization with other Ikaros proteins (Sun et al., 1996).

Ikaros is the founding member of the Ikaros family of transcription factors. Using degenerate primers against the C-terminal domain, the close relative Aiolos (encoded by *Ikzf3*) was discovered (Morgan et al., 1997). Shortly, another family member, Helios (encoded by *Ikzf2*), was found through its interaction with Ikaros (Hahm et al., 1998). Both Aiolos and Helios show a high degree of sequence homology to Ikaros, especially within the zinc finger domains, and their expression is predominantly confined to lymphoid lineages (Hahm et al., 1998; Morgan et al., 1997). Two additional distantly related family members, Eos (*Ikzf4*) and Pegasus (*Ikzf5*), are more widely expressed and are detected in lineages other than haematopoietic cells (Honma et al., 1999; Perdomo et al., 2000).

Ikaros itself is alternatively spliced, producing at least eight isoforms (Figure 1.2). Each isoform contains a distinct composition of N-terminal zinc fingers and a shared C-terminal protein interaction domain (Hahm et al., 1994; Molnar and Georgopoulos, 1994; Payne et al., 2003). The N-terminal zinc fingers determine Ikaros isoform DNA binding affinity and sequence-specificity. Zinc fingers 2 and 3 are essential for DNA binding, and recognize the core consensus sequence (G)GGAA(A). However, to achieve higher binding affinity and subsequently stronger regulation of transcription, additional zinc fingers 1 and/or 4 are also required (Cobb et al., 2000; Hahm et al., 1994; Molnar and Georgopoulos, 1994). Recently, an elegant study from the Smale lab on mouse models with deleted zinc finger 1 or 4 revealed that the Ikaros isoforms containing zinc fingers 1 or 4 regulate distinct sets of genes during lymphocyte development (Schjerven et al., 2013). Mice expressing Ikaros lacking zinc finger 1 show severely impaired expression of Igμ at the pro-B stage. However, in mice with deletion of Ikaros zinc finger 4, early B cell development is only mildly affected (Schjerven et al., 2013).

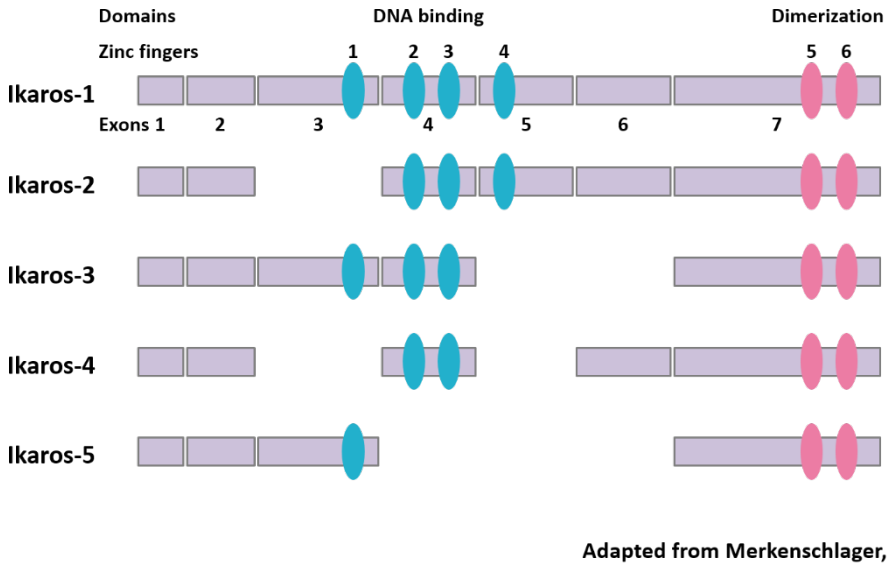

Figure 1.2 Schematic illustration of Ikaros domain structure

The cartoon shows the structure of Ikaros isoforms 1-5. The ellipses are representative of zinc fingers, with the blue eclipses at N-terminus responsible for DNA binding, and the red eclipses at C-terminus responsible for dimerization. All isoforms contain C-terminus and vary at the N-terminus. Additional isoforms are not shown in this figure (Payne et al., 2003).

Genetic studies revealed that Ikaros is critically involved in haematopoiesis, particularly during lymphocyte development (Merkenschlager, 2010). An Ikaros-deficient mouse strain was generated by deletion of *Ikzf1* exon 7, which destabilises Ikaros protein. These Ikaros-null mice lack B cells, NK cells, and foetal T cells (Wang et al., 1996). The development of T lymphocytes is restored in adult mice, however the differentiation is defective with an increased number of CD4 single positive cells at the expense of CD4 CD8 double positive precursor cells. A more severe phenotype was observed in Ikaros mutant mice homozygous for deletion of *Ikzf1* exon 3 and 4 (zinc finger 1-3), which produces short Ikaros proteins deficient in DNA binding. These mice lack not only B, T and NK cells, but also their earliest defined progenitors (Georgopoulos et al., 1994). The varied severity between these two Ikaros mutants can be explained by the interactions between Ikaros and family members. The recovery of T cell development in Ikaros-null mice suggests the ability of other Ikaros family members to compensate for Ikaros function (Wang et al., 1996). However in mice expressing the non-DNA binding Ikaros isoform, these short Ikaros proteins interact with other family

members and produce non-functional Ikaros complexes, therefore posing a dominant negative effect and abolishing the compensation.

Additionally, mice heterozygous for dominant negative Ikaros rapidly develop T cell leukaemia (Winandy et al., 1995). This suggests a role of Ikaros as a tumour suppressor. In support of this, *IKZF1* deletion is observed in more than 80% of patients suffering from the oncogenic tyrosine kinase BCR-ABL$^+$ acute lymphoblast leukaemia (ALL) (Mullighan et al., 2008). Using mouse models with selected deletions of Ikaros N-terminal zinc fingers, Smale and colleagues recently discovered that the zinc fingers 2-4 of Ikaros protein are essential for the tumour suppression functions of Ikaros, in both T malignancies and the BCR-ABL$^+$ B-ALL (Schjerven et al., 2013).

The expression of Ikaros gradually increases during early B cell development (Ferreiros-Vidal et al., 2013). In pro-B cells, Ikaros is essential for V-DJ rearrangement by activating the recombination machinery and ensuring correct accessibility and compaction of the *IgH* locus (Reynaud et al., 2008). At the transition from cycling pre-B cells to resting pre-B cells, Ikaros, together with elevated level of Aiolos, functions to silence the expression of the SLC component λ5 and VpreB (Thompson et al., 2007). Ikaros and Aiolos also down-regulate c-Myc (Ma et al., 2010), and subsequently induce cell cycle arrest in G1 (Ferreiros-Vidal et al., 2013). Remarkably, simple overexpression of Ikaros in a cycling pre-B cell line is sufficient to drive global transcriptional changes that mimic the transition from cycling to resting pre-B cells (Ferreiros-Vidal et al., 2013). This *in vitro* study is supported by research using conditional *Ikzf1* knockout mice (Heizmann et al., 2013; Schwickert et al., 2014). Deletion of *Ikzf1* in pro-B cells results in a complete block at the cycling pre-B stage. Restoration of Ikaros, but not Aiolos, rescues the differentiation into the resting pre-B cells (Heizmann et al., 2013; Schwickert et al., 2014). These studies emphasize the essential role of Ikaros in early B cell development.

1.2 Transcriptional regulation in B cell development

B cell lineage commitment is achieved by the establishment of lineage-specific transcriptional programmes, which involves the activation of lineage-specific genes, and the silencing of inappropriate genes. This is largely determined by the key transcription factors required for B cell development.

To understand how these unique gene expression patterns are orchestrated during development is a formidable task. Fundamentally, transcription of mRNA is carried out by the core RNA polymerase II (RNAPII) transcription machinery based on the genomic DNA. However in eukaryotes, DNA is largely inaccessible to the transcription machinery, as it is packaged into macromolecules with proteins, termed chromatin. Here, a few important mechanisms involved in modulating RNAPII and chromatin status during transcriptional regulation are discussed.

1.2.1 RNA polymerase II

The enzymatic activity of DNA-dependent RNA polymerase was first discovered by Weiss and Gladstone in rat liver nuclei (Weiss and Gladstone, 1959). In 1969, the RNA polymerases I, II, and III were first separated and identified by Roeder and Rutter (Roeder and Rutter, 1969). RNA polymerase I was found in the nucleoli, and II and III were in the nucleoplasm (Roeder and Rutter, 1970). The functional specificity of RNA polymerases was resolved based on their differential sensitivities to α-amanitin by Chambon's and Roeder's groups (Gniazdowski et al., 1970; Kedinger et al., 1970; Weinmann et al., 1974; Weinmann and Roeder, 1974). RNA polymerase II (RNAPII) was found to transcribe mRNA.

For effective mRNA transcription, RNAPII is first recruited to gene promoters, and assembled into the pre-initiation complex (PIC) together with the general transcription factors (GTFs) (step1). This transcription machinery then unwinds double-stranded DNA (dsDNA) to form an open complex (OC) (step2). After transcription initiation, RNAPII polymerises mRNA and escapes promoters (step3). This early elongating RNAPII is subsequently paused at promoter-proximal regions (step4). For effective elongation, RNAPII needs to be released from pausing (step5). Transcription is thus productive along the entire body of the gene (step6). Following that, RNAPII is terminated when it encounters the transcription termination signal (step7), and perhaps recycled for a new round of transcription (step8) (Fuda et al., 2009).

All these steps are delicately assisted and regulated by a complex set of factors, and each step can be potentially rate-limiting to transcription. To understand transcriptional regulation, RNAPII serves as a useful target to study the steps and factors involved in transcriptional

regulation. Here, the regulation of RNAPII at initiation and elongation steps is further discussed (Figure 1.3, 1.4).

1.2.1.1 Transcription initiation

RNAPII is the core of the transcription machinery. RNAPII is composed of 12 subunits, namely Rpb1-12, with a total mass of about 500kD (kilodaltons) (Cramer et al., 2000; Young, 1991). Rpb1 and Rpb2 form the central mass of the enzyme. They position on opposite sides of a cleft, at the bottom of which lies the catalytic site of the enzyme (Cramer et al., 2000). Rpb1 has a unique C-terminal domain (CTD). It contains up to 52 tandem repeats of the heptad sequence YSPTSPS (Tyrosine- Serine- Proline- Threonine- Serine- Proline- Serine). Rpb1-CTD extends from the catalytic core of RNAPII and lies at the nascent mRNA exit site (Cramer et al., 2001). Rpb1-CTD can be phosphorylated at multiple positions in a programmed way during transcription initiation and elongation (Bentley, 2014). It acts as important scaffold for the assembly of factors regulating the synthesis and the processing of mRNA transcripts (Corden, 2013; Hahn, 2004).

RNAPII can unwind DNA double helix, polymerise RNA and proofread the nascent transcript. However, on its own, RNAPII is not able to recognize promoters or initiate transcription. A minimal set of general transcription factors (GTFs), namely TFIIB, -D, -E, -F, -H, is required (Grunberg and Hahn, 2013; Liu et al., 2013). The TATA-binding protein (TBP), which normally occurs as a subunit of TFIID, marks the promoter through its interactions with TATA, and bends DNA by approximately 90 degrees forming an assembly platform for PIC (Kim et al., 1993a; Kim et al., 1993b). This TBP-DNA interaction can be facilitated and stabilised by TFIIA (Bleichenbacher et al., 2003; Geiger et al., 1996; Tan et al., 1996). TFIIB bridges TBP and RNAPII (Hahn, 2004). TFIIF, identified as a RNAPII loading factor, enters the PIC together with RNAPII (Roeder, 1996; Sopta et al., 1985). TFIIE is primarily a loading factor for TFIIH (Holstege et al., 1995; Pan and Greenblatt, 1994). TFIIH is the only GTF possessing ATP-dependent enzymatic activities. TFIIH contains CDK7/Kin28 (cycling-dependent kinase, CDK), XPD/Rad3 (DNA helicase) and XPB/Ssl2 (DNA translocase), and seven other subunits (Egly and Coin, 2011). These GTFs are essential to recruit RNAPII to gene promoters and initiate transcription.

Step 1: the assembly of pre-initiation complex (PIC)

The assembly steps of the PIC remain to be further elucidated, since recent studies point to two distinct pathways of human and yeast PIC assembly. Describing the human PIC, TBP, TFII-A, -B and RNAPII first form a complex with DNA. This is followed by sequential addition of TFII-F, -E and finally –H (He et al., 2013). While describing the yeast PIC, an intermediate complex containing TBP, TFII-A, -B, -E, -H is first assembled onto the DNA, and subsequently, TFIIF and RNAPII are added (Murakami et al., 2013).

The assembly of the PIC is the first rate-limiting step in RNAPII transcription. It is regulated by cell type- and DNA sequence-specific transcription factors, and is assisted by transcription cofactors. Transcription cofactors can be broadly categorised into two classes. One class contains proteins or complexes that can modify histones or remodel chromatin in an ATP-dependent manner (this is further discussed in section 1.2.2). The other class includes factors that directly interact with the core transcription machinery to modulate transcription, such as Mediator and SAGA (Grunberg and Hahn, 2013).

Mediator is a multisubunit complex composed of four separate modules: head, middle, tail, CDK/kinase (Ansari and Morse, 2013). It bridges transcription factors with the transcription machinery. Mediator head module interacts with RNAPII Rbp1-CTD. This interaction is stabilized by the TFIIF (Bernecky et al., 2011). Meditor interacts with transcription factors at multiple interfaces (Borggrefe and Yue, 2011). For example, Mediator directly interacts with the transcription factor GATA1 during erythropoiesis. Conditional deletion of the Mediator subunit MED1 abolishes the expression of β-globin, and blocks erythroid development (Stumpf et al., 2010). In pro-B cells, Mediator colocalizes with key transcription factors for B cell development, such as PU.1, Ebf1, E2A and Foxo1, and marks enhancer regions that are important for the specification of B cell identity (Whyte et al., 2013).

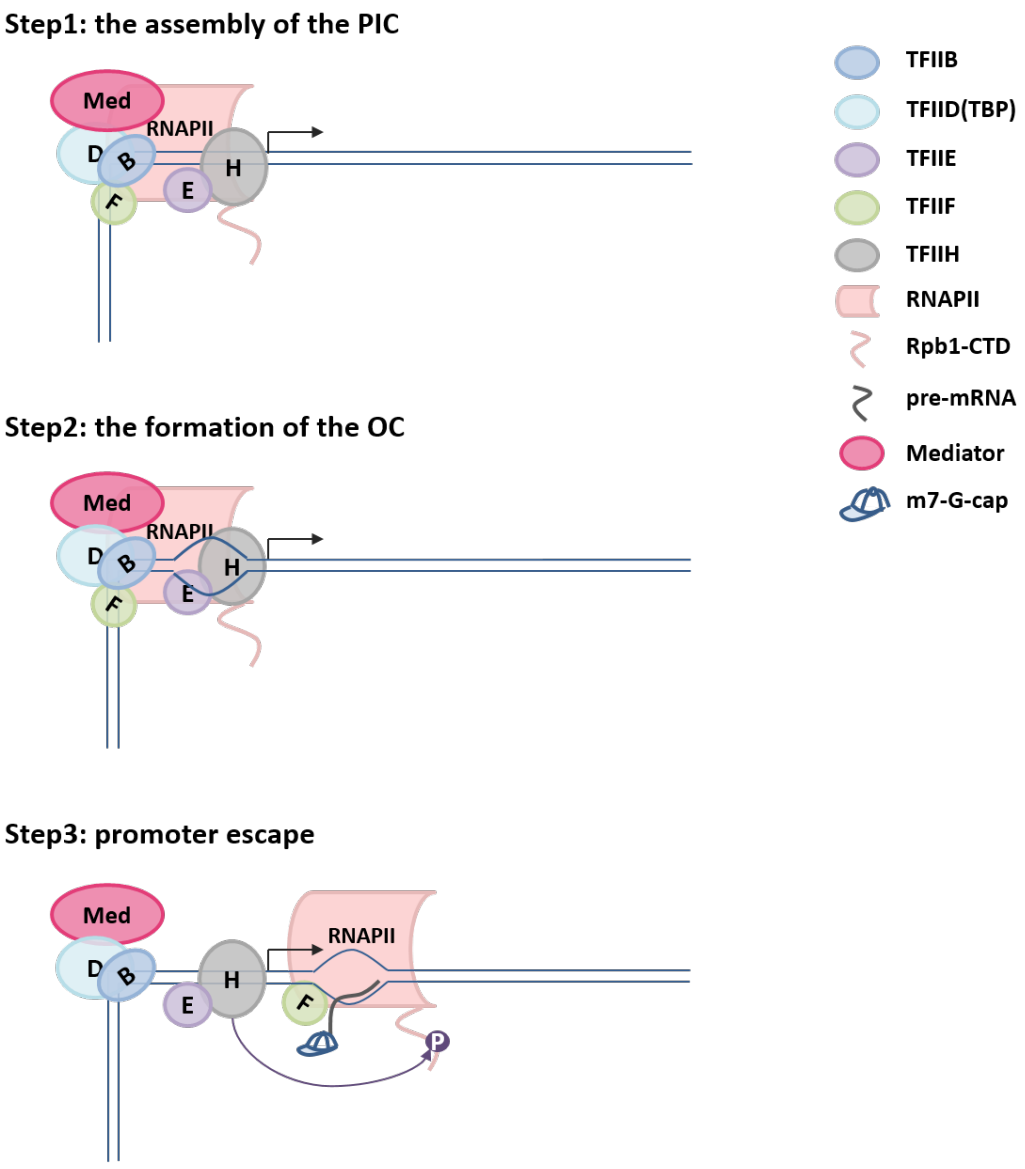

Figure 1.3 Schematic illustration of transcription initiation

Transcription initiation starts from the assembly of the pre-initiation complex (PIC) at gene promoter. This involves general transcription factors TFII-B, -D, -E, -F, -H, and RNAPII, and can be assisted by transcription cofactors, such as the Mediator complex. Following this, the formation of the open complex (OC) is recognized by the generation of single-stranded DNA (ssDNA) by the XPB subunit of TFIIH. Promoter escape to accomplish transcription initiation is accompanied by the phosphorylation of Rpb1-CTD serine5 by the Cdk7 subunit of TFIIH, dissociation of RNAPII from most of the general transcription factors, and m7-G-capping at the 5' of pre-mRNA.

Step 2: the formation of the open complex (OC)

The formation of the open complex (OC, or open PIC) features the unwinding of dsDNA, thus creating a 'transcription bubble' (Fuda et al., 2009). TFIIH is required to melt the promoter dsDNA and form the open complex (Grunberg et al., 2012; Kim et al., 2000). The DNA translocase subunit of TFIIH, XPB/Ssl2, inserts 15bp of downstream DNA into the RNAPII cleft by right-handed threading. Combined with the fixed position of upstream DNA, the rotation then leads to DNA unwinding (Grunberg et al., 2012).

The formation of the OC has recently been discovered to be the second rate-limiting step during transcription initiation in eukaryotes (Kouzine et al., 2013). Casellas and colleagues developed ssDNA-seq to quantify the melting of dsDNA. In naïve B cells, most genes that are induced upon activation are already bound by RNAPII. However, the generation of ssDNA at promoters, which indicates the formation of the OC, is only observed after B cell activation. This is accompanied by the stimulated expression of TFIIH (Kouzine et al., 2013).

Step 3: promoter escape

Following the formation of the OC, the template strand of DNA is orientated to the catalytic site of RNAPII by TFIIB (Kostrewa et al., 2009; Liu et al., 2010). The OC then scans downstream for transcription start site (TSS). The selection of TSS is facilitated by TFIIB, TFIIF, and additional assisting factors (Kostrewa et al., 2009; Liu et al., 2013; Sainsbury et al., 2013). Following this, RNAPII starts polymerising RNA. This is accompanied by the conformational changes of RNAPII-TFIIB, which leads to the dissociation of TFIIB, other GTPs and Mediator from RNAPII (Sainsbury et al., 2013). Subsequently, RNAPII escapes the promoter and proceeds to early elongation. TFIIH also plays an important role in RNAPII promoter escape. The kinase subunit of TFIIH, CDK7, phosphorylates serine5 on the Rpb-CTD, and aids RNAPII breaking contact with promoter-bound factors (Jeronimo and Robert, 2014; Saunders et al., 2006; Wong et al., 2014).

1.2.1.2 Transcription elongation

After successful promoter escape, early elongating RNAPII can be paused at 20-60nt downstream of the TSS. This RNAPII promoter proximal pausing mechanism was first described for *Drosophila* heat-shock genes (Rougvie and Lis, 1988). In mammalian cells, the control of RNAPII pause-release is also a highly regulated rate-limiting step during transcription (Figure 1.4) (Guenther et al., 2007; Rahl et al., 2010).

Step 4/5: RNAPII pause-release

RNAPII promoter proximal pausing is imposed by two factors, the 5,6-dichloro-1-β-D-ribofuranosylbenzimidazle (DRB) sensitivity-inducing factor (DSIF) and negative elongation factor (NELF). To reverse their effect, positive transcription elongation factor (P-TEFb) is required and allows for productive elongation (Zhou et al., 2012). P-TEFb is a nuclear-localized cyclin-dependent kinase (CDK), containing cyclins T1/T2 and the catalytic subunit CDK9. P-TEFb functions in releasing paused RNAPII by phosphorylating NELF subunit NELFe (Fujinaga et al., 2004), DSIF subunit hSpt5 (Chen et al., 2009), and serine2 on the Rpb1-CTD (Ramanathan et al., 2001). Phosphorylated NELF is dissociated from RNAPII, and phosphorylated DSIF functions as a positive elongation factor (Peterlin and Price, 2006). In addition, the hyperphosphorylated Rpb1-CTD, conveniently located at the pre-mRNA exit site (Cramer et al., 2001), serves as an important scaffold for the binding of RNA processing complexes and other positive elongation factors to facilitate transcription elongation (Bentley, 2014; Zhou et al., 2012).

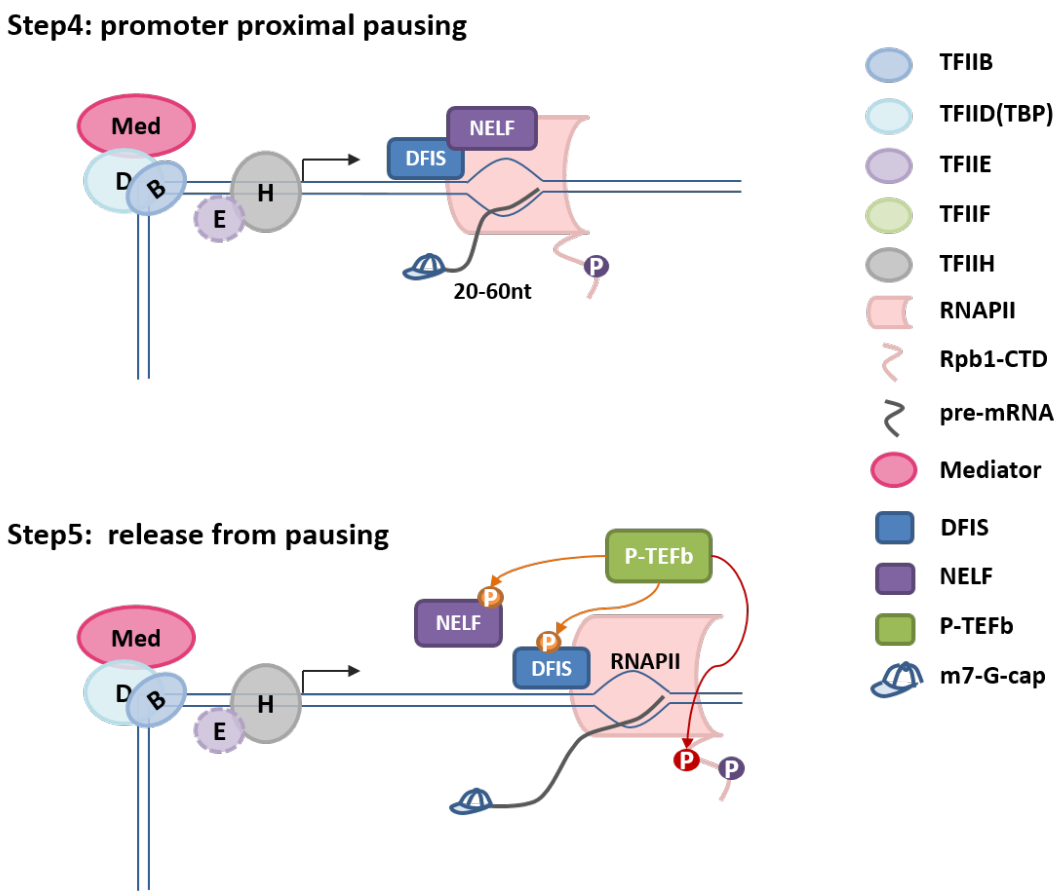

Figure 1.4 Schematic illustration of transcription elongation control

After promoter escape (Figure 1.3), RNAPII is paused at the promoter proximal region, after producing approximately 20-60nt of pre-mRNA. The pausing is imposed mainly by two factors, NELF and DFIS. Productive elongation need to overcome the pausing by P-TEFb, which phosphorylates NELF, DFIS and Rpb1-CTD serine2. This leads to the dissociation of NELF from RNAPII, transformation of DFIS to positively assisting elongation, and recruitment of mRNA processing complexes.

Because paused RNAPII requires P-TEFb for productive elongation, regulating the activity and localization of P-TEFb is essential for proper gene expression. P-TEFb is sequestered in an inactive state by the RNA-binding protein HEXIM1/2 and 7SK snRNP (containing 7SK RNA, LARP7 and MePCE) (Li et al., 2005b; Nguyen et al., 2001; Yang et al., 2001). Reversing the association with 7SK snRNP plays a major role in delivering the active form of P-TEFb.

In one way, the release of P-TEFb can be mediated through direct interaction with Brd4, a bromodomain protein of the BET family (bromodomain and extraterminal) (Jang et al., 2005; Yang et al., 2005). Brd4 recognizes acetylated histones, particularly acetylated histone H4K5/K8/K12 (Hargreaves et al., 2009). Brd4 then directs P-TEFb to these hyperacetylated gene promoters. Interference with Brd4 by siRNA or BET inhibitors, such as JQ1 and I-BET, impairs P-TEFb recruitment to the gene promoters with paused RNAPII. This leads to decreased phosphorylation of Rpb1-CTD serine2, and subsequently suppresses inducible gene expression (Filippakopoulos et al., 2010; Hargreaves et al., 2009; Nicodeme et al., 2010). Additionally, a small fraction of P-TEFb can be activated though its association with the super elongation complex (SEC) (Smith et al., 2011). P-TEFb/SEC can be recruited to paused RNAPII through MED26 of the Mediator complex (Takahashi et al., 2011) or PAFc (polymerase-associated factor complex) (He et al., 2011), and subsequently increases the release of paused RNAPII. P-TEFb/SEC can also be targeted to distinct genomic loci associated with disease progression. For example, the *MLL* gene (mix lineage leukaemia) generates in-frame fusions with translocation partners including the genes encoding components of SEC. The fusion proteins thereby bring P-TEFb/SEC to MLL target genes for activation, and therefore induces leukemic transformation (Lin et al., 2010a).

Transcription factors can impose their effects on RNAPII through modulating the pause-release. For example, c-Myc directly interacts with P-TEFb, and enhances transcription at target genes without changing the recruitment of the transcription machinery (Rahl et al., 2010). Elevated c-Myc, either by ectopic overexpression or physiological stimulation, invades active promoters and enhancers in embryonic stem cells, lymphocytes and B-cell leukaemia cell lines. Through interactions with P-TEFb, chromatin invasion by c-Myc leads to increased binding of CDK9 to c-Myc bound promoters, increased phosphorylation of Rpb1-CTD serine2, and subsequently, universally amplified transcription (Lin et al., 2012; Nie et al., 2012).

Once released from pausing, RNAPII elongates at a speed of ~3.8Kb/min on the human genome (Singh and Padgett, 2009), until encountering termination signals.

1.2.2 Nucleosomes as barriers to transcription

In eukaryotes, genomic DNA is packaged into chromatin, and the fundamental structural unit of chromatin is the nucleosome. Nucleosomes were first discovered due to the regular patterns on nuclease digestion and electron microscopic analysis of chromatin (Hewish and Burgoyne, 1973; Olins and Olins, 1974; Woodcock et al., 1976). They consist of a histone octamer with ~147bp of DNA tightly wrapped around (Luger et al., 1997). Nucleosomes are connected by short 'linker DNA' into a linear array, forming the primary structure of chromatin. Linear arrays of nucleosomes are further compacted into chromatin fibres through interactions between neighbouring nucleosomes. Subsequent fibre-fibre interactions contribute to the formation of more condensed higher order structures of chromatin (Luger et al., 2012; Tremethick, 2007). This high order structure partitions the chromatin into less condensed and transcriptionally active euchromatin, and densely packed and transcriptionally inert heterochromatin (Luger et al., 2012).

The compaction of genomic DNA into chromatin has a profound influence on transcription. It occludes the genomic DNA from being accessible to most transcription factors and regulatory cofactors, as well as the transcription machinery (Fuda et al., 2009). For transcription, this organized and compacted chromatin is made accessible in a highly regulated manner. The regulation of nucleosomes is fundamental to the generation of alternative chromatin structure.

1.2.2.1 Nucleosome distribution

The genome-wide distribution of nucleosomes shares common features among eukaryotes. In the majority of the genome, nucleosomes are regularly spaced. The length of spacing varies among different cell types in human and, within the same cell type, active chromatin shows shorter spacing than found in repressed heterochromatin (Valouev et al., 2011). However in many functional regions, nucleosomes are often depleted, creating a nucleosome-free region (NFR). These NFRs are observed at transcription start sites (TSSs), transcription termination sites (TTSs), and enhancers (Struhl and Segal, 2013). Specifically, nucleosomes surrounding the TSS, starting from the -1 (upstream) and +1 (downstream) nucleosomes, are well positioned and phased (Kaplan et al., 2009; Valouev et al., 2011), and this phasing pattern fades away as RNAPII signal decreases (Schones et al., 2008).

The nucleosome positioning in the genome is affected by DNA sequence. Nucleosome formation is optimal when bendable AA/AT/TA/TT dinucleotide occurs ~10bp periodically and interacts with histones (Brogaard et al., 2012; Drew and Travers, 1985; Segal et al., 2006). In contrast, homopolymeric poly(dA:dT) is rigid and favours nucleosome depletion (Hughes et al., 2012; Raveh-Sadka et al., 2012). However, DNA sequence is not the only determinant of nucleosome positioning, since nucleosomes assembled *in vitro* based on DNA sequence alone do not fully agree with their *in vivo* distribution. For example, reconstitution of human chromatin *in vitro* reveals a 'container' model that favours nucleosome formation (Valouev et al., 2011). This model states that high GC content favours nucleosome formation, and this nucleosome formation is enhanced by being surrounded by AT-rich repelling elements. However, this GC/AT preference is not observed *in vivo* in primary human cells (Valouev et al., 2011). As another example, *in vitro* reconstituted yeast chromatin does not show strongly positioned +1 nucleosome (Zhang et al., 2009).

In addition to the intrinsic DNA sequence preference, the chromatin environment is an important determinant of nucleosome positioning. With the addition of yeast whole cell lysate and ATP, Pugh and colleagues were able to reproduce a native nucleosome distribution *in vitro*, including the well positioned nucleosomes surrounding the TSSs (Zhang et al., 2011). As another example, transcription is fine-tuned by manipulating nucleosome-disfavouring sequences. However, the level of gene expression is dominantly determined by the binding affinity of transcription factors (Raveh-Sadka et al., 2012). Therefore, transcription factors, together with chromatin modifiers, override the intrinsic DNA preference and regulate the accessibility of functional regulatory DNA elements. This is particularly important to modify the transcription landscape and mediate cell differentiation.

1.2.2.2 Nucleosome composition and dynamics

The nucleosome consists of ~147bp of DNA wrapped around a histone octamer, which is composed of two copies each of the histones H2A, H2B, H3 and H4. The nucleosome is stabilised by a multitude of protein-protein interactions within the histone octamer, and by the interactions between the histone octamer and the entire length of nucleosomal DNA (Andrews and Luger, 2011; Luger et al., 1997). Histone H2A dimerizes with H2B, while H3 dimerizes with H4. The $(H3\text{-}H4)_2$ tetramer is formed due to a strong four-helix bundle

interaction between two H3 proteins (Luger et al., 1997). Two H2A-H2B heterodimers interact with the $(H3\text{-}H4)_2$ tetramer through a weaker four-helix bundle interaction between H2B and H4 (Luger et al., 1997). Additionally, the association of H2A-H2B dimers within the nucleosome is strengthened by contacts between the two H2A histones. The nucleosome core can be viewed as three spatial domains, the $(H3\text{-}H4)_2$ tetramer and two H2A-H2B dimers. The $(H3\text{-}H4)_2$ tetramer lies at the 'central region' of the DNA wrap, governing ~80bp DNA. H2A-H2B dimers dock at the DNA 'entry' and 'exit' sites of the nucleosome, associating with ~35bp DNA each (Bintu et al., 2012; Talbert and Henikoff, 2010).

Nucleosome assembly and disassembly are highly structured processes (Figure 1.5). A study of salt-induced nucleosome disassembly suggests that the first step is the dissociation of the H2A-H2B dimers from the $(H3\text{-}H4)_2$ tetramer. This is followed by the release of H2A-H2B dimers from the nucleosomal DNA and lastly, the $(H3\text{-}H4)_2$ tetramer is removed from DNA (Bohm et al., 2011). The reverse of this process is the primary assembly pathway. During nucleosome (dis)-assembly, simultaneous steps are possible (Andrews and Luger, 2011).

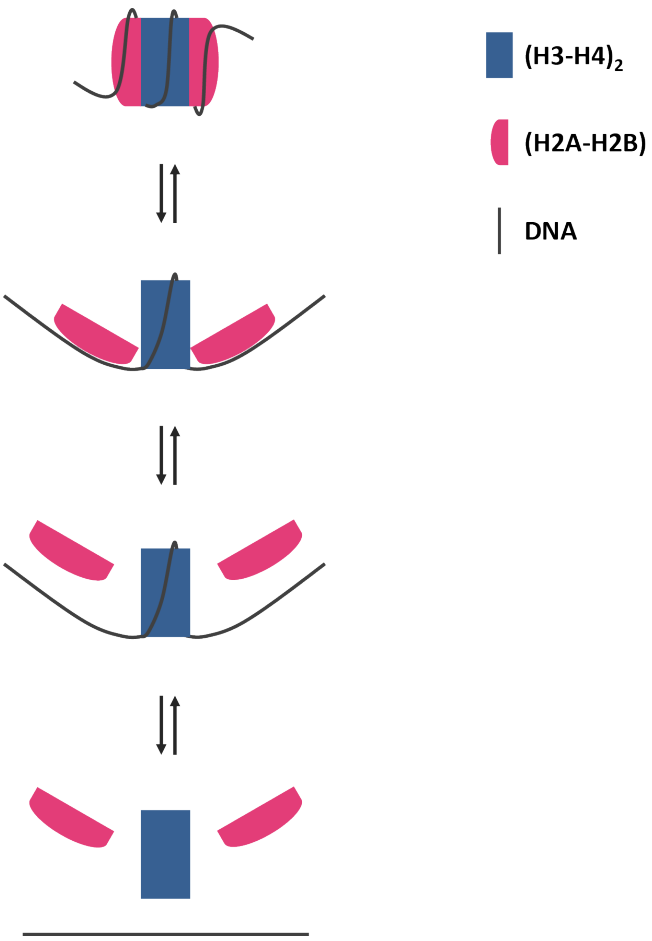

Figure 1.5 Schematic illustration of nucleosome (dis)-assembly

The first step in nucleosome disassembly is the dissociation of the H2A-H2B dimer from the $(H3\text{-}H4)_2$ tetramer. It is followed by H2A-H2B dimer release from the DNA. And lastly, the $(H3\text{-}H4)_2$ tetramer is removed from DNA. The reverse of this process is the primary assembly pathway. This schematic is adapted from (Bohm et al., 2011).

The study of nucleosome structure and its (dis)-assembly processes suggests that the spatial domains of nucleosomes are independently controlled. Indeed, the $(H3\text{-}H4)_2$ tetramer is more stably associated with DNA *in vivo* (Xu et al., 2010). The $(H3\text{-}H4)_2$ tetramer, governing the central region of DNA wrapping, determines the strength of the barrier to elongating RNAPII *in vitro* (Bintu et al., 2012). Transcription by RNAPII can disrupt H2A-H2B dimers, without changing the position of the $(H3\text{-}H4)_2$ tetramer (Kireeva et al., 2002). Due to the independently controlled domains of nucleosomes, accessibility to DNA can be generated by

partial disassembly of the nucleosome. For example, to initiate V(D)J recombination during B cell development, recombination signal sequences (RSSs) need to be accessible to the recombination machinery. The generation of RSS accessibility is not achieved by complete disassembly of the nucleosome core, but by transiently evicting H2A-H2B dimers, thereby exposing ~35bp DNA (Bevington and Boyes, 2013).

The nucleosome is not a static entity. The protein-protein interactions between the spatial domains and the protein-DNA interactions between the core histones and the nucleosomal DNA are intrinsically dynamic. Nucleosomal DNA undergoes spontaneous partial unwrapping off the histone surface and rewraps, which makes the nucleosomal DNA transiently accessible (Li et al., 2005a). DNA unwraps fastest at the DNA entry site of the nucleosome, and the kinetics slow down dramatically as DNA elements locate increasingly inside the nucleosome (Tims et al., 2011). Interestingly, this nucleosome intrinsic unwrapping/rewrapping dynamic is still observed in folded chromatin fibres (Poirier et al., 2008). In addition, the interactions between the spatial domains of the nucleosome core are also dynamic. The nucleosomes go through dynamic disassembly and assembly, termed turnover. By directly measuring newly incorporated histones, nucleosomes are shown to turn over in both yeast and *Drosophila* cells. Nucleosome turnover is more rapid at regulatory elements and active genes (Deal et al., 2010; Dion et al., 2007; Rufiange et al., 2007). Furthermore, this turnover happens to both the H2A/H2B dimer and the $(H3/H4)_2$ tetramer. The H2A/H2B dimer turns over much faster than the $(H3/H4)_2$ tetramer in both intra- and intergenic regions (Jamai et al., 2007).

The spontaneously dynamic histone-DNA and histone-histone interactions provide another means to transiently expose DNA binding sites to regulatory factors. This transient exposure of DNA is hypothesised to be captured by 'pioneer transcription factors', and subsequently induce a cascade of events to further open up chromatin and facilitate transcription (Tims et al., 2011). Because of this dynamic nature of nucleosomes, some nucleosomes are labelled 'fragile' in the yeast genome. These fragile nucleosomes show higher sensitivity to Micrococcal nuclease (MNase) digestion and salt concentration. They mainly flank the promoters of transcriptionally poised genes, allowing for swift up-regulation upon cellular signals (Xi et al., 2011).

Taken together, regulatory DNA elements can be transiently exposed to transcription factors due to the spontaneous nucleosome dynamics. These dynamics can be influenced by the

factors that induce changes in nucleosome stability, including the incorporation of histone variants, or post-translational modifications of histones (Weber and Henikoff, 2014). In addition, nucleosomes can be partially disrupted at certain spatial domains (Ballare et al., 2013), or totally disassembled to allow for DNA access by more transcription factors and the transcription machinery (Agalioti et al., 2000; Petesch and Lis, 2008). This process is carried out by ATP-dependent chromatin remodelers. These topics are further discussed in the following sections.

1.2.2.3 Histone variants and histone chaperones

Sequence divergence is observed in core histones, giving rise to histone variants. Whilst the expression of the 'canonical' histones is restricted to S phase of the cell cycle, histone variants are expressed and incorporated into nucleosomes throughout the cell cycle (Osley, 1991; Talbert and Henikoff, 2010). Since the first histone variant was discovered by West and Bonner (West and Bonner, 1980), histone variants have been attracting a lot of attention due to their profound influence on nucleosome stability as well as biological processes ranging from transcriptional regulation to genome stability.

The highest degree of histone sequence divergence is observed in the histone H2A and H3 family. While histone H2A variant H2A.X is mainly involved in DNA damage response, H2A.B, MacroH2A, H2A.Z, and histone H3 variant H3.3 have been shown to be involved in transcriptional regulation (Bonisch and Hake, 2012).

H2A.B (H2A.Bbd or H2A.Lap1) is found only in mammals and is highly tissue-specific. Compared to canonical H2A, H2A.B is considerably shorter and less stable (Bonisch and Hake, 2012). An H2A.B-containing nucleosome protects ~30bp less DNA against Micrococcal nuclease (MNase) digestion (Doyen et al., 2006). In both mouse and human, H2A.B is associated with active genes (Soboleva et al., 2012; Tolstorukov et al., 2012). MacroH2A, found mainly in vertebrates, contains a distinct non-histone globular (macro) domain. MacroH2A is enriched on the inactive female X chromosome (Costanzi and Pehrson, 1998) and senescence-associated heterochromatic foci (Zhang et al., 2005b), suggesting a role in transcriptional repression. Histone variant H2A.Z is almost universally expressed and highly conserved between species (Talbert and Henikoff, 2010). Despite the overall similarity

of its structure to that of canonical H2A, H2A.Z fulfils unique functions and is essential to many organisms including mouse and human (Bonisch and Hake, 2012).

H2A.Z is not uniformly distributed in the genome. It is enriched at gene promoters and enhancers in mammalian cells (Barski et al., 2007; Raisner et al., 2005; Schones et al., 2008). H2A.Z is also incorporated into the strongly positioned +1 nucleosome immediately downstream of the TSS, and a few well positioned nucleosomes further downstream, but is relatively depleted over the rest of the gene bodies (Barski et al., 2007; Tropberger et al., 2013). The enrichment of H2A.Z is positively correlated with transcriptional activity, chromatin accessibility, and active histone modifications (Conerly et al., 2010; Hu et al., 2013). In contrast, the enrichment of H2A.Z is anti-correlated with DNA methylation during B cell lymphomagenesis (Conerly et al., 2010). This implicates a role of H2A.Z in active transcription.

H2A.Z poses its influence on transcription through modulating the stability of nucleosomes, with H2A.Z shown to destabilise nucleosomes *in vivo* (Weber and Henikoff, 2014). H2A.Z-containing nucleosomes protect only ~120bp DNA from MNase digestion in human T cells (Tolstorukov et al., 2009) and embryonic stem cells (ESCs) (Hu et al., 2013). The incorporation of H2A.Z enhances the dynamics of nucleosomes. This favours nucleosome removal at regulatory regions during transcription. For example, H2A.Z deposition leads to decreased nucleosome occupancy and increased chromatin accessibility at promoters and enhancers in ESCs. This is important for the binding of key active and repressive regulatory complexes (Creyghton et al., 2008; Hu et al., 2013). Knockdown of H2A.Z compromises the self-renewal and differentiation abilities of ESCs (Hu et al., 2013). During the specification of ESCs into endoderm/hepatic fate, H2A.Z works together with the transcription factor Foxa2, mediating nucleosome depletion at lineage-specific genes and also facilitating their activation (Li et al., 2012).

In addition to favouring the access to regulatory regions, H2A.Z also facilitates transcription elongation. In *Drosophila*, H2A.Z deposition enhances the turnover of the +1 nucleosome. Depletion of H2A.Z results in a stronger barrier to RNAPII during transcription elongation (Weber et al., 2014).

Deposition and removal of H2A.Z is an active process. In yeast, the general histone H2A/H2B chaperone Nap1 and Chz1 preferentially bind H2A.Z over H2A (Luk et al., 2007; Straube et al., 2010). These chaperones act as reservoirs for histone H2A.Z, and deliver it to

the ATP-dependent chromatin remodeler Swr1. Swr1 catalyses the exchange of H2A.Z for canonical H2A (Luk et al., 2010; Mizuguchi et al., 2004; Watanabe et al., 2013). The removal of H2A.Z from chromatin is catalysed by the chromatin remodeler Ino80 (Papamichos-Chronakis et al., 2011). In mammalian cells, the equivalent of Swr1 falls into two distinct complexes, P400/Tip60 and SRCAP. Recently, ANP32E, a H2A.Z-specific histone chaperone in human, was discovered as part of the P400/Tip60 complex, but not SRCAP (Mao et al., 2014; Obri et al., 2014).

Histone H3 variant H3.3 differs from canonical histone H3 only by four to five amino acids, and yet it displays a distinct role in the regulation of transcription (Filipescu et al., 2013). H3.3 is widely distributed in the genome, and is observed at regulatory regions, gene bodies, and heterochromatin (Weber and Henikoff, 2014). Histone H3.3 does not alter nucleosome dynamics *in vitro*, agreeing with its high similarity in structure to canonical H3 (Thakar et al., 2009). However *in vivo*, H3.3 deposition facilitates chromatin accessibility to regulatory complexes. In ESCs, depletion of H3.3 reduces nucleosome turnover, and decreases the binding of the repressive complex PRC2 (polycomb repressive complex 2) (Banaszynski et al., 2013). This *in vivo* property of H3.3 to destabilise the nucleosome can be attributed to its interactions with partners. Felsenfeld and colleagues reported that H3.3-containing nucleosomes, when present together with H2A.Z, are highly unstable. H2A.Z/H3.3-containing nucleosomes are more sensitive to salt concentration and are easily disrupted (Jin and Felsenfeld, 2007). They flank the active promoters, enhancers and insulator regions. Due to their instability, these nucleosomes are more easily replaced by non-histone DNA binding proteins, therefore favouring transcriptional regulation (Jin et al., 2009). In support of this, H3.3-containing nucleosomes turn over at different speed depending on the genomic regions, with the turnover being the fastest at promoters and enhancers which are associated with active histone marks and histone H2A.Z, intermediate at gene bodies, and slowest at telomeres (Kraushaar et al., 2013).

Two histone chaperones are responsible for H3.3 incorporation: HIRA (histone regulator A), and DAXX (death-associated protein) together with ATP-dependent chromatin remodeler ATRX. The former incorporates H3.3 into genic and euchromatic regions (Banaszynski et al., 2013), while the latter deposits H3.3 to pericentrometic and telomeric heterochromatin regions (Goldberg et al., 2010).

1.2.2.4 Histone modifications and histone-modifying enzymes

Histones can be post-translationally modified by methylation, acetylation, phosphorylation, sumoylation, and other modifications. These post-translational modifications (PTMs) appear on both the globular structure of the nucleosome core, and the N-terminal tails of histones. Histone tails extend away from the nucleosome core, and are involved in interactions with neighbouring nucleosomes or regulatory factors (Luger et al., 1997). Histone modifications have a profound impact on chromatin dynamics and transcriptional regulation (Kouzarides, 2007). They can be categorised into those that correlate with transcriptional activation, and those that correlate with transcriptional repression. Histone modifications affect transcription by altering the stability and dynamics of nucleosomes, or by recruiting or occluding other non-histone proteins (Kouzarides, 2007).

Acetylation was the first described histone modification (Phillips, 1963). Acetylated histones are mainly associated with active genes (Tropberger et al., 2013; Wang et al., 2008). The positive effect of histone acetylation on transcription is due to the altered stability and dynamics of the nucleosome. Acetylation of lysine (K) residues on the histones neutralises their positive charge. Since DNA is negatively charged, lysine acetylation thereby weakens the charge-dependent interactions between histones and nucleosomal DNA. In this way, histone acetylation increases the nucleosome dynamics, thus making the nucleosomal DNA more accessible to transcription factors and the transcription machinery (Zentner and Henikoff, 2013).

The tails of histone H3 and H4 can be acetylated at multiple sites. They positively affect transcriptional outcomes due to a cumulative effect on charge neutralisation, rather than the acetylation of specific lysines (Zentner and Henikoff, 2013). This is supported by a study that investigates the effects of lysine-to-arginine mutations on transcription. Arginine (R) is used to mimic the positively charged, but unable to be acetylated lysines (K). It is hypothesised that if the charge neutralisation effect on transcription is cumulative, mutations on the specific lysine residues should affect the same set of genes. Indeed, specific K→R mutations of the H4 tail at K5, K8, and K12 affect nearly identical group of genes. Furthermore, combined mutations enhance this transcription deregulation (Dion et al., 2005). In support of this, lysine-to-glutamine mutations on the H3 tail, which mimics the acetylated lysines, revealed that these lysine residues have generally redundant roles on transcription (Martin et al., 2004). In addition to acetylation on the histone tails, acetylation also occurs on the

globular domain of the nucleosome core. Lysine acetylation near the nucleosome DNA entry/exit regions (H3K56Ac) modulates nucleosome partial unwrapping (Neumann et al., 2009), and those near the centre of the nucleosome directly facilitates nucleosome disassembly *in vitro* (Simon et al., 2011). Acetylation of H3K64 and H3K122, which lie within the nucleosome globular domain, favours nucleosome disassembly, and directly facilitates active transcription *in vivo* (Di Cerbo et al., 2014; Tropberger et al., 2013).

In addition to modulating the physical properties of the nucleosome, acetylated histones are recognised by histone 'readers'. In this way, histone modifications serve as docking sites for the binding of regulatory proteins, and signal downstream events. Histone acetylation is recognised by a specific reader module, the bromodomain (Zentner and Henikoff, 2013). Brd4 recognizes acetylated histone H4, and directs P-TEFb to these gene promoters and enhances RNAPII elongation (Hargreaves et al., 2009). Hyperacetylation of H4 and deposition of H2A.Z together signal the binding of Brd2, and subsequently induces active transcription (Draker et al., 2012).

Lysine residues on histones are acetylated by histone acetyltransferases (HATs), and are deacetylated by histone deacetylases (HDACs) (Allis et al., 2007). Histone deacetylation by HDACs are mostly related to transcription inactivation. For example, HDAC SIRT7 binds its target gene promoters and deacetylates H3K18. This leads to the transcriptional repression of its target genes (Barber et al., 2012). Yeast HDACs Sir2 and Clr3 facilitate the establishment and maintenance of heterochromatin. This is achieved by their role in repressing active transcription and decreasing histone turnover rate, as well as bringing in the H3K9-specific histone methyltransferase Clr4 (Alper et al., 2013; Buscaino et al., 2013). In addition to the role of HDACs in repressing transcription, HDACs are also found at actively transcribed genes. They work together with HATs, and control the dynamics of histone acetylation at active genes (Wang et al., 2009). Interestingly, HDAC6 is only associated with active genes at the promoters and particularly at the gene bodies in mammalian cells (Wang et al., 2009). In addition, the half-lives of histone acetylations are a few minutes for many events (Barth and Imhof, 2010). These observations support the mechanism, as proposed in yeast (Carrozza et al., 2005; Huh et al., 2012) and *Drosophila* (Rincon-Arano et al., 2012), that acetylated histones loosen DNA-histone interactions to allow RNAPII traveling, but are rapidly deacetylated to promote chromatin assembly after transcription, therefore preventing cryptic transcription.

In contrast to acetylation, lysine methylation can have both positive and negative effects on transcription, depending on the lysine residue methylated. Methylations on H3K4, K36 and K79 are associated with active transcription, while H3K9Me2/3, H3K27Me2/3 are usually found at inactive heterochromatin (Barski et al., 2007).

H3K4Me3 facilitates active transcription by recruiting the chromatin modifiers and other downstream effector proteins. Readers for H3K4Me3 include the PHD (plant homeo domain) module, chromodomain, and other modules (Yun et al., 2011). H3K4Me3 is recognised by TAF3, a subunit of the general transcription factor TFIID, through its PHD module. This directly links H3K4Me3 to the recruitment of the transcription machinery (Vermeulen et al., 2007). H3K4Me3 also facilitates the recruitment of the chromatin remodeler Chd1 (chromodomain helicase DNA binding protein 1) to gene promoters, and subsequently opens up chromatin and stimulates transcription (Bartke et al., 2010; Lin et al., 2011). However, H3K4Me3 density is not proportional to the transcription level. H3K4Me3 is found at active gene promoters as well as poised ones (Guenther et al., 2007). Furthermore, significant reduction of H3K4Me3 by deleting the histone methyltransferase SET1/MLL complex (Dpy-30 subunit) does not dramatically down-regulate the transcription of active genes in ESCs (Jiang et al., 2011).

In a similar manner to H3K4Me3, H3K9Me3 is recognised by the chromodomain of the heterochromatin protein 1 (HP1). This is important for gene silencing and chromatin compaction (Bannister et al., 2001; Lachner et al., 2001).

Histone modifications and histone modifiers cross-talk with each other and co-regulate transcription (Bartke et al., 2010; Vermeulen et al., 2010). For example, H3K4Me3 methyltransferase SET1 complex (SET1C) is recruited to gene promoters through direct interactions with the HAT p300, and they work cooperatively to facilitate transcription (Tang et al., 2013). In yeast, histone methyltransferase Set2 methylates H3K36, which is observed at active gene bodies. Set2 also recruits HDAC Rpd3S to active genes to repress cryptic transcription on the gene bodies (Carrozza et al., 2005).

1.2.2.5 Chromatin remodelers

The reorganisation of chromatin structure is carried out by ATP-dependent chromatin remodelers. The targeting of chromatin remodelers to chromatin depends on specific histone modifications and is facilitated by context-specific transcription factors. The chromatin remodelers directly bind nucleosomes and subsequently catalyse nucleosome repositioning or eviction, or alter nucleosome composition (Clapier and Cairns, 2009). An ATPase domain is shared by all chromatin remodelers. Depending on their additional unique domains, chromatin remodelers are categorised into four different families, namely the CHD (chromodomain helicase DNA binding) family, the SWI/SNF (switching defective/sucrose nonfermenting) family, the INO80 (inositol requiring 80) family, and ISWI (imitation switch) family (Clapier and Cairns, 2009).

The CHD family members Mi-2α/Chd3 and Mi-2β/Chd4 contain two PHD domains, two chromodomains and an ATPase domain (Clapier and Cairns, 2009; Woodage et al., 1997). To remodel nucleosomes, the ATPase activity of Mi-2 is stimulated by chromatin, but not by free histones or DNA (Wang and Zhang, 2001). The PHD domains of Mi-2β are required to facilitate transcriptional regulation. PHD1 and -2 function individually to bind histone H3 tails. Mutations in these two domains compromise the ability of Mi-2β to restrain *Mb-1* expression, even to the same level as Mi-2β knockdown (Musselman et al., 2012).

Mammalian Mi-2 (predominantly Mi-2β) exists in the Mi-2/NuRD (nucleosome remodelling and deacetylase) complex. In addition to the ATPase subunit Mi-2, the Mi-2/NuRD complex also contains histone deacetylases HDAC1/2, methyl CpG binding domain proteins MBD2/3, metastasis-associated proteins MTA1-3, and histone-binding proteins/retinoblastoma-binding proteins PBBP4, -7 (Tong et al., 1998; Xue et al., 1998; Zhang et al., 1998). The Mi-2/NuRD complex is the only complex possessing both chromatin remodelling and histone deacetylation functions.

The Mi-2/NuRD complex has been associated with transcriptional repression in different systems (Curtis and Griffin, 2012; Kaji et al., 2006; McDonel et al., 2009; Reynolds et al., 2012). As examples in the B cell compartment, Mi-2/NuRD subunit MTA3 was shown to directly interact with the transcription factor Bcl-6 in B lymphocytes. The MTA3-Mi-2/NuRD complex is required for transcriptional repression by Bcl-6, as knockdown of MTA3 results in up-regulated expression of Bcl-6 target genes (Fujita et al., 2004). During EBF and Pax5-mediated *Mb-1* activation, the Mi-2/NuRD complex limits *Mb-1* activation level. Mi-

2/NuRD restrains the increase in chromatin accessibility, and limits DNA demethylation at the *Mb-1* promoter. Knockdown of Mi-2β fails to restrain the transcription activities and results in stronger *Mb-1* activation (Gao et al., 2009). These observations also highlight the unique feature of the Mi-2/NuRD complex to combine different transcriptional regulatory processes, including nucleosome reorganization, histone modifications and DNA methylation.

In addition to the role in transcriptional repression, Mi-2 has also been associated to transcriptional activation. During T cell differentiation, Mi-2β directly interacts with the *Cd4* enhancer, and positively regulates *Cd4* expression (Williams et al., 2004). Furthermore, Mi-2β is reported to be critical for self-renewal and lineage commitment of HSCs, which involves the activation of lineage-specific genes (Yoshida et al., 2008). The activating role of Mi-2β may be an indication of Mi-2β functioning outside of the Mi-2/NuRD complex. In support of this idea, Mi-2β N-terminal domain has been reported to be associated with the chromatin remodeler Brg1 (Shimono et al., 2003).

Brg1, or Brm, is the ATPase subunit of the SWI/SNF complex (also known as BAF). In addition to Brg1/Brm, the mammalian SWI/SNF complex contains 9 to 11 other subunits. The composition of the SWI/SNF is partially different between cell types, and their functions are not well understood (Wu et al., 2009). These additional subunits may be involved in regulating the recruitment, the assembly and/or the activity of the SWI/SNF complex (Schubert et al., 2013; Wu et al., 2009; Yang et al., 2007). Brg1/Brm, both the SWI/SNF complex-associated and the isolated, is able to alter histone-DNA interactions. Brg1 can produce a stably remodelled di-nucleosome from a mono-nucleosome template, or transfer the histone octamer from donor nucleosomes to acceptor DNA (Phelan et al., 2000).

Brg1/Brm plays an important role in opening up chromatin and activating transcription. Knockdown of Brg1/Brm inhibits the activation of *Mb-1* mediated by EBF and Pax5 during B cell development (Gao et al., 2009). The SWI/SNF complex is required to maintain the expression of *Myc* in leukaemia cells, by essentially maintaining the accessibility at the enhancers and facilitating the binding of the transcription factors to DNA (Shi et al., 2013).

Contrary to the role of Brg1/Brm in increasing chromatin accessibility and activating transcription, a recent genome-wide study showed that knockdown of Brg1 disrupts the nucleosome landscape at promoters, and decreases overall nucleosome occupancy. Knockdown of Brg1 also leads to the up-regulation of Brg1 target genes (Tolstorukov et al., 2013). The dual roles of the Brg1/Brm SWI/SNF complex in both transcriptional activation

and repression may be due to the variations in the composition and activity of the complex in a cell type-specific manner.

1.3 Ikaros and transcriptional regulation

Ikaros has both activating and repressing effects on transcription (Ferreiros-Vidal et al., 2013; Heizmann et al., 2013; Merkenschlager, 2010; Schjerven et al., 2013; Schwickert et al., 2014).

Ikaros was first discovered to bind the regulatory element of *Cd3δ*, and activate its transcription in lymphocytes (Georgopoulos et al., 1992). This original concept of Ikaros being an activator was first challenged by the observations that in B and T lymphocytes and early B cell progenitors, Ikaros proteins form clusters at pericentromeric heterochromatin, where silent genes are colocalised (Brown et al., 1999; Brown et al., 1997; Klug et al., 1998). This observation lead to the hypothesis that Ikaros may recruit its target genes to heterochromatic compartments, where repressive proteins are enriched, to maintain the silent state of target genes. This hypothesis is supported by the finding that several inactive genes adopt a position away from heterochromatin regions in resting B cells, and upon activation, these genes move towards heterochromatin concomitantly with the up-regulation of Ikaros and the clustering of Ikaros at heterochromatin (Brown et al., 1999). The targeting of Ikaros to heterochromatin is achieved through direct DNA binding, and requires the C-terminal zinc fingers to form Ikaros dimers or multimers (Cobb et al., 2000; Trinh et al., 2001).

Ikaros binding in the genome co-occurs with several transcription factors important for haematopoiesis, including EBF, E2A, Pax5, PU.1 and IRF4 (Ferreiros-Vidal et al., 2013; Schwickert et al., 2014). This colocalisation may indicate possible competitions or collaborations between Ikaros and other transcription factors. Indeed, Ikaros directly binds the *Igll1* promoter to down-regulate the transcription, and mutation in the Ikaros DNA binding domain or the deletion of a single Ikaros binding site abolishes the gene repression (Sabbattini et al., 2001; Thompson et al., 2007). EBF1 also binds the *Igll1* promoter, and activates transcription (Martensson and Martensson, 1997). Ikaros and EBF1 compete with each other and balance the expression of *Igll1* in pre-B cells (Thompson et al., 2007). Similarly, Ikaros competes with the transcription activator Elf1 to regulate the expression of *Dntt* in thymocytes (Trinh et al., 2001). In yolk sac erythroid cells, Ikaros binds to the human γ-globin promoter and facilitates the binding of the transcription factor GATA1. Together,

Ikaros and GATA1 promote the transcription of human γ-globin by increasing the PIC assembly and the phosphorylation of RNAPII serine2 by Cdk9 (Bottardi et al., 2011).

Ikaros also regulates transcription through its association with chromatin modifiers. This was first demonstrated by Georgopoulos and colleagues using a yeast two hybrid assay (Kim et al., 1999). Ikaros interacts with chromatin remodelers Mi-2/NuRD and Brg1-SWI/SNF complexes (Kim et al., 1999), as well as corepressors Sin3 (Koipally et al., 1999) and CtBP (Koipally and Georgopoulos, 2000). In erythroid cells, Ikaros facilitates the recruitment of Brg1 to activate the human γ-globin gene (Bottardi et al., 2011). In thymocytes, Ikaros is predominantly associated with the Mi-2/NuRD complex (Sridharan and Smale, 2007). Ikaros and Mi-2β both bind the *Cd4* silencer and regulate *Cd4* expression during T cell development (Naito et al., 2007). Loss of either Ikaros or Mi-2β leads to the activation or repression of the *Cd4* locus, respectively. Interestingly, this deregulation can be rescued by double mutation of Ikaros and Mi-2β (Naito et al., 2007). Genome-wide profiling of Ikaros and Mi-2β binding in double-positive (DP) thymocytes confirmed that Ikaros colocalises with Mi-2β at both promoters and enhancers, particularly at active genes (Zhang et al., 2012). Ikaros appears to inhibit the binding of Mi-2β, as loss of Ikaros leads to increased binding of Mi-2β and decreased H3K9Ac (Zhang et al., 2012). However in pro-B cells, contrasting observations were reported (Schwickert et al., 2014). In pro-B cells, Ikaros preferentially binds to active promoters and enhancers, and these binding sites are overlapped with Mi-2β only at the promoters, but not the enhancers. Further contrasting the observations in thymocytes, loss of Ikaros in pro-B cells does not lead to the redistribution of Mi-2β binding, nor a global decrease of H3K9Ac (Schwickert et al., 2014). The differences observed in thymocytes and pro-B cells may be due to the different roles of Ikaros in thymocytes and pro-B cells, or the differences in the experimental strategies.

Ikaros protein itself can be post-translationally modified, which modulates its functions. Ikaros is dynamically phosphorylated within the regions encoded by exon 3 and 7 during the cell cycle. Ikaros is hypophosphorylated in G1 and hyperphosphorylated after entry into S phase (Gomez-del Arco et al., 2004). The phosphorylation of Ikaros inhibits its ability to impede the G1-S transition (Gomez-del Arco et al., 2004). Phosphorylations at alternative sites within Ikaros have been linked to both facilitating and inhibiting Ikaros nuclear localization and DNA binding (Gurel et al., 2008; Uckun et al., 2012). Additional means for the regulation of Ikaros function is via sumoylation. The sumoylation of Ikaros reduces its

ability to repress transcription, possibly by reducing the interactions with chromatin modifiers (Gomez-del Arco et al., 2005).

To regulate transcription, Ikaros directly binds DNA. The mechanisms include competition or collaboration with other transcription factors, interaction with the transcription machinery, recruitment of chromatin modifiers, and spatial compartmentalization in the nucleus. The activities of Ikaros can be controlled by post-transcriptional modifications. The potential of Ikaros to act as a repressor or activator therefore depends on the cellular context in a stage-specific manner.

1.4 Aims of this thesis

The principal aim of this study is to understand the kinetics and mechanisms of Ikaros-mediated transcriptional regulation. By applying an inducible Ikaros system to pre-B cells, the changes in chromatin status are identified. Furthermore, the kinetics of these regulatory events are monitored at high temporal resolution, and subsequently the order of events is comprehended. Following these observations, between the possible early and later events, causal relationships are investigated.

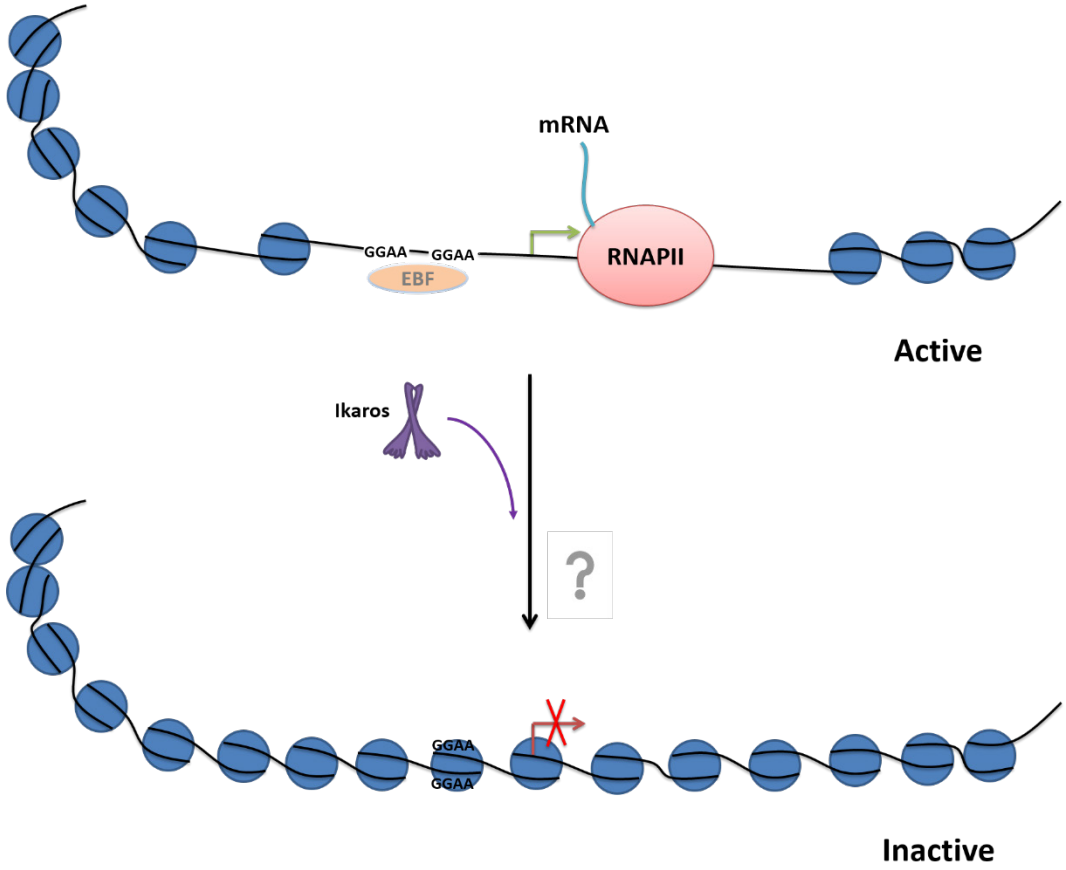

Figure 1.6 Aim of this study

The principle aim of this study is to understand the kinetics and mechanisms of Ikaros-mediated transcriptional regulation. During transcriptional down-regulation, introducing Ikaros to a negatively regulated target gene can change the locus from an active state to an inactive state. This may feature outcompeting transcription activators, the loss of RNAPII, and compaction of the gene promoter. This study aims to investigate what changes are induced in chromatin status by Ikaros, and what is the order of these events. Furthermore, between possible early events and late events, the causal relationships are also evaluated.

2 Materials and methods

2.1 Cell culture

All cells were maintained at 37°C in a humidified chamber with 5% (v/v) CO_2.

The B3 pre-B cell cells, isolated and cloned from a lymphoma occurring in an IL-7 transgenic mouse (Fisher et al., 1995), were cultured in Iscove's Modified Dulbecco's Medium (IMDM, Invitrogen), supplemented with 10% (v/v) foetal calf serum (FCS) (Biosera), and antibiotics (100U/ml Penicillin and 100µg/ml Streptomycin) (GIBCO, Invitrogen). The culturing concentration was maintained between 0.5-3×10^6 cells/ml by splitting the cells every two days.

The 293T packaging cells were cultured in Dulbecco's Modified Eagle Medium (DMEM, Invitrogen), supplemented with 10% (v/v) foetal calf serum (FCS) (Biosera), 2mM L-Glutamine, antibiotics (100U/ml Penicillin and 100µg/ml Streptomycin), and 50µM β-mercaptoethanol (GIBCO, Invitrogen), and were expanded every two days.

Frozen stocks of cell vials were generated by resuspending 1×10^6 cells in 1ml of FCS containing 10% (v/v) DMSO (Sigma), cooled down in Mr Frosty freezing container in -80°C freezer for 24 hours , and kept in liquid nitrogen.

2.2 Cloning

2.2.1 shRNA design

Work related to shRNA targeting *Ikzf1* (encodes for Ikaros) and *H2afz* (encodes for H2A.Z) were discussed in discussion and presented as supplementary figures.

The sequence of untranslated region (UTR) and coding region of the gene was used as reference for the design of siRNA. 19 or 21 nuclear tides (nt) targeting sequence was designed using the designer of small interfering RNA (DSIR) algorism (http://biodev.extra.cea.fr/DSIR/DSIR.html), the siDesign algorism by Dharmacon (http://dharmacon.gelifesciences.com/design-center/), the siRNA Wizard algorism by

InvivoGen (http://www.sirnawizard.com/), or Sigma MISSION shRNA. Top hits were screened for off-targets using NCBI blast. The first two targeting sequences against H2A.Z were taken from published data designed by Dr Keji Zhao's lab, NIH-NHLBI, USA (Hu et al., 2013). Selected hits were then fit in shRNA hairpin by inserting a loop of TTCAAGAGA between the sense strand and the anti-sense strand of siRNA, and also adding restriction enzyme site BglII overhang at 5' and XhoI at 3' for further cloning into pQsupR plasmid. Detailed sequence of shRNA targeting *Ikzf1* and *H2afz* was listed in Table I.1.

2.2.2 shRNA cloning

All enzymes used for cloning were purchased from New England Labs.

The pQsupR control plasmid and the plasmids with shRNA inserts targeting Mi-2β or Brg1/Brm were generated by Dr Stephen Smale's lab, UCLA (Ramirez-Carrozzi et al., 2006), and were purchased from Addgene.

The pQsupR plasmid was also used for the house designed shRNA cloning. shRNA cloning protocol was obtained from Dr Jesus Gil's lab, MRC CSC, with kind help from Dr Selina Raguz. To clone the shRNA into the retroviral plasmid, the pQsupR control plasmid (1µg) was first digested with BglII/XhoI, and linearized plasmid backbone was purified from 1% agarose gel using QIAquick gel extraction kit (Qiagen). To prepare shRNA insert, the forward and reverse shRNA oligos were ordered from Sigma, and resuspended in sterile water at 100µM. The forward and reverse oligos were then annealed by combining 2.5µl of each oligos with 95µl of 1× ligation buffer (from T4 DNA ligase kit), heating at 100 °C for 30s, and cooling down at room temperature. 1µl of annealed shRNA and 1µl of purified pQsupR backbone were ligated using 1µl (400U) of T4 DNA ligase at room temperature for 2 hours. Ligation background control was included by performing same ligation procedure but adding 1µl of H_2O instead of shRNA insert.

2.2.3 Inducible Ikaros vector from IRES-GFP to IRES-mCherry

The inducible Ikaros plasmid designed by previous PhD student, Ben Taylor, was in a MSCV (murine stem cell virus) retroviral plasmid containing IRES-GFP (IRES stands for internal

ribosome entry site) (more details in section 3.1). To change IRES-GFP to IRES-mCherry, the sequences of IRES and mCherry were amplified using Phusion high fidelity DNA polymerase from pMIG plasmid (MSCV vector containing IRES-GFP) and fluorescent reporter vector (from Rory Blevins, a previous PhD student in the lab), respectively. Primers used for amplification contains either appropriate restriction enzyme sites or complimentary sequence allowing to join cDNA fragments by PCR sewing (Table I.2). Both joint IRES-mCherry cDNA and inducible Ikaros MSCV plasmid with IRES-GFP were digested with EcoRI/SalI, purified and ligated as described before, generating inducible Ikaros MSCV plasmid with IRES-mCherry. Inducible control plasmid with IRES-mCherry was produced in parallel.

2.2.4 Bacteria transformation and plasmid DNA isolation

Ligation products were delivered into competent DH5α *E.coli*. To do so, 5µl of ligation product was mixed with 20µl of 5× KCM buffer (0.5M KCl, 0.15M $CaCl_2$, 0.25M $MgCl_2$), and topped up to 100µl with H_2O. The 100µl mixture was then combined with 100µl DH5α bacteria. The bacteria mix was kept on ice for 20 minutes and room temperature for 10 minutes, before plating onto lysogeny broth (LB) agar plates supplemented with 50µl/ml ampicillin and incubating at 37 °C overnight. Individual colonies were picked and grew in 3ml of LB supplemented with ampicillin. Minipreps of individual colonies were screened by appropriate restriction enzyme digestion and subsequently DNA sequencing by MRC genomics facility. Selected colonies were then inoculated and plasmids were isolated using maxipreps kit (Qiagen).

2.3 Transfection and infection

2.3.1 Transfection and virus collection

The viral packaging genes *gag* and *pol* are stably integrated in the 293T fibroblast packing cell line.

The MSCV retroviral particles for inducible Ikaros were produced by 293T fibroblasts using calcium phosphate transfection protocol as previous described (Cobb et al., 2000). In brief, the 293T fibroblasts were cultured in 10cm dish to around 40% confluence in 9ml medium. The formation of DNA-containing precipitates was produced by adding 500µl of 2× HEBS (12mM Dextrose, 50mM HEPES, 10mM KCl, 280mM NaCl, 1.5mM $Na_2HPO_4 \cdot 2H_2O$ in sterile water, pH7.05) drop by drop to 500µl of 0.4M $CaCl_2$ solution with 4µg of MSCV plasmid DNA and 4µg of pCL-Eco envelop helper plasmid DNA. The transfection solution containing DNA precipitates were then added to the cells drop by drop. Fresh medium was then fed to the cells after 12 hours and 24 hours of transfection. Supernatant of 3.5ml containing retroviral particles were collected after 36 hours, 48 hours and 60 hours of transfection, and pooled for infection.

The pQsupR retroviral particles for shRNA were produced by 293T fibroblasts using Lipofectamine 2000 (Invitrogen) as described in the standard Invitrogen protocol (http://tools.lifetechnologies.com/content/sfs/manuals/Lipofectamine_2000_Reag_protocol.pdf). In brief, the 293T fibroblasts were cultured in 10cm dish to around 90% confluence in 12ml medium. The transfection solution was generated by combining 1.5ml Opti-MEM (Invitrogen) medium containing 60µl Lipofectamine 2000 with another 1.5ml Opti-MEM medium containing 16µg of pQsupR plasmid DNA and 16µg of pCL-10A1 helper envelop plasmid DNA. The combined solution was kept at room temperature for 20 minutes before adding to the cells drop by drop. The transfection solution was kept with the cells for 12 hours and fresh medium was fed to the cells after 12 hours and 24 hours. Supernatant containing retroviral particles were collected after 36 hours, 48 hours and 60 hours of transfection, and pooled for infection.

2.3.2 Infection

Lymphocytes, including B3 pre-B cells and JE131 thymocytes, were infected in 6-well plates. 2×10^6 cells were plated with 3ml of retroviral supernatant, supplemented with 10mM pH 7.6 HEPES and 4µg/ml polybrene (Sigma-Aldrich). The spin infection was then performed at 2500rpm for 1.5 hours in 37°C. For infection with shRNA retrovirus, the cells were further kept with the virus in the incubator for 3 hours after spin infection. At last, the infected cells were fed with fresh medium.

To infect fibroblasts, the cells were cultured in 10cm dish to 60% confluence. The cells were then maintained in 4ml of viral supernatant supplemented with 10mM pH 7.6 HEPES and 4μg/ml polybrene (Sigma-Aldrich) for 6 hours in the incubator before changing to fresh medium.

2.4 Ikaros induction

Ectopic inducible Ikaros was induced from cytoplasm to the nucleus by adding 0.5μM 4-hydroxytamoxifen (4OHT, Sigma-Aldrich). Since *Myc* (an Ikaros target gene of interest and a key player in transcription) can be up-regulated by ethanol (EtOH), the carrier for 4OHT (Leach et al., 1999; Nakahara et al., 2003; Paice et al., 2002; Yagle and Costa, 1999), to reduce concentration of ethanol during treatment, 4OHT was resuspended at 20mM in 95% EtOH as stock. To perform time course study, Ikaros was induced for different time prior to sample collection, and processed at the same time for downstream analyses.

2.5 Fluorescent activated cell sorting (FACS)

2.5.1 Cell sorting

Cellular fluorescent level was assessed using BD LSRII or FACSCalibur flow cytometer, and cell sorting was performed on BD FACSAria II or III cell sorter. To sort, cells were pelleted and resuspended in sorting buffer [10% (v/v) FCS in PBS-/- (PBS stands for phosphate-buffered saline)] at around 10×10^6 cells/ml, and passed through cell-strainer cap into 12x75mm polypropylene tubes to further remove cell lumps. Samples were then submitted to MRC flow cytometry facility to sort for cells expressing specific window of fluorescent proteins (GFP or mCherry).

2.5.2 Cell cycle analysis by propidium iodide (PI) staining

Cells were washed once with cold PBS-/-. 0.5×10^6 cells were resuspended in 300μl of propodium iodide (PI) staining buffer [PBS-/- supplemented with 50μg/ml propidium iodide (Sigma-Aldrich), 10μg/ml RNase A (Life Technologies, NY, USA), and 0.05% v/v NP40

(Calbiochem, Merck Millipore)], and incubated on ice for 30 minutes. PI profile was analysed using a BD LSRII flow cytometer. Live cells were identified using forward scatter (FSC) and side scatter (SSC) profiles, and doublets were discriminated using FSC-W/FSC-A gating. Data were analysed using FlowJo software.

2.6 Immunofluorescence (IF)

Fibroblasts were cultured in 6-well plates with sterile coverslips at the bottom. Suspension cells after required treatment were plated into 12-well plates with poly-L-lysine coated coverslips (BioCoat) for 10 minutes at the bottom. Coverslips were then washed with PBS and fixed with 4% paraformaldehyde (PFA) in PBS for 10 minutes at room temperature. Fixed samples were washed in PBS, and were permeabilised with 0.5% Triton X-100 for 5 minutes. Samples were subsequently incubated in blocking solution [3% normal goat serum (Vector), 0.1% Triton X-100 in PBS] for 30 minutes at room temperature in a humid chamber. Primary antibody was diluted 1:1000 in blocking solution (Table I.3), and added to the samples for 1 hour at room temperature or incubated overnight at 4 °C in a humid chamber. Coverslips were washed 3 times in PBS and incubated with secondary antibodies coupled with appropriate fluorophores (Molecular Probes) that were diluted in blocking solution for 1 hour at room temperature in a dark humid chamber. Cells were then washed 3 times in PBS and mounted in Vecatshield (Vector Laboratories) with DAPI (0.1µg/ml).

Samples were visualised using a TCS SP5 Leica laser scanning confocal microscope. Microscope settings and laser power were kept constant among samples. Images were processed using Leica Confocal software and Adobe Photoshop CS5.

2.7 Western blot

2.7.1 Protein quantification

Cells were pelleted and washed once in cold PBS supplemented with protease inhibitor cocktail (Roche). Cell pellet was then resuspended in 1 volume of cold PBS, topped with 1 volume of 2× sample buffer [100mM Tris (pH 6.8), 20% glycerol, 2% sodium dodecyl sulphate (SDS)] at the concentration of 1×10^6 cells in total volume of 100µl. Samples were

incubated at 95 °C for 10 minutes. Protein concentration was measured using the Pierce™ BCA Protein Assay Kit (Thermo Scientific) according to manufacturer's instructions. After quantification, 10% (v/v) β-mercaptoethanol and 0.002% bromophenol blue were added to protein samples, and kept at -20°C.

Otherwise, if protein quantification was not required, after washing with PBS, 1×10^6 cells was resuspended in 50µl PBS and topped with 50µl 2× sample buffer containing β-mercaptoethanol and bromophenol blue, and incubated at 95 °C for 10 minutes.

2.7.2 Cell fractionation

To fractionate the B3 cells to cytoplasmic fraction and nuclear fraction, cells were first washed once with cold PBS supplemented with protease inhibitor cocktail. Cells were resuspended in cold cell lysis buffer [10mM HEPES (pH 7.9), 10mM KCl, 1.5mM $MgCl_2$, 0.34mM sucrose, 10% glycerol, 1mM DTT, 0.1% Triton X] at 1×10^6 cells/20µl, and lysed on ice for 5 minutes. Sample was then span down at 1300 rcf for 5 minutes at 4°C. Supernatant was collected and used as cytoplasmic fraction after removing debris by centrifuging at 25000 rcf for 10 minutes in 4°C. The pellet was washed once with cold cell lysis buffer without Triton X before lysed with nuclear lysis buffer (3mM EDTA, 0.2mM EGTA, 1mM DTT) 1×10^6 cells/20µl for 30 minutes on ice, and used as nuclear fraction. 1 volume of 2× sample buffer [100mM Tris (pH 6.8), 20% glycerol, 2% sodium dodecyl sulphate (SDS), 10% (v/v) β-mercaptoethanol, 0.002% bromophenol blue] was added to both cytoplasmic and nuclear fractions and boiled at 95°C for 10 minutes. The nuclear fraction was further sonicated at high speed for 3 cycles of 15s on/off. To load on gel, same volume of each fraction was loaded.

2.7.3 Western blotting

The quantity of protein loading varies depending on protein of interest. Together with dilution of primary and secondary antibody, information can be found in Table I.3.

Proteins, together with the Benchmark pre-stained protein ladder (Invitrogen) as size reference, were loaded on a SDS-polyacrylamide gel, consisting 4 % stacking gel [4% (w/v)

acrylamide, 125mM Tris-HCl (pH 6.8), 0.1% SDS, 0.067% ammonium persulphate (APS), 0.12% N,N,N'-tetramethylethylenediamine (TEMED)] and a 10 % acrylamide resolving gel [10 % acrylamide, 390 mM Tris-HCl (pH 8.8), 0.1 % SDS, 0.05 % APS, 0.1 % TEMED]. For large proteins, such as Rbp1, Chd4, Brg1 and Brm, 4–15% precast polyacrylamide gel (Bio-Rad) was used. Proteins were separated by running the gel in running buffer (25mM Tris base, 192mM glycine, 0.1% SDS)), using Bio-Rad minigel system for 1-1.5 hours at 30mA per gel. Proteins were transferred to a Protan nitrocellulose transfer membrane (Schleicher & Schuell Bioscience) using the Trans-Blot® SD Semi-Dry Transfer Cell (BioRad) in transfer buffer [48mM Trizma base, 39mM glycine, 0.037% (w/v) SDS and 20% v/v methanol]. The transfer was performed for 1.5 hours at 140mA/25v/gel. The membrane was then incubated for half an hour in blocking buffer [5% (w/v) fat free milk powder (Marvel), 1.2g/L Tris (pH 7.4), 8.75g/L NaCl] followed by incubation with the primary antibody (diluted in blocking buffer) for 1 hour at room temperature or at 4°C overnight with agitation. Membranes were then washed three times for ten minutes in wash buffer [1.2g/L Tris (pH 7.4), 8.75g/L NaCl] before incubation with horseradish peroxidise-coupled secondary antibodies (α-rabbit and α-mouse antibodies were purchased from Amersham and used at 1:5000 dilution in blocking buffer) for 1h at room temperature. After washes of secondary antibody, detection was done using the Luminata Crescendo Western HRP Substrate (Millipore) following manufacturer's instructions with Kodak X-Omat photographic films.

2.8 Gene expression quantification

2.8.1 RNA extraction and reverse transcription

RNA extraction was performed using the QIAshredder and RNeasy Mini kits (Qiagen). Residual DNA was eliminated using DNA-free kit (Ambion), according to manufacturer's instructions.

Reverse transcription was performed using Superscript First-Strand Synthesis system (Invitrogen). In brief, 500ng of total RNA was combined with 1µl of 10mM dNTP mix and 1µl of 0.25µg/µl random primers, topped up to 11µl with RNase-free H_2O. The mix was incubated at 65°C for 5 minutes and left on ice for 1 minute before adding 1µl of 0.1M DTT, 4µl of 5× first strand buffer, 1µl of RNaseOUT and 1µl of 200U/µl Superscirpt III reverse

transcriptase. The reaction mixture was then incubated at 25°C for 5 minutes, at 50°C for 1 hour, and at 75°C for 15 minutes. cDNA was then diluted 10× before analysed using real-time quantitative PCR (RT-qPCR).

2.8.2 Real-time quantitative PCR (RT-qPCR)

Primers used for RT-qPCR analysis were listed in Table I.4 and I.5.

To design primers, reference sequence was obtained from UCSC genome browser. Primers were designed using Primer3 (http://frodo.wi.mit.edu/primer3/), and screened for off-targets using UCSC in silico PCR tools. The amplification efficiency and linearity of each primer pair was determined using sequential 2-fold dilutions genomic DNA (for testing of qPCR primers for nascent mRNA and ChIP). Primers presenting good linear fits of the C(t) versus logarithm of the genomic DNA concentration (R2>0.99) and amplification efficiencies within the range of 1.8 – 2.2 were selected.

A reaction mix was composed of 2X SYBR Green qPCR mastermix (Qiagen), 0.3mM primers, and 1-2µl of cDNA or ChIPed DNA in a final volume of 12µl. RT-qPCR was performed using the following program: reaction was activated by incubating at 95°C for 15 minutes, then a cycle of denaturising at 94°C for 15 seconds, annealing at 60°C for 30 seconds, and elongating at 72°C for 30 seconds was repeated 40 times. Fluorescence was read at 72°C, 75°C, 78°C and 83°C. The melting curve was determined from 72-90°C at 0.2°C intervals. qPCR quantification was performed using a Chromo4 Opticon or a Bio-Rad CFX96 Real-Time qPCR machine, and was analysed using Opticon Monitor 3 Software or CFX96 Manager Software, respectively. Relative abundance of detected sequences was calculated using the ΔΔC(t) method (Pfaffl, 2001). In brief, C(t) is the number of amplification cycles after which fluorescence of PCR products can be detected above background. Suppose qPCR products are amplified exponentially, i.e. amplification efficiency is close to 2, the relative abundance of the gene or region of interest (C(t)1) compared to a control (C(t)2) can be calculated as $2^{-\Delta C(t)1}/2^{-\Delta C(t)2}$. For gene expression, housekeeping genes were used for normalisation. ChIP-qPCR analysis follows the same principle but normalization was different and was discussed in relevant context.

2.9 Micrococcal nuclease (MNase) assay

2.9.1 MNase digestion

30×10^6 cells were collected in 18ml of complete medium and cross-linked in 1% formaldehyde by adding 2ml of fixation buffer (0.5mM EGTA pH 8.0, 100mM NaCl, 1mM EDTA, 50mM HEPES pH 8.0, 10% Formaldehyde in sterile H_2O). Cells were incubated for 10 minutes at room temperature on a rotating platform, and fixation was stopped by adding glycin to the final concentration of 140mM. Fixed cells were then centrifuged at 4°C for 5 minutes at 1700rpm, and washed twice with cold PBS. Cell pellet was then resuspended in 0.5ml of cell lysis buffer (5mM PIPES pH 8.0, 85mM KCl, 0.5% NP-40 in sterile H_2O) supplemented with protease inhibitor cocktail (Roche), 0.15mM Spermine (Sigma), and 0.5mM Spermidine (Sigma), and lysed on ice for 20 minutes. Sample was then pelleted at 4°C for 10 minutes at 900 rcf, and washed once in 1ml of cold MNase $CaCl_2$- buffer (10mM Tris-HCl, pH 7.4, 15mM NaCl, 60mM KCl) supplemented with 0.15mM Spermine and 0.5mM Spermidine. Sample was then resuspended in MNase $CaCl_2$+ buffer (10mM Tris-HCl, pH 7.4, 15mM NaCl, 60mM KCl, 1mM $CaCl_2$) supplemented with 0.15mM Spermine and 0.5mM Spermidine at 2×10^6 cells in 100µl, and digested with MNase (Roche) at 200U/ml in room temperature for 10 minutes. Digestion was stopped by adding 20µl/2×10^6 cells of stop buffer (100mM EDTA, 10mM EGTA). As undigested control, 2×10^6 cells were treated in parallel without adding MNase.

To map nucleosome positioning, 120µl of digested or undigested control chromatin was supplemented with 80µl MNase $CaCl_2$- buffer, 1% SDS, 50µg/ml proteinase K, and 100µg/ml RNase A, and incubated at 37°C for 2 hours and 65°C overnight. DNA was extracted with using a phenol/chloroform protocol, and precipitated with ethanol and sodium acetate (pH 5.2). Precipitated DNA was washed once in cold 70% ethanol, and dried pellet was resuspended in 50µl sterile H_2O. To check the efficiency of digestion, 10µl of digested and undigested DNA were analysed using agarose gel electrophoresis. Afterwards, DNA was subject to quantification using pigogreen before analysis by RT-qPCR or sequencing.

To use MNase digested chromatin for chromatin immunoprecipitation (ChIP), after digestion, chromatin was supplemented with protease inhibitor cocktail and sonicated for 4 minutes at 4°C with 30 seconds on, and 30 seconds off using a Bioruptor® (Diagenode). Un-sonicated

chromatin and debris were span down at 25000rcf for 15 minutes at 4°C and supernatant was taken for IP. Before IP, chromatin was supplemented with 0.1% SDS, 0.1% sodium deoxycholate, and 1% Triton X-100.

2.9.2 Picogreen quantification

PicoGreen® dsDNA quantitation assay kit was purchased from Life Technologies. As an ultrasensitive nucleic acid stain, it has the advantage of detecting as little as 25 pg/ml of dsDNA in the presence of ssDNA, RNA, and free nucleotides. Quantification was carried out according to the manufacturer's instructions. Particularly, for MNase assay DNA quantification, standard curve was made from a maximum of 100ng DNA 6 sequential 2-fold dilutions, and 1µl of extracted DNA was used in the assay. Fluorescence was read by Bio-rad CFX96 RT-qPCR machine. After quantification, DNA was diluted to 2ng/µl, and 1µl was used per qPCR reaction.

2.10 Chromatin immunoprecipitation (ChIP)

2.10.1 Histone and histone modification ChIP

Chromatin for histone and histone modification ChIP was fragmented by MNase digestion as described in section 2.8.1. For all IPs, 10µl of Dynabeads® Protein A or G (Life Technologies) was first washed twice with cold RIPA standard buffer (140mM NaCl, 10mM Tris-HCl pH 7.5, 1mM EDTA pH 8.0, 0.5mM EGTA pH 8.0, 1% Triton X-100, 0.1% SDS, 0.1% sodium deoxycholate), and incubated with antibody of interest for 3 hours at 4°C on a rotating platform. Antibodies used and antibody to beads ratios were specified in table I.3. Saturated antibody was washed away by RIPA standard buffer on a magnetic stand before incubating beads/antibody with chromatin overnight at 4°C. For each histone and histone modification IP, 50µl chromatin was combined with 150µl RIPA standard buffer and was added to beads/antibody in 300µl tube stripes. For histone acetylation ChIP, 5mM sodium butyrate (inhibitor for HDAC class I and II) and 10mM nicotinamide (inhibitor for HDAC class III) were supplemented to the chromatin on top of protease inhibitor cocktail. Unbound

chromatin and non-specific binding was washed away sequentially by RIPA standard buffer, RIPA high salt buffer (500mM NaCl, 10mM Tris-HCl pH 7.5, 1mM EDTA pH 8.0, 0.5mM EGTA pH 8.0, 1% Triton X-100, 0.1% SDS, 0.1% sodium deoxycholate), RIPA LiCl buffer (250mM LiCl, 10mM Tris-HCl pH 7.5, 1mM EDTA pH 8.0, 0.5mM EGTA pH 8.0, 1% Triton X-100, 0.1% SDS, 0.1% sodium deoxycholate), and TE buffer (10mM Tris-HCl, 1mM EDTA, pH 7.5). Washed beads were resuspended in 200µl of histone ChIP elution buffer (25mM Tris, 1mM EDTA, pH 9.2) with 100µg/ml Proteinase K and 100µg/ml RNase A, and incubated in PCR machine at 37°C for 30 minutes, 65°C for 6 hours and 95°C for 10 minutes. For qPCR analysis, 5µl of supernatant was used per reaction in a total volume of 30µl.

2.10.2 RNAPII ChIP

RNAPII ChIP protocol from Dr Ana Pombo's lab, MDC Germany, was used with adjustment (http://www.epigenesys.eu/images/stories/protocols/pdf/20111121162410_p48.pdf). Briefly, cells were fixed and washed as described in MNase assay. Fixed cells were then lysed in swelling buffer (25mM HEPES, 1.5mM MgCl2, 10mM KCl, 0.1% NP-40, pH 7.9) at 50×10^6 cells/ml on ice for 15 minutes. Lysed cells were centrifuged at 900 rcf for 10 minutes at 4°C and resuspended in sonication buffer (140mM NaCl, 50mM HEPES, 1mM EDTA, 1% Triton X-100, 0.1% SDS, 0.1% sodium deoxycholate, pH 7.9) at 50×10^6 cells/ml. Fragmentation of chromatin was done by sonication at high speed for 25 minutes at 4°C with 30 seconds on, and 30 seconds off using a Bioruptor® (Diagenode). Un-sonicated chromatin and debris were span down at 25000rcf for 15 minutes at 4°C and supernatant was taken for IP. Chromatin was quantified by doing 10-fold dilution in 0.1M NaOH and measured by nanodrop. 140µg chromatin was used per IP. IP incubation was done as described for histone ChIP. Unbound chromatin and non-specific binding was washed away sequentially by sonication buffer, wash buffer A (500mM NaCl, 50mM HEPES, 1mM EDTA, 1% Triton X-100, 0.1% SDS, 0.1% sodium deoxycholate, pH 7.9), wash buffer B (250mM LiCl, 50mM HEPES, 1mM EDTA, 0.5% NP-40, 0.5% sodium deoxycholate, pH 8.0), and TE buffer (10mM Tris-HCl, 1mM EDTA, pH 7.5). Washed beads were resuspended in 300µl of elution buffer (50mM Tris, 1mM EDTA) with 1% SDS, 50µg/ml Proteinase K and 100µg/ml RNase A, and incubated at 37°C for 2 hours, 65°C overnight with agitation. DNA was extracted using a pheonol/chloroform protocol and precipitated with ethanol and sodium acetate. For qPCR analysis, 1µl out of 50µl was used per reaction in a total volume of 12µl.

2.10.3 Ikaros ChIP

Ikaros ChIP followed the same protocol as for RNAPII ChIP, except for the preparation of chromatin. Briefly, 100×10^6 cells was washed once in PBS-/- and resuspended in 35ml PBS-/- containing 1mM Disuccinimidyl glutarate (DSG, Thermo Scientific), and incubated on a rotating platform for 30 minutes at room temperature. Cells were then washed and resuspended in PBS, and fixed again with 1% formaldehyde as described in section 2.8.1. After cell lysis as described, pellet was resuspended in nuclear lysis buffer (50mM Tris-HCl pH 8.1, 10mM EDTA pH 8.0, 0.5% SDS) and incubated on ice for 5 minutes before sonication for 15 minutes. 50µg chromatin was used per IP.

2.11 Sequencing library preparation

MNase assay and ChIP DNA sequencing libraries were prepared using NEBNext Ultra™ DNA Library Prep Kit for Illumina according to manufacturer's instructions. Particularly, 50ng DNA from MNase assay and 10ng DNA from ChIP or input were used to prepare the library, and during PCR amplification step, 10 and 14 cycles were used, respectively. No size-selection step was performed for MNase DNA sequencing libraries, and a size-selection of 200-400bp after PCR amplification was performed for ChIP library. The libraries were differentially indexed for multiplexing during sequencing.Library quality was checked on a DNA high sensitivity chip using bioanalyser at MRC genomics centre. Sequencing was performed on Illumina high-throughput sequencer at MRC genomics centre.

2.12 Bioinformatics analysis

2.12.1 Reference data and Gene Annotation

All genome sequences, their respective indices and gene annotations used were downloaded for the NCBI37 Mouse genome build from Illumina IGenomes repositories. (http://support.illumina.com/sequencing/sequencing_software/igenome.html)

2.12.2 Sequencing alignment

Single-end and paired-end sequences for RNAPII and MNase digested data respectively were aligned using BWA version 0.7.4 and SAM files generated using the relevant single or paired-end modes. Following sequence alignment, SAM files were sorted and indexed using samtools version 0.1.18 to created indexed BAM files. The quality of all datasets and predicted fragment lengths for single end data were analysed using ChIPQC Bioconductor package. Coverage files in the form of normalised BigWigs were generated for polymerase II data using rtracklayer package with coverage depth normalised to total reads outside of known mm9 blacklists. To calculate normalised coverage per base for MNase data, paired-end reads were first reconstructed into complete fragments in silico and coverage calculated from these fragments normalised to total reads outside of mm9 blacklisted regions.

Following sequence alignment and quality assessment, RNAPII counts within 500bp pstream and 50bp downstream of transcription start sites (TSSs) and in remaining genes were calculated and travelling ratios for all genes evaluated as the reads in TSS regions over those in remaining genes. Counting was performed using ChIPQC bioconductor package.

2.12.3 Coverage plots of genes

Coverage plots over genes were created using the Sogi Bioconductor package. Coverage plots of RNAPII data over genes was created using predicted fragment lengths and normalised to total reads outside mm9 blacklisted regions. Coverage plots of MNase data over genes was performed using the predicted centre of MNase fragments derived from paired-end data.

3 An inducible system to study Ikaros-mediated transcriptional regulation

3.1 Inducible Ikaros

To study the kinetics and mechanisms underlying Ikaros-mediated transcriptional regulation, our lab has devised an inducible Ikaros system. In this system, full length Ikaros (Ikaros-1) is fused with the ligand-binding domain of estrogen receptor (ERt2) at the C-terminus, and is HA-tagged at the N-terminus (Figure 3.1). This HA-Ikaros-ERt2 is cloned into a murine stem cell virus (MSCV) vector. Additionally, IRES-GFP (Internal Ribosome Entry Site, green fluorescent protein) is cloned downstream of HA-Ikaros-ERt2, so that the HA-Ikaros-ERt2 fusion protein and the GFP protein are translated from the same transcript. In this way, the GFP protein can be used as an indicator of the level of inducible Ikaros expression. The transcription of HA-Ikaros-ERt2-IRES-GFP is driven by the 5' MSCV long terminal repeat.

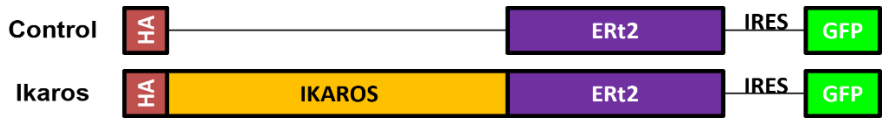

Figure 3.1 Schematic illustration of inducible Ikaros system

The illustration shows inducible control (top) and inducible Ikaros (bottom) MSCV retroviral vectors. Control vector contains HA-ERt2, while Ikaros vector contains HA-Ikaros-ERt2. Either fusion protein is translated from the same transcript as GFP.

In this study, the inducible Ikaros system was introduced to the mouse pre-B cell line B3, which was used as a model for cycling pre-B cells. To obtain this, retroviral particles carrying inducible Ikaros plasmid were produced by 293T packaging cells, and were used to infect B3 pre-B cells. To obtain a less heterogeneous infected cell population, the cells were sorted for GFP within a high and narrow GFP positive window using flow cytometry, and this level was maintained throughout this study.

After introducing to cells, HA-Ikaros-ERt2 fusion protein is constitutively expressed but tethered to heat shock proteins in the cytoplasm. Following the addition of 4-hydroxytamoxifen (4OHT), a ligand of ERt2, Ikaros fusion protein is released and led into the nucleus by its Nuclear Localization Signal (NLS). B3 cells express endogenous Ikaros, and this inducible system is designed to allow for an increase in the dosage of Ikaros in the nucleus upon induction with 4OHT. Admittedly, estrogen receptors form stable dimers upon ligand binding (Tamrazi et al., 2002); however, Ikaros dimerization or multimerization is essential for its function (Cobb et al., 2000; Trinh et al., 2001). Here, the properties of the inducible Ikaros system were well characterised.

3.2 Translocation of inducible Ikaros is fast and efficient

To test the efficiency and timing of inducible Ikaros translocation from cytoplasm to nucleus, the localisation of inducible Ikaros was monitored by immunofluorescence (IF) microscopy (Figure 3.2). Inducible Ikaros fusion protein was detected by anti-HA antibody (red), while the nucleus was marked with DAPI (blue), a fluorescent stain that binds to AT-rich regions of DNA. Without Ikaros induction (4OHT 0min), almost all of the inducible Ikaros was in the cytoplasm. As soon as 15 minutes after Ikaros induction (4OHT 15min), a proportion of inducible Ikaros was observed in the nucleus. After 2 hours of Ikaros induction (4OHT 2h), almost all the inducible Ikaros had translocated into the nucleus. It is noteworthy that inducible Ikaros formed clusters at pericentromeric heterochromatin, as previously described (Brown et al., 1997). This pericentromeric targeting of Ikaros requires its DNA binding ability (Cobb et al., 2000), and therefore showed that inducible Ikaros binds to DNA.

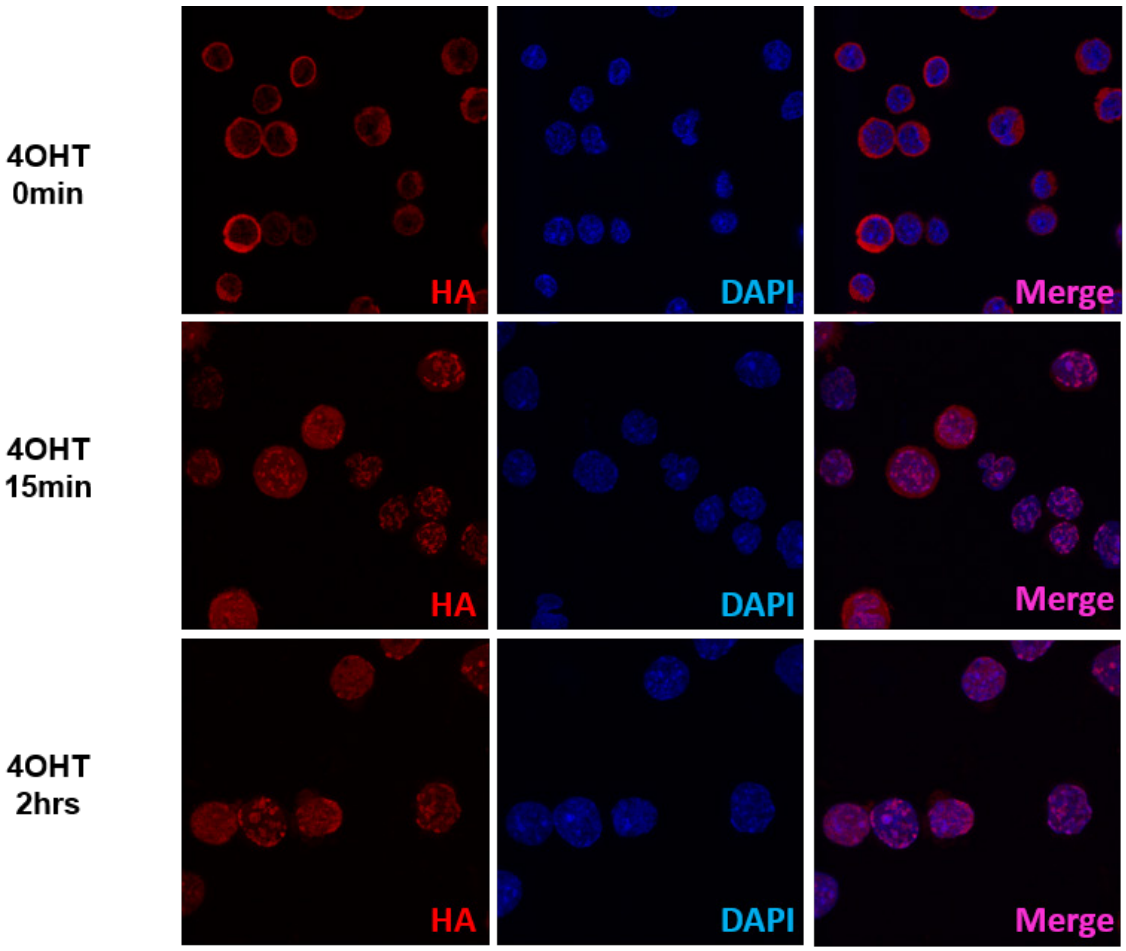

Figure 3.2 Translocation of inducible Ikaros by Immunofluorescence

Pictures show Ikaros translocation before induction (top), and 15min (middle) and 2h (bottom) after induction. Inducible Ikaros was recognized by anti-HA antibody (red) on left column, nucleus was marked by DAPI (blue) in the middle column, and the merged picture was shown on the right.

To validate Ikaros translocation, cells were lysed and fractionated into cytoplasmic and nuclear fractions, and protein extracts from each fraction were analysed by western blotting. The quality of fractionation was controlled by blotting with antibodies that recognise proteins specific for each fraction, i.e. tubulin for cytoplasm and histone H3 for nucleus (Figure 3.3). Anti-HA antibody was used to identify inducible Ikaros (Figure 3.3A). Before Ikaros induction (4OHT 0min), almost all of the inducible Ikaros was present in the cytoplasmic fraction (CYT). After 15 minutes of induction (4OHT 15min), inducible Ikaros signal in the cytoplasm (CYT) decreased and that in the nucleus (NL) increased. After 2 hours of

induction (4OHT 2h), almost all of inducible Ikaros was seen in the nuclear fraction. This was also validated with an anti-Ikaros antibody, recognising both ectopic Ikaros fusion protein (expected size ~95KDa) and endogenous Ikaros (expected size ~57KDa) (Figure 3.3A). Therefore, data from western blotting presented similar timing and efficiency of Ikaros translocation as shown by IF. Taken together, the results have shown that the translocation of inducible Ikaros from cytoplasm to nucleus is fast in its response to 4OHT induction, and is efficient in that a large proportion translocates within a short time window.

A further advantage of using anti-Ikaros antibody is to comprehend the relationship between the ectopic and endogenous Ikaros. From the loading of whole cell lysate (WCL) in the western blot (Figure 3.3A), it was observed that the level of ectopic Ikaros was comparable to endogenous Ikaros. This is important to the system since Ikaros mRNA expression mildly increases during B cell development (Ferreiros-Vidal et al., 2013; Heizmann et al., 2013; Schwickert et al., 2014), and such a dosage increase of Ikaros is able to drive the transition from cycling to resting pre-B stage (Ferreiros-Vidal et al., 2013). In this sense, the level of inducible Ikaros in B3 cells is likely to be physiological in the context of haematopoiesis. Furthermore, it is worth noting that before Ikaros induction, a small fraction of inducible Ikaros was in the nucleus, while most of the endogenous Ikaros was in the cytoplasm. After induction with 4OHT, the level of endogenous Ikaros in the nuclear fraction also increased. This could be because inducible and endogenous Ikaros interact with each other and form dimers or multimers (Sun et al., 1996), thereby reciprocally influencing the localization of each other.

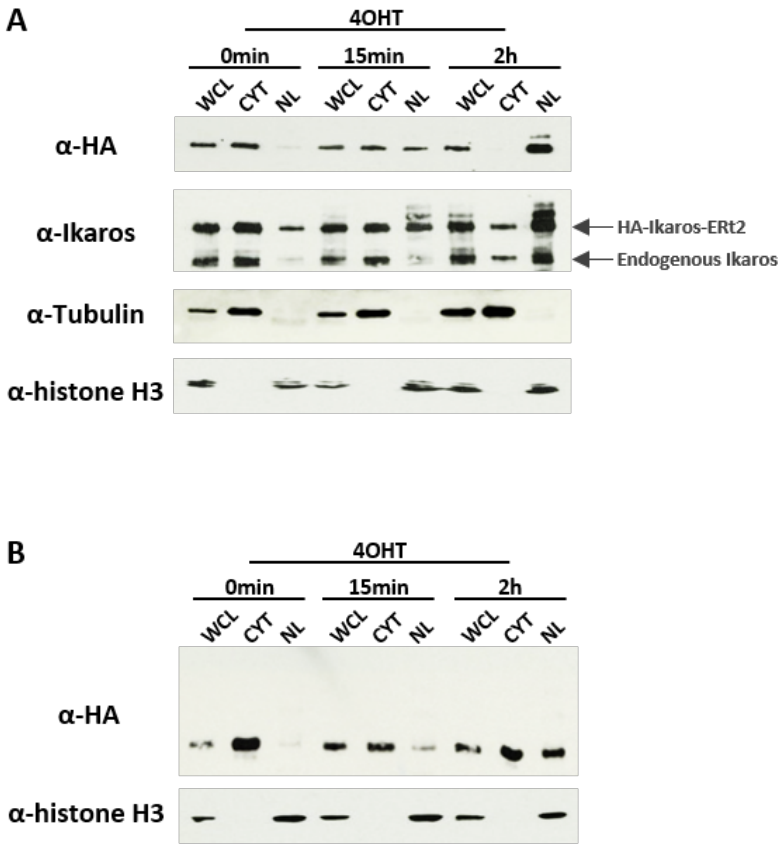

Figure 3.3 Translocation of inducible Ikaros by western blotting

B3 cells with inducible Ikaros vector (A) and with control vector (B) were lysed and fractionated into cytoplasmic and nuclear fractions, and protein extracts from whole cells lysate (WCL), cytoplasm (CYT) and nucleus (NL) were loaded in the western blot. Inducible Ikaros was detected by either anti-HA or anti-Ikaros antibodies. Anti-tubulin and anti-histone H3 were used as controls for cytoplasmic and nuclear fractions. The localization of inducible Ikaros was monitored before induction, and after 15 minutes and 2 hours of induction.

Interestingly, after Ikaros induction, both anti-HA and anti-Ikaros antibodies recognized one or two additional bands in the nuclear fractions, higher than the expected Ikaros fusion protein band, and the signals were stronger as more fusion protein translocated (Figure 3.3A). This could be due to post-translational modifications of the fusion protein after translocation into the nucleus. In this case, it is important to identify whether the modifications happened to the HA-Ikaros or the ERt2 part of the fusion protein. To this end, control cells carrying inducible control vector (HA-ERt2, Figure 3.1) were included (Figure 3.3B). After 4OHT

induction in the control cells, HA-ERt2 fusion protein travelled into the nucleus in a similar manner as inducible Ikaros. However, no extra bands were observed, indicating that translocated HA-ERt2 fusion protein was not post-translationally modified. Thus, it was more likely that inducible Ikaros was post-translationally modified after travelling into the nucleus.

3.3 Inducible Ikaros is functional

Ikaros target genes in B3 cells have been identified through an integrative analysis of ChIP-seq binding data and gene expression profiling (Ferreiros-Vidal et al., 2013). To ask whether inducible Ikaros is functional, a selection of target genes that show strong Ikaros binding and are highly responsive to Ikaros overexpression were chosen as candidate genes for this study, namely *Igll1, Myc, Ccnd2* for down-regulation, and *Lig4, Zfp36* for up-regulation.

3.3.1 Inducible Ikaros binds to Ikaros target genes

The pericentromeric clustering of inducible Ikaros suggested that inducible Ikaros binds to DNA (Figure 3.2) (Cobb et al., 2000). I first tested the ability of inducible Ikaros to bind to known Ikaros target genes. To this end, Ikaros chromatin immunoprecipitation (ChIP) was performed before or after 3 hours of Ikaros induction, followed by RT-qPCR (real-time quantitative PCR). Ikaros binding was quantified as enrichment over input, and exemplified with two target genes, down-regulated *Igll1* and up-regulated *Zfp36.* Neighbouring primers flanking expected Ikaros binding sites were used to produce high-resolution profiles of Ikaros binding (Figure 3.4). Using anti-Ikaros antibody, both endogenous and inducible Ikaros were detected. Before Ikaros induction (Ikaros-0h), at the *Igll1* locus, Ikaros binding was observed from 300bp upstream to the transcription start site (TSS) and peaked around 200bp upstream. After 3 hours of induction (Ikaros-3h), enrichment of Ikaros binding almost doubled at the pre-bound region, and also mildly extended to 100-200bp downstream of the TSS. At the *Zfp36* locus, weak but above background binding signal was observed both upstream and downstream of the TSS before induction (Ikaros-0h). After induction (Ikaros-3h), Ikaros binding was up to three times stronger, with a better defined peak shape at 300-600bp upstream and TSS-100bp downstream. Increased Ikaros binding after induction suggested

inducible Ikaros binding to target genes. The fold change in Ikaros binding after induction is not expected to be comparable among Ikaros targets, considering the differential binding affinity and local chromatin architecture for different target genes.

Inducible Ikaros binding was also confirmed using an anti-HA antibody (Figure 3.4). After 3 hours of Ikaros induction (HA-3h), Ikaros targeted sites showed strong binding of inducible Ikaros. It was worth noting that there was weak inducible Ikaros binding before induction (HA-0h). This corresponded to the leaking of the inducible Ikaros into the nucleus before induction, possibly through interactions with endogenous Ikaros, as seen in translocation data by western blotting (Figure 3.3A).

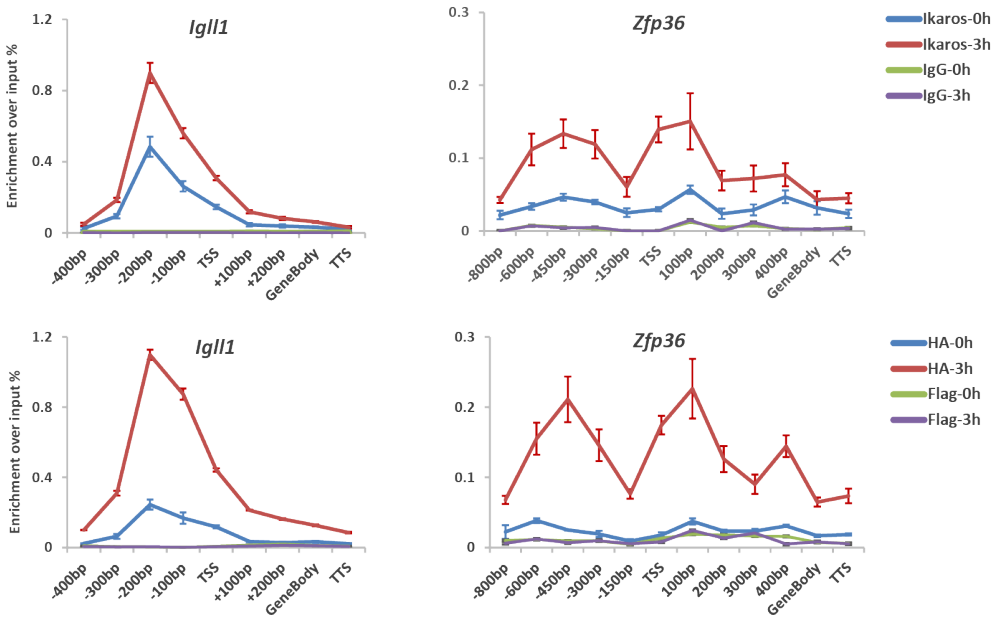

Figure 3.4 Ectopic inducible Ikaros binds to expected Ikaros binding sites

Top row shows Ikaros binding by ChIP-qPCR using α-Ikaros antibody before (blue line) and after (red) induction, and Ikaros targets *Igll1* and *Zfp36*. IgG negative controls are shown in green and purple. Bottom row shows Ikaros ChIP using α-HA antibody. Data shown is an average of three biological replicates.

3.3.2 Inducible Ikaros regulates transcription

To test the function of inducible Ikaros, the expression of selected target genes was monitored after Ikaros induction using reverse transcription and qPCR. To capture the immediate changes in transcription, intronic primers amplifying primary transcripts were used. As a carrier control, inducible Ikaros cells were treated with ethanol (EtOH) in parallel with 4OHT. To control for the effect of 4OHT, control cells carrying empty vector (Figure 3.1, 3.3B) were also treated with EtOH or 4OHT. Gene expression was normalized to stably expressed housekeeping genes *Ubc* and *Ywhaz*. No significant changes were observed in the expression of target genes under either control condition (Figure 3.5). Thus, for simplicity, only analysis for Ikaros induced conditions are shown in this study.

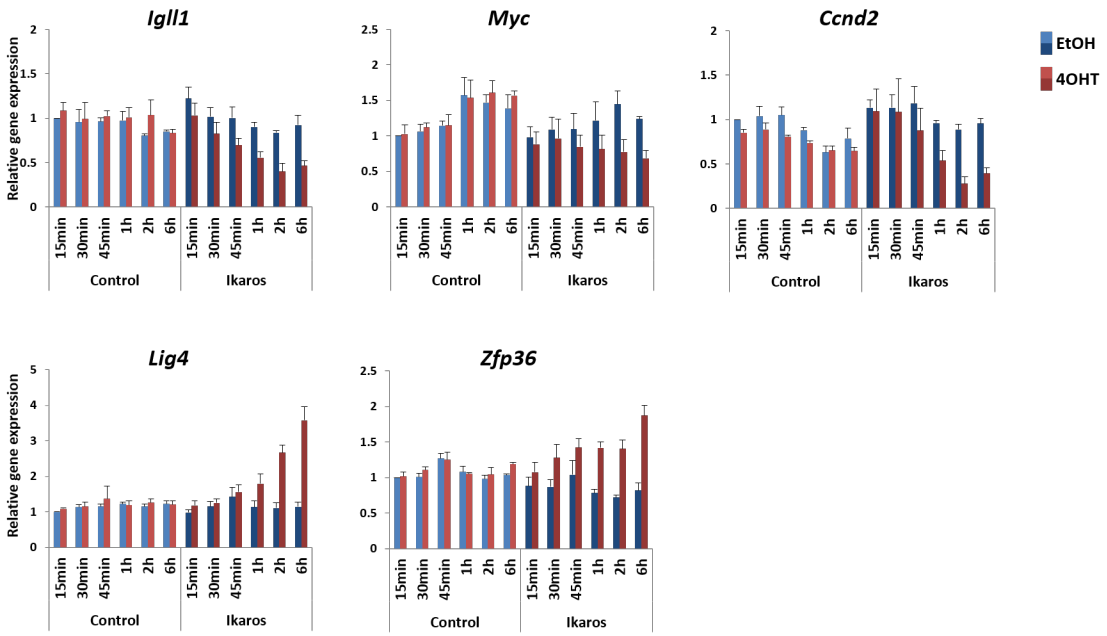

Figure 3.5 Transcriptional regulation in Ikaros induction and control conditions

Figure shows relative gene expression profiles of B3 cells with control vector and B3 cells with inducible Ikaros vector treated with EtOH as control (in blue) or 4OHT to induce Ikaros (in red), for 15min. 30min, 45min, 1h, 2h or 6h. Relative gene expression was calculated by normalizing to housekeeping genes *Ubc* and *Ywhaz*, and further normalized to control vector-EtOH-15min sample. Top row shows Ikaros down-regulated genes *Igll1*, *Myc* and *Ccnd2*, and bottom row shows Ikaros up-regulated genes *Lig4* and *Zfp36*. Only inducible Ikaros cells treated with 4OHT showed significant changes after treatment. Data shown was the average of three biological replicates.

To emphasise the trend of gene expression changes after Ikaros induction, relative expression to housekeeping genes was further normalized to the un-induced sample, taking 0min as value 1. After 5 minutes of Ikaros induction, the negatively regulated genes, *Igll1* and *Myc,* were significantly down-regulated (Figure 3.6). The expression of *Ccnd2* was significantly reduced after 15 minutes of Ikaros induction. The repression level of down-regulated genes also became progressively stronger during induction. The strongest repression of *Myc* (to ~35%) and *Ccnd2* (to ~20%) was reached within 1 hour of Ikaros induction, whilst the down-regulation of *Igll1* progressed until 6 hours after Ikaros induction. At these selected genes, different response kinetics and strength of regulation were observed. *Igll1* presented the most immediate (5 minutes) and strongest repression (to less than 5%).

The positively regulated Ikaros target genes, *Lig4* and *Zfp36*, were significantly up-regulated after 15 minutes and 5 minutes of induction, and achieved a 4-fold and a 2.5-fold of increase after 6 hours of induction, respectively (Figure 3.6).

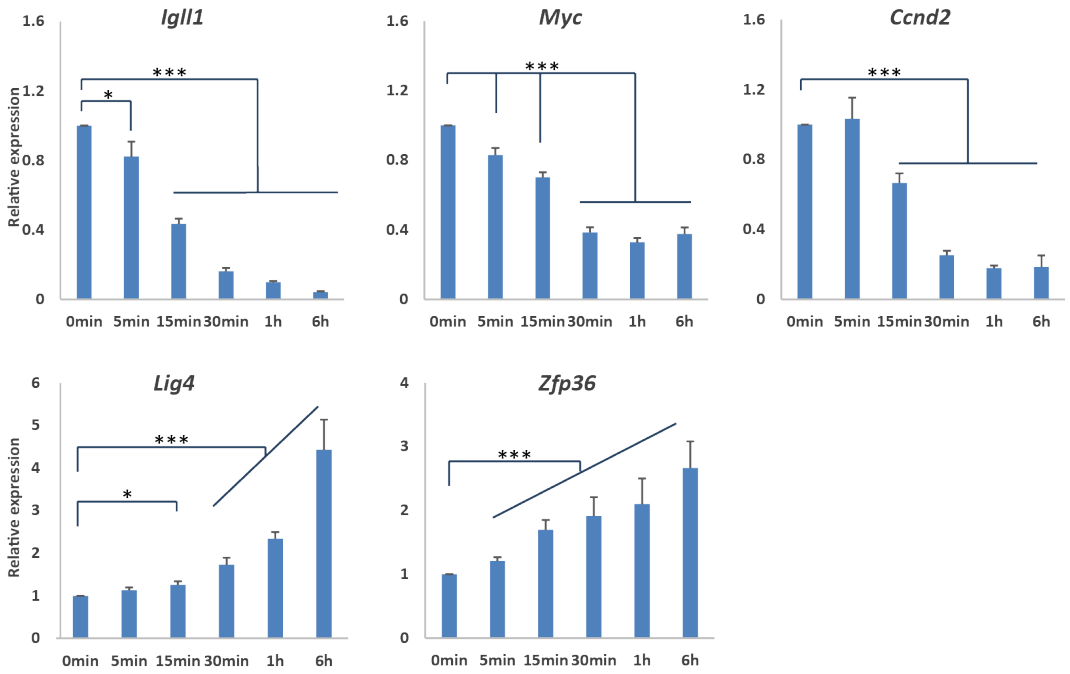

Figure 3.6 Inducible Ikaros regulates transcription of candidate target genes

Graphs show relative gene expression of candidate Ikaros target genes after 0min, 5min, 15min, 30min, 1h and 6h of Ikaros induction. Top row shows gene expression for down-regulated *Igll1*, *Myc* and *Ccnd2*, bottom row for up-regulated *Lig4* and *Zfp36*. Data shown was an average of three biological replicates. Student T-test P value: * $p<0.05$, *** $p<0.01$.

3.3.3 Inducible Ikaros results in cell cycle arrest

Finally, I tested whether Ikaros induction results in cell cycle arrest. DNA content was used as the readout for different cell cycle phases. Propidium iodide (PI), an intercalating agent and fluorescent molecule which binds to nucleic acids, was used to stain DNA in cells and was measured by flow cytometry. PI profiles and cell cycle analysis were presented after 0, 2, 6, 12 and 16 hours of Ikaros induction (Figure 3.7). Before induction, B3 cells with inducible Ikaros were cycling with a profile of 35% of G1, 46% of S and 13% of G2 phase. There were no significant differences in the cell cycle profiles after 2h, 6h or 12h of induction. Only after 16h of Ikaros induction was the cell cycle arrest observed with an accumulation of G1 stage cells up to 53% and a decrease of both S and G2 cells. Therefore, inducible Ikaros resulted in cell cycle arrest at G1 after 16 hours of induction.

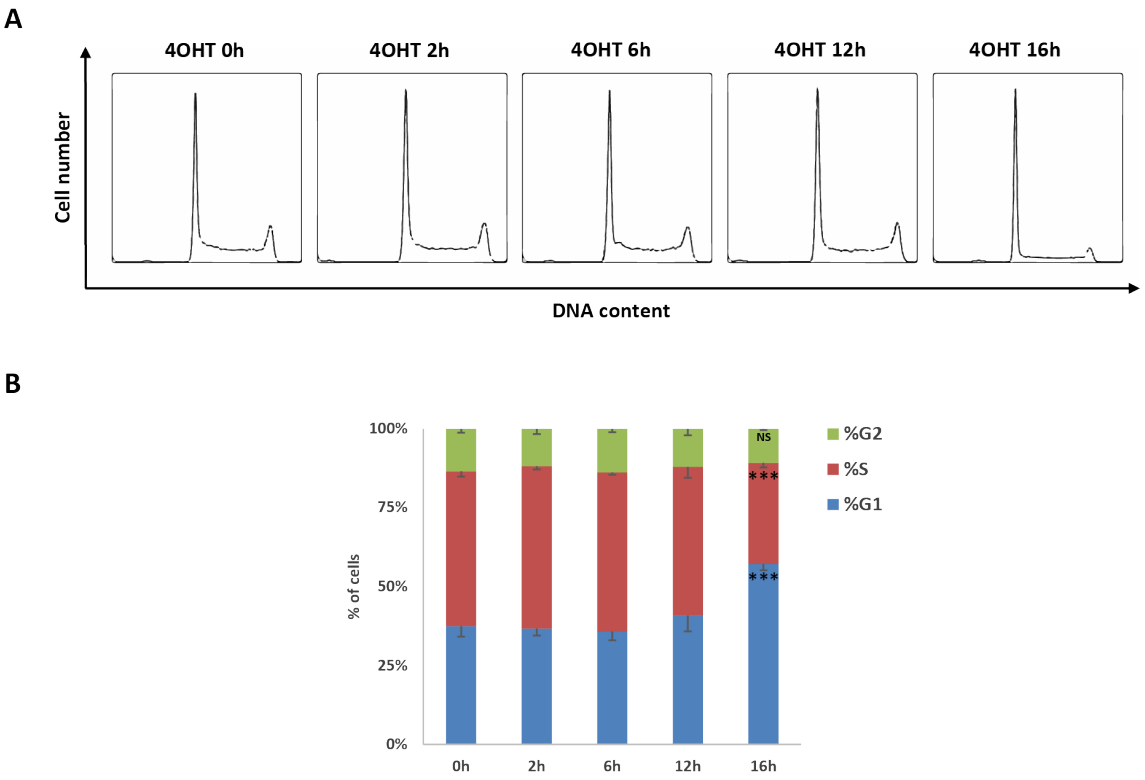

Figure 3.7 Inducible Ikaros results in cell cycle arrest

(A) shows cell cycle profiles by PI staining after 0, 2, 6, 12 and 16 hours of Ikaros induction. (B) shows quantification of cells in different cell cycle stages: blue for G1, red for S, and green for G2 phase. Data shown was an average of three biological replicates. Student T-test P value: *** $p<0.01$

3.4 Discussion

In this chapter, I have characterised the inducible Ikaros system in B3 pre-B cells. Inducible Ikaros translocation into the nucleus was observed as soon as 15min after induction by 4OHT, analysed by both IF and western blotting. This translocation was almost complete after 2 hours of Ikaros induction. Translocation of inducible Ikaros was then confirmed to lead to functional changes in the nucleus. Inducible Ikaros first bound to the binding sites of Ikaros target loci. Secondly, inducible Ikaros regulated transcription of the target genes, which consequently resulted in cell cycle arrest. Taken together, the inducible Ikaros system is not only fast and efficient, but also functional.

At the transcription level, inducible Ikaros can induce changes within minutes of induction, providing a powerful system to study the dynamics of transcriptional regulation at high temporal resolution in mammalian cells. Furthermore, this transcriptional regulation occurs long before cell cycle arrest (which occurs after 16 hours of Ikaros induction). Thus, the inducible Ikaros system is suitable to study the direct effects of Ikaros on transcription, and the kinetics of Ikaros-mediated regulatory events during transcriptional regulation.

After Ikaros induction, the regulation of gene expression was not only fast, but also became stronger with time after 4OHT treatment. The kinetics of transcriptional regulation may depend on how much and how fast ectopic Ikaros translocates. Therefore, the stability of the level of inducible Ikaros and the reproducibility of 4OHT treatment are required to compare the observations from different experiments. Hence, the expression levels of inducible Ikaros were carefully maintained according to their GFP levels, and the cells were always induced in the same way as described in materials and methods.

Ikaros can be phosphorylated (Cho et al., 2008; Gomez-del Arco et al., 2004; Gurel et al., 2008; Uckun et al., 2012) or SUMOylated (Gomez-del Arco et al., 2005), and these modifications can both positively and negatively regulate Ikaros function. To further identify the types of modifications observed (Figure 3.3) and their functional roles, more analyses need to be done. It will however not be included in this project.

4 Genome-wide profiling of Ikaros-mediated changes in chromatin status

To understand the influence of Ikaros on chromatin status, I profiled genome-wide RNAPII binding and nucleosome occupancy before and after Ikaros induction. In concert, the analysis of both RNAPII and nucleosomes allowed for the genome-wide profiling of Ikaros-mediated changes in chromatin status.

The bioinformatics analysis in this chapter was done by Dr Thomas Carroll.

4.1 Ikaros mediates changes in RNA polymerase II profiles

To ask whether Ikaros can modulate RNAPII profiles at target genes, total RNAPII density, including initiated but paused and productively elongating, was compared before and after Ikaros induction, using chromatin immunoprecipitation for RNAPII followed by high-throughput sequencing (ChIP-seq). An antibody that recognises Rbp1 N-terminus, thus the total RNAPII regardless of its phosphorylation state at the CTD, was used for ChIP.

4.1.1 Sequencing library preparation and sequencing quality

B3 pre-B cells with inducible Ikaros were treated for 6 hours with 4OHT for Ikaros induction or with ethanol treatment for the control. This time point was selected since strong changes in transcription were observed at selected target genes after 6 hours of induction (Figure 3.6) and the cell cycle was not yet affected (Figure 3.7). Fragmented chromatin was used for RNAPII ChIP, and chromatin without IP (input) was used to control for any genomic or sonication bias. DNA fragments from both IP and input were selected for sizes between 100-300bp, and the samples from two biological replicates were used to generate sequencing libraries for the Illumina HiSeq2500 sequencer. The libraries were sequenced at single-end for 50 cycles, generating 50bp reads.

Libraries were sequenced in depth, with the library of RNAPII ChIP before Ikaros induction from replicate1 (Rep1-RNAPII-0h) being the highest obtaining 81 million reads, and the library of input before Ikaros induction from replicate2 (Rep2-INPUT-0h) being the lowest obtaining 17 million reads (Table 4.1).

The first quality control step is the mapping rate. Sequencing reads were aligned to mouse genome mm9. All ChIP libraries showed high percentage of unique mapping, with similar mapping percentages of 85% ~ 94% (Table 4.1).

Table 4.1 RNAPII ChIP-seq general statistics

Libraries	Total Reads	Mapped reads	Mapped%	Duplication%
Rep1-RNAPII-0h	81,646,769	77,028,433	94%	33%
Rep1-RNAPII-6h	49,283,217	41,740,022	85%	59%
Rep1-INPUT-0h	23,241,633	15,970,663	69%	28%
Rep1-INPUT-6h	47,277,191	43,157,432	91%	22%
Rep2-RNAPII-0h	78,566,451	69,637,707	89%	52%
Rep2-RNAPII-6h	64,854,713	59,581,374	92%	32%
Rep2-INPUT-0h	17,071,938	10,701,144	63%	25%
Rep2-INPUT-6h	47,270,265	40,972,794	87%	21%

Another general quality control of sequencing is duplication rate. It is the percentage of reads with the same start and end positions (duplicates) over the total amount of reads in each library. Here, two libraries showed high duplication rates of 50% ~ 60% (Table 4.1). Duplicates exist due to various reasons. First, they come from real biological signals. For ChIP-seq, genomic regions with strong binding affinity for the protein of interest, or regions with consistent binding among the cell population, are highly enriched during IP, thereby more likely to be duplicated during sequencing. Second, sequencing saturation also leads to high duplication rate. Third, duplication can be caused by PCR amplification during library preparation. If the DNA sample used to generate a sequencing library is not complex enough, over-amplification by PCR during library preparation results in artefacts observed as duplicates. In this particular case, RNAPII often stalls at narrow promoter proximal regions, which gives a high possibility of duplication in these regions. Further, Rep1-RNAPII-6h (59%

duplication) and Rep2-RNAPII-0h (52% duplication) each obtained 50 and 80 million reads, increasing the possibility of duplication due to sequencing saturation. Admittedly, it was difficult to rule out the possibility of PCR over-amplification during library preparation. It is hard to estimate the contribution of each factor to duplication rate. However, it is suggested that one should be very cautious when removing duplicates during ChIP-seq analysis, since it more strongly removes true biological signal than background noise (Carroll et al., 2014). Removing duplicates has been tested for the analysis, but RNAPII signals at promoter proximal regions were strongly reduced (data not shown). Hence, analysis for RNAPII ChIP-seq was carried out without removing duplicates.

Rep1-RNAPII-0h showed a duplication rate of 30%, similar to Rep2-RNAPII-6h; meanwhile, Rep2-RNAPII-0h showed a similar duplication rate to Rep1-RNAPII-6h. Since biological replicates were processed at the same time during ChIP and library preparation, which made them technically very comparable, libraries were matched up according to their duplication rate across biological replicates. To compare among samples, normalised signal was obtained by scaling to sequencing depth. Normalized sequencing data was then used for downstream analyses.

4.1.2 RNA polymerase II profile and its change mediated by Ikaros

RNAPII profile

To assess the profile of RNAPII binding genome wide, I first asked if RNAPII sequencing data reflected transcriptional activity. To this end, RNAPII density of the 1000 top expressed genes was compared to the 1000 bottom expressed genes (Figure 4.1). Gene lists based on expression level were obtained from published B3 pre-B cell microarray data (Ferreiros-Vidal et al., 2013). To generate the profiles, genomic regions were segregated to 4 sections: 1) TSS, as from -30bp to +300bp relative to TSS, 2) TTS, as from -300bp to +300bp relative to TTS, 3) gene body, as the remaining part of the gene, and 4) intergenic region, as the rest of the genome (Rahl et al., 2010). Reads mapped to the gene body were normalized according to gene length. RNAPII density was then calculated using reads per million (RPM).

The RNAPII profile of top expressed genes showed a strong peak just downstream of the TSS, agreeing with the extensive promoter proximal pausing. There was higher than background RNAPII signal along the gene body, followed by a small peak just downstream of the TTS, reflecting the termination process (Figure 4.1). In contrast, the RNAPII profile of the bottom expressed genes did not show RNAPII binding at the TSS, gene body or TTS. Hence, this sequencing dataset lives up to the expected RNAPII distribution profile, and discriminates active from inactive genes.

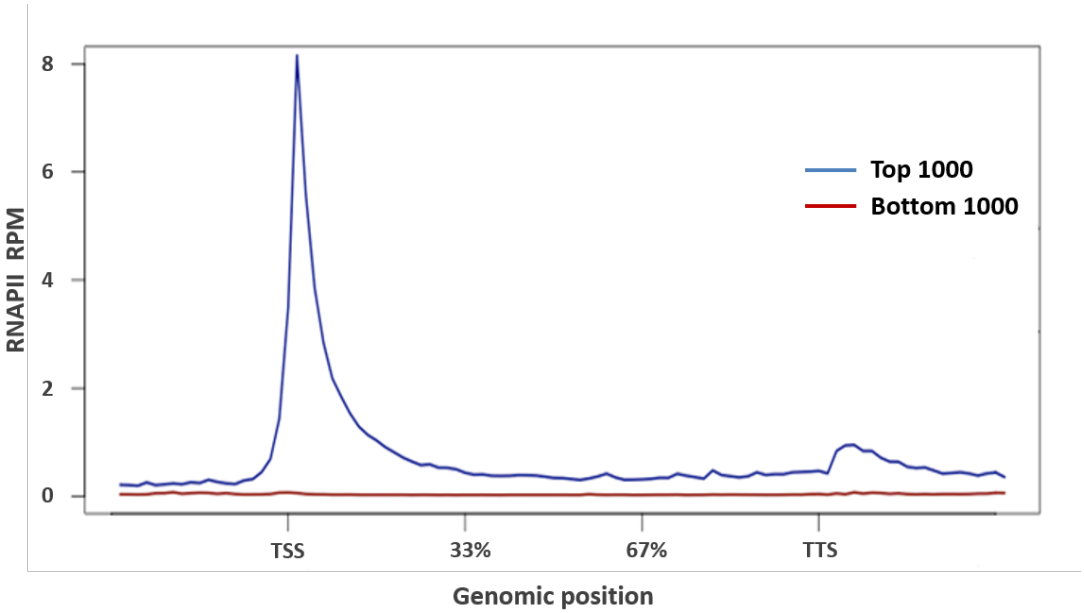

Figure 4.1 RNAPII coverage across intragenic region of active genes and inactive genes

RNAPII density calculated as reads per million (RPM) was plotted along the intragenic region, of top expressed 1000 genes (blue) and bottom expressed 1000 genes (red).

Changes in RNAPII profile mediated by Ikaros

To evaluate RNAPII profiles before and after Ikaros induction, selected target genes were first examined. At the down-regulated *Igll1*, *Myc* and *Ccnd2,* the TSSs showed strong RNAPII binding before Ikaros induction, and lower binding was observed at the gene bodies and TTSs. After Ikaros induction, the RNAPII signal was significantly decreased at the TSSs and gene bodies of these negatively regulated genes (Figure 4.2A). The changes at *Igll1* were

the most dramatic, as the RNAPII signal was almost gone after 6 hours of induction. RNAPII binding at the *Myc* locus reduced to about ½ after 6 hours of Ikaros induction, both at the TSS and the gene body. *Ccnd2* lost ¾ of RNAPII binding at the TSS and almost all at the gene body. The decreases in RNAPII binding at these down-regulated genes were to different extents. This is in agreement with the gene expression data (Figure 3.6). The up-regulated genes, *Lig4* and *Zfp36*, showed increased RNAPII binding after Ikaros induction (Figure 4.2B). This increase appeared more obvious at the TSSs. *Rex1* (*Zfp42*) and *Acta1* (encodes for α-actin) were used in this study as controls for inactive genes in B3 cells, as they are not expressed and do not contain any Ikaros binding sites within 1Mb region (Ferreiros-Vidal et al., 2013). There was no RNAPII binding observed at these inactive control loci at the same scale (Figure 4.2C). This confirmed the RNAPII profile of the bottom expressed 1000 genes (Figure 4.1). No enriched RNAPII signal was observed in input samples at any loci.

A

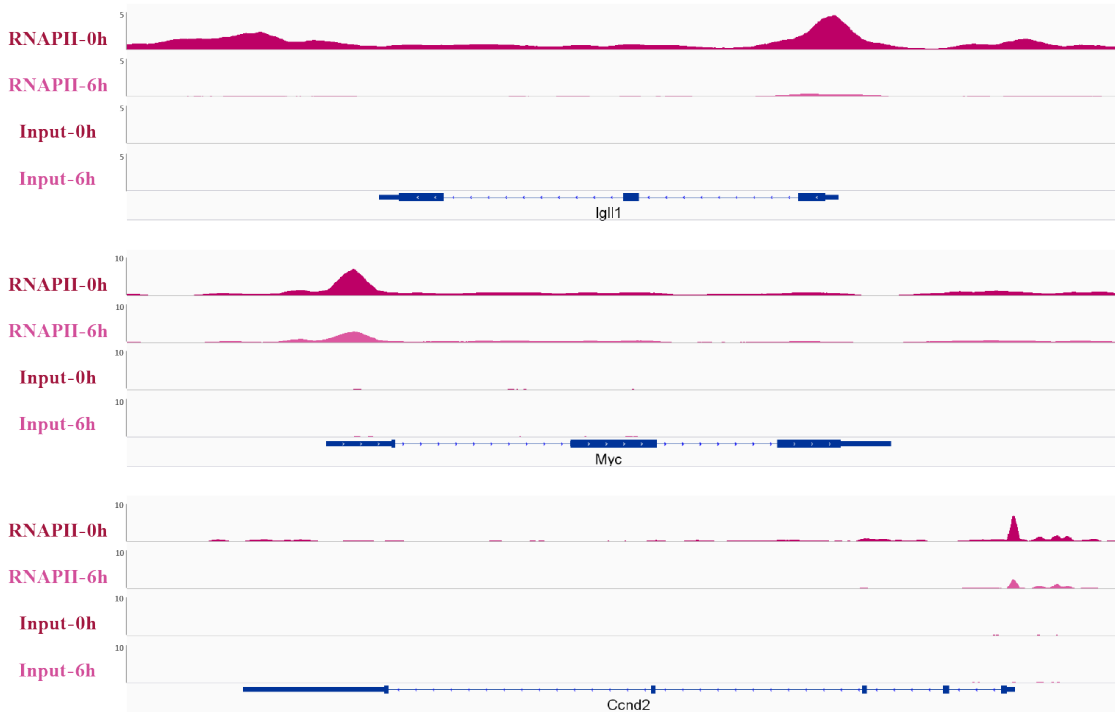

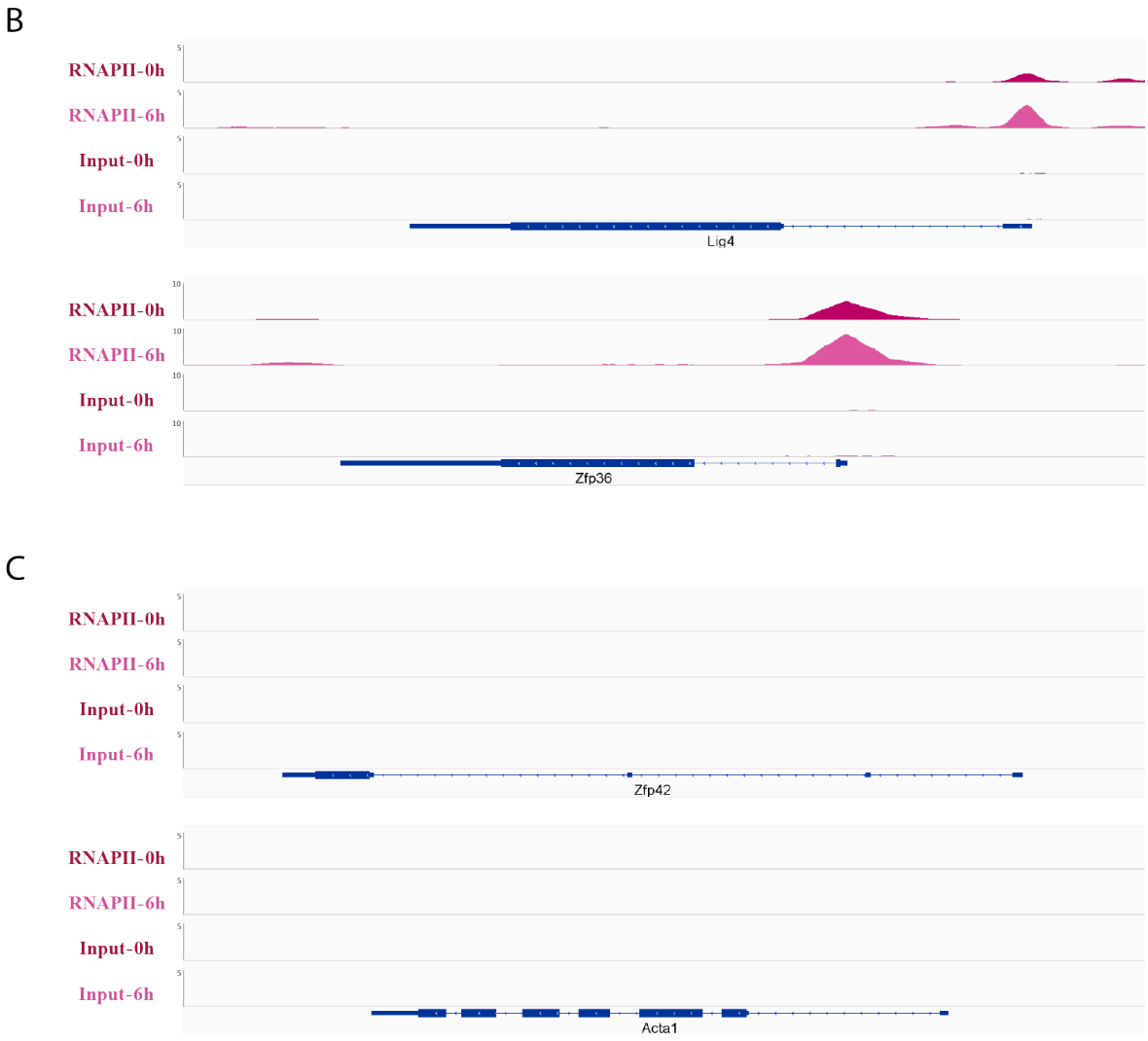

Figure 4.2 RNAPII profile changes during Ikaros induction at selected loci

RNAPII profile changes during Ikaros induction at (A) down-regulated *Igll1, Myc, Ccnd2*, (B) up-regulated *Lig4, Zfp36*, and (C) negative control *Rex1(Zfp42), Acta1*. Each picture presents coverage profiles of RNAPII-0h, RNAPII-6h, Input-0h and Input-6h at the same scale.

Next, additional Ikaros targets were examined, based on the microarray gene expression profiling data in B3 cells after Ikaros overexpression (Ferreiros-Vidal et al., 2013). The subsets of regulated genes were selected with the criteria that they were significantly regulated (corrected p value < 0.05), either down-regulated or up-regulated, after 6 hours of Ikaros induction and the regulation of gene expression remained significant in the same

direction after 48 hours of Ikaros overexpression. The list came down to 117 genes for down-regulation and 68 genes for up-regulation. The RNAPII profiles for these two sets of genes were generated as previously described. The down-regulated gene set showed general decrease of RNAPII density at the TSS, gene body and TTS (Figure 4.3). In contrast to the down-regulated set of genes, the up-regulated set of genes showed an increase in RNAPII density at the TSS, milder increases were also observed at the gene body and TTS. This indicates that the changes observed at selected loci are not special cases, and are representative of overall RNAPII profile changes at Ikaros regulated genes following Ikaros induction.

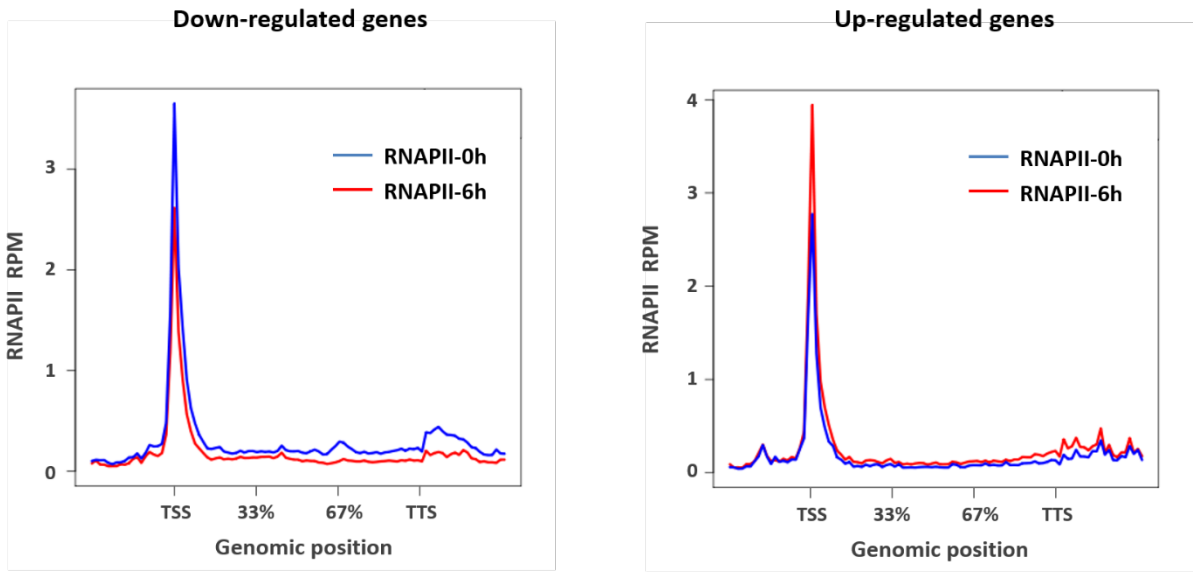

Figure 4.3 RNAPII coverage profile changes during Ikaros induction at regulated genes

RNAPII densities calculated as RPM were plotted along the intragenic region. Picture (left) shows RNAPII coverage profiles after 0h (blue line) and 6h (red line) of Ikaros induction for down-regulated Ikaros target genes; picture (right) shows RNAPII coverage profiles after 0h (blue line) and 6h (red line) of Ikaros induction for up-regulated Ikaros target genes.

c-Myc is a universal amplifier of expressed genes by facilitating RNAPII pause-release, and this facilitating effect is reversed by *Myc* knock-down or c-Myc inhibitors (Lin et al., 2012; Nie et al., 2012; Rahl et al., 2010). Importantly, *Myc* is an Ikaros target gene that is immediately down-regulated after Ikaros induction (Figure 3.6). *Myc* mRNA and c-Myc protein have very short half-lives (Hann and Eisenman, 1984). It was therefore a concern that after 6 hours of Ikaros induction, down-regulated *Myc* may lead to global reduction in RNAPII elongation. This would subsequently result in decreased transcription, and thereby introduce a bias on the interpretation of the genes regulated by Ikaros. To address this possibility, global RNAPII profiles were analysed before and after 6 hours of Ikaros induction (Figure 4.4). Before Ikaros induction, expressed genes contributed to the RNAPII signals along the intragenic region, highlighting RNAPII pausing at the TSS and transcription termination immediately downstream of the TTS. Importantly, no difference in the global RNAPII profile was observed after Ikaros induction. This suggests that the down-regulation of *Myc* does not globally reduce RNAPII elongation after 6 hours of Ikaros induction. This also supports the idea that the changes in RNAPII profiles are selective for Ikaros target genes.

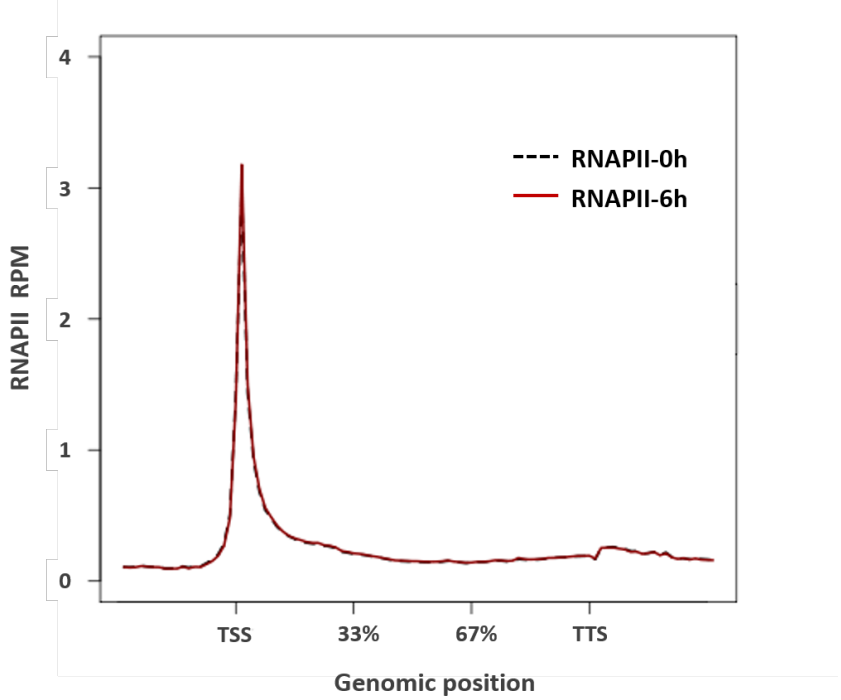

Figure 4.4 Global RNAPII coverage profiles before and after Ikaros induction

RNAPII density calculated as reads per million (RPM) was plotted along intragenic region. Global RNAPII coverage profiles were compared before (black dash line) and after 6 hours of Ikaros induction (red line).

Taken together, RNAPII profiling is consistent with the expected RNAPII genome-wide distribution, which not only discriminates actively transcribed genes from inactive ones, but also reflects rate-limiting processes during RNAPII traveling. Further, inducible Ikaros is shown to introduce changes in RNAPII binding selectively at Ikaros target genes, and the changes are in agreement with regulation at the transcriptional level.

4.1.3 Ikaros mediates changes in RNA polymerase II recruitment and elongation

I next asked whether Ikaros regulates RNAPII through modulating RNAPII recruitment or elongation. Recruitment level can be quantified using the RNAPII density proximal to the promoter. The efficiency of elongation was quantified using the RNAPII travel ratio (TR) (Rahl et al., 2010). The TR measures the ratio between the RNAPII density in the promoter (-30bp to +300bp of TSS) and in the gene region. More efficient RNAPII elongation results in less RNAPII at the promoter region and more at the gene body, and a lower TR.

For simplicity, it is assumed that the elongation rate, which reflects the speed of RNAPII travelling on the chromatin template, remains constant (Ehrensberger et al., 2013). Figure 4.5 left panel illustrates how down-regulation can be achieved. In the first scenario, Ikaros regulates RNAPII only at the level of recruitment, but does not influence elongation efficiency, so that TR remains the same before and after Ikaros induction (Figure 4.5A-L). In this case, RNAPII density decreases to the same extent at the promoter and the gene region. Preliminary examination showed that the Ikaros target gene *Myc* fell into this category of regulation. Second, Ikaros may not influence RNAPII recruitment, but increase RNAPII pausing (Figure 4.5B-L). In this scenario, the RNAPII density at the promoter remains or slightly increases due to stronger pausing, whilst RNAPII density in the gene region is reduced and the TR is higher after 6 hours of Ikaros induction. Third, Ikaros may reduce both RNAPII recruitment and elongation (Figure 4.5C-L). In this situation, RNAPII density at the promoter is reduced after Ikaros induction, while signal at the gene region is reduced even more as a consequence of both decreased recruitment and increased pausing. The Ikaros target gene *Ccnd2* appeared to fit this model. Finally, Ikaros may reduce RNAPII density at the promoter region, and less efficiently at the gene body (Figure 4.5D-L). Figure 4.5R illustrates four possible RNAPII regulation scenarios during Ikaros-mediated transcriptional

up-regulation. To examine whether Ikaros regulates RNAPII through one dominant mechanism or different mechanisms for different subsets of target genes, statistical tests will be used.

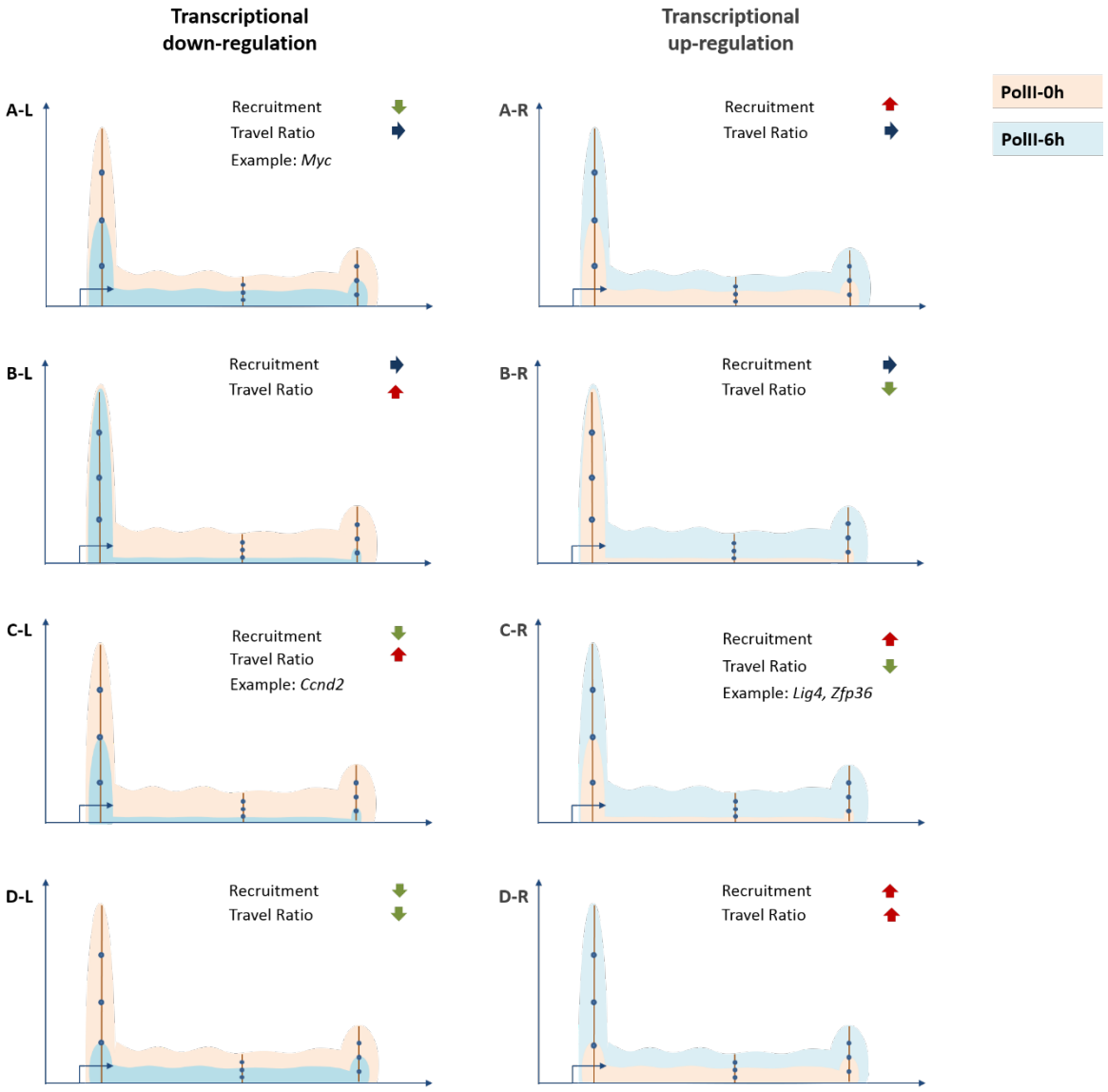

Figure 4.5 Schematic of possible Ikaros-mediated RNAPII regulation scenarios

Left panel shows possible regulation scenarios of down-regulated genes, while right panel shows those for up-regulated genes. Yellow area presents RNAPII density before Ikaros induction, while blue area presents that after 6 hours of Ikaros induction. Each scenario represents the possible combinations of regulation and recruitment and elongation levels. Each dot on the line at either TSS, gene body or TTS indicated of ¼ of RNAPII density, and it was intended to be representative of simplified percentage changes.

4.2 Ikaros mediates changes in the nucleosome landscape

4.2.1 Methodology

To determine nucleosome position, I used Micrococcal nuclease (MNase) to digest chromatin. MNase is derived from *Staphylococcus aureus* and is a relatively non-specific endo-exonuclease that digests both single-stranded and double-stranded nucleic acids. Treating chromatin with MNase, naked DNA is exposed for digestion, whilst DNA that is tightly wrapped around nucleosome is protected. In this way, DNA fragments that survive MNase digestion reveal the position of nucleosomes. To minimise nucleosome sliding during MNase treatment, cells were cross-linked with 1% formaldehyde. To balance the requirement of high resolution mapping for mono-nucleosome and the risk of over-digestion, MNase treatment was optimised to obtaining mostly mono-nucleosomes and minor di-nucleosomes (Barski et al., 2007; Schones et al., 2008). Digestion efficiency was checked using DNA agarose gel electrophoresis. DNA fragments purified from digested chromatin were subjected to high-throughput sequencing (MNase-seq) to determine the nucleosome landscape before and after Ikaros induction. I have received very helpful advice from Dr Steven Henikoff, FHCRC, USA, on how to conduct these experiments.

Canonical nucleosome consists of eight core histones with 147bp of DNA wrapping around it (Luger et al., 1997). However, nucleosomes *in vivo* are highly dynamic. They can be partially unwrapped (Tims et al., 2011) or partially composed (Henikoff et al., 2011), or contain histone variants (Weber and Henikoff, 2014). These nucleosomes may protect shorter lengths of DNA (Henikoff et al., 2011). For the purpose of mapping all types of nucleosomes, it was crucial that sequencing libraries were prepared using a specifically optimised protocol to bypass any size cut-off procedure. To discriminate between differentially composed nucleosomes (fully, partial or variant-containing), it is important to be able to calculate the precise length of each DNA fragment sequenced. To this end, libraries went through pair-end sequencing for 50 cycles at each end using an Illumina HiSeq2500 genome sequencer.

A total of 200 million reads were generated for MNase-0h and 220 million for MNase-6h (Table 4.2). Sequencing reads were mapped against the mouse genome mm9. Libraries showed 97% and 98% unique mapping, respectively. An additional quality control for pair-end sequencing is the pairing rate. 92% of reads from both libraries were paired with its mate

within a 1kb distance in the genome. This corresponded to 90 million and 100 million sequenced fragments for MNase-0h and MNase-6h, respectively. The mouse genome is 2.8×10^9 bp and considering there is a nucleosome every 200bp on average in the genome (Zhang and Pugh, 2011), mouse chromatin contains around 14 million nucleosomes. In this sense, the sequencing achieved 6-7 times coverage. The duplication rate for both libraries was around 10%, consistent with the high complexity of nucleosome positioning in the genome and indicative of a high library quality.

Table 4.2 Nucleosome sequencing general statistics

Libraries	**Total reads**	**Mapped reads**	**Mapped%**	**Paired reads**	**Paired%**	**Duplicates%**
MNase-0h	195,647,692	190,255,641	97%	179,586,712	92%	11%
MNase-6h	223,900,854	218,460,712	98%	205,098,842	92%	11%

For genome-wide analysis, true DNA fragments were re-generated by filling in the gap between read pairs. Following that, fragment lengths were calculated and their distribution plotted (Figure 4.6). MNase-0h and MNase-6h showed strong agreement in their fragment length distributions and both peaked around 150bp, corresponding to fully-composed stable mono-nucleosomes. Fragments shorter than 150bp were well preserved, representative of DNA protected by differentially composed nucleosomes, and other subnucleosome-sized particles, including transcription factors, the transcription machinery, and other large regulatory complexes. There was also a minor proportion of fragments that were longer than 150bp, indicating that chromatin was not over-digested by MNase.

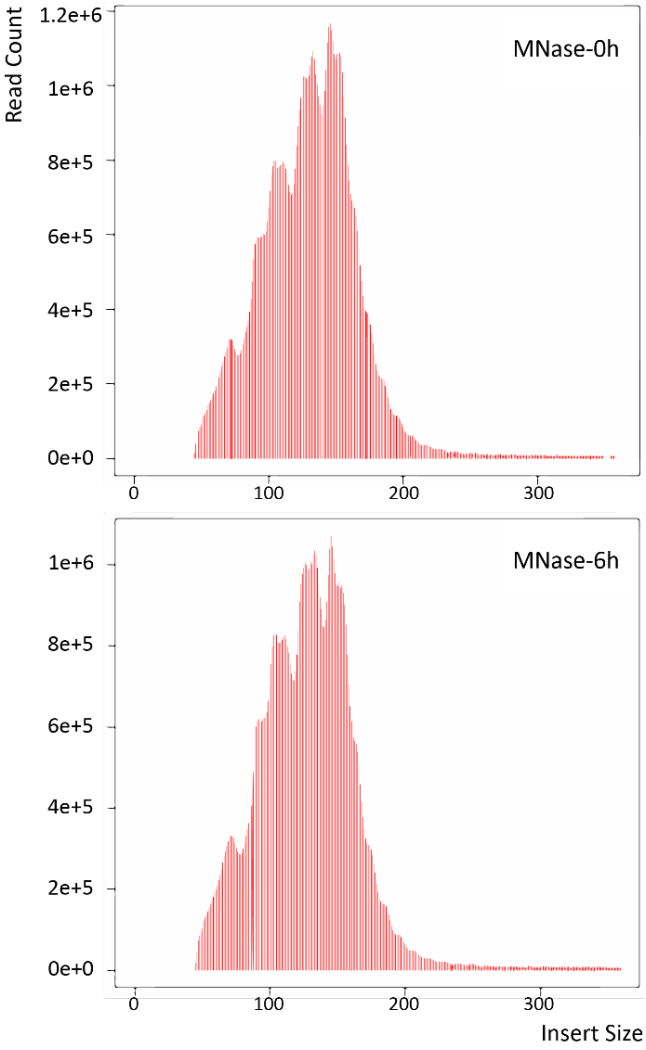

Figure 4.6 Fragment size distribution of nucleosome sequencing

Figure shows insert fragment size distribution of nucleosome sequencing before (top) and after (bottom) 6 hours of Ikaros induction, with x-axis being insert size and y-axis being read count. The distributions of fragments in two libraries were very similar.

4.2.2 The nucleosome landscape is changed by Ikaros

The genome-wide distribution of nucleosomes features both well positioned and phased nucleosomes surrounding the TSS (Struhl and Segal, 2013). To evaluate the quality of the MNase-seq dataset, I first examined whether my sequencing captured this feature (Figure 4.7A). As expected, nucleosomes were depleted at the TSS. The -1 and +1 nucleosomes were well positioned relative to the TSS. +2 to +5 nucleosomes were also phased, and phasing was

lost at more distant nucleosomes. The phasing pattern was less obvious in nucleosomes upstream of the TSS.

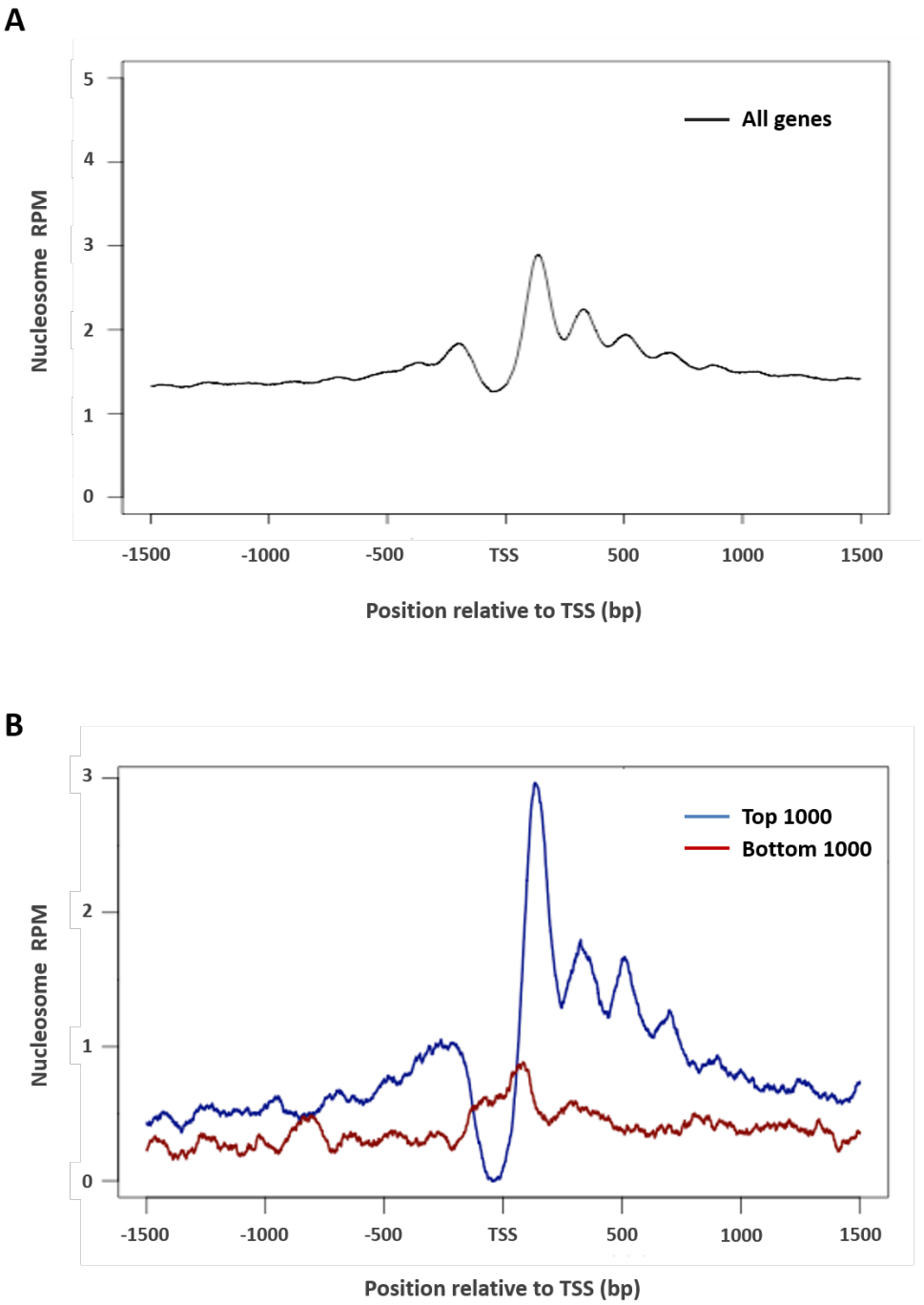

Figure 4.7 Nucleosome distribution around TSS

Graph highlights nucleosomes surrounding the TSS, with their density calculated as RPM. A shows nucleosome distribution of all genes, and B shows that of top (blue line) and bottom (red line) expressed genes.

The positioning and phasing pattern of nucleosomes surrounding the TSS is positively correlated with the level of gene expression (Schones et al., 2008). To test this correlation, nucleosome profiles surrounding the TSS were generated separately for the top 1000 expressed genes and bottom 1000 expressed genes (Figure 4.7B), as described for the RNAPII analysis (Figure 4.1). Highly expressed genes showed strong nucleosome depletion at the TSS. The +1 nucleosome was well positioned with a pronounced phasing pattern of downstream nucleosomes. In contrast, at silent genes, the TSS was occupied by nucleosomes and there was no phasing pattern either upstream or downstream of the TSS. Interestingly, +1 nucleosomes of silent genes seemed to shift closer to the TSS compared to the +1 nucleosomes in highly expressed genes. Hence, this MNase-seq dataset reflected the expected nucleosome distribution at the genome-wide level.

Next, the nucleosome landscape was evaluated before and after Ikaros induction at selected target genes. The nucleosomes occupying promoters and TSSs were examined, which best reflect transcriptional activities (Struhl and Segal, 2013). RNAPII profiles were included to illustrate transcriptional activities. The down-regulated *Igll1* promoter was almost depleted of nucleosomes before Ikaros induction. After 6 hours of Ikaros induction, the promoter was highly occupied by nucleosomes, reflecting reduced promoter accessibility (Figure 4.8). This change was particularly strong immediately upstream of the TSS. The negatively regulated *Myc* promoter showed a milder increase in nucleosome occupancy. All three down-regulated genes examined shared an interesting feature after Ikaros induction, which was the increase of nucleosome occupancy at sites that were occupied by RNAPII before Ikaros induction. The nucleosomes neighbouring RNAPII appeared to close in after Ikaros induction, filling the gap previously occupied by RNAPII (Figure 4.8). This data suggested that Ikaros may mediate changes in nucleosome positioning and occupancy, thereby controlling promoter accessibility during transcriptional regulation. Particularly, Ikaros could be involved in the possibly active competition between nucleosomes and RNAPII at the TSS.

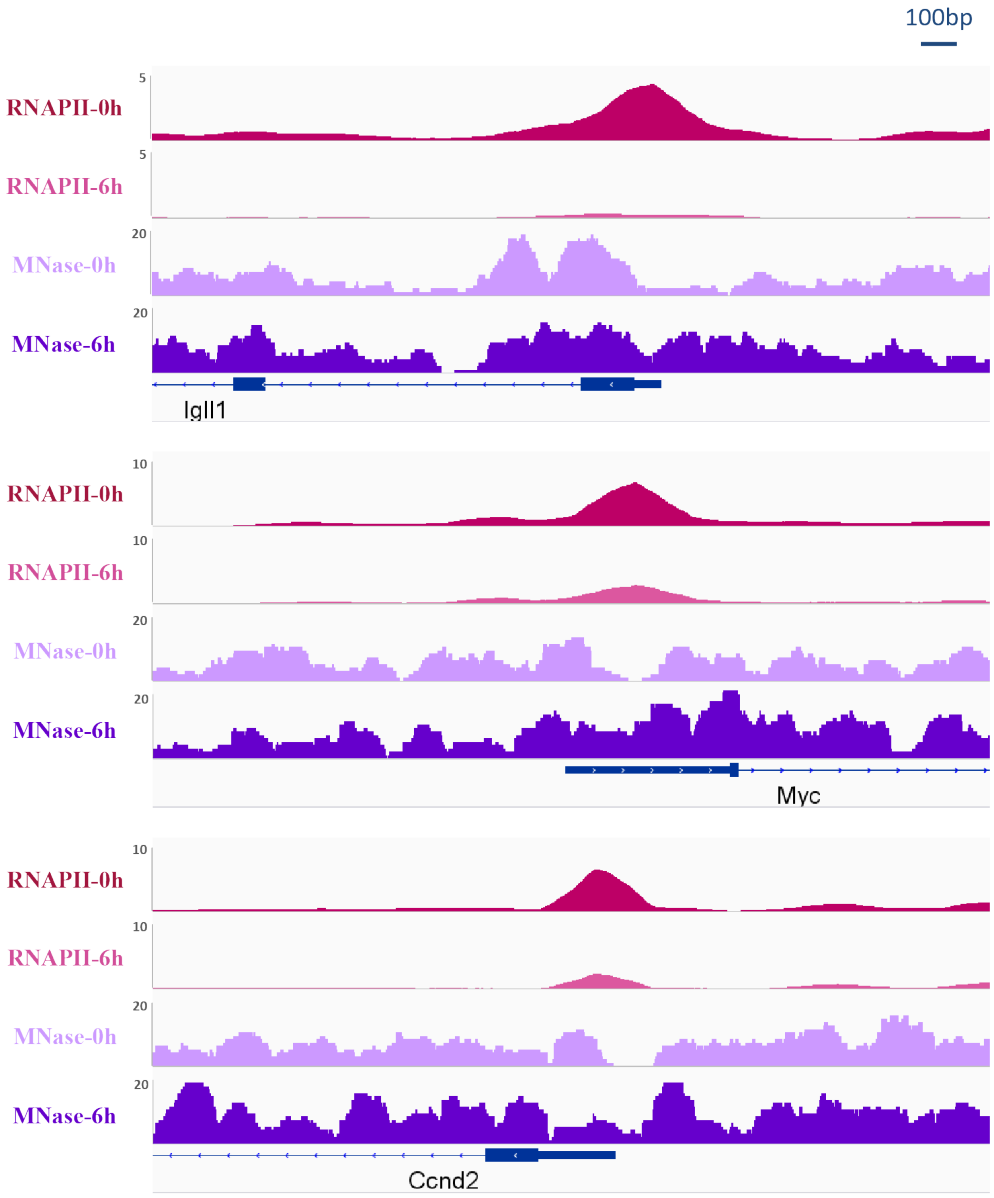

Figure 4.8 The nucleosome landscapes at down-regulated gene promoters

Figure shows the nucleosome landscape at promoters and downstream of the TSSs of down-regulated *Igll1* (Top), *Myc* (middle) and *Ccnd2* (Bottom). At each locus, the profiles of RNAPII before (dark pink), and after Ikaros induction (light pink), nucleosome before (light purple), and after (dark purple) Ikaros induction, and reference gene position were presented.

In contrast, up-regulated genes like *Zfp36* showed mildly decreased nucleosome occupancy at the promoter after Ikaros induction (Figure 4.9). The promoter of *Lig4* did not show obvious

nucleosome occupancy changes before and after Ikaros induction. This could be due to active transcription before Ikaros induction, though at lower level, which has already made the promoter relatively accessible. Interestingly, at the TSSs of both these up-regulated genes, the nucleosomes neighbouring RNAPII appeared to be more apart from each other after Ikaros induction, creating a bigger gap for RNAPII.

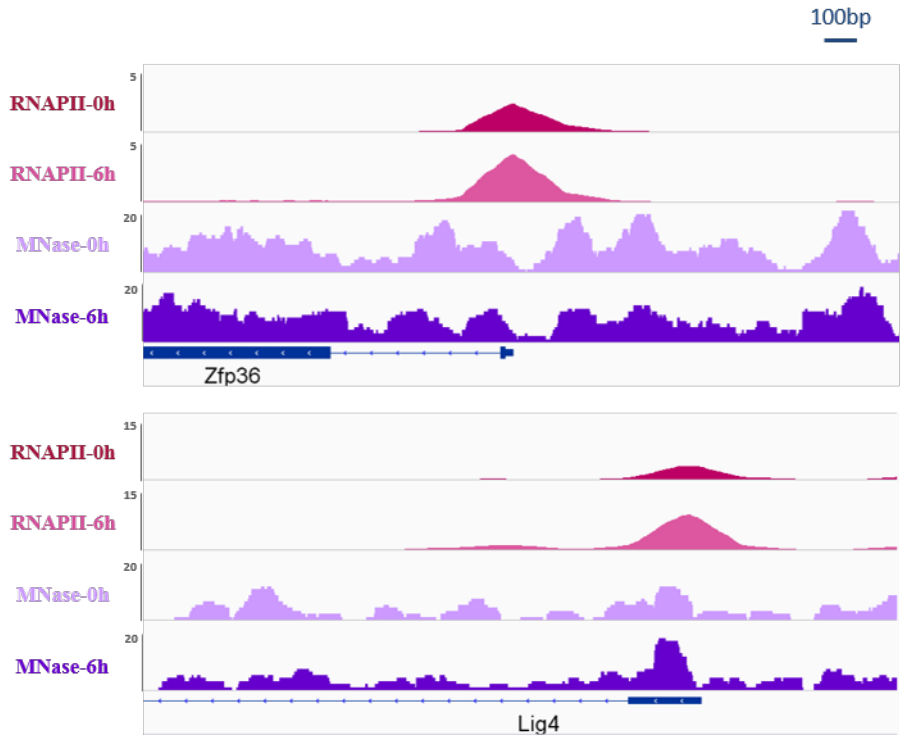

Figure 4.9 Nucleosome landscape at up-regulated and control gene promoters

Figure shows the nucleosome landscape at the promoter and downstream of the TSS of up-regulated *Zfp36* (Top), *Lig4* (bottom). At each loci, the profiles of RNAPII before (dark pink), and after Ikaros induction (light pink), nucleosome before (light purple), and after (dark purple) Ikaros induction, and reference genome were presented.

4.2.3 Mapping of differentially composed nucleosomes

To investigate whether Ikaros regulates nucleosome composition, DNA fragments were divided into 4 size classes: >140bp for stable and fully composed nucleosomes, 110-140bp for partial nucleosomes possibly with one dynamic pair of the H2A-H2B dimer or containing

destabilising histone variants, 80-110bp for more dynamic and destabilised nucleosomes, and <80bp for subnucleosome-sized particles (Henikoff et al., 2011).

Taking the down-regulated *Igll1* as an example (Figure 4.10), the majority of sequenced fragments were grouped as >140bp, consistent with the analysed fragment length distribution (Figure 4.6). Ikaros increased nucleosome occupancy at the *Igll1* promoter and TSS after Ikaros induction (labelled as total). With careful inspection, the increase appeared mainly, if not only, in the size classes of 110-140bp and >140bp. This suggested that Ikaros preferentially incorporated or exchanged for more intact and stable nucleosomes to the *Igll1* locus during repression. No increase was observed in the size classes of 80-110bp and <80bp, which corresponded to the binding of destabilised nucleosomes or chromatin regulatory complexes. Consistent with this notion, at the up-regulated *Zfp36* locus, the decrease in nucleosome occupancy seen in total was mainly contributed by the nucleosomes that protects longer piece of DNA (Figure 4.10). The sequencing coverage at the fractions of partial nucleosomes and subnucleosome-sized particles were not deep, and consequently were less reliable to examine the changes in the composition of nucleosomes. To ask whether Ikaros is able to manipulate the composition of nucleosomes to favour the direction of its transcriptional regulation, nucleosome composition is further examined in later sections.

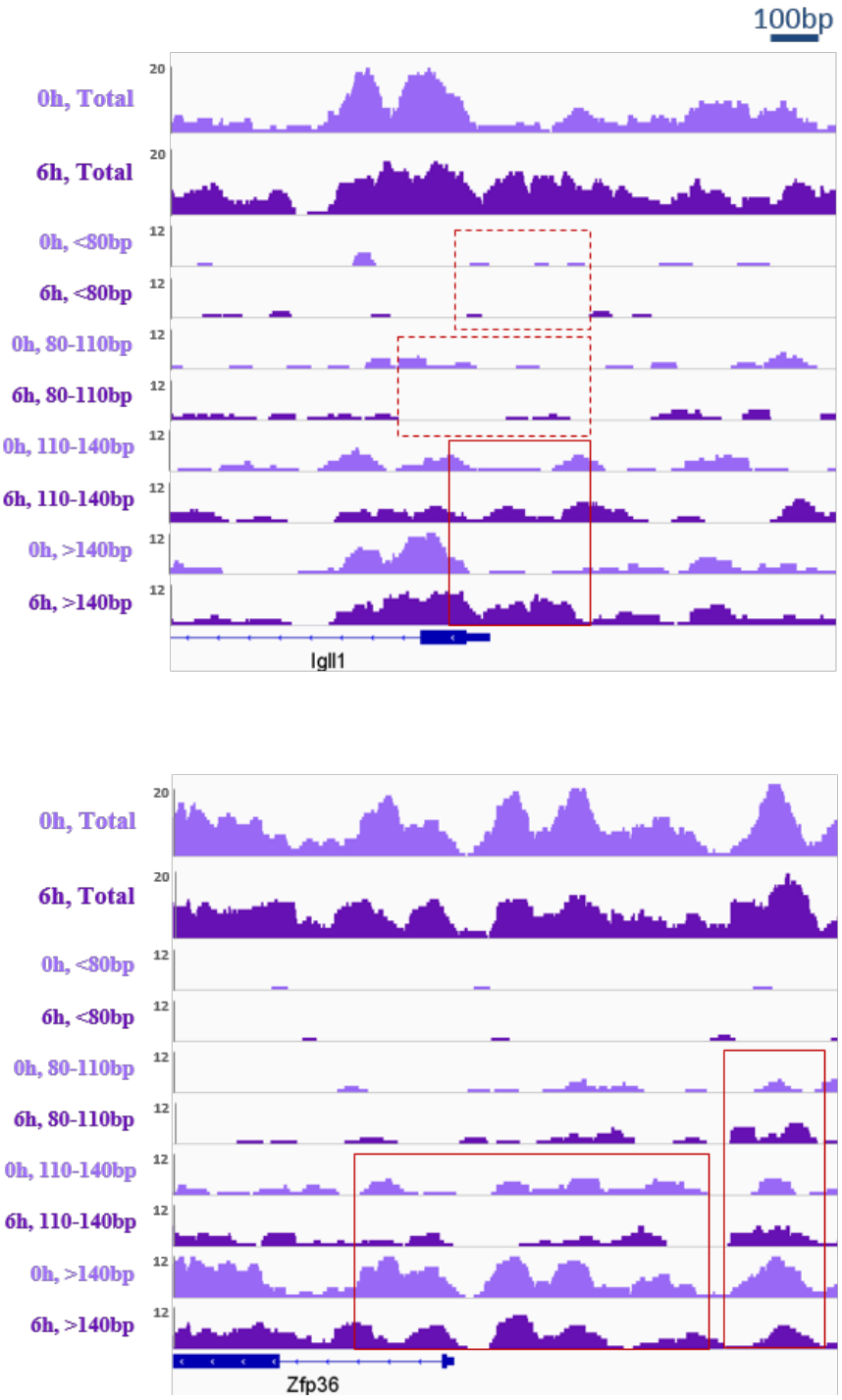

Figure 4.10 Nucleosome landscape based on the composition of nucleosomes

Nucleosome landscape at *Igll1* (top) and *Zfp36* (bottom) of total nucleosomes, and subnucleosome particles protecting <80bp DNA, partial nucleosomes protect 80-110bp, 110-140bp and more than 140bp DNA, before and after Ikaros induction.

4.3 Discussion

Here, the genome-wide profiles of RNAPII and nucleosome were determined in B3 pre-B cells before and after Ikaros induction. These profiles set out the landscape of chromatin status, and revealed striking changes in RNAPII binding and promoter accessibility mediated by Ikaros. They suggest possible mechanisms used by Ikaros to regulate transcription. Furthermore, they also help focus on particular loci to study the kinetics and mechanisms of Ikaros-mediated transcriptional regulation in depth.

RNA polymerase II profiles

The binding of RNAPII was determined by high quality ChIP-seq. Whilst no RNAPII binding was observed at silent genes, the binding of RNAPII at active genes reflected the promoter proximal pausing, elongation at the gene body, and the termination process (Figure 4.1). Confident with the quality of RNAPII profiling, we have shown that Ikaros modulated the RNAPII density selectively at Ikaros target genes (Figure 4.2, 4.3). At the down-regulated genes, an obvious decrease in RNAPII binding was observed after 6 hours of Ikaros induction, in contrast to an increase at the up-regulated genes. Moreover, the degree of change in RNAPII binding faithfully reflected the strength of Ikaros regulation on the transcriptional level (Figure 3.6), with *Igll1* being the strongest among down-regulated targets, and the down-regulation being more dramatic than the up-regulation.

To take the analysis to the next level, the regulation of RNAPII by Ikaros will be examined at two rate-limiting steps, the recruitment and the elongation (Figure 4.5), and categorise the genes regulated by Ikaros depending on the scenarios of RNAPII regulation, and to test whether there is a dominant mechanism used by Ikaros to regulate RNAPII. To this end, a high quality set of differentially expressed genes after Ikaros induction is required. So far, the gene expression profiling to identify Ikaros target genes was done using microarray (Ferreiros-Vidal et al., 2013). Though it has been very informative and instructive, there is the limitation that the probes used in the array are designed from exons, thereby only recognising differential expression at the level of mature transcripts. Additionally, the B3 cells used to generate the microarray dataset express lower level of inducible Ikaros, therefore the transcriptional changes are relatively milder (Figure 3.5 and Figure 3.6). These factors together lead to a potential loss of target genes that can be identified. Our collaborators, the

STATegra consortium, profiled gene expression by RNA-seq after 0h, 2h, and 6h of Ikaros induction, in B3 cells expressing comparable level of inducible Ikaros to this study. When the dataset is available, the classification of Ikaros target genes according to its RNAPII regulation mechanisms will be tested.

Recently, the rate-limiting step of RNAPII promoter melting has been discovered in eukaryotes (Kouzine et al., 2013), and it would be of interest to investigate whether Ikaros can regulate promoter melting. In that study, Casellas and colleagues developed ssDNA-seq to measure the extent of promoter melting. The generation of ssDNA leads to a shift of the RNAPII peak at the TSS downstream by about 18bp (Kouzine et al., 2013). Therefore, before uptaking the technique of ssDNA-seq, the RNAPII binding profile of the differentially regulated genes will be zoomed in to examine whether there is a shift of RNAPII after Ikaros induction.

Nucleosome landscape

Nucleosome landscapes were determined using MNase-seq. Digestion by MNase to mostly the mono-nucleosome level allows for high-resolution mapping of nucleosome positioning. The data showed that Ikaros modulated promoter accessibility during transcriptional regulation. After 6 hours of Ikaros induction, an increase in nucleosome occupancy was observed at the negatively regulated gene promoters (Figure 4.8). The up-regulated gene promoters showed no increase or a mild decrease in nucleosome occupancy (Figure 4.9).

It is interesting to test whether Ikaros can further control the composition of nucleosomes to favour the direction of transcriptional regulation (Figure 4.10). For example, at the down-regulated *Igll1* locus, Ikaros preferentially deposited nucleosomes that protect longer piece of DNA. There was no increase observed in the size class of 80-110bp corresponding to the destabilised nucleosomes. A series of factors can contribute to the stability of the nucleosomes and consequently the length of DNA they protect, including the nucleosome integrity, the incorporation of histone variants and the histone modifications. The composition of nucleosomes needs further investigation. Furthermore, the size class of <80bp corresponds to the binding of transcription factors and chromatin modifiers. Should a decrease in these subnucleosome-sized particles be statistically significant, it may be due to direct effects of Ikaros to remove these regulatory complexes. It may also be an indirect effect of Ikaros decreasing promoter accessibility.

The current sequencing depth however has limited the strength of further investigation. So far, a 6-7 coverage depth of nucleosome sequencing was achieved from one biological replicate. It is suggested that ideal high-resolution mapping of nucleosomes requires at least 15-30 coverage depth (personal communications with Dr Steven Henikoff). Attempts were made to generate another sequencing replicate, however these were unsuccessful due to unresolved low pairing rate from pair-end sequencing.

Should ideal sequencing depth be achieved from more than one biological replicate, more in depth analyses can be done using the nucleosome landscapes. First, it is important to assess whether the modulation of promoter accessibility is observed at other Ikaros regulated genes. Further, it would be interesting to ask whether the strength of nucleosome occupancy regulation positively correlates with the strength of transcriptional regulation. Next, it is intriguing to investigate whether the existence of partially composed nucleosome favours transcription in mammalian cells. In yeast and *Drosophila*, they correlate with genes poised for activation and are therefore suggested to favour transcription (Weber et al., 2010; Weiner et al., 2010; Xi et al., 2011). However in mouse ESCs, Rando and colleagues found little correlation between the footprints of these partially unwrapped or less stably bound nucleosomes and the transcriptional activities (Carone et al., 2014). Taking advantage of the mapping of the differentially composed nucleosomes, we can examine the correlation of the partial nucleosomes with transcriptional activities in mammalian cells.

RNA Polymerase II vs nucleosomes

RNAPII and nucleosome occupancy at gene promoters were both regulated by Ikaros. Though the changes were to different extents, one unifying feature was the anti-correlation of RNAPII binding and nucleosome occupancy around the TSSs. The competition between RNAPII and nucleosomes, whether active or passive, needs to be further explored. For instance, it is possible that Ikaros increases the binding of one factor, thus making the DNA binding regions unavailable to the other. To answer this question, it would be helpful to study the kinetics of changes in chromatin mediated by Ikaros, to see if one change appears before another.

5 Kinetics of Ikaros-mediated changes in chromatin status

Ikaros modulates both the RNAPII binding and promoter accessibility of its target genes (Figure 4.8, 4.9). Here, I zoomed in the time frame to investigate the kinetics of changes in chromatin status during Ikaros-mediated transcriptional regulation. Furthermore, based on these kinetics, the order of events occurred during transcriptional regulation was evaluated.

5.1 Kinetics of changes in RNA polymerase II mediated by Ikaros

To examine how fast Ikaros can change RNAPII density, I performed RNAPII ChIP-qPCR in a time course of Ikaros induction, namely 0 minutes, 5 minutes, 15 minutes, 30 minutes, 1 hour and 6 hours (Figure 5.2). The antibody used for RNAPII ChIP recognizes total RNAPII, as described previously (section 4.1). ChIP enrichment, defined as percentage over input, was used to evaluate the binding of RNAPII.

The quality of RNAPII ChIP-qPCR was first evaluated before Ikaros induction (Figure 5.1). At the promoters of negative control genes *Acta1* and *Rex1*, RNAPII enrichment was not detectable. At the promoters of active genes such as *Igll1*, *Myc* and *Ccnd2*, a significant RNAPII enrichment of 0.8-1.6% over input was observed. *Lig4* and *Zfp36* are not silent in B3 cells, therefore enrichment of RNAPII was also observed at these loci before Ikaros induction. Moreover, within each locus, RNAPII enrichment was the highest at the TSSs, and lower at the gene bodies and TTSs (enrichment of less than 0.5% over input), as expected (Guenther et al., 2007) (Figure 4.1).

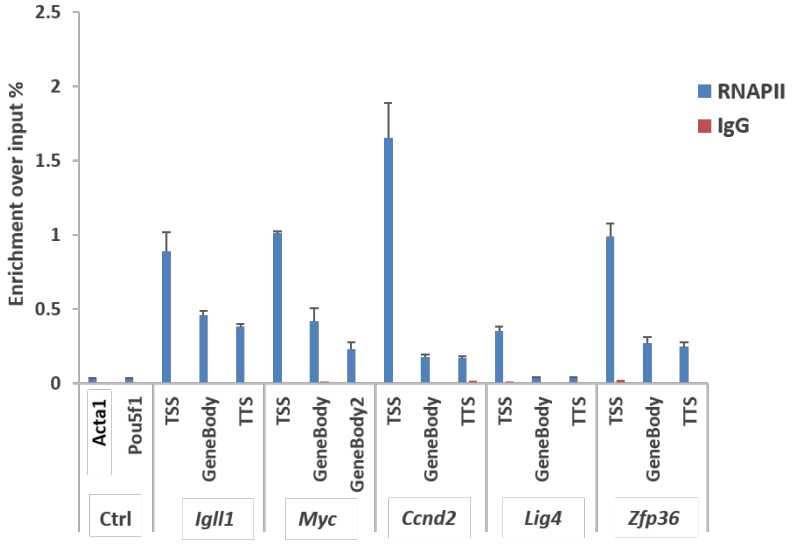

Figure 5.1 RNAPII enrichment at selected Ikaros target genes and control genes before induction

The enrichment of RNAPII (blue) and negative control antibody IgG (red) was examined at the promoters of inactive genes Acta1 and Pou5f1, and the promoters, gene bodies and TTSs of the Ikaros target genes *Igll1*, *Myc*, *Ccnd2*, *Lig4* and *Zfp36*. Data shown was the average of three biological replicates.

After Ikaros induction, the binding of RNAPII decreased at the negatively regulated genes *Igll1*, *Myc* and *Ccnd2*. Strikingly, RNAPII was significantly down-regulated as soon as 15 minutes after Ikaros induction at the *Igll1* and *Ccnd2* promoters, and 30 minutes at the *Myc* promoter. Down-regulation became progressively stronger during Ikaros induction at all three genes, and the strongest repression level seemed to be obtained within 1 hour after induction (Figure 5.2). Comparing the repression level of these down-regulated genes, *Igll1* had the strongest effect within 6 hours of induction, with a ~80% reduction compared to the ~50% decreases at *Myc* and *Ccnd2*. This is in agreement with the changes in mRNA transcription (Figure 3.6) and in RNAPII genome-wide profiling (Figure 4.2).

The up-regulated genes *Lig4* and *Zfp36* showed increased RNAPII binding after Ikaros induction. The kinetics of the increases were relatively slower compared to down-regulation, with significant increases observed after 1 hour of Ikaros induction. The level of regulation was also milder compared to repression, with increases less than 2-fold.

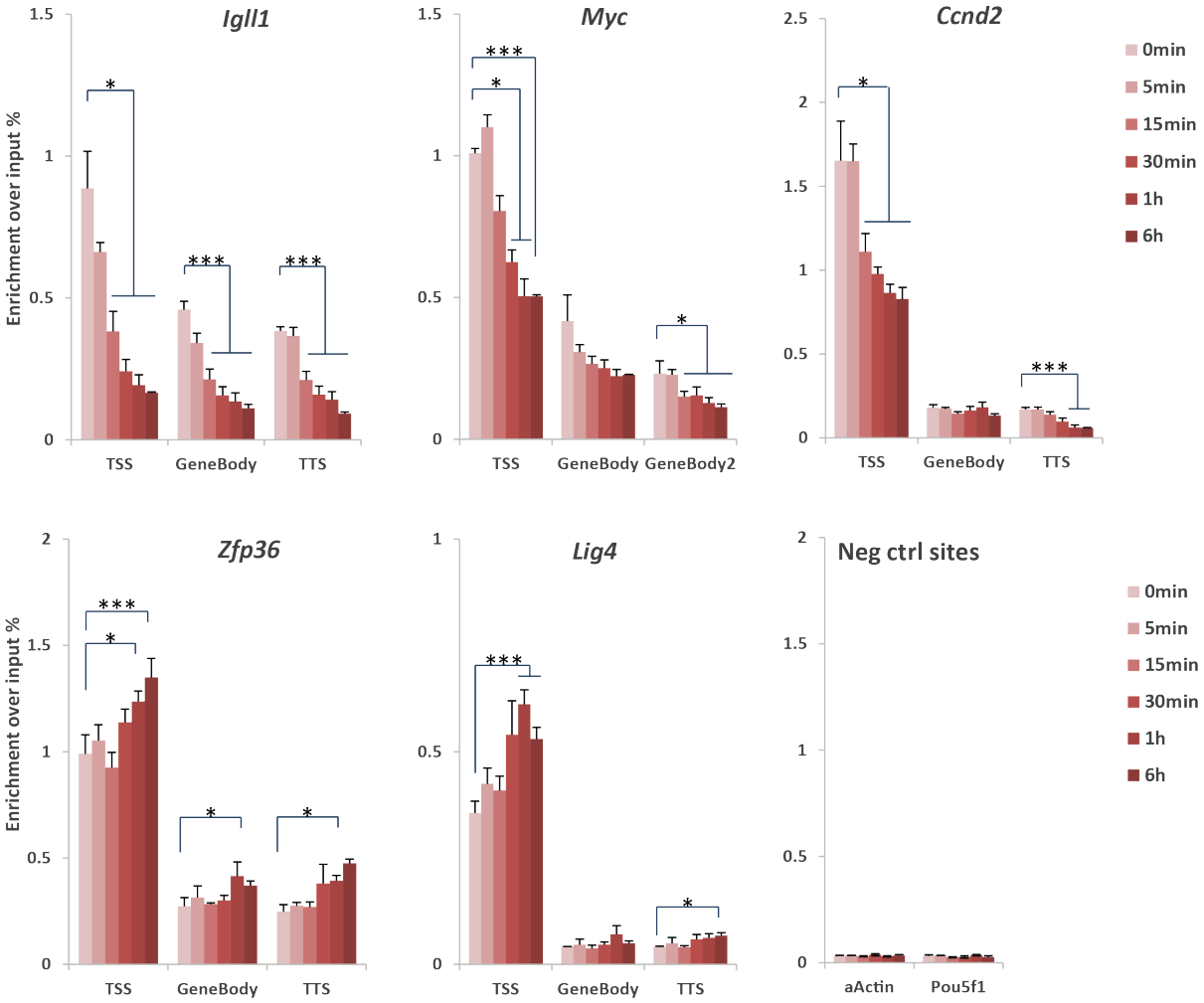

Figure 5.2 Kinetics of changes in RNAPII after Ikaros induction

Graphs show RNAPII enrichment at TSS, gene body, and TTS of Ikaros-regulated (top panel being down-regulated, bottom panel being up-regulated) genes and negative control genes (bottom right), after 0min, 5min, 15min, 30min, 1h and 6h of Ikaros induction. Data shown was an average of three biological replicates. P value: *<0.05, ***<0.01.

Taken together, the binding of RNAPII rapidly responds to Ikaros induction at target genes and the changes in RNAPII faithfully agree with mRNA transcriptional regulation. Thus, inducible Ikaros system is proved to be a powerful and reliable system to monitor the kinetics of the regulatory events mediated by Ikaros.

5.2 Kinetics of changes in nucleosome occupancy mediated by Ikaros

Next, the dynamics of promoter accessibility was monitored using a MNase-qPCR assay. To capture the kinetics, the MNase assay was performed in the same time course as for RNAPII, namely 0 minutes, 5 minutes, 15 minutes, 30 minutes, 1 hour and 6 hours after Ikaros induction.

To quantify nucleosome occupancy, firstly, DNA concentration was accurately measured (described in detail in section 2.9.2) and 2ng of either MNase digested or undigested DNA were used per qPCR reaction. Nucleosome occupancy was calculated by normalizing the signal from digested to that of undigested, in order to correct for any possible genomic bias. The promoter of the inactive control gene *Rex1*, which should be stably occupied by nucleosomes, was used as an internal control. To further correct for variations introduced by DNA quantification, the digested/undigested signal of the locus of interest was further normalized to that of the *Rex1* promoter. Finally, to emphasize the kinetics of changes in nucleosome occupancy at specific loci, fold changes of the normalized nucleosome occupancies after Ikaros induction were calculated against the 0min un-induced sample (Figure 5.2). Though complicatedly normalized, each step was carefully examined and little technical noise was observed (data not shown). As a positive control, the repressed gene *Acta1* promoter showed similar nucleosome occupancy compared to *Rex1* (data not shown), and remained unchanged during Ikaros induction (Figure 5.3). At the selected Ikaros target loci, qPCR primers used were marked in the nucleosome profiling snapshots with upstream to downstream in the genome as left to right in the graph.

At the down-regulated gene *Igll1* promoter (primers: Promoter and TSS), nucleosome occupancy was significantly increased to 5-fold as soon as 5 minutes after Ikaros induction, immediately making the promoter less accessible. Within 6 hours of induction, the increase of nucleosome occupancy reached about 18-fold compared to the un-induced situation. In contrast, nucleosome occupancy remained unchanged at an upstream (Upstream-1) and a downstream site (+1 nucleosome). This supports the idea that nucleosomes at the promoters are highly regulated, compared to those at the gene bodies and intergenic regions (Struhl and Segal, 2013). Likewise, down-regulated *Myc* also showed a significant increase in nucleosome occupancy. The kinetics were slower and milder compared to the *Igll1* locus, with a significant increase first observed after 15 minutes of induction which reached to 3-

fold within 6 hours. Similar to the kinetics of RNAPII binding, the changes in nucleosome occupancy were mostly obtained within 1 hour after Ikaros induction.

In contrast to the decreased chromatin accessibility at the down-regulated gene promoters after Ikaros induction, nucleosome occupancy at the up-regulated *Lig4* and *Zfp36* promoters were progressively reduced, making the promoters more accessible. The kinetics were also slower compared to down-regulation, with a significant decrease observed within 30 minutes to 1 hour after induction. This is similar to the kinetics seen in RNAPII binding.

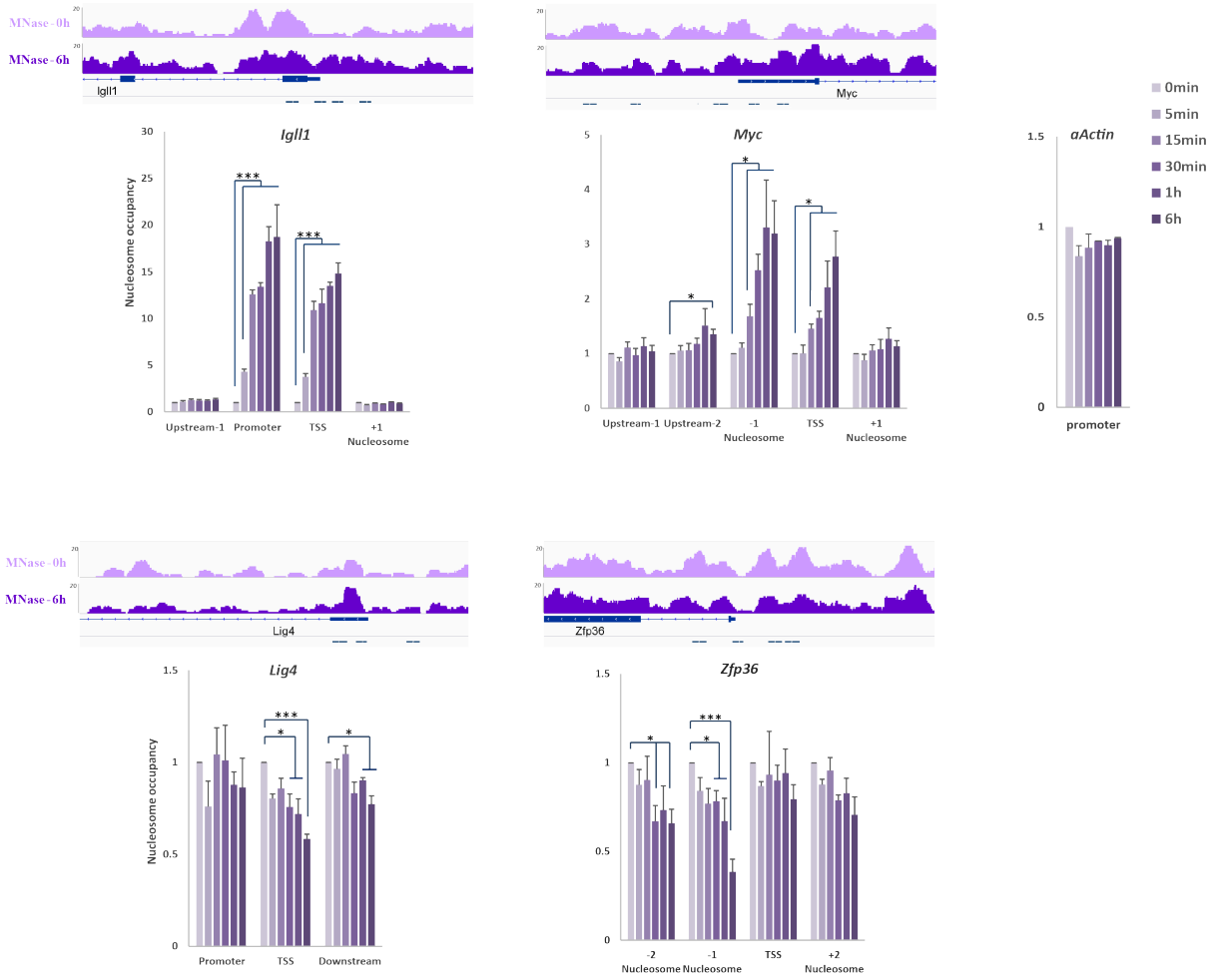

Figure 5.3 Kinetics of nucleosome positioning mediated by Ikaros

Graphs show nucleosome occupancy at promoters of Ikaros-regulated (top panel being down-regulated, bottom panel being up-regulated) and control loci (top right), after 0min, 5min, 15min, 30min, 1h and 6h of Ikaros induction. qPCR primers used were marked in the nucleosome profiling snapshots with upstream to downstream in the genome as left to right in the graph. Data shown was an average of three biological replicates. P value: *<0.05, ***<0.01.

5.3 Kinetics of changes in nucleosome composition mediated by Ikaros

The nucleosome landscape after Ikaros induction captured changes in different size classes of nucleosomal DNA (Figure 4.10). The difference in the length of DNA protected from MNase digestion reflected the variations in nucleosome stability (Luger et al., 2012; Xi et al., 2011). Here, the composition of the nucleosome was examined at the level of nucleosome integrity and the incorporation of histone variants. Further, the kinetics of changes in nucleosome compositions were monitored after Ikaros induction.

5.3.1 Nucleosome integrity

The nucleosome core can be viewed as three independently controlled spatial domains. The $(H3\text{-}H4)_2$ tetramers are more stably associated with DNA, governing the 'central region' of the DNA wrap. H2A-H2B dimers are more dynamic, docking at the DNA 'entry' and 'exit' sites of the nucleosome (Bintu et al., 2012; Rhee et al., 2014; Talbert and Henikoff, 2010). The ratio between H2B and H3 can be used as an indication of how intact the nucleosome is (Bevington and Boyes, 2013; Kireeva et al., 2002). To examine the integrity of nucleosome composition, enrichment of histone H2B and H3 was quantified after Ikaros induction by ChIP.

To achieve clearer boundaries between nucleosomes, I optimized the ChIP protocol by using MNase digested chromatin for IP. This was adapted from a native MNase-ChIP protocol from Keji Zhao's lab. Briefly, as for MNase assay, cross-linked chromatin was fragmented by MNase digestion to mostly mono-nucleosome level, and this chromatin lysate was used for IP to analyse the composition of nucleosomes.

To test whether the protocol has worked, the mapping of nucleosome by histone H3 MNase-ChIP was compared to that by MNase-qPCR. Theoretically, these two methods should produce similar results on nucleosome occupancy. In the MNase-ChIP, there is no unbiased genomic input control, since the chromatin fragmented by MNase treatment has been enriched for regions protected by nucleosomes. Therefore enrichment of histone H3 at the locus of interest was quantified by normalizing to that of the promoter of the internal control *Rex1*. As expected, the nucleosome occupancy analysed using these two methods was highly comparable over the same time course after Ikaros induction (Figure 5.4). At the *Igll1* locus,

both methods showed the same kinetics of increase in nucleosome occupancy, as well as a similar fold change. This confirmed that the newly developed MNase-ChIP protocol was highly reliable.

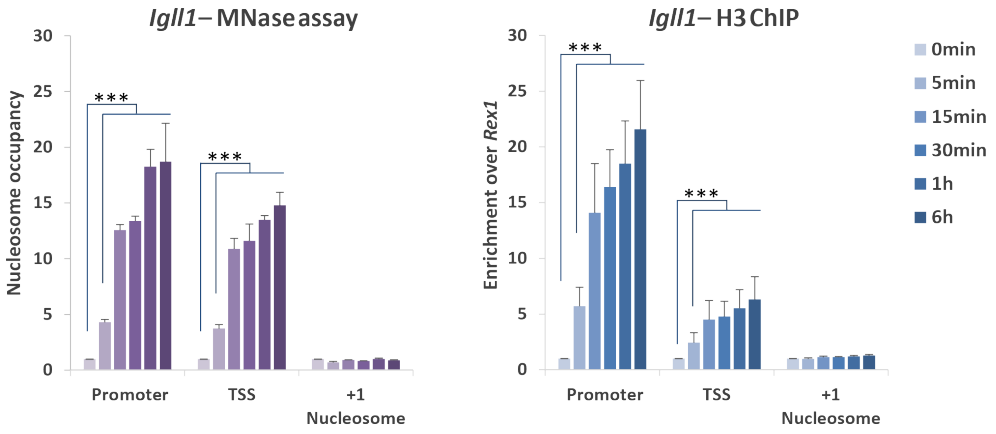

Figure 5.4 Nucleosome occupancy measured by MNase assay and histone H3 MNase-ChIP

Nucleosome occupancy measured by MNase assay (left) and histone H3 MNase-ChIP (right) showed very similar kinetics and fold change at *Igll1* locus after Ikaros induction. Data shown was an average of three and five biological replicates, respectively. P value: ***<0.01.

Following this, the integrity of nucleosomes was investigated after Ikaros induction (Figure 5.5). The control locus *Rex1* did not show any significant changes of H2B enrichment over H3, therefore the integrity of nucleosomes remained the same after Ikaros induction. At the down-regulated *Igll1* promoter, there was an increased H2B/H3 ratio after Ikaros induction, significantly after 6 hours of induction. Similar changes were observed at the negatively regulated *Ccnd2* promoter, with a significant increase observed after 1 hour of Ikaros induction. This suggests that those re-positioned or deposited nucleosomes, which decrease the accessibility of the down-regulated promoters, are more fully composed. This perhaps further decreases the chance of access to nucleosomal DNA by non-histone DNA-binding proteins, thereby acting synergistically to favour transcriptional down-regulation. In contrast, the up-regulated promoters appeared to be the other way around (Figure 5.5). At the *Lig4* locus, a significant decrease in H2B/H3 ratio was observed within 30 minutes of Ikaros

induction, indicating that the nucleosomes became more partially composed on top of the decreased occupancy (Figure 5.3). These partial nucleosomes are more likely to expose DNA regulatory regions, thus further favouring nucleosomal DNA accessibility to DNA binding proteins during transcriptional up-regulation.

In conclusion, Ikaros modulates nucleosome integrity to favour transcriptional regulation towards either direction. This supports the observations in the nucleosome landscapes of different size classes of nucleosomal DNA (Figure 4.10). Furthermore, the kinetics of changes in nucleosome integrity appear to be slower.

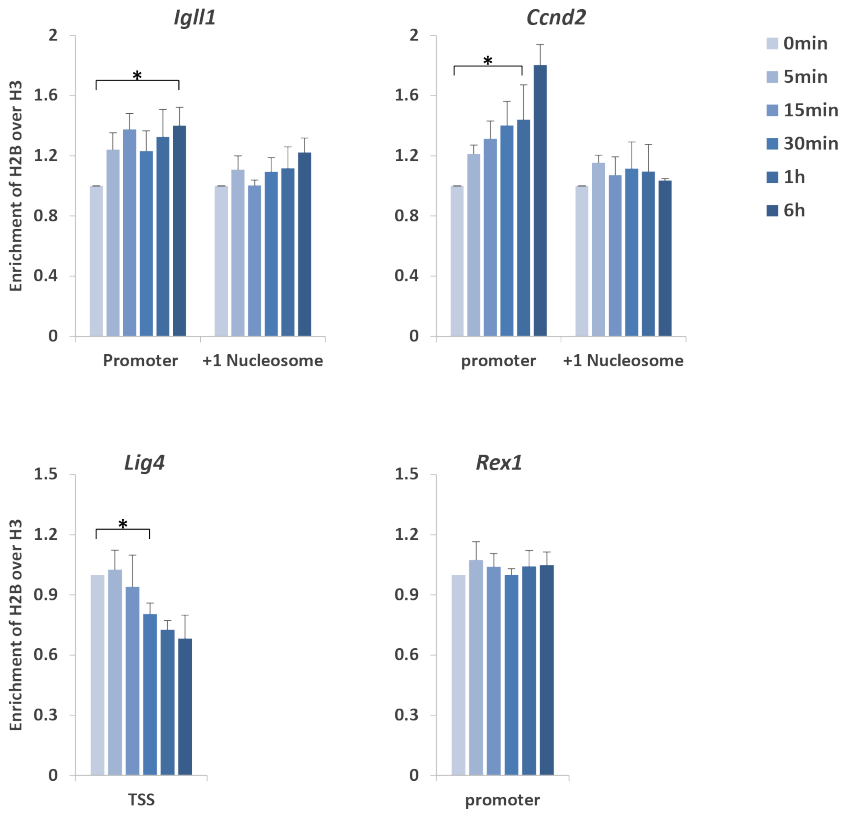

Figure 5.5 Kinetics of changes in nucleosome intactness mediate by Ikaros

Graphs show nucleosome intactness measured by enrichment of H2B/H3 at the promoters of Ikaros-regulated (top panel being down-regulated, bottom panel being up-regulated) and control loci (bottom right), after 0min, 5min, 15min, 30min, 1h and 6h of Ikaros induction. Data shown was an average of three biological replicates. P value: *<0.05.

5.3.2 Histone variant H2A.Z

Histone variants can alter nucleosome stability during transcriptional regulation (Weber and Henikoff, 2014). H2A.Z is one of the most conserved histone variants between species. H2A.Z-containing nucleosomes protect ~120bp of DNA *in vivo* (Hu et al., 2013; Tolstorukov et al., 2009), and are reported to play an important role in poising genes for transcriptional activation (Weber and Henikoff, 2014). Here, the involvement of histone H2A.Z during Ikaros-mediated transcriptional regulation was investigated.

Using the same MNase-ChIP technique, H2A.Z enrichment was examined. Here, I focused on the involvement of H2A.Z in the composition of nucleosomes, rather than its distribution in the genome. For this purpose, the influence of nucleosome occupancy was ruled out by normalizing histone H2A.Z to H3. Surprisingly, at the down-regulated *Igll1* locus, strong incorporation of H2A.Z was observed at the nucleosomes surrounding the TSS (Figure 5.6). In particular, at the +1 nucleosome, the incorporation of H2A.Z was significantly increased as soon as 5 minutes after Ikaros induction, and reached to 6-fold within 6 hours. *Igll1* was not an exception. Similar effects were seen at the negatively regulated *Myc* and *Ccnd2*. The increases in the incorporation of H2A.Z reached about 1.5-fold within 6 hours at the +1 nucleosomes, appearing milder compared to the changes at *Igll1*. The data suggested that Ikaros mediates H2A.Z incorporation during gene repression. In contrast, the involvement of H2A.Z at the up-regulated genes appeared to be the other way around. At the positively regulated *Lig4* and *Zfp36* loci, decreases of H2A.Z were observed (Figure 5.6). Whilst only ~20% reduction in H2A.Z involvement was observed at the -2 nucleosome at the *Zfp36* locus, nucleosomes surrounding the *Lig4* TSS showed reduced H2A.Z involvement as soon as 15 minutes after Ikaros induction and reached 40~60% reduction within 6 hours.

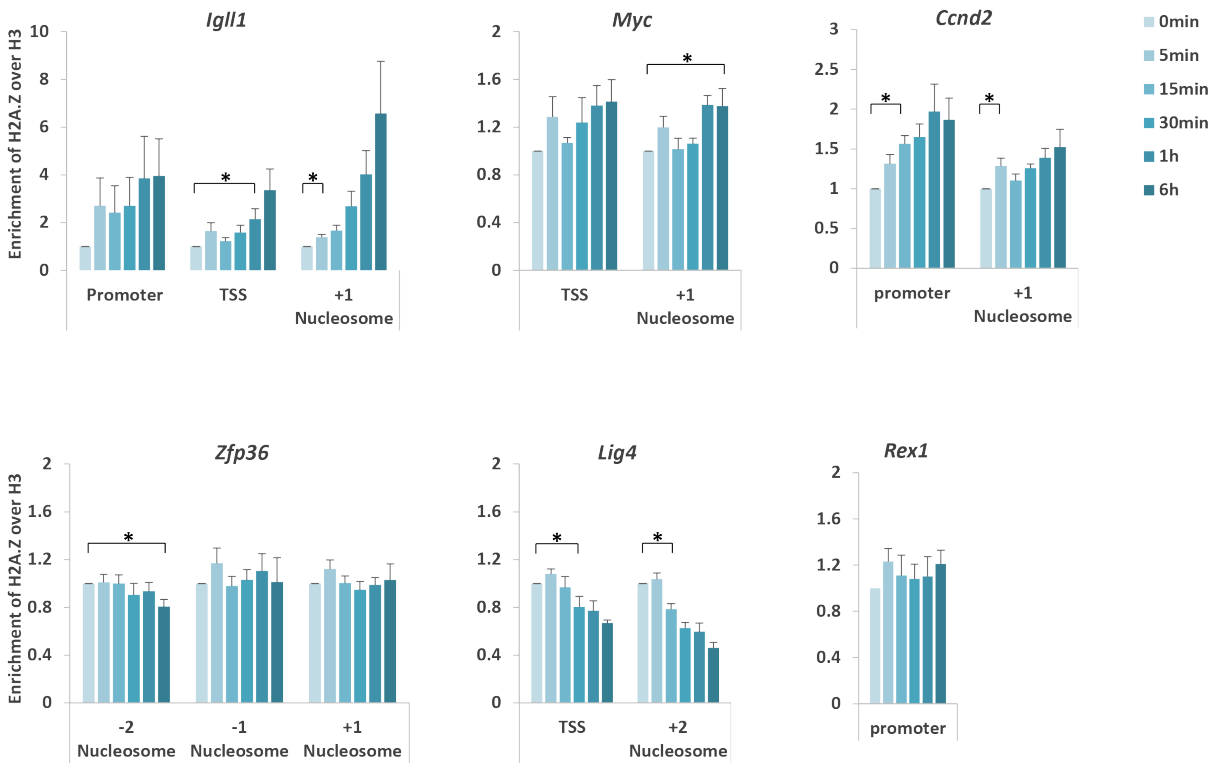

Figure 5.6 Kinetics of the changes in H2A.Z mediated by Ikaros

Graphs show H2A.Z involvement at promoters of Ikaros-regulated (top panel being down-regulated, bottom panel being up-regulated) and control loci (bottom right), after 0min, 5min, 15min, 30min, 1h and 6h of Ikaros induction. Data shown was an average of three biological replicates. P value: *<0.05.

Canonical histone H2A was also examined after Ikaros induction (Figure 5.7). At the down-regulated *Igll1* and *Myc* loci, contrasting the increased involvement of variant H2A.Z, decreases in canonical H2A were observed at the nucleosomes surrounding the TSSs. While the decrease was significant but mild at *Igll1*, the strongest and fastest change was observed at the *Myc* locus. An 'inconsistent' increase of H2A involvement was observed at the *Ccnd2* promoter (interpreted later, Figure 5.8). At the up-regulated loci, significantly increased involvement of H2A was observed near the TSSs (Figure 5.7). In general, the changes of H2A.Z and H2A were mainly opposite to each other, although not perfectly complementary in either fold change or kinetics.

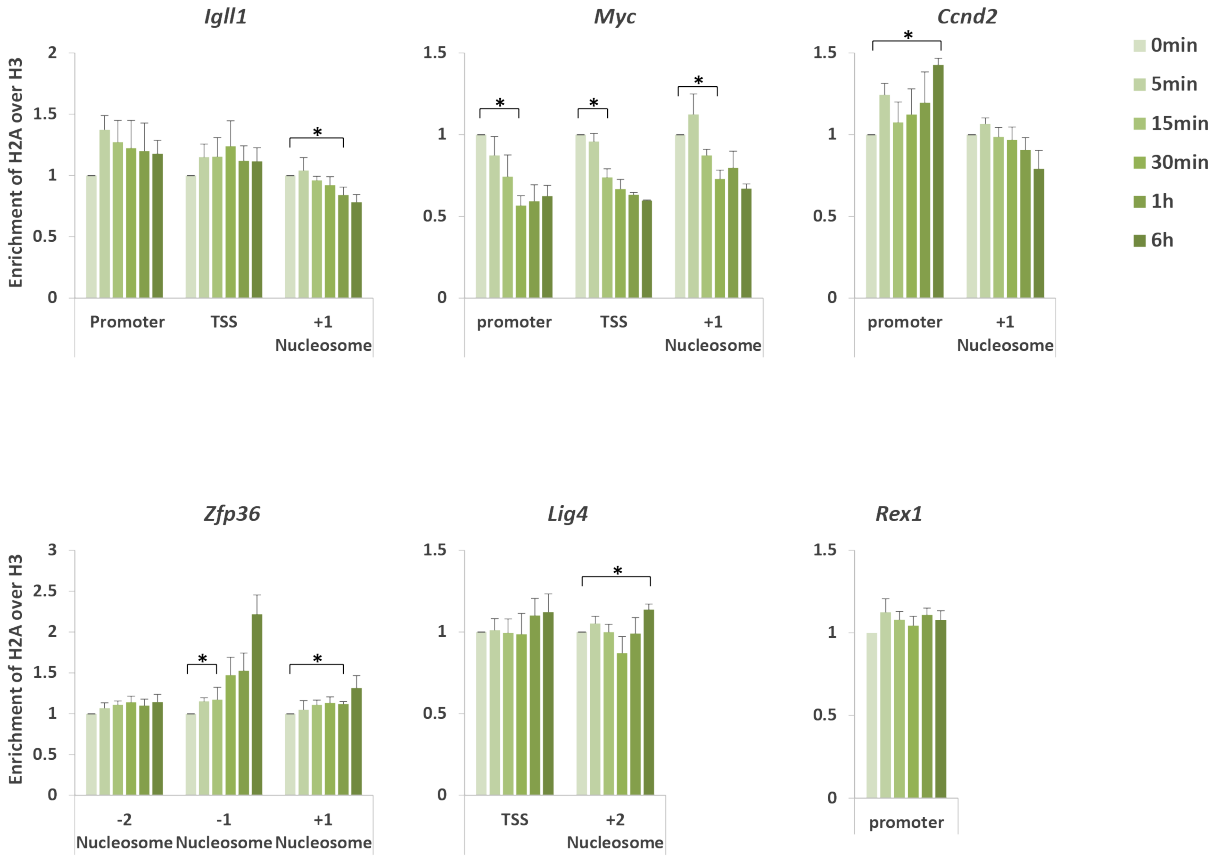

Figure 5.7 Kinetics of the changes in H2A mediated by Ikaros

Graphs show H2A.Z involvement at promoters of Ikaros-regulated (top panel being down-regulated, bottom panel being up-regulated) and control loci (bottom right), after 0min, 5min, 15min, 30min, 1h and 6h of Ikaros induction. Data shown was an average of three biological replicates. P value: *<0.05.

The non-perfect but roughly complementary changes in H2A.Z and H2A lead to the question whether there was an active exchange between the canonical histone H2A and histone variant H2A.Z. Histone H2A and variants are deposited or removed as (H2A-H2B) dimers (Burgess and Zhang, 2013; Luk et al., 2010; Morrison and Shen, 2009; Ranjan et al., 2013). Considering that Ikaros mediates the changes in nucleosome integrity (Figure 5.5), it was a better idea to answer this question by normalizing histone H2A.Z or H2A to H2B, thus correcting for the number of (H2A-H2B) dimers in the nucleosome.

Remarkably, the increased incorporation of H2A.Z at the *Igll1* locus was still observed after normalizing to H2B (Figure 5.8A). This suggested that the increase is not only due to nucleosomes getting more fully composed, but that there is a selective incorporation of H2A.Z. This was accompanied by minor loss of H2A (Figure 5.8A). Similar effects were observed at the *Myc* and *Ccnd2* loci (Figure 5.8B, C). This supported the idea that there is an active exchange of H2A.Z for H2A during Ikaros-mediated transcriptional repression. Interestingly, the 'inconsistent' increase of H2A at the *Ccnd2* promoter was gone after normalizing to H2B, suggesting that the increase was because the nucleosomes were getting fully composed. In contrast, the exchange of H2A.Z for H2A was not observed at the up-regulated loci of *Lig4* and *Zfp36* or the control locus *Rex1* (Figure 5.9).

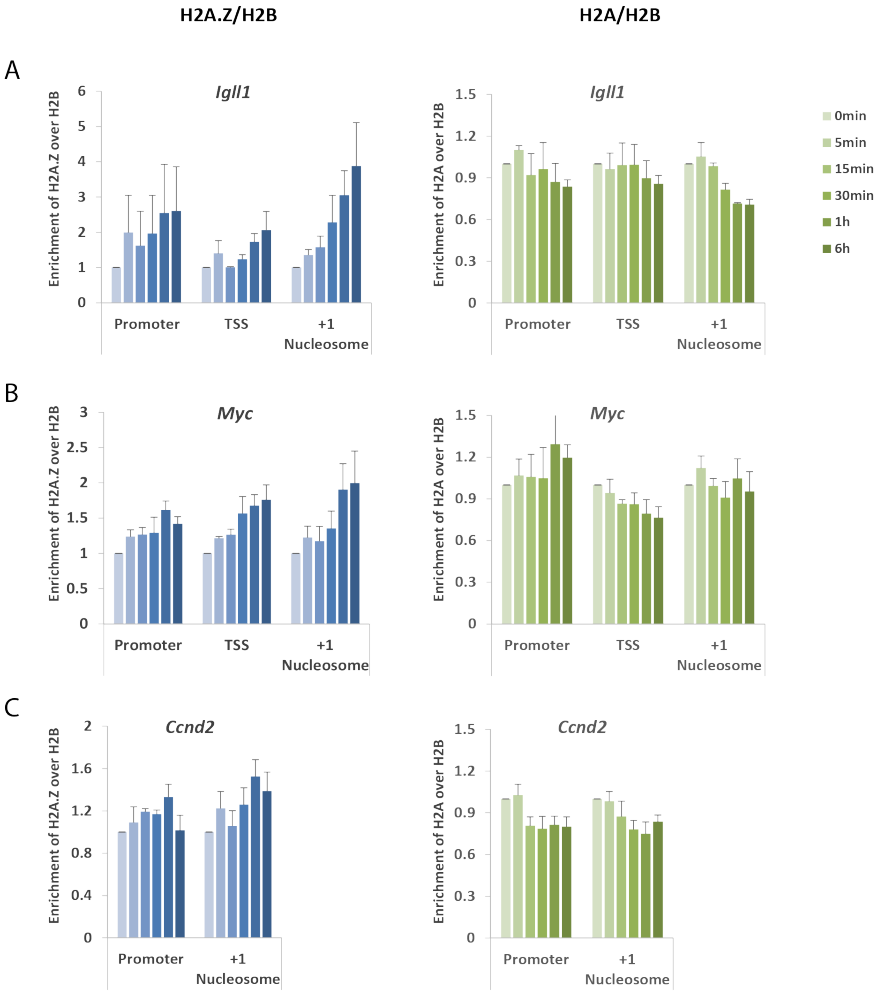

Figure 5.8 Kinetics of the exchange between histone H2A.Z and H2A mediated by Ikaros at down-regulated genes

Enrichment of H2A.Z (left) and H2A (right) over H2B at the promoters of down-regulated *Igll1*, *Myc* and *Ccnd2* promoters. Data shown was the average of three biological replicates.

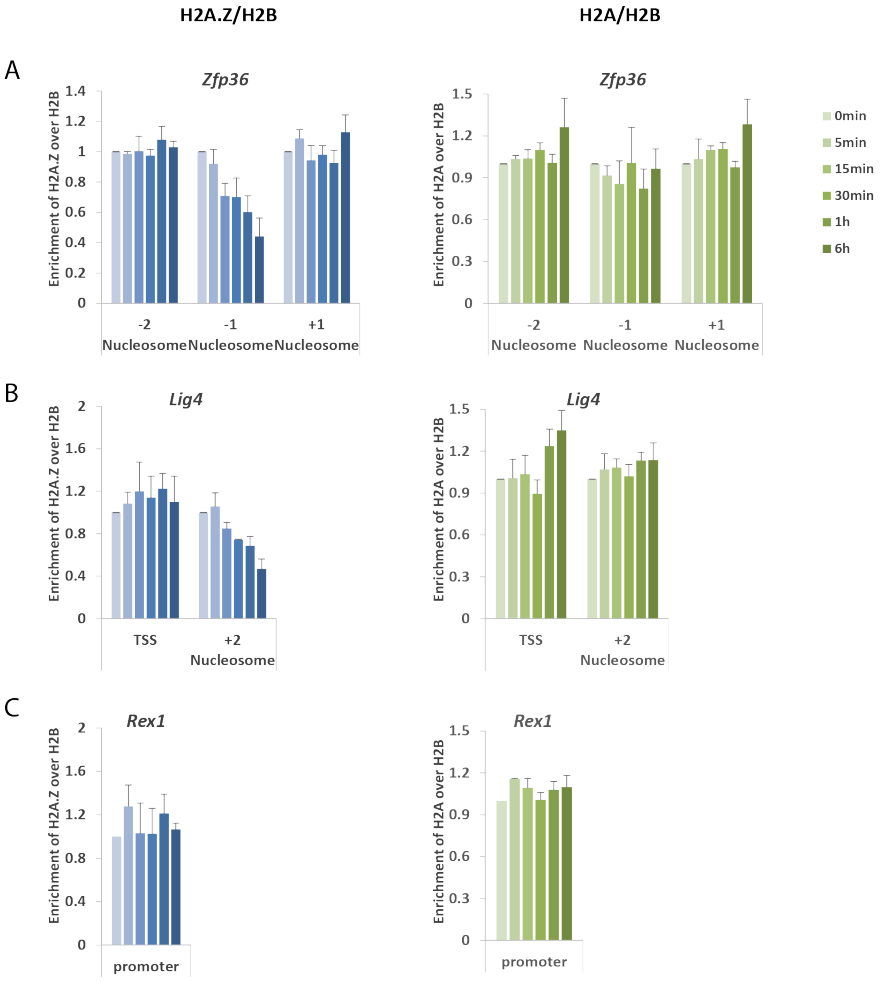

Figure 5.9 Kinetics of the exchange between histone H2A.Z and H2A mediated by Ikaros at up-regulated and control genes

Enrichment of H2A.Z (left) and H2A (right) over H2B at the promoters of up-regulated *Zfp36*, *Lig4* and control *Rex1* promoters. Data shown was the average of three biological replicates.

Additionally, an individual H2A.Z-nucleosome can contain two H2A.Z histones (homotypic), or one H2A.Z and one H2A (heterotypic). Structural analysis predicts that heterotypic H2A.Z will cause a major structural clash between H2A-H2A.Z interactions, therefore destabilizing the nucleosome (Suto et al., 2000). In mouse trophoblast stem cells, only heterotypic H2A.Z nucleosomes mark the TSSs of active genes (Nekrasov et al., 2012). To examine the composition of H2A.Z-containing nucleosomes, one reliable way is to perform sequential

H2A.Z H2A ChIP (Nekrasov et al., 2012; Weber et al., 2010). Another less accurate way to guess the composition is by comparing the fold changes of H2A/H2B and H2A.Z/H2B. Since chromatin IP is not 100% efficient, it is probably reasonable to assume that homotypic H2A.Z (ZZ) would have a better chance of being IPed using H2A.Z antibody than heterotypic H2A/H2A.Z (AZ). Following this idea, if the increased incorporation of H2A.Z is due to the exchange from AA to AZ, the fold increase in H2A.Z/H2B should be higher than the fold decrease in H2A/H2B. Similar deduction can be used for the exchange from AZ to ZZ: the fold increase in H2A.Z/H2B may still be observed, but it should be less than the fold decrease in H2A/H2B. Another potential source of the increased incorporation of H2A.Z is the exchange from AA to ZZ. In this case, the fold increase in H2A.Z/H2B would ideally be the same as the fold decrease in H2A/H2B. Following this theory, the fold changes of H2A.Z/H2B and H2A/H2B were calculated after 6 hours of Ikaros induction (Figure 5.10). At down-regulated *Igll1* and *Myc*, the fold increases in H2A.Z/H2B were higher than the fold decreases in H2A/H2B, favouring the possibility that the incorporation of H2A.Z happened from AA to AZ.

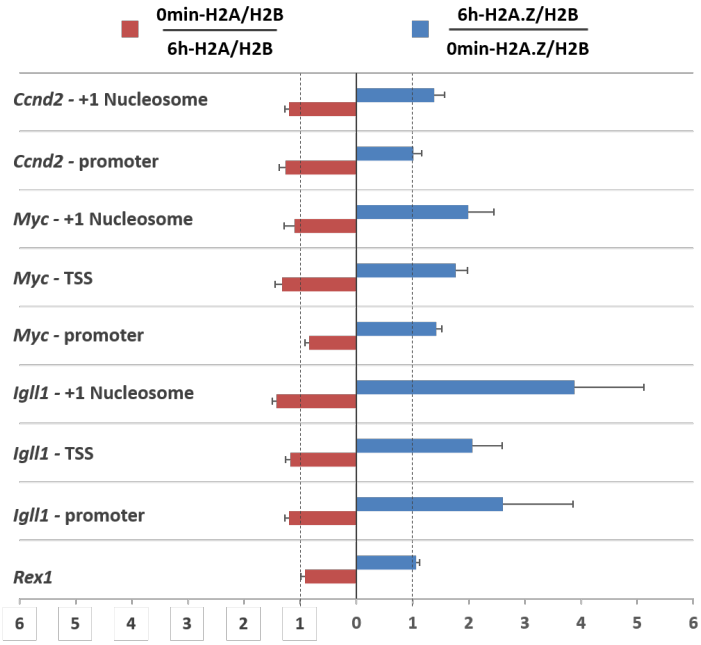

Figure 5.10 Fold change of H2A and H2A.Z enrichment over H2B

Fold decrease of enrichment of H2A over H2B was calculated by normalizing 0min enrichment to 6h enrichment (in red, on the left). Fold increase of enrichment of H2A.Z over H2B was calculated by normalizing 6h enrichment to 0min enrichment (in blue, on the right). Fold change of 1 (no change between 0min and 6h) was marked with dash line. Data shown is an average of three biological replicates.

5.4 Kinetics of changes in histone modifications mediated by Ikaros

Next, I asked whether Ikaros influences histone modifications during transcriptional regulation. Acetylations on the histone H3 and H4 tails were first investigated by MNase-ChIP, using antibodies anti-acetyl-histone H3 (K9, K14, K18, K23, K27) and anti-acetyl-histone H4 (K5, K8, K12, K16).

Histone modification signals were normalized to histone H3 to correct for nucleosome occupancy. Positive and negative controls were examined, where inactive genes showed no enrichment of histone acetylations and good enrichment was observed at active genes (data not shown). The trend of the changes was emphasized by normalizing enrichment signals to the un-induced 0min condition.

After Ikaros induction, a gradual decrease in acetylated histone H3 was observed at the down-regulated *Igll1*, *Myc* and *Ccnd2* promoters (Figure 5.11). The up-regulated *Zfp36* and *Lig4* promoters showed an increase in the acetylation level at histone H3. Similar to histone H3, deacetylation of histone H4 was observed at the down-regulated *Igll1* promoter (Figure 5.12). At the *Myc* and *Ccnd2* loci, deacetylation of H4 appeared mild after Ikaros induction. Meanwhile, increased H4 acetylation was observed at the up-regulated *Zfp36* and *Lig4* promoters.

In general, the data suggested that Ikaros mediates histone deacetylation during gene repression, and facilitates histone acetylation during transcriptional up-regulation. Compared to the kinetics and strength of changes in RNAPII binding and nucleosome occupancy, histone acetylation and deacetylation appeared much milder. It is worth noting that there was an increase of acetylation level after 5 minutes of Ikaros induction at the *Igll1* promoter. This was likely due to technical reasons, which will be further discussed in section 5.6 (Figure S2).

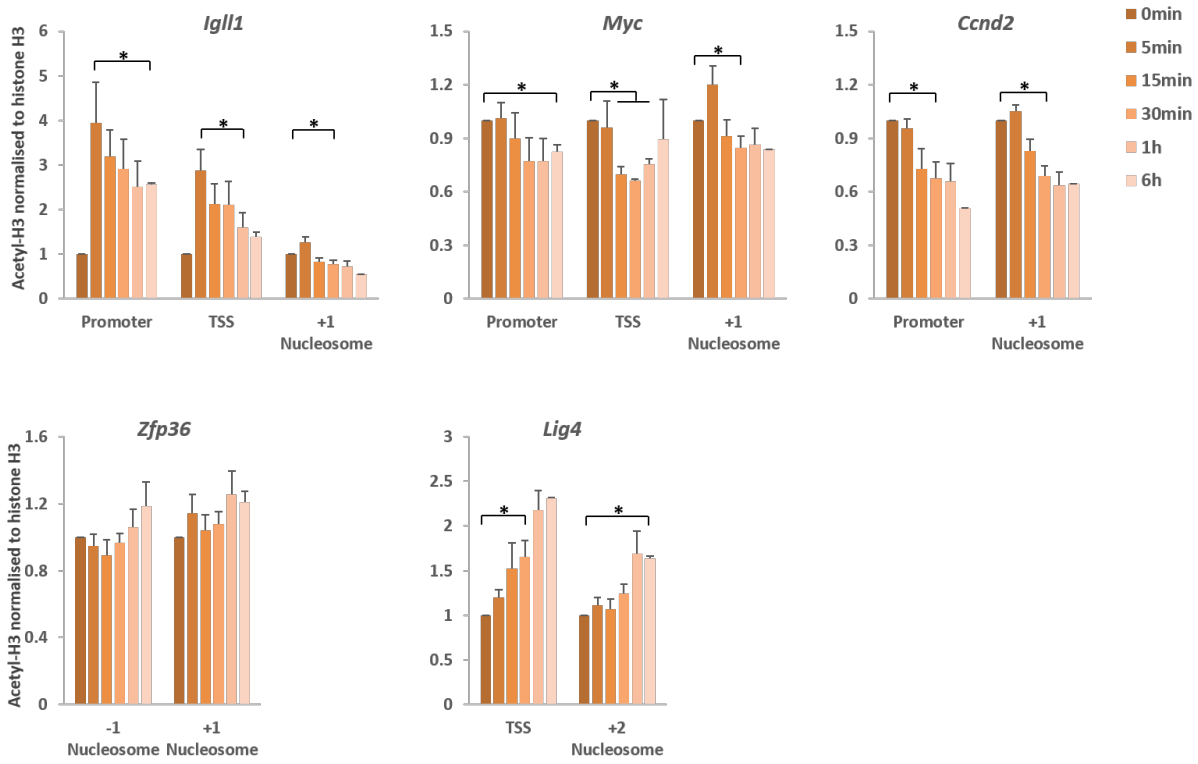

Figure 5.11 Kinetics of changes in acetyl-histone H3 mediated by Ikaros

Graphs show acetyl-histone H3 at the promoters of Ikaros-regulated genes (top panel being down-regulated, bottom panel being up-regulated) after Ikaros induction. Data shown here was the average of five biological replicates. P value: *<0.05.

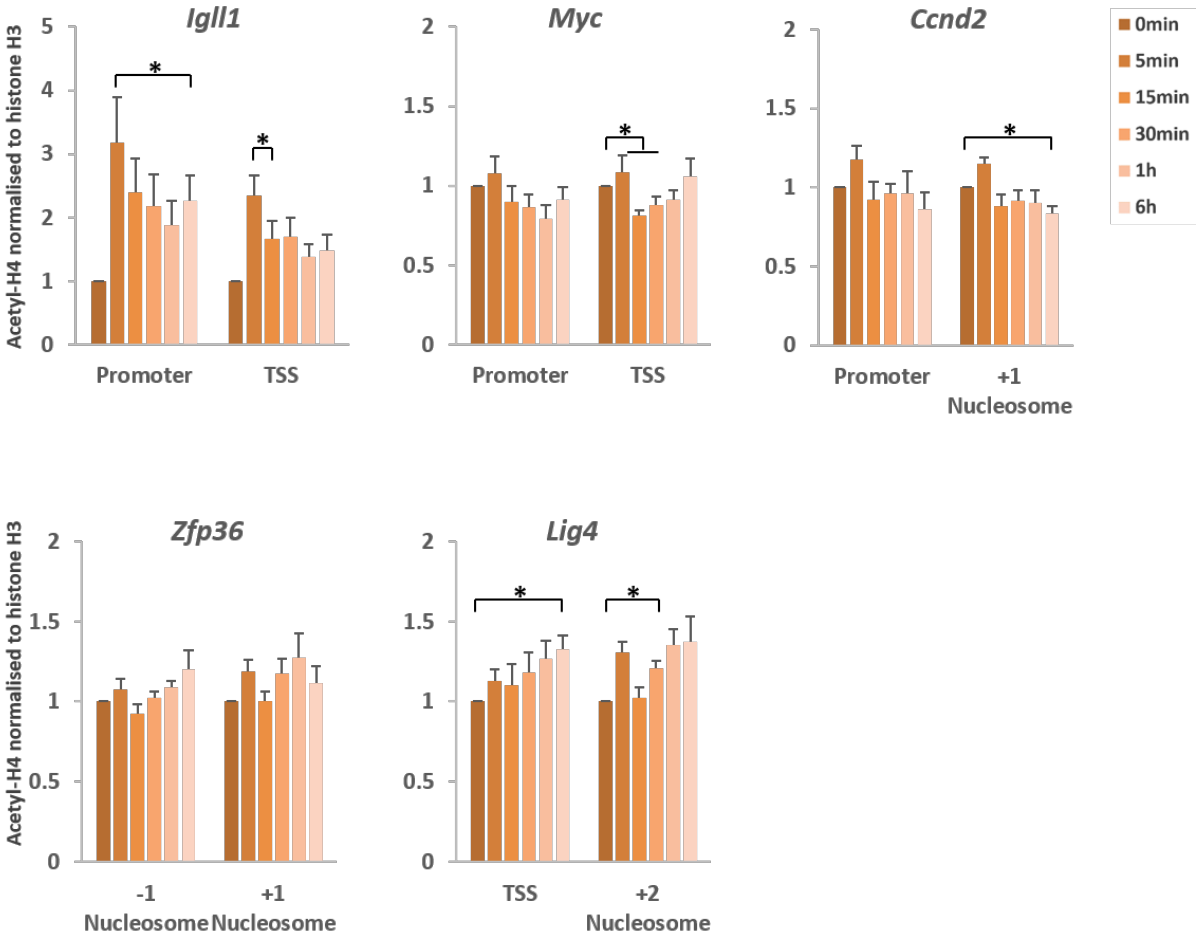

Figure 5.12 Kinetics of changes in acetyl-histone H4 mediated by Ikaros

Graphs show acetyl-histone H4 at the promoters of Ikaros-regulated genes (top panel being down-regulated, bottom panel being up-regulated) after Ikaros induction. Data shown here was the average of five biological replicates. P value: *<0.05.

Following this, another well characterised active histone mark, H3K4Me3 was examined (Figure 5.13). A minor decrease was observed at the *Igll1* promoter, while the *Myc* and *Ccnd2* promoters remained mostly unchanged. A subtle increase was observed at the up-regulated *Zfp36* promoter. In general, the changes in H3K4Me3 appeared slow and mild, suggesting that methylation or demethylation of H3K4 is not an early event during Ikaros-mediated transcriptional regulation.

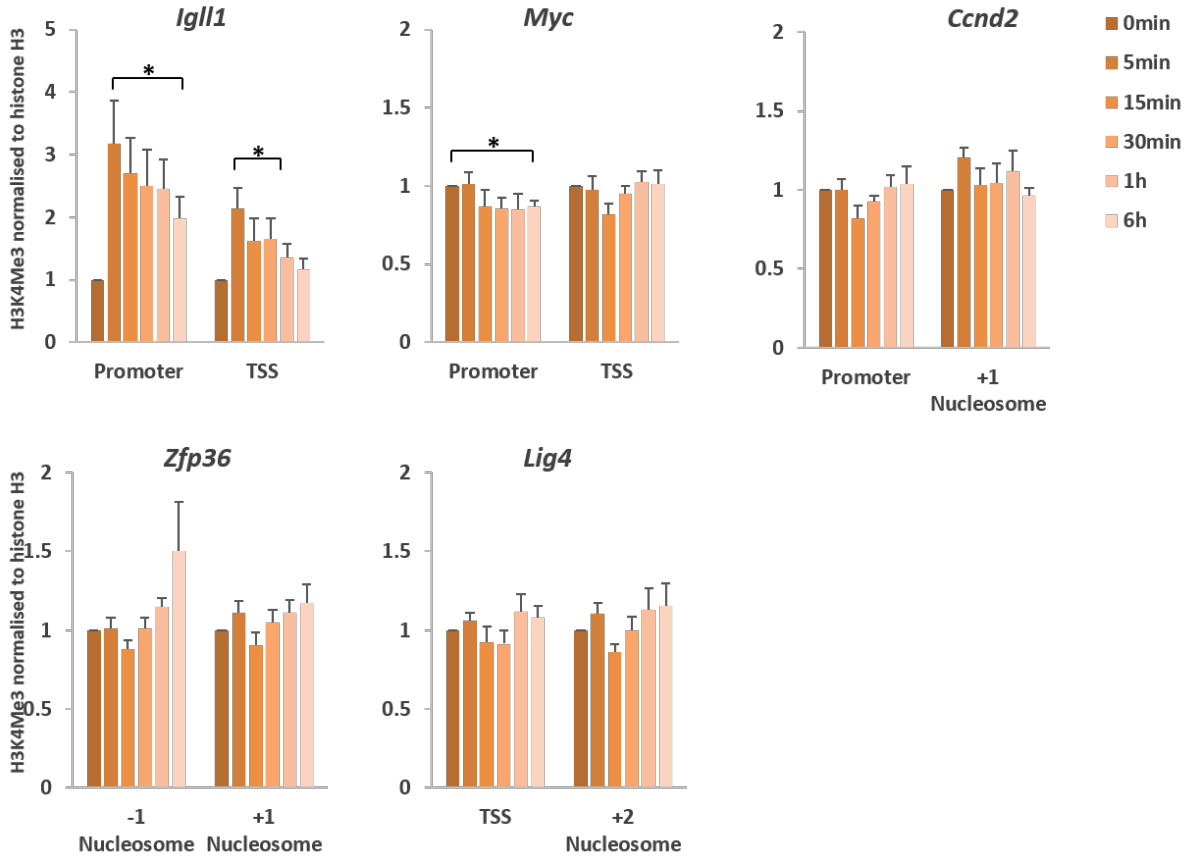

Figure 5.13 Kinetics of changes in H3K4Me3 mediated by Ikaros

Graphs show histone modification H3K4Me3 at the promoters of Ikaros-regulated genes (top panel being down-regulated, bottom panel being up-regulated) after Ikaros induction. Data shown here was the average of five biological replicates. P value: *<0.05.

In terms of repressive histone marks, attempts have been made to examine H3K9Me3. However, it was technically unsuccessful. I used a widely accepted antibody for ChIP (ab8898), but my ChIP result did not discriminate positive loci from negative loci after normalizing to histone H3 signals, either in mouse ESCs or B3 pre-B cells.

5.5 The order of events

Ikaros regulates transcription of its target genes through a variety of regulatory events. Ikaros modulates the binding of RNAPII and nucleosome occupancy at regulated promoters. Additionally, Ikaros also influences the composition of nucleosomes and post-translational modifications on histones.

In general, changes at the down-regulated promoters appeared stronger than the up-regulated gene promoters. More importantly, the kinetics of these changes were monitored at high temporal resolution. Based on the kinetics, the order of events was comprehended at the model locus *Igll1* (Figure 5.14). RNAPII binding and nucleosome occupancy at this promoter appeared to respond the fastest after Ikaros induction. Not only were the changes significant only after 5 or 15 minutes of induction, but the strongest level of regulation was achieved early. Here, I used the shape of a growth curve, including lag phase, log phase, and stationary phase (Figure S1), to help discriminate and illustrate the trend and timing of these regulatory events. It looked as if the change in the occupancy of RNAPII and nucleosome started off from 'log phase', and reached 'stationary phase' within at least 1 hour of Ikaros induction. Subsequently, H2A.Z was incorporated at the promoter proximal region. This increase seemed to start from the 'lag phase', and the 'log phase'-like increase appeared perhaps after 30 minutes of Ikaros induction. The change in H2B was even slower than H2A.Z incorporation. Histone deacetylation and the decrease of H3K4Me3 showed almost linear changing curve. As the transcription output, *Igll1* gene expression started with a short 'lag phase', and then progressed into 'log phase'. There seemed to be a minor delay of the kinetics of transcription compared to that of RNAPII binding, consistent with biological expectations. The *Myc* locus presented a similar order of events (data not shown).

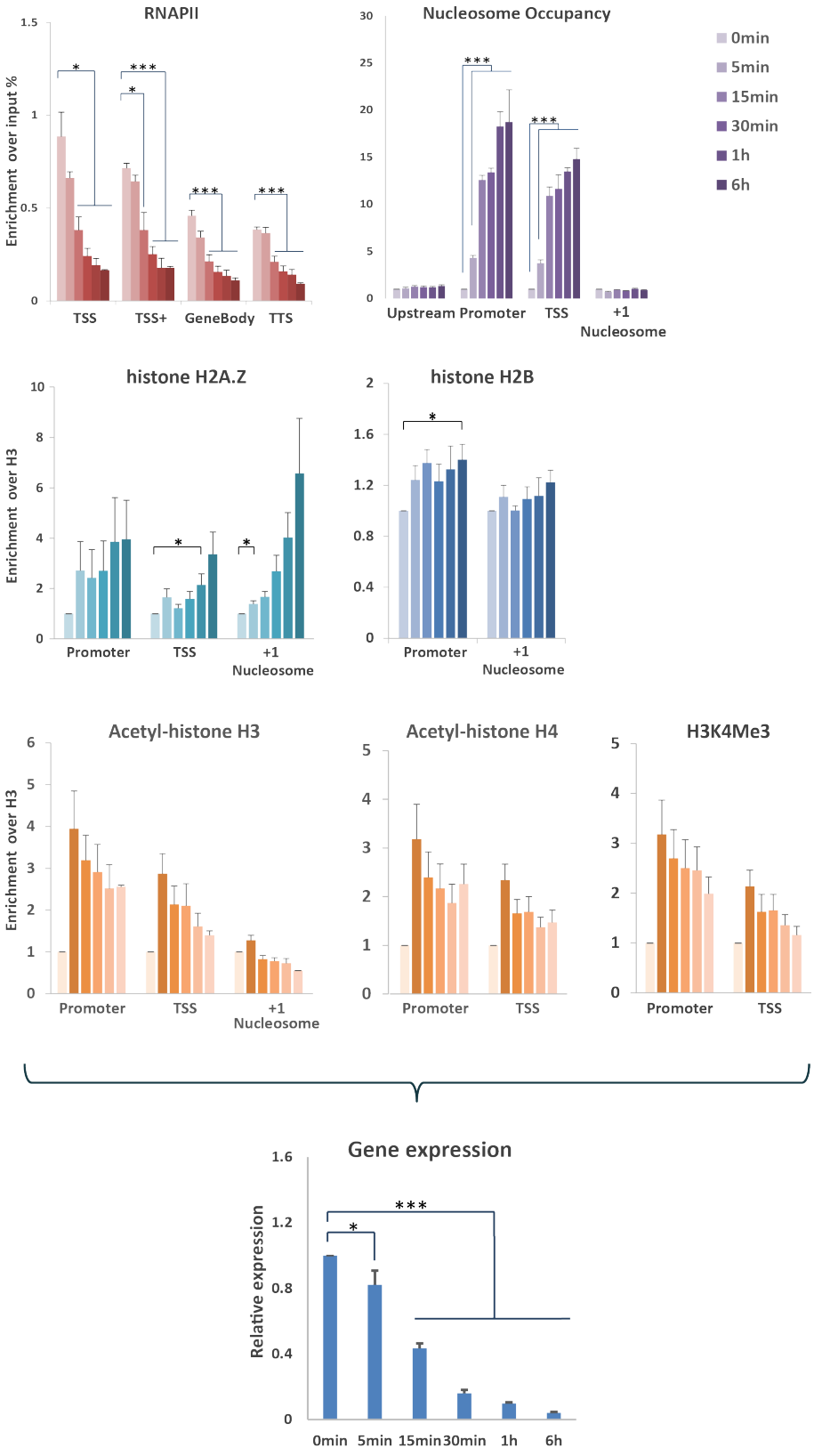

Figure 5.14 The order of regulatory events during Ikaros-mediated *Igll1* repression

Graphs shows changes in RNAPII and nucleosome density (top), nucleosome composition (middle), and histone modifications (bottom) during Ikaros-mediated Igll1 repression (the end)

To interpret the order from a different way, fold changes of the regulatory events were plotted against time after Ikaros induction. The kinetics of RNAPII binding and mRNA expression were first compared (Figure 5.15A). The trend lines that best fit were polynomial algorithm by the order of 2. Comparison of the fitted trend lines showed that the changes of RNAPII appeared earlier than those in mRNA. Next, similar analysis was applied to the kinetics of changes in nucleosomes surrounding the TSS. The increase in nucleosome occupancy appeared ahead of the incorporation of H2A.Z and the increase in histone H2B (Figure 5.15B). Using this method however, it was difficult to compare increased changes to decreased ones. So the kinetics of changes in RNAPII and nucleosome occupancy were not compared.

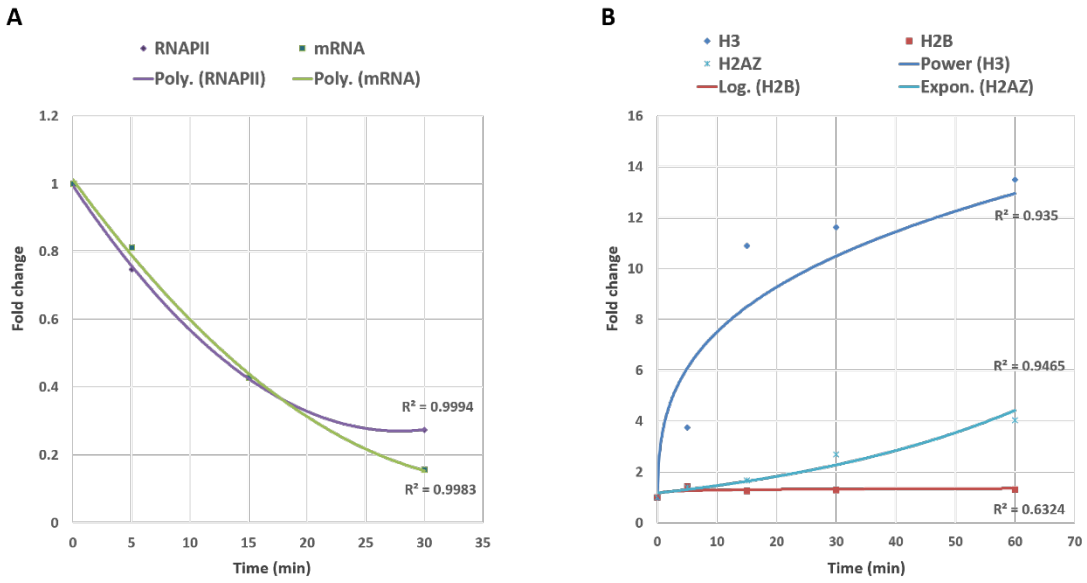

Figure 5.15 Interpretation of the order of regulatory events using fitted trend lines

The observed fold changes in chromatin status was plotted against time of Ikaros induction, and the best fitting trend lines were calculated. (A) compares RNAPII to mRNA. (B) compares nucleosome occupancy measured by H3, nucleosome intactness measured by H2B/H3, and incorporation of H2A.Z at the nucleosome closest to *Igll1*'s TSS.

In summary, based on the kinetics of changes in regulatory events during Ikaros-mediated transcriptional repression, the regulation of RNAPII and nucleosome occupancy appeared to happen early. Subsequently, active histone modifications were reduced and H2A.Z was incorporated.

5.6 Discussion

The order of regulatory events

The study of the order of regulatory events is important to understand the process of transcriptional regulation. It has the advantage of inferring possible causal relationships between these events without perturbing the system. However, the order is difficult to clarify due to the lack of high temporal resolution. In mammalian cells, the order of regulatory events has been monitored along the developmental process. For example, during the differentiation of ESCs to endoderm/hepatic progenitor cells, activation of the developmental genes first requires H2A.Z-mediated binding of the transcription factor Foxa2. Foxa2 then recruits chromatin remodelers to H2A.Z-containing nucleosomes, and this subsequently leads to the loss of these nucleosomes and eventually transcriptional activation (Li et al., 2012). In another study, Crabtree and colleagues reported the sequential process of HP1-mediated gene silencing at the resolution of days. This process involves the early increase of H3K9Me3 and loss of H3K4Me3, followed by a gradual loss of H3K27Ac and much later, DNA methylation (Hathaway et al., 2012). In *Drosophila*, the activation process of a heat shock gene *Hsp70* has been studied at high temporal resolution (Petesch and Lis, 2008). Lis and colleagues showed that the loss of nucleosomes at the gene body occurs first within 30 seconds of heat shock, and is independent of RNAPII binding. However, the relevance of this observation to mammalian cells remains to be tested.

In this study, the changes in chromatin status mediated by Ikaros were not only evaluated, but also timed at a high temporal resolution. The down-regulated genes were more sensitive to Ikaros induction compared to the up-regulated, in terms of the response time and the strength of regulation. Therefore, I focused on transcriptional down-regulation, and used *Igll1* and *Myc* as model loci.

To interpret the order of the regulatory events, their kinetics curves were compared, rather than the first time point when significant changes were first observed. This is because each aspect of chromatin status is evaluated using different techniques, or different antibodies. This introduces different levels of technical variation that biological changes need to overcome in order to appear significant. Giving credibility to the interpretation by comparing kinetics curves, the kinetic curve of gene expression showed a minor delay compared to that of RNAPII binding. Among the regulatory events examined, the regulation of RNAPII

binding and promoter accessibility appeared early. Subsequently, histone deacetylation and the decrease in H3K4Me3 were observed, as well as the incorporation of H2A.Z.

Interestingly, genome-wide profiling of chromatin status showed that the occupancy of RNAPII and nucleosomes are negatively correlated around TSSs. From kinetics studies here, it is still difficult to distinguish which of these two regulatory events happens first. The anti-correlation and the similar kinetics in the regulation of RNAPII and nucleosomes have heated up the question of whether both events are directly or independently regulated by Ikaros.

The incorporation of histone variant H2A.Z during gene repression

H2A.Z favours the destabilisation of nucleosomes *in vivo*, and is associated with transcriptional activation (Weber and Henikoff, 2014). It is therefore surprising to see the substitution of H2A.Z for H2A during Ikaros-mediated transcriptional repression. Further investigation is required to understand the role of H2A.Z.

First, an individual H2A.Z-nucleosome can contain two H2A.Z histones (homotypic), or one H2A.Z and one H2A (heterotypic). Preliminary examination favours the possibility that the incorporation of H2A.Z happened from AA to AZ (Figure 5.10). This does not help explain the incorporation of H2A.Z during Ikaros-mediated gene repression, as heterotypic H2A.Z is predicted to favour the destabilisation of the nucleosomes (Suto et al., 2000).

Recently, more attention has been brought to the acetylation of H2A.Z. In mouse ESCs, acetylated histone H2A.Z correlates with transcriptional activities better than total H2A.Z (Hu et al., 2013). Similar results were also seen in human cancer cells (Valdes-Mora et al., 2012), supporting the idea that acetylated H2A.Z is more responsible for transcriptional activation. Furthermore, even when H2A.Z/H3.3 containing nucleosomes are strongly unstable *in vivo*, nucleosome containing only H2A.Z does not have dramatic alterations in their stability (Jin and Felsenfeld, 2007). Taken together, the nucleosome destabilizing ability of H2A.Z could be due to a combination of the composition and post-translational modifications of nucleosomes.

The major role of H2A.Z in transcription is poising genes for activation and facilitating the opening of chromatin. Although a loss of H2A.Z might be observed upon activation, it is usually attributed to the loss of the H2A.Z marked nucleosome (Conerly et al., 2010; Li et al., 2012; Papamichos-Chronakis et al., 2011; Zhang et al., 2005a). In this sense, to poise a gene

for activation, an incorporation of H2A.Z may be observed. Indeed, this was seen in a study from Craig Peterson's lab (Papamichos-Chronakis et al., 2011). In yeast, the expression of *KAR4* is oscillated during the cell cycle, with it being inactive in G2/M and active in G1. At the *KAR4* promoter, H2A.Z is more enriched when *KAR4* is inactive than when it is active. Dr Peterson explains it as H2A.Z marking and poising the genes for activation during cell cycle progression (personal communication).

In the case of Ikaros-mediated gene repression, incorporation of H2A.Z was observed at all the *Igll1*, *Myc* and *Ccnd2* loci in B3 pre-B cells. *Igll1* encodes for pre-BCR component λ5, which need to be silenced upon differentiation (Merkenschlager, 2010). It is therefore biologically unlikely that H2A.Z needs to poise *Igll1* for reactivation. In addition, *Myc* and *Ccnd2* facilitate cell cycle progression, but they won't be immediately needed upon differentiation (Clark et al., 2014).

It is possible that H2A.Z incorporation is due to the fact the histone variants are expressed in all cell cycle stages. They are probably most available to close up active promoters when transcriptional repression occurred outside of S phase. To address this possibility, it is important to examine the incorporation of H2A.Z mediated by Ikaros at different cell cycle stages.

Finally, it is important to entertain the possibility of H2A.Z being actively involved in Ikaros-mediated gene repression. To this end, it would be useful to examine transcriptional regulation by Ikaros in H2A.Z-deficient cells. Attempts have been made to knockdown H2A.Z in B3 cells using shRNA and siRNA. However, it has not yet been successful. In the future, this question is worth further investigation.

A technical issue of histone modification ChIP at the *Igll1* locus

It is unusual to see a dramatic increase in histone acetylation after 5 minutes of Ikaros induction at the *Igll1* locus. The acetylation levels observed later seemed more comparable to that after 5 minutes of Ikaros induction, rather than 0 minutes (Figure 5.11, 5.12). After careful examination, the 'jump' of the acetylation level after 5 minutes of Ikaros induction was likely due to technical issues.

To focus on the processes of acetylation and deacetylation, the levels of histone acetylation were normalised to histone H3 to correct for nucleosome occupancy. Before Ikaros induction,

the *Igll1* promoter was almost totally depleted of nucleosomes (Figure 4.8). The low enrichment of H3 at 0min was likely to compromise the normalisation. Since Ikaros induction rapidly increased nucleosome occupancy at the promoter (Figure 5.3), H3 enrichment measured after 5 minutes of induction was able to bring the normalisation to an accurate range.

This is supported by the following observations. First, the jump from 0min to 5min was only strongly observed at the *Igll1* promoter, where nucleosomes were highly depleted before induction (Figure 4.8), and dramatically increased after Ikaros induction (Figure 5.3). Second, this hypothesis was tested using sonicated chromatin for ChIP. MNase treatment breaks down chromatin to mostly mono-nucleosomes, leaving sharp nucleosome boundaries. Sonication, however, breaks down chromatin randomly. Therefore, sonicated chromatin fragments are likely to contain more than one nucleosome. In this sense, sonicated chromatin would contain higher background, and consequently make it easier to meet the requirement for accurate normalisation. In support of this, whilst a 15-20 fold increase in nucleosome occupancy was observed using MNase-qPCR or MNase-ChIP at the *Igll1* promoter, only a 4-fold increase was observed using sonicated chromatin (Figure S.2A). This suggested that ChIP using sonicated chromatin contains higher background. Following this, using sonicated chromatin, histone modification ChIP data from two biological replicates showed that the jump from 0min to 5min was almost gone (Figure S.2B).

Admittedly, I still cannot rule out the possibility that the 'jump' is a biological response to Ikaros induction. It is possible that when Ikaros needs to bring in nucleosomes to close up the *Igll1* promoter, nucleosomes surrounding this active transcription environment, which may be carrying acetylation marks, are recruited. Subsequently, histone deacetylation processes come into action to facilitate transcriptional repression. In this case, a 'jump' followed by deacetylation can also be observed.

6 Mechanisms of Ikaros-mediated regulatory events

The kinetics of changes in regulatory events during gene repression suggested that the regulation of RNAPII binding and nucleosome occupancy happens early, and the changes in nucleosome composition and histone modifications occur later. However, this order needs to be further tested; and more importantly, it remains an unanswered question whether the temporal order of these events is a reflection of causal relationships. Here, I first investigated the relationship between the early regulation of RNAPII binding and nucleosome occupancy. After this, the contribution of the later histone deacetylation to transcriptional down-regulation was tested.

6.1 Nucleosome regulation does not depend on RNAPII density

The changes in nucleosome and RNAPII occupancy mediated by Ikaros appeared to follow similar kinetics in an anti-correlated manner (Figure 4.8, 5.2, 5.3). It is possible that nucleosomes and RNAPII are both directly and independently regulated by Ikaros. It is also possible that Ikaros controls only one event. When nucleosomes and RNAPII actively compete for DNA binding at the promoters, the other event is consequently changed.

To test whether the increase in nucleosome occupancy during Ikaros-mediated gene repression is a consequence of reduced RNAPII density, nucleosome occupancy after Ikaros induction was monitored under the condition where the influence of RNAPII was ruled out through its targeted degradation. To degrade RNAPII *in vivo*, triptolide (TPL) was used. Triptolide is a diterpene triepoxide isolated from a traditional Chinese medicine. It inhibits the ATPase activity of TFIIH subunit XPB, and longer or stronger treatment leads to proteasome-dependent Rbp1 degradation (Manzo et al., 2012; Titov et al., 2011; Vispe et al., 2009; Wang et al., 2011), and therefore it has been used to block RNAPII initiation (Henriques et al., 2013; Jonkers et al., 2014).

To achieve rapid RNAPII degradation in B3 cells, cells were treated with 1μM TPL. The degradation conditions were tested after 30 minutes, 1 hour, 2 hours, 3 hours and 4 hours of

TPL treatment, and the cells treated with DMSO, the carrier for TPL, were used as a control. The kinetics of degradation were analysed by western blot (Figure 6.1A). Cells treated with TPL showed decreased RNAPII signal after 2 hours of treatment, and almost all RNAPII signal was gone after 3 hours of treatment.

Next, to make sure that the reduction of RNAPII protein was functional, mRNA production was examined. From the same number of cells, a mild decrease of total mRNA quantity was observed after 2 hours of TPL treatment (data not shown). In addition, assuming the degradation is functional, short lived mRNA should be more affected than long lived mRNA, and for an individual gene, primary transcripts should show more dramatic changes than mature transcripts. Therefore, mRNA from the same number of cells treated with DMSO or TPL was used for transcription analysis (Figure 6.1B). As the TPL treatment progressed, mRNA levels of all genes examined were reduced, consistent with the reduction in the quantity of total mRNA. More importantly, short lived mRNA *Ccnd2* and *Myc* showed earlier reduction than long lived housekeeping genes *Gapdh* and *Ubc*, and the *Igll1* primary transcripts decreased faster than its mature transcripts. The minor increases after 30 minutes of TPL treatment at *Gapdh, Ubc* and *Igll1* were likely due to a bias in cell counting. In brief, TPL was shown to efficiently degrade RNAPII and impair transcription in B3 cells.

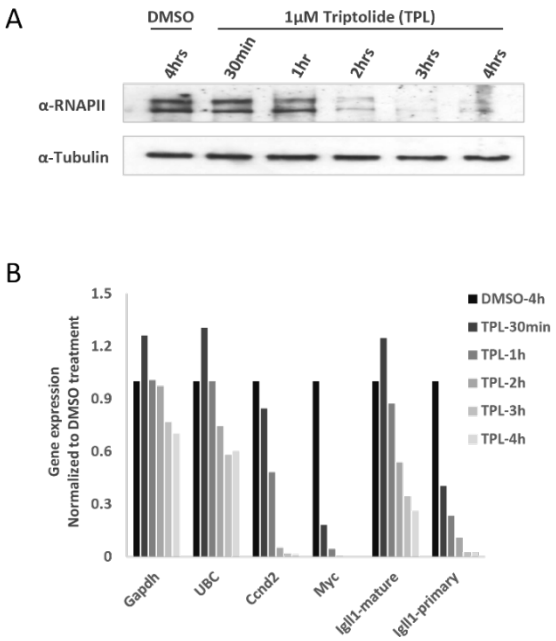

Figure 6.1 Triptolide (TPL) is used to degrade RNAPII

B3 cells were tested with 1μM TPL treatment for 30 minutes, 1 hour, 2 hours, 3 hours and 4 hours. Carrier DMSO was used as control. RNAPII degradation was analysed by (A) western blotting and (B) gene expression analysis by qPCR.

To balance the efficiency of RNAPII degradation and the risk of dramatic cellular changes due to impaired transcription, inducible Ikaros B3 cells were pre-treated with TPL for 3 hours to degrade RNAPII. DMSO treatment was included as a control. After the pre-treatment, Ikaros was induced in a time course of up to 1 hour (Figure 6.2A). To assess the efficiency of RNAPII degradation, RNAPII binding at the TSSs of Ikaros target genes was first evaluated by ChIP-qPCR (Figure 6.2B). In cells treated with DMSO, RNAPII was enriched at the promoter of the active control gene *Actb*, but not the promoter of the inactive *Rex1*. Decreased binding of RNAPII was observed at the down-regulated *Igll1* and *Myc* promoters after Ikaros induction (as in Figure 5.2). In cells treated with TPL, RNAPII binding was abolished at the promoters of all these genes (Figure 6.2B).

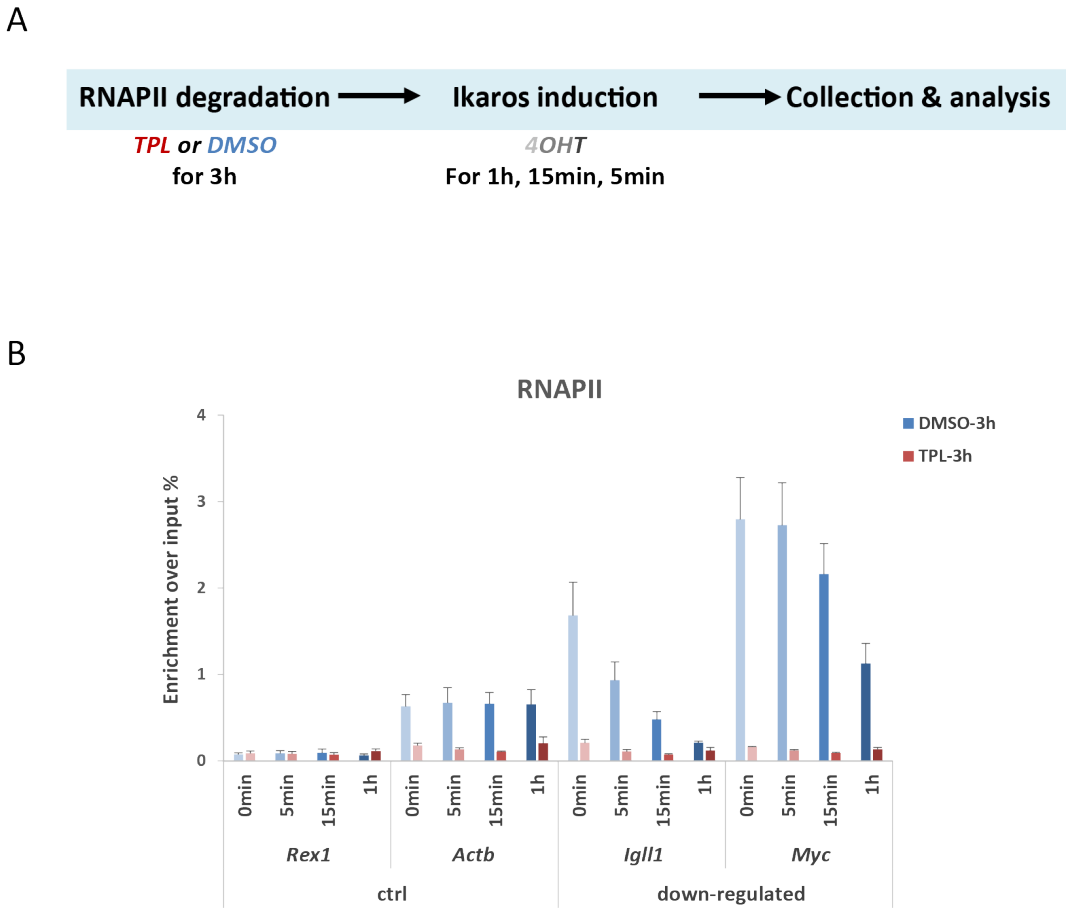

Figure 6.2 RNAPII is efficiently deleted at gene promoters

(A) Schematic design of the RNAPII degradation experiment. (B) RNAPII density at the gene promoters including the negative control *Rex1*, positive control *Actb*, and down-regulated *Igll1* and *Myc*. Graph showed that RNAPII was efficiently deleted with TPL treatment. Data shown was an average of three biological replicates.

Following the efficient degradation of RNAPII, changes in nucleosome occupancy after Ikaros induction were investigated using MNase-qPCR (Figure 6.3). For credibility, analyses of RNAPII binding and nucleosome occupancy were done using the same preparation of chromatin. To focus on whether the increase in nucleosome occupancy was due to RNAPII giving away DNA binding sites, the same primers were used to examine RNAPII binding and nucleosome occupancy at the TSSs. Interestingly, before Ikaros induction (0min), very similar levels of nucleosome occupancy were observed in cells treated with TPL and those treated with DMSO. This suggested that when RNAPII is no longer bound, nucleosomes do not occupy the TSSs of *Igll1* and *Myc*. Therefore, the nucleosome occupancy at these two promoters is highly regulated at the basal level in B3 cells. After Ikaros induction, increases in nucleosome occupancy were observed at the TSSs of *Igll1* and *Myc* in the cells pre-treated with DMSO (as in Figure 5.3). Importantly, TPL treatment did not result in any differences in the kinetics or the fold changes of the increases in nucleosome occupancy at these loci after induction (Figure 6.3). Therefore, at Ikaros negatively regulated model loci *Igll1* and *Myc*, the regulation of nucleosome occupancy was independent of the changes in RNAPII binding. This data suggested that nucleosome occupancy may be directly regulated by Ikaros.

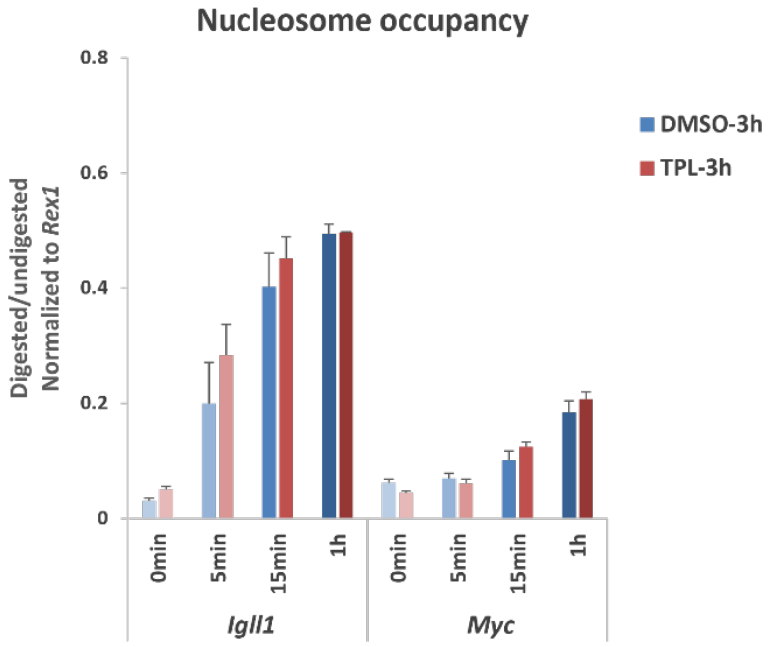

Figure 6.3 Nucleosome occupancy regulated by Ikaros after TPL or DMSO treatment

Graph shows nucleosome occupancy after Ikaros induction with TPL (red) or DMSO (blue) pre-treatment. No significant difference was observed at either baseline level or the kinetics of regulation between control condition and RNAPII degraded condition. This was average of three biological replicates.

6.2 Nucleosome regulation influences transcription by RNAPII

Next, the influence of the changes in nucleosome occupancy on the regulation of RNAPII binding was examined. To this end, instead of creating a histone-deficient condition, the regulation of nucleosome was interfered with to dissect its influence on the modulation of RNAPII binding. To interfere with the regulation of nucleosomes, it was important to find the chromatin remodeler(s) that work with Ikaros. Mi-2β, the catalytic subunit of the Mi-2/NuRD complex, is a top candidate. Ikaros and Mi-2β co-regulate the expression of *Cd4* during T cell development (Naito et al., 2007). Mi-2β co-localizes with Ikaros in thymocytes and pro-B cells (Schwickert et al., 2014; Zhang et al., 2012), and in B3 cells, Ikaros was shown to interact with Mi-2β by co-IP (Ben Taylor, unpublished).

First, Mi-2β was silenced in B3 cells via RNA interference (Ramirez-Carrozzi et al., 2006). In brief, shRNA sequence against the Mi-2β gene (*Chd4*) was inserted into a pQsupR retroviral plasmid (Figure 6.4A). The plasmid also contained GFP and puromycin N-acetyl-transferase (PAC) conferring puromycin resistance. To distinguish the transduction of inducible Ikaros and Mi-2β shRNA (both containing GFP), I replaced the original fluorophore GFP in the inducible Ikaros plasmid to mCherry (details in section 2.2.3) (Figure 6.4B), and generated mCherry positive B3 cells expressing inducible Ikaros. Following that, these cells were infected with retroviral particles containing shRNA targeting Mi-2β. After infection, approximately 10% of GFP positive cells were obtained under optimised conditions. Additionally, knock-down of Mi-2β was lethal to B3 cells. Therefore, the cells after one day of shRNA infection were supplemented with 20μM pan caspase inhibitor in culture, thus blocking cell apoptosis at an early stage. This dosage of pan caspase inhibitor was optimised to be able to block programmed cell death, while the concentration of the carrier DMSO (0.1% final) was not toxic to the cells (data not shown). After 2 days of shRNA infection, the cells were sorted for the GFP positive population using flow cytometry to enrich for shRNA-containing cells. The efficiency of Mi-2β knock-down was examined using western blotting after 1, 2 or 3 days of sorting. The first clean knock-down was observed two days after sorting. Therefore, the sorted GFP positive cells were then kept in culture for 2 days to establish the Mi-2β knock-down condition before Ikaros induction (Figure 6.4C). Each biological replicate started from fresh infection, and Mi-2β knock-down efficiency was individually confirmed using western blotting (Figure 6.4D).

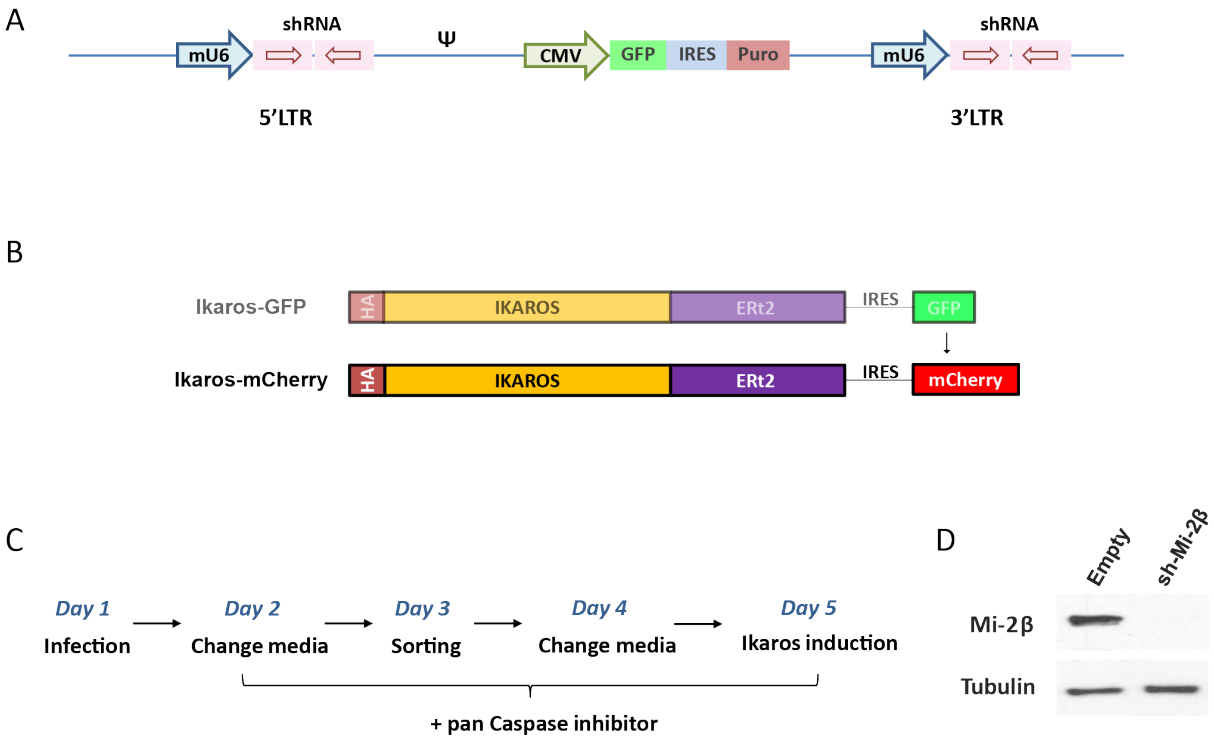

Figure 6.4 shRNA knockdown of Mi-2β

(A) Schematic design of shRNA against Mi-2β in pQsupR plasmid, in which shRNA was transcribed from the mU6 promoter. The plasmid also contains GFP and puromycin selection site transcribed from the CMV promoter (Ramirez-Carrozzi et al., 2006). The fluorophore in inducible Ikaros plasmid was changed from original GFP to mCherry (B). (C) Timeline of shRNA knock-down experiment. (D) Mi-2β was efficiently knocked down with shRNA, shown by western blotting. Each biological replicate started from fresh infection, and the efficiency of knock-down was individually validated.

Following the efficient knockdown of Mi-2β, the next step was to test whether Mi-2β was involved in Ikaros-mediated nucleosome regulation. For this purpose, Ikaros was induced in shRNA control and Mi-2β knock-down cells in parallel, and nucleosome occupancy was monitored using MNase-qPCR (Figure 6.5). In control cells (Empty), the negatively regulated *Igll1* and *Myc* promoters showed an increase in nucleosome occupancy (as in Figure 5.3). In detail, significant increases were observed after 5 minutes of Ikaros induction at the *Igll1* promoter and after 15 minutes at the *Myc* promoter. After 2 hours of induction, nucleosome occupancy increased to 8-fold and 2.5-fold at the *Igll1* and *Myc* promoters, respectively. In contrast, in Mi-2β knock-down cells (sh-Mi2), at the *Igll1* promoter, nucleosome occupancy

increased significantly only after 15 minutes of Ikaros induction, and to 3-fold after 2 hours. At the *Myc* promoter, a significant increase to 1.7-fold was observed only after two hours of Ikaros induction (Figure 6.5). The control locus *Acta1* showed no significant changes of nucleosome occupancy after Ikaros induction in either control or Mi-2β knock-down cells.

The data showed that the Mi-2β knock-down not only delayed the kinetics of nucleosome regulation mediated by Ikaros, but also compromised the magnitude of regulation. On the other hand, the results also confirmed that changes in nucleosome occupancy mediated by Ikaros were, at least partially, through the chromatin remodeler Mi-2β.

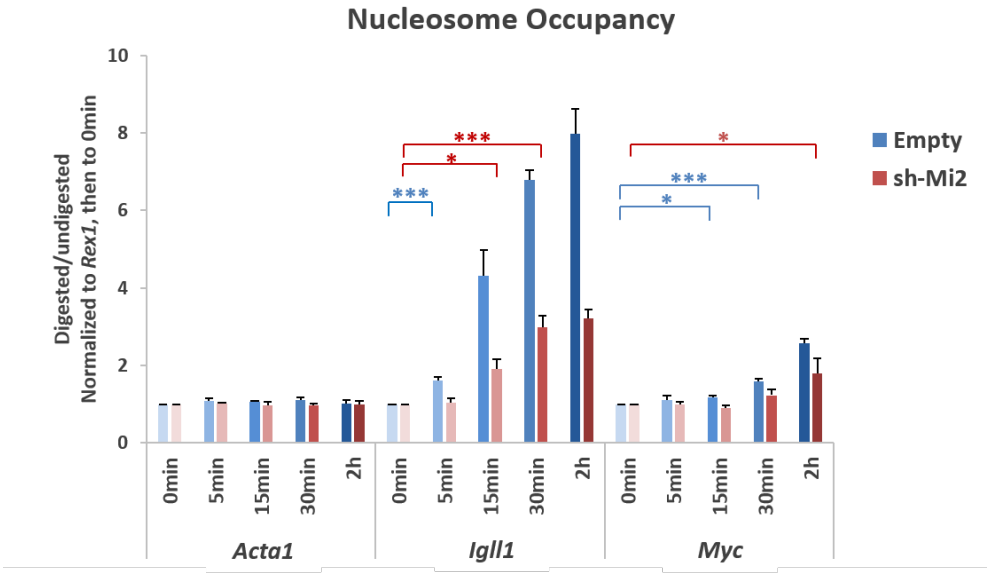

Figure 6.5 Nucleosome regulation mediated by Ikaros is impaired under Mi-2β knock-down condition

Nucleosome occupancy was measured using MNase assay during Ikaros induction in control cells (blue) and Mi-2β knock-down cells (red). After Mi-2β knock-down, nucleosome regulation mediated by Ikaros was delayed and compromised at *Igll1* and *Myc* loci. Data shown was an average of five independent biological replicates. P value: *<0.05, ***<0.01.

Next, the influence of the compromised nucleosome regulation on mRNA transcription was examined. To this end, Ikaros was induced in control and Mi-2β knock-down cells in parallel, and mRNA transcription was monitored by qPCR analysis (Figure 6.6). In control cells, the expression of *Igll1* and *Myc* were both significantly down-regulated after 15 minutes of Ikaros induction, and achieved approximately 60% repression after two hours of induction. In contrast, in Mi-2β knock-down cells, *Igll1* and *Myc* were significantly down-regulated only after two hours of Ikaros induction, with a milder reduction of 40% (Figure 6.6). Therefore, interference with nucleosome regulation mediated by Ikaros, resulted in delayed and compromised gene repression.

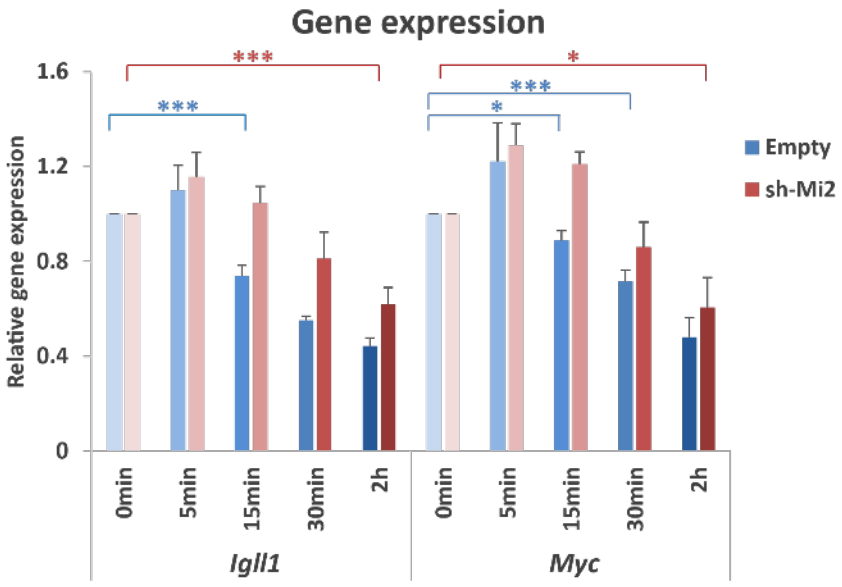

Figure 6.6 Gene expression regulation by Ikaros is impaired under Mi-2β knock-down condition

Gene expression was quantified by qPCR during Ikaros induction in control cells (blue) and Mi-2β knock-down cells (red). After Mi-2β knock-down, gene expression regulation by Ikaros was delayed and compromised. Data shown here was an average of five independent biological replicates. P value: *<0.05, ***<0.01.

The compromised transcriptional regulation resulting from the interference with nucleosome reorganization indicated that the regulation of nucleosome occupancy is probably upstream of the control of RNAPII binding. To test this hypothesis, it would be ideal to monitor the binding of RNAPII in Mi-2β knock-down cells after Ikaros induction. However, such delicate

comparison requires high quality RNAPII ChIP, which needs a large number of cells. From the five biological replicates attempted, despite striking differences in RNAPII enrichment at positive and negative loci, the capturing of biological differences was inefficient (data not shown).

Taken together, the data suggested that the regulation of nucleosome occupancy is probably an upstream event of the control of RNAPII binding, and affects the transcriptional repression.

To understand how Ikaros utilises Mi-2β to reorganise nucleosomes, the binding of Mi-2β was examined by ChIP-qPCR after Ikaros induction at down-regulated loci *Igll1* and *Myc*, and control loci *Pou5f1* and *Rex1* (Figure 6.7). However, no significant changes were observed after Ikaros induction within each locus. This is further discussed in section 6.4.

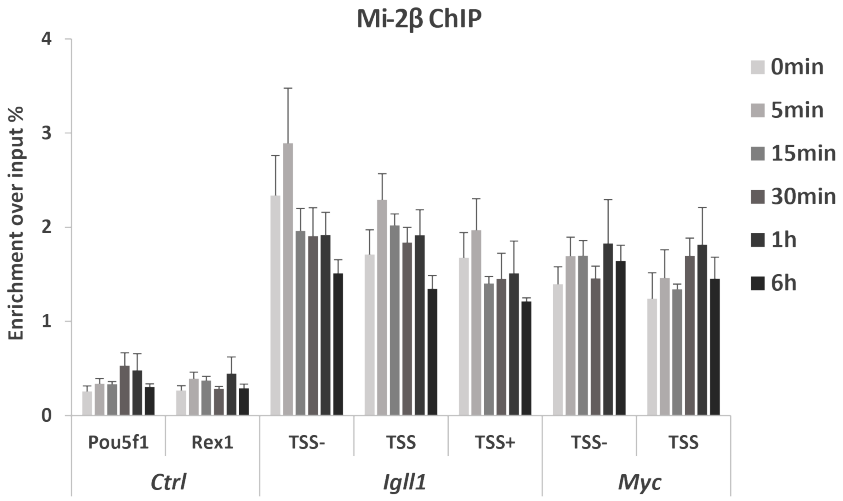

Figure 6.7 Mi-2β binding during Ikaros induction

Graphs show Mi-2β enrichment around the TSS of Ikaros down-regulated target genes *Igll1* and *Myc*, and control genes, after 0min, 5min, 15min, 30min, 1h and 6h of Ikaros induction. Data shown was an average of three biological replicates.

Additionally, one can argue that the delayed gene repression is not directly due to the compromised nucleosome regulation, but is because the Mi-2β deficient cells are stressed, since knockdown of Mi-2β leads to cell apoptosis. To answer this question, chromatin remodeler Brg1/Brm knockdown was done in parallel using shRNA targeting both Brg1 and

Brm (Ramirez-Carrozzi et al., 2006) (Figure 6.8A). Cultured with caspase inhibitor, the control B3 cells proliferated 2.5 times within 24 hours, the Mi-2β knockdown cells divided around 1.5 times a day, but the Brg1/Brm knockdown barely divided after knockdown (data not shown). Therefore, perhaps the Brg1/Brm knockdown cells should suffer more than the Mi-2β knockdown cells. In this sense, if the delayed gene repression was due to cellular stress, the delay should be more obvious in the Brg1/Brm knockdown cells. However, it was the other way around (Figure 6.8B). The gene repression was similar in the Brg1/Brm knockdown cells as in control cells. This suggested that the side effect of apoptosis block was not the main reason to cause the delayed and compromised transcriptional repression. However, the influence of cellular stress due to the interference with Mi-2β on chromatin remodelling needs to be further addressed.

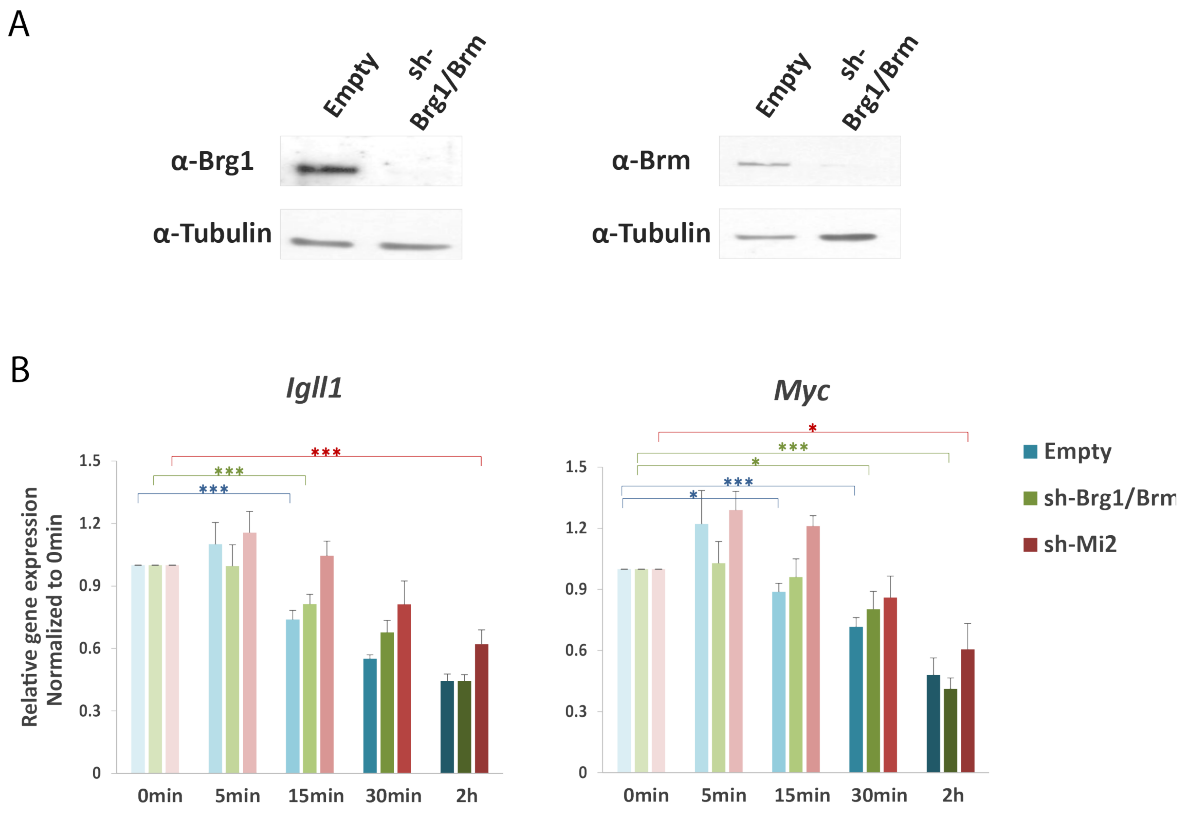

Figure 6.8 Effect of Brg1/Brm knock-down on Ikaros-mediated transcriptional regulation

(A) Brg1/Brm was efficiently knocked down in B3 pre-B cells using shRNA. (B) Gene expression was quantified by qPCR during Ikaros induction in control cells (blue), Brg1/Brm knock-down cells (green) and Mi-2β knock-down cells (red). After both Brg1/Brm and Mi-2β knock-down, gene expression regulation by Ikaros was delayed and compromised, while Mi-2β knock-down showed more severe effect. Data shown is an average of five independent biological replicates. P value: *<0.05, ***<0.01.

6.3 Histone deacetylation is not necessary to initiate gene repression

During Ikaros-mediated gene repression, histone deacetylation was observed and appeared to be a later event (Figure 5.11, 5.12). Interestingly, class I histone deacetylases (HDACs) HDAC1/2 are present in the Mi-2β/NuRD complex (Reynolds et al., 2013). Here, the role of histone deacetylation during Ikaros-mediated transcriptional repression was investigated.

First, histone deacetylation was blocked by HDAC inhibitor trichostatin A (TSA). TSA is a hydroxamic acid, and blocks class I and II HDACs activities by binding to their zinc-containing catalytic domain (Kim and Bae, 2011). In B3 cells, TSA alone induced transcriptional changes at as little as 5ng/ml (data not shown). The inhibitory effect of TSA was then tested at 1ng/ml using western blotting with antibodies recognising acetylated histone H3 and H4 (Figure 6.9). TSA treatment at 1ng/ml for 1 hour strongly increased the acetylations of histone H3 and H4 in inducible Ikaros B3 cells (Figure 6.9).

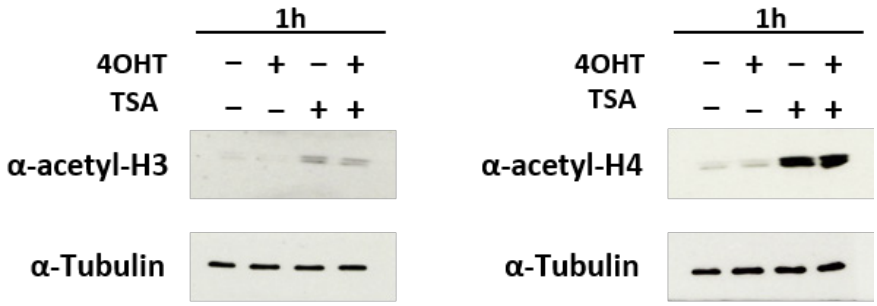

Figure 6.9 TSA treatment leads to a global increase in histone H3 and H4 acetylation

Cells treated with 1ng/ml TSA for 1h showed global increase in histone acetylation at H3 (left) and H4 (right), and the effect was not compromised by inducing Ikaros with 4OHT. This is a representation of three biological replicates.

To test specifically whether Ikaros-induced histone deacetylation was blocked with 1ng/ml TSA treatment, the level of histone acetylation was monitored after 1 hour of Ikaros induction in the cells treated with TSA or the carrier ethanol (Figure 6.10). To prevent introducing hyperacetylation at the baseline level, cells were not pre-treated with TSA. At the

Igll1 and *Myc* promoters, Ikaros induction lead to significant histone deacetylation at histone H3 and H4 in ethanol treated cells. In contrast, in TSA treated cells, Ikaros induction did not induce histone deacetylation. Therefore, 1ng/ml TSA treatment efficiently blocks histone deacetylation by Ikaros. It is worth noting that at *Igll1* locus, TSA treatment decreased the histone acetylation level compared to ethanol treatment. This could be due to the readjusted histone acetylation and deacetylation equilibrium introduced by TSA (Makarona et al., 2014).

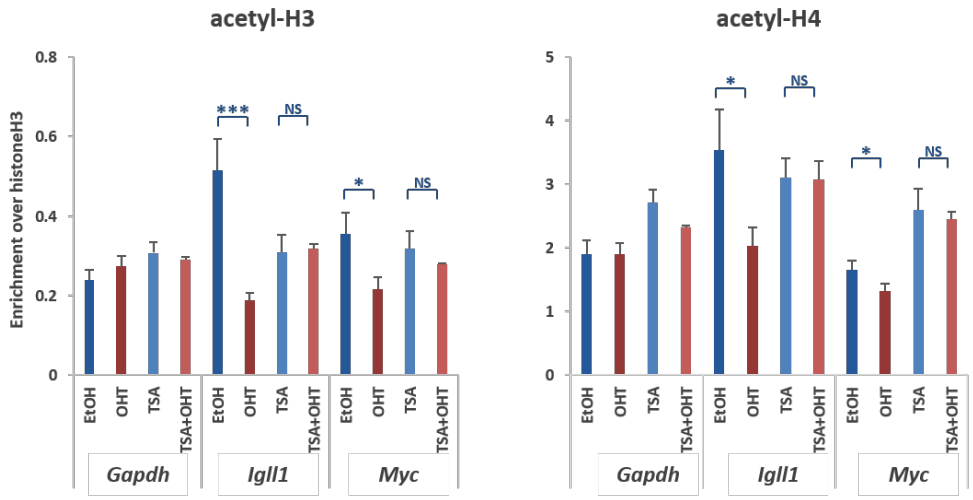

Figure 6.10 TSA impaired histone deacetylation mediated by Ikaros

Histone acetylation of H3 and H4 tails were examined by ChIP at the *Igll1* and *Myc* loci. Ikaros was induced by 4OHT (red bars) with or without TSA treatment for 1h. Data shown was the average of three biological replicates. NS: not significant, student t-test P value >0.05 *: p value <0.05, ***: p value <0.01.

Following this, nucleosome occupancy was examined under these conditions (Figure 6.11). In ethanol treated cells, Ikaros induction increased nucleosome occupancy at the *Igll1* and *Myc* promoters. TSA treatment for 1 hour did not significantly alter the baseline level of nucleosome occupancy before Ikaros induction. Furthermore, in the TSA treated cells, Ikaros induction resulted in similar levels of increase in nucleosome occupancy as in the control cells. Therefore, the regulation of nucleosome occupancy at the promoters was independent of histone deacetylation.

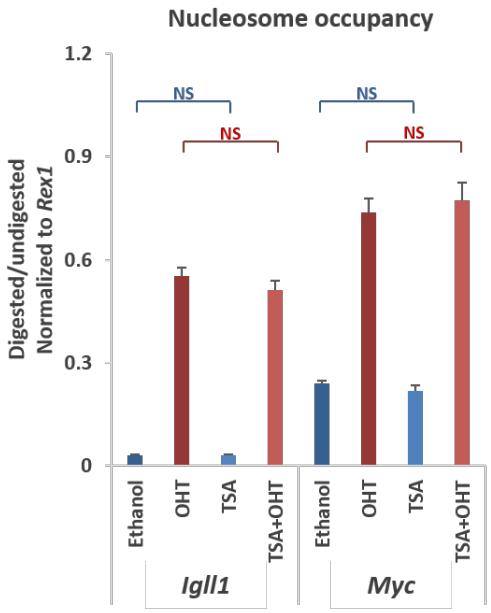

Figure 6.11 TSA treatment does not impair nucleosome reorganization by Ikaros

Ikaros was induced by 4OHT (red bars) with or without TSA treatment for 1h. At the down-regulated *Igll1* and *Myc* promoters, TSA treatment did not alter the nucleosome reorganization mediated by Ikaros. Data shown here was the average of three biological replicates. NS: not significant, p value > 0.05.

Next, the binding of RNAPII was analysed under the same conditions (Figure 6.12). In ethanol treated cells, *Igll1* and *Myc* showed decreased binding of RNAPII after Ikaros induction. TSA treatment for 1 hour alone mildly but not significantly decreased RNAPII at the *Igll1* and *Myc* loci. Furthermore, Ikaros induction in the TSA treated cells reduced the binding of RNAPII to the same level as in the control cells. Thus, the regulation of RNAPII was independent of histone deacetylation.

Finally, gene expression was directly examined (Figure 6.12). The gene expression data agreed faithfully with RNAPII binding, and that Ikaros induced down-regulation of *Igll1* and *Myc* were not influenced by the blocked histone deacetylation.

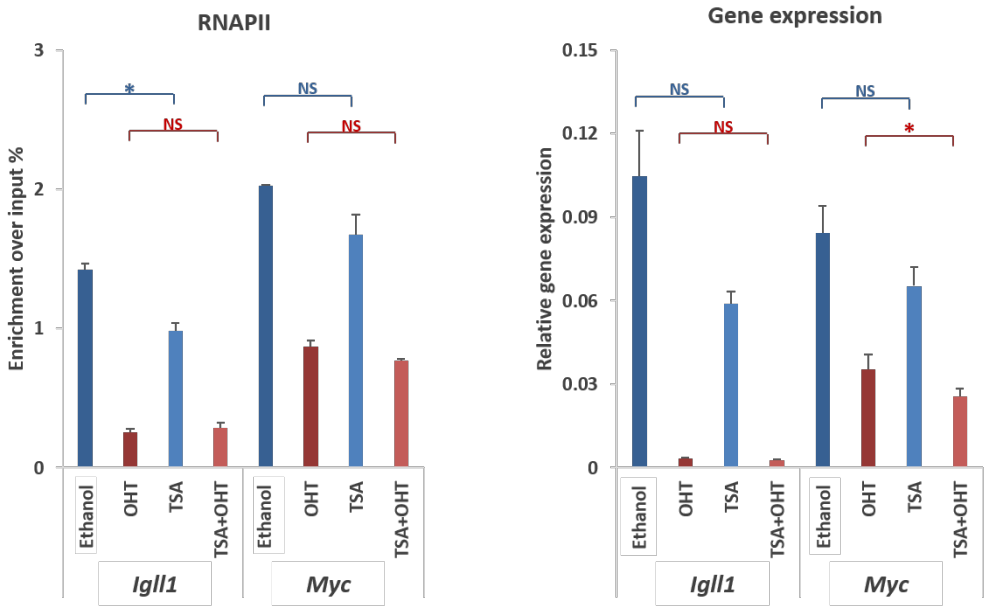

Figure 6.12 TSA treatment does not impair RNAII and transcription regulated by Ikaros

Ikaros was induced by 4OHT (red bars) with or without TSA treatment for 1h. At down-regulated *Igll1* and *Myc* promoters, TSA treatment did not alter the changes in RNAPII mediated by Ikaros (left). Transcriptional regulation of *Igll1* and *Myc* was not compromised either (right). Data show here was the average of three biological replicates. NS: not significant, p value > 0.05, *: p value <0.05.

In summary, without decreasing the histone acetylation level, Ikaros was still able to increase nucleosome occupancy, reduce RNAPII binding and eventually, down-regulate gene expression to the same level. The data also supported the finding from the kinetics study that histone deacetylation appeared to be a later event during Ikaros-mediated transcriptional repression.

6.4 Discussion

I carried out mechanistic tests on the observed order of regulatory events in chromatin during Ikaros-mediated transcriptional repression. Nucleosome repositioning appeared to be directly regulated by Ikaros, not through the influence of RNAPII binding, since degradation of RNAPII did not result in or alter nucleosome reorganization. On the other hand, when the regulation of nucleosome occupancy was compromised by interfering with chromatin remodeler Mi-2β, transcriptional regulation was delayed. This indicated that the regulation of RNAPII density was, at least partially, influenced by nucleosome occupancy at the promoters. After testing the causal relationship between the early events of RNAPII and nucleosome regulation, the involvement of a seemingly later change, histone deacetylation, was examined. The block of histone deacetylation did not alter the regulation of nucleosome and RNAPII density, and histone deacetylation was not necessary to initiate gene down-regulation. This supported the kinetics study that histone acetylation was a later event during Ikaros-mediated transcriptional repression. These mechanistic tests not only support the kinetics studies, but also shed light on the causal relationships between these regulatory events.

Mi-2β in Ikaros-mediated transcriptional repression

In Mi-2β knock-down cells, the increase in nucleosome occupancy mediated by Ikaros was not only delayed, but also milder. This is the first direct evidence that Ikaros regulates nucleosome positioning through Mi-2β in the B cell compartment.

It remains to be answered how Ikaros utilises Mi-2β to regulate promoter accessibility. Interestingly, the enrichment of Mi-2β at the regulated promoters did not significantly change after Ikaros induction (Figure 6.7). It is possible that the quality of the ChIP was not good enough. ChIP for chromatin remodelers has been considered difficult. In this ChIP, the enrichment at the silent genes *Pou5f1* and *Rex1*, presumably not bound by Mi-2β (Schwickert et al., 2014; Zhang et al., 2012), was not dramatically different from the enrichment of the Mi-2β regulated promoters. Thus, a better quality ChIP may be required. Furthermore, strictly speaking, the ChIP enrichment of Mi-2β does not necessarily reflect Mi-2β binding to DNA. Mi-2β interacts with Ikaros in B3 cells (Ben Taylor, unpublished). The ChIP enrichment can be due to the interaction of Mi-2β with the DNA binding protein Ikaros. After

induction, increased dosage of Ikaros may help the pre-associated Mi-2β molecules bind DNA. Additionally, Ikaros may also influence the stability or activity of Mi-2β in the context of NuRD complex. How Ikaros utilises Mi-2β to reposition nucleosomes is still an open question.

The knockdown of Mi-2β did not totally abolish nucleosome reorganization mediated by Ikaros. It is possible that there were still a fraction of Mi-2β proteins left after knock-down. They may facilitate Ikaros to reorganise nucleosome positioning to a lesser level. Another possibility is that Mi-2β is not the only chromatin remodeler that works with Ikaros (Kim et al., 1999; Morris et al., 2014; Sridharan and Smale, 2007). There may be cooperative regulation of the nucleosome reorganisation between the chromatin remodelers, and therefore transcriptional repression is not totally abolished after the knockdown of Mi-2β (Morris et al., 2014).

Histone deacetylation in Ikaros-mediated gene repression

HDACs in human are divided into four classes: Zn^{2+} dependent class I (HDAC1, 2, 3, 8), class II (HDAC4, 5, 6, 7, 9, 10), class IV (HDAC11), and NAD+ dependent class III (Sirt1-7) (Delcuve et al., 2012). To identify which HDACs work with Ikaros to deacetylate histones during transcriptional repression, HDAC1 and 2 are top candidates. They are part of the Mi-2/NuRD complex as well as the corepressors Sin3 and CtBP, which interact with Ikaros (Kim et al., 1999; Sridharan and Smale, 2007). HDAC1 and 2 exhibit a high degree of homology, and form homo- and heterodimers between each other. They work together but also have distinct roles depending on the cell types (Delcuve et al., 2012). To test the involvement of HDAC1/2 in Ikaros-mediated histone deacetylation, more specific HDAC inhibitors to HDAC1/2 can be used, such as MS-275 (Quintas-Cardama et al., 2011) or BRD8430 (Frumm et al., 2013). Furthermore, since Mi-2β plays a vital part in Ikaros-mediated gene repression in B3 cells, it would be interesting to test the role of HDAC1/2 in the context of the Mi-2/NuRD complex.

It is worth emphasizing that this study does not argue against the importance of histone acetylation or deacetylation during transcriptional regulation, but raises the point that histone deacetylation is not necessary to initiate transcriptional repression mediated by Ikaros.

7 Discussion

7.1 Overview

In B3 pre-B cells, I applied an inducible Ikaros system to monitor the changes in chromatin status mediated by Ikaros at a high temporal resolution. By adding 4OHT, inducible Ikaros translocated into the nucleus quickly and efficiently. This led to significant changes in transcription of selected Ikaros target genes as early as 5 minutes after induction, and induced cell cycle arrest after 16 hours of induction. This inducible Ikaros system serves as a powerful tool to study the kinetics and mechanisms of Ikaros-mediated transcriptional regulation.

Genome-wide profiling of RNAPII and nucleosome density after 6 hours of Ikaros induction revealed that Ikaros decreased promoter accessibility and RNAPII binding during transcription down-regulation, and *vice versa* during up-regulation. Time course studies at selected model loci indicted that changes in nucleosome occupancy and RNAPII binding were early events during Ikaros-mediated transcriptional repression. These experiments also revealed later changes in histone modifications and nucleosome composition, including the integrity of nucleosomes and the incorporation of the histone variant H2A.Z.

Once the order of chromatin-based events during Ikaros-mediated transcriptional repression was clarified, I began to address the causal relationships between these events. Changes in RNAPII and nucleosome occupancy both occurred very early, and appeared in an anti-correlated manner. Investigating the relationship between these events, I found that RNAPII was not required for the maintenance of a nucleosome-free region at Ikaros target promoters. On the other hand, interference with chromatin remodelers that regulate nucleosome occupancy compromised the regulation of RNAPII binding by Ikaros. This suggests a direct role for Ikaros in directing chromatin remodelling and nucleosome occupancy upstream of the regulation of RNAPII binding. Decreased histone acetylation was not necessary to initiate Ikaros-mediated transcriptional repression, and histone deacetylation appeared to be a later event than increased nucleosome occupancy and reduced RNAPII binding.

In this study, I applied an inducible system of the key transcription factor Ikaros to a well-defined and critical developmental stage during early B cell development. The observations

in this study not only improved the understanding of how Ikaros mediates transcriptional changes during early B cell development, but also provided direct evidence for the order and causal relationships between regulatory events during transcriptional regulation in high eukaryotes.

Figure 7.1 Cartoon of the mechanisms used by Ikaros to down-regulate transcription

This cartoon illustrates the sequence of the regulatory events and mechanisms used by Ikaros to down-regulate transcription. In an active transcription state (A) a gene promoter is highly accessible to transcription factors, including Ikaros and EBF, and is bound by RNAPII. The neighbouring nucleosomes around the TSS are modified with active histone marks, including acetylation. Induction of Ikaros (B) increase the binding of Ikaros at the pre-bound binding site in the regulated promoter, possibly forming dimer or multimers with Ikaros itself or family members. This may also out compete the transcription factors involved in activating the gene, such as EBF (discussed in section 7.3). (C) Subsequently, Ikaros induction increases the nucleosome occupancy at the negatively regulated promoter. This process is facilitated by chromatin remodeler Mi-2β. (D) The increase of nucleosome occupancy results in or facilitates the decrease in RNAPII binding. Following these events, H2A.Z is incorporated into the TSS neighbouring nucleosomes (Ei) and histones are deacetylated (Eii). After these initial regulatory events, transcription of Ikaros down-regulated gene may be further silenced by other mechanisms (F). It probably leads to the full closure of the promoter and loss of all active histone marks and RNAPII binding.

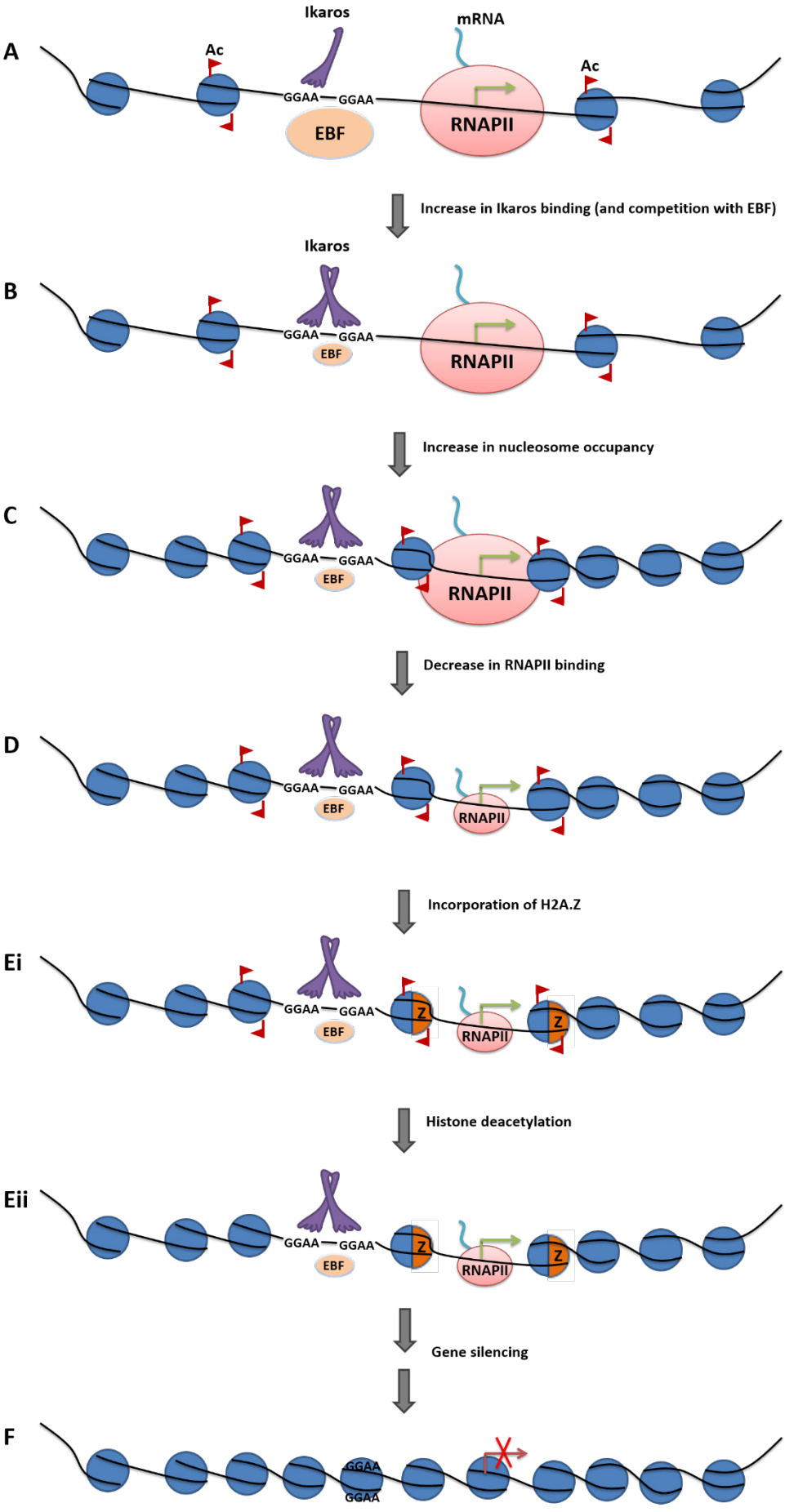
A
Ikaros
mRNA
Ac
Ac
GGAA
GGAA
EBF
RNAPII
Increase in Ikaros binding (and competition with EBF)
B
Ikaros
GGAA
GGAA
EBF
RNAPII
Increase in nucleosome occupancy
C
GGAA
GGAA
EBF
RNAPII
Decrease in RNAPII binding
D
GGAA
GGAA
EBF
RNAPII
Incorporation of H2A.Z
Ei
GGAA
GGAA
EBF
Z
RNAPII
Z
Histone deacetylation
Eii
GGAA
GGAA
EBF
Z
RNAPII
Z
Gene silencing
F
GGAA
GGAA

7.2 Ikaros works together with Mi-2β to regulate transcription

Ikaros physically interacts with Mi-2β in T cells (Kim et al., 1999) and in B3 pre-B cells (Ben Taylor, unpublished). Here, I provide direct evidence that Ikaros works with Mi-2β to increase nucleosome occupancy at negatively regulated promoters in pre-B cells, and that this regulatory event is critical to Ikaros-mediated gene repression, as knock-down of Mi-2β interferes with increased nucleosome occupancy mediated by Ikaros, and subsequently delays the changes in transcription.

How does Ikaros cooperate with Mi-2β? Although the binding of Ikaros substantially overlaps with that of Mi-2β at permissive promoters in both thymocytes and pro-B cells (Schwickert et al., 2014; Zhang et al., 2012), there is disagreement on the effect of Ikaros on Mi-2β binding. In thymocytes, Ikaros reportedly inhibits the binding of Mi-2β, as loss of Ikaros leads to increased Mi-2β binding (Zhang et al., 2012). However in pro-B cells, loss of Ikaros does not lead to the redistribution of Mi-2β binding, arguing against the role of Mi-2β in controlling the chromatin changes at Ikaros-regulated gene promoters (Schwickert et al., 2014). My results support the idea that Ikaros cooperates with Mi-2β to down-regulate transcription, and this co-regulation is positively co-ordinating, rather than inhibitory as seen in thymocytes (Naito et al., 2007; Zhang et al., 2012).

It remains to be discovered how an increased level of Ikaros leads to an increase in nucleosome occupancy mediated by Mi-2β. Preliminary data shows that increased Ikaros binding does not influence the binding of Mi-2β to regulated promoters (Figure 6.7). Therefore, Ikaros does not seem to control the recruitment of Mi-2β in pre-B cells. Perhaps Ikaros stabilizes the interactions between Mi-2β and nucleosomes by binding to DNA and interacting with Mi-2β, or by changing the local chromatin conformation. Ikaros may also increase Mi-2β activity by controlling the stability and activity of Mi-2β in the context of Mi-2/NuRD.

Mi-2β may work independently of the NuRD complex (Naito et al., 2007; Shimono et al., 2003), or in the context of NuRD complex. The Mi-2β/NuRD complex possesses histone deacetylation activity due to HDAC1/2 subunits (Reynolds et al., 2013) and histone deacetylation is observed after Ikaros induction. It would be very interesting to test whether this histone deacetylation observed is due to HDAC1/2. If so, the next question would be whether HDAC1/2 functions in the context of NuRD complex.

7.3 Ikaros decreases RNA polymerase II binding during transcription repression

In this study, Ikaros was shown to reduce RNAPII binding during transcriptional regulation, through reducing recruitment and/or down-regulating pause-release. The reduction of RNAPII binding at down-regulated genes is at least partly due to the increase in nucleosome occupancy at the promoters mediated by Ikaros, thereby precluding access of the transcription machinery to DNA. Therefore, the regulation of RNAPII binding by Ikaros can be downstream of the regulation of nucleosome occupancy.

There is another possibility that Ikaros can reduce RNAPII binding indirectly. Ikaros may mediate a decrease in RNAPII binding through competing with transcription factors. Ikaros is thought to compete with the transcription factor EBF1 in pre-B cells, where they both bind to the *Igll1* promoter to balance its expression (Thompson et al., 2007). In cycling pre-B cells, Ikaros induction leads to the down-regulation of *Igll1*. I performed EBF1 ChIP to examine the binding of EBF1 after Ikaros induction at the *Igll1* promoter (Figure S3). Both Ikaros and EBF binding peaks are positioned around 200bp upstream of the TSS. After 3 hours of Ikaros induction, Ikaros binding increases to almost 2-fold, while EBF1 binding reduces to half. Since the binding sites of Ikaros and EBF1 overlap in the *Igll1* promoter, it is possible that increased Ikaros binding blocks the binding of EBF1. Reduced EBF1 binding may decrease RNAPII recruitment to *Igll1*. Competition between Ikaros and EBF may be a general mechanism for decreased RNAPII recruitment in B cell progenitors, where 52% of EBF1 binding peaks overlap with Ikaros (Ferreiros-Vidal et al., 2013; Lin et al., 2010b).

These observations, however, do not rule out the possibility that Ikaros may directly regulate RNAPII, in a pathway that is independent of decreasing promoter accessibility or competing with transcription activators. In erythroid cells, to activate transcription, Ikaros reportedly regulates the transcription machinery by recruiting the PIC component TBP and interacting with Cdk9 to promote RNAPII elongation (Bottardi et al., 2013; Bottardi et al., 2011). In this study, the genome-wide profiling of RNAPII binding in B3 pre-B cells suggested Ikaros may modulate RNAPII at both recruitment and elongation levels under different scenarios (section 4.1.3). Further analysis may reveal one or more dominant mechanisms used by Ikaros to regulate RNAPII during B cell development.

7.4 The competition between RNAPII and nucleosomes

Viewed simplistically, transcriptional regulation could be described as a fight between RNAPII and nucleosomes. These two are the principle components of the complicated battlefield of transcription. The rest of the transcriptional regulatory events are either positively or negatively, directly or indirectly, affecting either RNAPII or nucleosomes to contribute to transcriptional regulation.

RNAPII pausing at promoter proximal sites is important for maintaining permissive chromatin architecture. As shown in *Drosophila*, two thirds of NELF-dependent genes are down-regulated in response to NELF-depletion. Examination of selected promoters shows significant increase in nucleosome occupancy due to loss of paused RNAPII upon NELF depletion (Gilchrist et al., 2008). This is further explained as the promoter sequences of NELF-dependent highly paused genes inherently favour the formation of nucleosomes, therefore loss of paused RNAPII leads to the promoter architectures adopting their natural feature (Gilchrist et al., 2010). Therefore, RNAPII dominantly competes with nucleosome at *Drosophila* promoters, and prevents nucleosomes from adopting their favourite positions. However, this competing mechanism remains to be seen in mammalian cells.

In this study, I provide initial evidence of this competition by demonstrating that RNAPII and nucleosome density are anti-correlated at both up-regulated and down-regulated gene promoters after Ikaros induction. Based on this observation, the changes in RNAPII and nucleosome density could be both dependent on Ikaros. It is also possible that one is directly regulated by Ikaros, and the change in the other is a passive consequence of the competition between RNAPII and nucleosomes. Furthermore, the changes in RNAPII and nucleosome density also follow similar kinetics, and appear earlier than other regulatory events examined. The almost simultaneous regulation further heats up the questions about the existence of active competition between RNAPII and nucleosomes, and the causal factors that induce these changes.

My experiments show that loss of RNAPII does not lead to increased nucleosome occupancy at Ikaros targets in contrast with observations in *Drosophila*. Preliminary prediction using parameters from the Segal lab suggests that the DNA sequences of both *Igll1* and *Myc* promoters favour the formation of nucleosomes (Kaplan et al., 2009). Admittedly, it is possible that the RNAPII degradation treatment (3 hours) is not long enough for nucleosomes to adopt their favourable positions. This also indicates that mammalian cells may use

different mechanisms from *Drosophila*, and that nucleosomes at gene promoters are highly regulated, rather than simply following the thermal dynamics. Furthermore, promoter accessibility is also tightly regulated during transcriptional regulation mediated by Ikaros, and this regulation is independent of RNAPII binding.

Bibliography

Agalioti, T., Lomvardas, S., Parekh, B., Yie, J., Maniatis, T., and Thanos, D. (2000). Ordered recruitment of chromatin modifying and general transcription factors to the IFN-beta promoter. Cell *103*, 667-678.

Allis, C.D., Berger, S.L., Cote, J., Dent, S., Jenuwien, T., Kouzarides, T., Pillus, L., Reinberg, D., Shi, Y., Shiekhattar, R.*, et al.* (2007). New nomenclature for chromatin-modifying enzymes. Cell *131*, 633-636.

Alper, B.J., Job, G., Yadav, R.K., Shanker, S., Lowe, B.R., and Partridge, J.F. (2013). Sir2 is required for Clr4 to initiate centromeric heterochromatin assembly in fission yeast. EMBO J *32*, 2321-2335.

Andrews, A.J., and Luger, K. (2011). Nucleosome structure(s) and stability: variations on a theme. Annual review of biophysics *40*, 99-117.

Ansari, S.A., and Morse, R.H. (2013). Mechanisms of Mediator complex action in transcriptional activation. Cellular and molecular life sciences : CMLS *70*, 2743-2756.

Bain, G., Maandag, E.C., Izon, D.J., Amsen, D., Kruisbeek, A.M., Weintraub, B.C., Krop, I., Schlissel, M.S., Feeney, A.J., van Roon, M.*, et al.* (1994). E2A proteins are required for proper B cell development and initiation of immunoglobulin gene rearrangements. Cell *79*, 885-892.

Ballare, C., Castellano, G., Gaveglia, L., Althammer, S., Gonzalez-Vallinas, J., Eyras, E., Le Dily, F., Zaurin, R., Soronellas, D., Vicent, G.P.*, et al.* (2013). Nucleosome-driven transcription factor binding and gene regulation. Molecular cell *49*, 67-79.

Banaszynski, L.A., Wen, D., Dewell, S., Whitcomb, S.J., Lin, M., Diaz, N., Elsasser, S.J., Chapgier, A., Goldberg, A.D., Canaani, E.*, et al.* (2013). Hira-dependent histone H3.3 deposition facilitates PRC2 recruitment at developmental loci in ES cells. Cell *155*, 107-120.

Bannister, A.J., Zegerman, P., Partridge, J.F., Miska, E.A., Thomas, J.O., Allshire, R.C., and Kouzarides, T. (2001). Selective recognition of methylated lysine 9 on histone H3 by the HP1 chromo domain. Nature *410*, 120-124.

Barber, M.F., Michishita-Kioi, E., Xi, Y., Tasselli, L., Kioi, M., Moqtaderi, Z., Tennen, R.I., Paredes, S., Young, N.L., Chen, K.*, et al.* (2012). SIRT7 links H3K18 deacetylation to maintenance of oncogenic transformation. Nature *487*, 114-118.

Barski, A., Cuddapah, S., Cui, K., Roh, T.Y., Schones, D.E., Wang, Z., Wei, G., Chepelev, I., and Zhao, K. (2007). High-resolution profiling of histone methylations in the human genome. Cell *129*, 823-837.

Barth, T.K., and Imhof, A. (2010). Fast signals and slow marks: the dynamics of histone modifications. Trends in biochemical sciences *35*, 618-626.

Bartke, T., Vermeulen, M., Xhemalce, B., Robson, S.C., Mann, M., and Kouzarides, T. (2010). Nucleosome-interacting proteins regulated by DNA and histone methylation. Cell *143*, 470-484.

Bentley, D.L. (2014). Coupling mRNA processing with transcription in time and space. Nature reviews Genetics *15*, 163-175.

Bernecky, C., Grob, P., Ebmeier, C.C., Nogales, E., and Taatjes, D.J. (2011). Molecular architecture of the human Mediator-RNA polymerase II-TFIIF assembly. PLoS biology *9*, e1000603.

Bevington, S., and Boyes, J. (2013). Transcription-coupled eviction of histones H2A/H2B governs V(D)J recombination. EMBO J *32*, 1381-1392.

Bintu, L., Ishibashi, T., Dangkulwanich, M., Wu, Y.Y., Lubkowska, L., Kashlev, M., and Bustamante, C. (2012). Nucleosomal elements that control the topography of the barrier to transcription. Cell *151*, 738-749.

Bleichenbacher, M., Tan, S., and Richmond, T.J. (2003). Novel interactions between the components of human and yeast TFIIA/TBP/DNA complexes. Journal of molecular biology *332*, 783-793.

Bohm, V., Hieb, A.R., Andrews, A.J., Gansen, A., Rocker, A., Toth, K., Luger, K., and Langowski, J. (2011). Nucleosome accessibility governed by the dimer/tetramer interface. Nucleic acids research *39*, 3093-3102.

Bonisch, C., and Hake, S.B. (2012). Histone H2A variants in nucleosomes and chromatin: more or less stable? Nucleic acids research *40*, 10719-10741.

Borggrefe, T., and Yue, X. (2011). Interactions between subunits of the Mediator complex with gene-specific transcription factors. Seminars in cell & developmental biology *22*, 759-768.

Bottardi, S., Mavoungou, L., Bourgoin, V., Mashtalir, N., Affar el, B., and Milot, E. (2013). Direct protein interactions are responsible for Ikaros-GATA and Ikaros-Cdk9 cooperativeness in hematopoietic cells. Mol Cell Biol *33*, 3064-3076.

Bottardi, S., Zmiri, F.A., Bourgoin, V., Ross, J., Mavoungou, L., and Milot, E. (2011). Ikaros interacts with P-TEFb and cooperates with GATA-1 to enhance transcription elongation. Nucleic acids research *39*, 3505-3519.

Brogaard, K., Xi, L., Wang, J.P., and Widom, J. (2012). A map of nucleosome positions in yeast at base-pair resolution. Nature *486*, 496-501.

Brown, K.E., Baxter, J., Graf, D., Merkenschlager, M., and Fisher, A.G. (1999). Dynamic repositioning of genes in the nucleus of lymphocytes preparing for cell division. Molecular cell *3*, 207-217.

Brown, K.E., Guest, S.S., Smale, S.T., Hahm, K., Merkenschlager, M., and Fisher, A.G. (1997). Association of transcriptionally silent genes with Ikaros complexes at centromeric heterochromatin. Cell *91*, 845-854.

Burgess, R.J., and Zhang, Z. (2013). Histone chaperones in nucleosome assembly and human disease. Nature structural & molecular biology *20*, 14-22.

Buscaino, A., Lejeune, E., Audergon, P., Hamilton, G., Pidoux, A., and Allshire, R.C. (2013). Distinct roles for Sir2 and RNAi in centromeric heterochromatin nucleation, spreading and maintenance. EMBO J *32*, 1250-1264.

Carone, B.R., Hung, J.H., Hainer, S.J., Chou, M.T., Carone, D.M., Weng, Z., Fazzio, T.G., and Rando, O.J. (2014). High-resolution mapping of chromatin packaging in mouse embryonic stem cells and sperm. Dev Cell *30*, 11-22.

Carroll, T.S., Liang, Z., Salama, R., Stark, R., and de Santiago, I. (2014). Impact of artifact removal on ChIP quality metrics in ChIP-seq and ChIP-exo data. Frontiers in genetics *5*, 75.

Carrozza, M.J., Li, B., Florens, L., Suganuma, T., Swanson, S.K., Lee, K.K., Shia, W.J., Anderson, S., Yates, J., Washburn, M.P.*, et al.* (2005). Histone H3 methylation by Set2

directs deacetylation of coding regions by Rpd3S to suppress spurious intragenic transcription. Cell *123*, 581-592.

Cedar, H., and Bergman, Y. (2011). Epigenetics of haematopoietic cell development. Nat Rev Immunol *11*, 478-488.

Chen, H., Contreras, X., Yamaguchi, Y., Handa, H., Peterlin, B.M., and Guo, S. (2009). Repression of RNA polymerase II elongation in vivo is critically dependent on the C-terminus of Spt5. PloS one *4*, e6918.

Cho, S.J., Huh, J.E., Song, J., Rhee, D.K., and Pyo, S. (2008). Ikaros negatively regulates inducible nitric oxide synthase expression in macrophages: involvement of Ikaros phosphorylation by casein kinase 2. Cellular and molecular life sciences : CMLS *65*, 3290-3303.

Clapier, C.R., and Cairns, B.R. (2009). The biology of chromatin remodeling complexes. Annual review of biochemistry *78*, 273-304.

Clark, M.R., Mandal, M., Ochiai, K., and Singh, H. (2014). Orchestrating B cell lymphopoiesis through interplay of IL-7 receptor and pre-B cell receptor signalling. Nat Rev Immunol *14*, 69-80.

Cobb, B.S., Morales-Alcelay, S., Kleiger, G., Brown, K.E., Fisher, A.G., and Smale, S.T. (2000). Targeting of Ikaros to pericentromeric heterochromatin by direct DNA binding. Genes & development *14*, 2146-2160.

Conerly, M.L., Teves, S.S., Diolaiti, D., Ulrich, M., Eisenman, R.N., and Henikoff, S. (2010). Changes in H2A.Z occupancy and DNA methylation during B-cell lymphomagenesis. Genome research *20*, 1383-1390.

Corden, J.L. (2013). RNA polymerase II C-terminal domain: Tethering transcription to transcript and template. Chemical reviews *113*, 8423-8455.

Costanzi, C., and Pehrson, J.R. (1998). Histone macroH2A1 is concentrated in the inactive X chromosome of female mammals. Nature *393*, 599-601.

Cramer, P., Bushnell, D.A., Fu, J., Gnatt, A.L., Maier-Davis, B., Thompson, N.E., Burgess, R.R., Edwards, A.M., David, P.R., and Kornberg, R.D. (2000). Architecture of RNA polymerase II and implications for the transcription mechanism. Science *288*, 640-649.

Cramer, P., Bushnell, D.A., and Kornberg, R.D. (2001). Structural basis of transcription: RNA polymerase II at 2.8 angstrom resolution. Science *292*, 1863-1876.

Creyghton, M.P., Markoulaki, S., Levine, S.S., Hanna, J., Lodato, M.A., Sha, K., Young, R.A., Jaenisch, R., and Boyer, L.A. (2008). H2AZ is enriched at polycomb complex target genes in ES cells and is necessary for lineage commitment. Cell *135*, 649-661.

Curtis, C.D., and Griffin, C.T. (2012). The chromatin-remodeling enzymes BRG1 and CHD4 antagonistically regulate vascular Wnt signaling. Mol Cell Biol *32*, 1312-1320.

Deal, R.B., Henikoff, J.G., and Henikoff, S. (2010). Genome-wide kinetics of nucleosome turnover determined by metabolic labeling of histones. Science *328*, 1161-1164.

Decker, T., Pasca di Magliano, M., McManus, S., Sun, Q., Bonifer, C., Tagoh, H., and Busslinger, M. (2009). Stepwise activation of enhancer and promoter regions of the B cell commitment gene Pax5 in early lymphopoiesis. Immunity *30*, 508-520.

DeKoter, R.P., and Singh, H. (2000). Regulation of B lymphocyte and macrophage development by graded expression of PU.1. Science *288*, 1439-1441.

Delcuve, G.P., Khan, D.H., and Davie, J.R. (2012). Roles of histone deacetylases in epigenetic regulation: emerging paradigms from studies with inhibitors. Clinical epigenetics *4*, 5.

Di Cerbo, V., Mohn, F., Ryan, D.P., Montellier, E., Kacem, S., Tropberger, P., Kallis, E., Holzner, M., Hoerner, L., Feldmann, A.*, et al.* (2014). Acetylation of histone H3 at lysine 64 regulates nucleosome dynamics and facilitates transcription. Elife (Cambridge) *3*, e01632.

Dion, M.F., Altschuler, S.J., Wu, L.F., and Rando, O.J. (2005). Genomic characterization reveals a simple histone H4 acetylation code. Proc Natl Acad Sci U S A *102*, 5501-5506.

Dion, M.F., Kaplan, T., Kim, M., Buratowski, S., Friedman, N., and Rando, O.J. (2007). Dynamics of replication-independent histone turnover in budding yeast. Science *315*, 1405-1408.

Doyen, C.M., Montel, F., Gautier, T., Menoni, H., Claudet, C., Delacour-Larose, M., Angelov, D., Hamiche, A., Bednar, J., Faivre-Moskalenko, C.*, et al.* (2006). Dissection of the unusual structural and functional properties of the variant H2A.Bbd nucleosome. EMBO J *25*, 4234-4244.

Draker, R., Ng, M.K., Sarcinella, E., Ignatchenko, V., Kislinger, T., and Cheung, P. (2012). A combination of H2A.Z and H4 acetylation recruits Brd2 to chromatin during transcriptional activation. PLoS genetics *8*, e1003047.

Drew, H.R., and Travers, A.A. (1985). DNA bending and its relation to nucleosome positioning. Journal of molecular biology *186*, 773-790.

Egly, J.M., and Coin, F. (2011). A history of TFIIH: two decades of molecular biology on a pivotal transcription/repair factor. DNA repair *10*, 714-721.

Ehrensberger, A.H., Kelly, G.P., and Svejstrup, J.Q. (2013). Mechanistic interpretation of promoter-proximal peaks and RNAPII density maps. Cell *154*, 713-715.

Ferreiros-Vidal, I., Carroll, T., Taylor, B., Terry, A., Liang, Z., Bruno, L., Dharmalingam, G., Khadayate, S., Cobb, B.S., Smale, S.T.*, et al.* (2013). Genome-wide identification of Ikaros targets elucidates its contribution to mouse B-cell lineage specification and pre-B-cell differentiation. Blood *121*, 1769-1782.

Filipescu, D., Szenker, E., and Almouzni, G. (2013). Developmental roles of histone H3 variants and their chaperones. Trends in genetics : TIG *29*, 630-640.

Filippakopoulos, P., Qi, J., Picaud, S., Shen, Y., Smith, W.B., Fedorov, O., Morse, E.M., Keates, T., Hickman, T.T., Felletar, I.*, et al.* (2010). Selective inhibition of BET bromodomains. Nature *468*, 1067-1073.

Fisher, A.G., Burdet, C., Bunce, C., Merkenschlager, M., and Ceredig, R. (1995). Lymphoproliferative disorders in IL-7 transgenic mice: expansion of immature B cells which retain macrophage potential. International immunology *7*, 415-423.

Frumm, S.M., Fan, Z.P., Ross, K.N., Duvall, J.R., Gupta, S., VerPlank, L., Suh, B.C., Holson, E., Wagner, F.F., Smith, W.B.*, et al.* (2013). Selective HDAC1/HDAC2 inhibitors induce neuroblastoma differentiation. Chemistry & biology *20*, 713-725.

Fuda, N.J., Ardehali, M.B., and Lis, J.T. (2009). Defining mechanisms that regulate RNA polymerase II transcription in vivo. Nature *461*, 186-192.

Fujinaga, K., Irwin, D., Huang, Y., Taube, R., Kurosu, T., and Peterlin, B.M. (2004). Dynamics of human immunodeficiency virus transcription: P-TEFb phosphorylates RD and dissociates negative effectors from the transactivation response element. Mol Cell Biol *24*, 787-795.

Fujita, N., Jaye, D.L., Geigerman, C., Akyildiz, A., Mooney, M.R., Boss, J.M., and Wade, P.A. (2004). MTA3 and the Mi-2/NuRD complex regulate cell fate during B lymphocyte differentiation. Cell *119*, 75-86.

Gao, H., Lukin, K., Ramirez, J., Fields, S., Lopez, D., and Hagman, J. (2009). Opposing effects of SWI/SNF and Mi-2/NuRD chromatin remodeling complexes on epigenetic reprogramming by EBF and Pax5. Proceedings of the National Academy of Sciences of the United States of America *106*, 11258-11263.

Geiger, J.H., Hahn, S., Lee, S., and Sigler, P.B. (1996). Crystal structure of the yeast TFIIA/TBP/DNA complex. Science *272*, 830-836.

Georgopoulos, K., Bigby, M., Wang, J.H., Molnar, A., Wu, P., Winandy, S., and Sharpe, A. (1994). The Ikaros gene is required for the development of all lymphoid lineages. Cell *79*, 143-156.

Georgopoulos, K., Moore, D.D., and Derfler, B. (1992). Ikaros, an early lymphoid-specific transcription factor and a putative mediator for T cell commitment. Science *258*, 808-812.

Gilchrist, D.A., Dos Santos, G., Fargo, D.C., Xie, B., Gao, Y., Li, L., and Adelman, K. (2010). Pausing of RNA polymerase II disrupts DNA-specified nucleosome organization to enable precise gene regulation. Cell *143*, 540-551.

Gilchrist, D.A., Nechaev, S., Lee, C., Ghosh, S.K., Collins, J.B., Li, L., Gilmour, D.S., and Adelman, K. (2008). NELF-mediated stalling of Pol II can enhance gene expression by blocking promoter-proximal nucleosome assembly. Genes & development *22*, 1921-1933.

Gniazdowski, M., Mandel, J.L., Jr., Gissinger, F., Kedinger, C., and Chambon, P. (1970). Calf thymus RNA polymerases exhibit template specificity. Biochemical and biophysical research communications *38*, 1033-1040.

Goldberg, A.D., Banaszynski, L.A., Noh, K.M., Lewis, P.W., Elsaesser, S.J., Stadler, S., Dewell, S., Law, M., Guo, X., Li, X.*, et al.* (2010). Distinct factors control histone variant H3.3 localization at specific genomic regions. Cell *140*, 678-691.

Gomez-del Arco, P., Koipally, J., and Georgopoulos, K. (2005). Ikaros SUMOylation: switching out of repression. Molecular and cellular biology *25*, 2688-2697.

Gomez-del Arco, P., Maki, K., and Georgopoulos, K. (2004). Phosphorylation controls Ikaros's ability to negatively regulate the G(1)-S transition. Molecular and cellular biology *24*, 2797-2807.

Grunberg, S., and Hahn, S. (2013). Structural insights into transcription initiation by RNA polymerase II. Trends in biochemical sciences *38*, 603-611.

Grunberg, S., Warfield, L., and Hahn, S. (2012). Architecture of the RNA polymerase II preinitiation complex and mechanism of ATP-dependent promoter opening. Nature structural & molecular biology *19*, 788-796.

Guenther, M.G., Levine, S.S., Boyer, L.A., Jaenisch, R., and Young, R.A. (2007). A chromatin landmark and transcription initiation at most promoters in human cells. Cell *130*, 77-88.

Gurel, Z., Ronni, T., Ho, S., Kuchar, J., Payne, K.J., Turk, C.W., and Dovat, S. (2008). Recruitment of ikaros to pericentromeric heterochromatin is regulated by phosphorylation. J Biol Chem *283*, 8291-8300.

Hahm, K., Cobb, B.S., McCarty, A.S., Brown, K.E., Klug, C.A., Lee, R., Akashi, K., Weissman, I.L., Fisher, A.G., and Smale, S.T. (1998). Helios, a T cell-restricted Ikaros family member that quantitatively associates with Ikaros at centromeric heterochromatin. Genes Dev *12*, 782-796.

Hahm, K., Ernst, P., Lo, K., Kim, G.S., Turck, C., and Smale, S.T. (1994). The lymphoid transcription factor LyF-1 is encoded by specific, alternatively spliced mRNAs derived from the Ikaros gene. Molecular and cellular biology *14*, 7111-7123.

Hahn, S. (2004). Structure and mechanism of the RNA polymerase II transcription machinery. Nature structural & molecular biology *11*, 394-403.

Hann, S.R., and Eisenman, R.N. (1984). Proteins encoded by the human c-myc oncogene: differential expression in neoplastic cells. Molecular and cellular biology *4*, 2486-2497.

Hardy, R.R., Carmack, C.E., Shinton, S.A., Kemp, J.D., and Hayakawa, K. (1991). Resolution and characterization of pro-B and pre-pro-B cell stages in normal mouse bone marrow. The Journal of experimental medicine *173*, 1213-1225.

Hargreaves, D.C., Horng, T., and Medzhitov, R. (2009). Control of inducible gene expression by signal-dependent transcriptional elongation. Cell *138*, 129-145.

Hathaway, N.A., Bell, O., Hodges, C., Miller, E.L., Neel, D.S., and Crabtree, G.R. (2012). Dynamics and memory of heterochromatin in living cells. Cell *149*, 1447-1460.

He, N., Chan, C.K., Sobhian, B., Chou, S., Xue, Y., Liu, M., Alber, T., Benkirane, M., and Zhou, Q. (2011). Human Polymerase-Associated Factor complex (PAFc) connects the Super Elongation Complex (SEC) to RNA polymerase II on chromatin. Proc Natl Acad Sci U S A *108*, E636-645.

He, Y., Fang, J., Taatjes, D.J., and Nogales, E. (2013). Structural visualization of key steps in human transcription initiation. Nature *495*, 481-486.

Heinz, S., Benner, C., Spann, N., Bertolino, E., Lin, Y.C., Laslo, P., Cheng, J.X., Murre, C., Singh, H., and Glass, C.K. (2010). Simple combinations of lineage-determining transcription factors prime cis-regulatory elements required for macrophage and B cell identities. Molecular cell *38*, 576-589.

Heizmann, B., Kastner, P., and Chan, S. (2013). Ikaros is absolutely required for pre-B cell differentiation by attenuating IL-7 signals. The Journal of experimental medicine *210*, 2823-2832.

Henikoff, J.G., Belsky, J.A., Krassovsky, K., MacAlpine, D.M., and Henikoff, S. (2011). Epigenome characterization at single base-pair resolution. Proceedings of the National Academy of Sciences of the United States of America *108*, 18318-18323.

Henriques, T., Gilchrist, D.A., Nechaev, S., Bern, M., Muse, G.W., Burkholder, A., Fargo, D.C., and Adelman, K. (2013). Stable pausing by RNA polymerase II provides an opportunity to target and integrate regulatory signals. Molecular cell *52*, 517-528.

Herzog, S., Reth, M., and Jumaa, H. (2009). Regulation of B-cell proliferation and differentiation by pre-B-cell receptor signalling. Nat Rev Immunol *9*, 195-205.

Hewish, D.R., and Burgoyne, L.A. (1973). Chromatin sub-structure. The digestion of chromatin DNA at regularly spaced sites by a nuclear deoxyribonuclease. Biochemical and biophysical research communications *52*, 504-510.

Holstege, F.C., Tantin, D., Carey, M., van der Vliet, P.C., and Timmers, H.T. (1995). The requirement for the basal transcription factor IIE is determined by the helical stability of promoter DNA. EMBO J *14*, 810-819.

Honma, Y., Kiyosawa, H., Mori, T., Oguri, A., Nikaido, T., Kanazawa, K., Tojo, M., Takeda, J., Tanno, Y., Yokoya, S.*, et al.* (1999). Eos: a novel member of the Ikaros gene family expressed predominantly in the developing nervous system. FEBS Lett *447*, 76-80.

Hu, G., Cui, K., Northrup, D., Liu, C., Wang, C., Tang, Q., Ge, K., Levens, D., Crane-Robinson, C., and Zhao, K. (2013). H2A.Z facilitates access of active and repressive complexes to chromatin in embryonic stem cell self-renewal and differentiation. Cell stem cell *12*, 180-192.

Hughes, A.L., Jin, Y., Rando, O.J., and Struhl, K. (2012). A functional evolutionary approach to identify determinants of nucleosome positioning: a unifying model for establishing the genome-wide pattern. Molecular cell *48*, 5-15.

Huh, J.W., Wu, J., Lee, C.H., Yun, M., Gilada, D., Brautigam, C.A., and Li, B. (2012). Multivalent di-nucleosome recognition enables the Rpd3S histone deacetylase complex to tolerate decreased H3K36 methylation levels. EMBO J *31*, 3564-3574.

Jamai, A., Imoberdorf, R.M., and Strubin, M. (2007). Continuous histone H2B and transcription-dependent histone H3 exchange in yeast cells outside of replication. Mol Cell *25*, 345-355.

Jang, M.K., Mochizuki, K., Zhou, M., Jeong, H.S., Brady, J.N., and Ozato, K. (2005). The bromodomain protein Brd4 is a positive regulatory component of P-TEFb and stimulates RNA polymerase II-dependent transcription. Molecular cell *19*, 523-534.

Jeronimo, C., and Robert, F. (2014). Kin28 regulates the transient association of Mediator with core promoters. Nature structural & molecular biology *21*, 449-455.

Jiang, H., Shukla, A., Wang, X., Chen, W.Y., Bernstein, B.E., and Roeder, R.G. (2011). Role for Dpy-30 in ES cell-fate specification by regulation of H3K4 methylation within bivalent domains. Cell *144*, 513-525.

Jin, C., and Felsenfeld, G. (2007). Nucleosome stability mediated by histone variants H3.3 and H2A.Z. Genes & development *21*, 1519-1529.

Jin, C., Zang, C., Wei, G., Cui, K., Peng, W., Zhao, K., and Felsenfeld, G. (2009). H3.3/H2A.Z double variant-containing nucleosomes mark 'nucleosome-free regions' of active promoters and other regulatory regions. Nat Genet *41*, 941-945.

Jonkers, I., Kwak, H., and Lis, J.T. (2014). Genome-wide dynamics of Pol II elongation and its interplay with promoter proximal pausing, chromatin, and exons. eLife *3*, e02407.

Jumaa, H., Hendriks, R.W., and Reth, M. (2005). B cell signaling and tumorigenesis. Annual review of immunology *23*, 415-445.

Kaji, K., Caballero, I.M., MacLeod, R., Nichols, J., Wilson, V.A., and Hendrich, B. (2006). The NuRD component Mbd3 is required for pluripotency of embryonic stem cells. Nat Cell Biol *8*, 285-292.

Kaplan, N., Moore, I.K., Fondufe-Mittendorf, Y., Gossett, A.J., Tillo, D., Field, Y., LeProust, E.M., Hughes, T.R., Lieb, J.D., Widom, J.*, et al.* (2009). The DNA-encoded nucleosome organization of a eukaryotic genome. Nature *458*, 362-366.

Kedinger, C., Gniazdowski, M., Mandel, J.L., Jr., Gissinger, F., and Chambon, P. (1970). Alpha-amanitin: a specific inhibitor of one of two DNA-pendent RNA polymerase activities from calf thymus. Biochemical and biophysical research communications *38*, 165-171.

Kim, H.J., and Bae, S.C. (2011). Histone deacetylase inhibitors: molecular mechanisms of action and clinical trials as anti-cancer drugs. American journal of translational research *3*, 166-179.

Kim, J., Sif, S., Jones, B., Jackson, A., Koipally, J., Heller, E., Winandy, S., Viel, A., Sawyer, A., Ikeda, T.*, et al.* (1999). Ikaros DNA-binding proteins direct formation of chromatin remodeling complexes in lymphocytes. Immunity *10*, 345-355.

Kim, J.L., Nikolov, D.B., and Burley, S.K. (1993a). Co-crystal structure of TBP recognizing the minor groove of a TATA element. Nature *365*, 520-527.

Kim, T.K., Ebright, R.H., and Reinberg, D. (2000). Mechanism of ATP-dependent promoter melting by transcription factor IIH. Science *288*, 1418-1422.

Kim, Y., Geiger, J.H., Hahn, S., and Sigler, P.B. (1993b). Crystal structure of a yeast TBP/TATA-box complex. Nature *365*, 512-520.

Kireeva, M.L., Walter, W., Tchernajenko, V., Bondarenko, V., Kashlev, M., and Studitsky, V.M. (2002). Nucleosome remodeling induced by RNA polymerase II: loss of the H2A/H2B dimer during transcription. Molecular cell *9*, 541-552.

Kitamura, D., Roes, J., Kuhn, R., and Rajewsky, K. (1991). A B cell-deficient mouse by targeted disruption of the membrane exon of the immunoglobulin mu chain gene. Nature *350*, 423-426.

Klug, C.A., Morrison, S.J., Masek, M., Hahm, K., Smale, S.T., and Weissman, I.L. (1998). Hematopoietic stem cells and lymphoid progenitors express different Ikaros isoforms, and Ikaros is localized to heterochromatin in immature lymphocytes. Proceedings of the National Academy of Sciences of the United States of America *95*, 657-662.

Koipally, J., and Georgopoulos, K. (2000). Ikaros interactions with CtBP reveal a repression mechanism that is independent of histone deacetylase activity. The Journal of biological chemistry *275*, 19594-19602.

Koipally, J., Kim, J., Jones, B., Jackson, A., Avitahl, N., Winandy, S., Trevisan, M., Nichogiannopoulou, A., Kelley, C., and Georgopoulos, K. (1999). Ikaros chromatin remodeling complexes in the control of differentiation of the hemo-lymphoid system. Cold Spring Harbor symposia on quantitative biology *64*, 79-86.

Kondo, M., Weissman, I.L., and Akashi, K. (1997). Identification of clonogenic common lymphoid progenitors in mouse bone marrow. Cell *91*, 661-672.

Kostrewa, D., Zeller, M.E., Armache, K.J., Seizl, M., Leike, K., Thomm, M., and Cramer, P. (2009). RNA polymerase II-TFIIB structure and mechanism of transcription initiation. Nature *462*, 323-330.

Kouzarides, T. (2007). Chromatin modifications and their function. Cell *128*, 693-705.

Kouzine, F., Wojtowicz, D., Yamane, A., Resch, W., Kieffer-Kwon, K.R., Bandle, R., Nelson, S., Nakahashi, H., Awasthi, P., Feigenbaum, L*., et al.* (2013). Global regulation of promoter melting in naive lymphocytes. Cell *153*, 988-999.

Kraushaar, D.C., Jin, W., Maunakea, A., Abraham, B., Ha, M., and Zhao, K. (2013). Genome-wide incorporation dynamics reveal distinct categories of turnover for the histone variant H3.3. Genome Biol *14*, R121.

Lachner, M., O'Carroll, D., Rea, S., Mechtler, K., and Jenuwein, T. (2001). Methylation of histone H3 lysine 9 creates a binding site for HP1 proteins. Nature *410*, 116-120.

Leach, R.E., Rout, U.K., Schultz, J.F., Saunders, D.E., and Armant, D.R. (1999). Ethanol elevates c-Myc levels in cultured mouse preimplantation embryos. Alcoholism, clinical and experimental research *23*, 778-784.

Li, G., Levitus, M., Bustamante, C., and Widom, J. (2005a). Rapid spontaneous accessibility of nucleosomal DNA. Nature structural & molecular biology *12*, 46-53.

Li, Q., Price, J.P., Byers, S.A., Cheng, D., Peng, J., and Price, D.H. (2005b). Analysis of the large inactive P-TEFb complex indicates that it contains one 7SK molecule, a dimer of HEXIM1 or HEXIM2, and two P-TEFb molecules containing Cdk9 phosphorylated at threonine 186. J Biol Chem *280*, 28819-28826.

Li, Z., Gadue, P., Chen, K., Jiao, Y., Tuteja, G., Schug, J., Li, W., and Kaestner, K.H. (2012). Foxa2 and H2A.Z mediate nucleosome depletion during embryonic stem cell differentiation. Cell *151*, 1608-1616.

Lin, C., Smith, E.R., Takahashi, H., Lai, K.C., Martin-Brown, S., Florens, L., Washburn, M.P., Conaway, J.W., Conaway, R.C., and Shilatifard, A. (2010a). AFF4, a component of the ELL/P-TEFb elongation complex and a shared subunit of MLL chimeras, can link transcription elongation to leukemia. Mol Cell *37*, 429-437.

Lin, C.Y., Loven, J., Rahl, P.B., Paranal, R.M., Burge, C.B., Bradner, J.E., Lee, T.I., and Young, R.A. (2012). Transcriptional amplification in tumor cells with elevated c-Myc. Cell *151*, 56-67.

Lin, H., and Grosschedl, R. (1995). Failure of B-cell differentiation in mice lacking the transcription factor EBF. Nature *376*, 263-267.

Lin, J.J., Lehmann, L.W., Bonora, G., Sridharan, R., Vashisht, A.A., Tran, N., Plath, K., Wohlschlegel, J.A., and Carey, M. (2011). Mediator coordinates PIC assembly with recruitment of CHD1. Genes Dev *25*, 2198-2209.

Lin, Y.C., Jhunjhunwala, S., Benner, C., Heinz, S., Welinder, E., Mansson, R., Sigvardsson, M., Hagman, J., Espinoza, C.A., Dutkowski, J.*, et al.* (2010b). A global network of transcription factors, involving E2A, EBF1 and Foxo1, that orchestrates B cell fate. Nature immunology *11*, 635-643.

Liu, X., Bushnell, D.A., and Kornberg, R.D. (2013). RNA polymerase II transcription: structure and mechanism. Biochimica et biophysica acta *1829*, 2-8.

Liu, X., Bushnell, D.A., Wang, D., Calero, G., and Kornberg, R.D. (2010). Structure of an RNA polymerase II-TFIIB complex and the transcription initiation mechanism. Science *327*, 206-209.

Lo, K., Landau, N.R., and Smale, S.T. (1991). LyF-1, a transcriptional regulator that interacts with a novel class of promoters for lymphocyte-specific genes. Mol Cell Biol *11*, 5229-5243.

Luger, K., Dechassa, M.L., and Tremethick, D.J. (2012). New insights into nucleosome and chromatin structure: an ordered state or a disordered affair? Nature reviews Molecular cell biology *13*, 436-447.

Luger, K., Mader, A.W., Richmond, R.K., Sargent, D.F., and Richmond, T.J. (1997). Crystal structure of the nucleosome core particle at 2.8 A resolution. Nature *389*, 251-260.

Luk, E., Ranjan, A., Fitzgerald, P.C., Mizuguchi, G., Huang, Y., Wei, D., and Wu, C. (2010). Stepwise histone replacement by SWR1 requires dual activation with histone H2A.Z and canonical nucleosome. Cell *143*, 725-736.

Luk, E., Vu, N.D., Patteson, K., Mizuguchi, G., Wu, W.H., Ranjan, A., Backus, J., Sen, S., Lewis, M., Bai, Y.*, et al.* (2007). Chz1, a nuclear chaperone for histone H2AZ. Mol Cell *25*, 357-368.

Ma, S., Pathak, S., Mandal, M., Trinh, L., Clark, M.R., and Lu, R. (2010). Ikaros and Aiolos inhibit pre-B-cell proliferation by directly suppressing c-Myc expression. Mol Cell Biol *30*, 4149-4158.

Makarona, K., Caputo, V.S., Costa, J.R., Liu, B., O'Connor, D., Iskander, D., Roper, D., Robertson, L., Bhatnagar, N., Terpos, E.*, et al.* (2014). Transcriptional and epigenetic basis for restoration of G6PD enzymatic activity in human G6PD-deficient cells. Blood *124*, 134-141.

Manzo, S.G., Zhou, Z.L., Wang, Y.Q., Marinello, J., He, J.X., Li, Y.C., Ding, J., Capranico, G., and Miao, Z.H. (2012). Natural product triptolide mediates cancer cell death by triggering CDK7-dependent degradation of RNA polymerase II. Cancer research *72*, 5363-5373.

Mao, Z., Pan, L., Wang, W., Sun, J., Shan, S., Dong, Q., Liang, X., Dai, L., Ding, X., Chen, S.*, et al.* (2014). Anp32e, a higher eukaryotic histone chaperone directs preferential recognition for H2A.Z. Cell research *24*, 389-399.

Martensson, A., and Martensson, I.L. (1997). Early B cell factor binds to a site critical for lambda5 core enhancer activity. Eur J Immunol *27*, 315-320.

Martin, A.M., Pouchnik, D.J., Walker, J.L., and Wyrick, J.J. (2004). Redundant roles for histone H3 N-terminal lysine residues in subtelomeric gene repression in Saccharomyces cerevisiae. Genetics *167*, 1123-1132.

Matthias, P., and Rolink, A.G. (2005). Transcriptional networks in developing and mature B cells. Nat Rev Immunol *5*, 497-508.

McDonel, P., Costello, I., and Hendrich, B. (2009). Keeping things quiet: roles of NuRD and Sin3 co-repressor complexes during mammalian development. The international journal of biochemistry & cell biology *41*, 108-116.

Merkenschlager, M. (2010). Ikaros in immune receptor signaling, lymphocyte differentiation, and function. FEBS letters *584*, 4910-4914.

Mizuguchi, G., Shen, X., Landry, J., Wu, W.H., Sen, S., and Wu, C. (2004). ATP-driven exchange of histone H2AZ variant catalyzed by SWR1 chromatin remodeling complex. Science *303*, 343-348.

Molnar, A., and Georgopoulos, K. (1994). The Ikaros gene encodes a family of functionally diverse zinc finger DNA-binding proteins. Mol Cell Biol *14*, 8292-8303.

Morgan, B., Sun, L., Avitahl, N., Andrikopoulos, K., Ikeda, T., Gonzales, E., Wu, P., Neben, S., and Georgopoulos, K. (1997). Aiolos, a lymphoid restricted transcription factor that interacts with Ikaros to regulate lymphocyte differentiation. EMBO J *16*, 2004-2013.

Morris, S.A., Baek, S., Sung, M.H., John, S., Wiench, M., Johnson, T.A., Schiltz, R.L., and Hager, G.L. (2014). Overlapping chromatin-remodeling systems collaborate genome wide at dynamic chromatin transitions. Nature structural & molecular biology *21*, 73-81.

Morrison, A.J., and Shen, X. (2009). Chromatin remodelling beyond transcription: the INO80 and SWR1 complexes. Nature reviews Molecular cell biology *10*, 373-384.

Morrison, S.J., Uchida, N., and Weissman, I.L. (1995). The biology of hematopoietic stem cells. Annual review of cell and developmental biology *11*, 35-71.

Mullighan, C.G., Miller, C.B., Radtke, I., Phillips, L.A., Dalton, J., Ma, J., White, D., Hughes, T.P., Le Beau, M.M., Pui, C.H., *et al.* (2008). BCR-ABL1 lymphoblastic leukaemia is characterized by the deletion of Ikaros. Nature *453*, 110-114.

Murakami, K., Elmlund, H., Kalisman, N., Bushnell, D.A., Adams, C.M., Azubel, M., Elmlund, D., Levi-Kalisman, Y., Liu, X., Gibbons, B.J., *et al.* (2013). Architecture of an RNA polymerase II transcription pre-initiation complex. Science *342*, 1238724.

Musselman, C.A., Ramirez, J., Sims, J.K., Mansfield, R.E., Oliver, S.S., Denu, J.M., Mackay, J.P., Wade, P.A., Hagman, J., and Kutateladze, T.G. (2012). Bivalent recognition of nucleosomes by the tandem PHD fingers of the CHD4 ATPase is required for CHD4-mediated repression. Proceedings of the National Academy of Sciences of the United States of America *109*, 787-792.

Naito, T., Gomez-Del Arco, P., Williams, C.J., and Georgopoulos, K. (2007). Antagonistic interactions between Ikaros and the chromatin remodeler Mi-2beta determine silencer activity and Cd4 gene expression. Immunity *27*, 723-734.

Nakahara, T., Hashimoto, K., Hirano, M., Koll, M., Martin, C.R., and Preedy, V.R. (2003). Acute and chronic effects of alcohol exposure on skeletal muscle c-myc, p53, and Bcl-2 mRNA expression. American journal of physiology Endocrinology and metabolism *285*, E1273-1281.

Nekrasov, M., Amrichova, J., Parker, B.J., Soboleva, T.A., Jack, C., Williams, R., Huttley, G.A., and Tremethick, D.J. (2012). Histone H2A.Z inheritance during the cell cycle and its impact on promoter organization and dynamics. Nature structural & molecular biology *19*, 1076-1083.

Neumann, H., Hancock, S.M., Buning, R., Routh, A., Chapman, L., Somers, J., Owen-Hughes, T., van Noort, J., Rhodes, D., and Chin, J.W. (2009). A method for genetically installing site-specific acetylation in recombinant histones defines the effects of H3 K56 acetylation. Molecular cell *36*, 153-163.

Nguyen, V.T., Kiss, T., Michels, A.A., and Bensaude, O. (2001). 7SK small nuclear RNA binds to and inhibits the activity of CDK9/cyclin T complexes. Nature *414*, 322-325.

Nicodeme, E., Jeffrey, K.L., Schaefer, U., Beinke, S., Dewell, S., Chung, C.W., Chandwani, R., Marazzi, I., Wilson, P., Coste, H., *et al.* (2010). Suppression of inflammation by a synthetic histone mimic. Nature *468*, 1119-1123.

Nie, Z., Hu, G., Wei, G., Cui, K., Yamane, A., Resch, W., Wang, R., Green, D.R., Tessarollo, L., Casellas, R., *et al.* (2012). c-Myc is a universal amplifier of expressed genes in lymphocytes and embryonic stem cells. Cell *151*, 68-79.

Nutt, S.L., Heavey, B., Rolink, A.G., and Busslinger, M. (1999). Commitment to the B-lymphoid lineage depends on the transcription factor Pax5. Nature *401*, 556-562.

O'Riordan, M., and Grosschedl, R. (1999). Coordinate regulation of B cell differentiation by the transcription factors EBF and E2A. Immunity *11*, 21-31.

Obri, A., Ouararhni, K., Papin, C., Diebold, M.L., Padmanabhan, K., Marek, M., Stoll, I., Roy, L., Reilly, P.T., Mak, T.W., *et al.* (2014). ANP32E is a histone chaperone that removes H2A.Z from chromatin. Nature *505*, 648-653.

Olins, A.L., and Olins, D.E. (1974). Spheroid chromatin units (v bodies). Science *183*, 330-332.

Osley, M.A. (1991). The regulation of histone synthesis in the cell cycle. Annual review of biochemistry *60*, 827-861.

Paice, A.G., Hesketh, J.E., Towner, P., Hirako, M., Peters, T.J., and Preedy, V.R. (2002). Alcohol increases c-myc mRNA and protein in skeletal and cardiac muscle. Metabolism: clinical and experimental *51*, 1285-1290.

Pan, G., and Greenblatt, J. (1994). Initiation of transcription by RNA polymerase II is limited by melting of the promoter DNA in the region immediately upstream of the initiation site. The Journal of biological chemistry *269*, 30101-30104.

Papamichos-Chronakis, M., Watanabe, S., Rando, O.J., and Peterson, C.L. (2011). Global regulation of H2A.Z localization by the INO80 chromatin-remodeling enzyme is essential for genome integrity. Cell *144*, 200-213.

Payne, K.J., Huang, G., Sahakian, E., Zhu, J.Y., Barteneva, N.S., Barsky, L.W., Payne, M.A., and Crooks, G.M. (2003). Ikaros isoform x is selectively expressed in myeloid differentiation. Journal of immunology *170*, 3091-3098.

Perdomo, J., Holmes, M., Chong, B., and Crossley, M. (2000). Eos and pegasus, two members of the Ikaros family of proteins with distinct DNA binding activities. J Biol Chem *275*, 38347-38354.

Peterlin, B.M., and Price, D.H. (2006). Controlling the elongation phase of transcription with P-TEFb. Mol Cell *23*, 297-305.

Petesch, S.J., and Lis, J.T. (2008). Rapid, transcription-independent loss of nucleosomes over a large chromatin domain at Hsp70 loci. Cell *134*, 74-84.

Pfaffl, M.W. (2001). A new mathematical model for relative quantification in real-time RT-PCR. Nucleic acids research *29*, e45.

Phelan, M.L., Schnitzler, G.R., and Kingston, R.E. (2000). Octamer transfer and creation of stably remodeled nucleosomes by human SWI-SNF and its isolated ATPases. Molecular and cellular biology *20*, 6380-6389.

Phillips, D.M. (1963). The presence of acetyl groups of histones. The Biochemical journal *87*, 258-263.

Poirier, M.G., Bussiek, M., Langowski, J., and Widom, J. (2008). Spontaneous access to DNA target sites in folded chromatin fibers. Journal of molecular biology *379*, 772-786.

Quintas-Cardama, A., Santos, F.P., and Garcia-Manero, G. (2011). Histone deacetylase inhibitors for the treatment of myelodysplastic syndrome and acute myeloid leukemia. Leukemia *25*, 226-235.

Rahl, P.B., Lin, C.Y., Seila, A.C., Flynn, R.A., McCuine, S., Burge, C.B., Sharp, P.A., and Young, R.A. (2010). c-Myc regulates transcriptional pause release. Cell *141*, 432-445.

Raisner, R.M., Hartley, P.D., Meneghini, M.D., Bao, M.Z., Liu, C.L., Schreiber, S.L., Rando, O.J., and Madhani, H.D. (2005). Histone variant H2A.Z marks the 5' ends of both active and inactive genes in euchromatin. Cell *123*, 233-248.

Ramanathan, Y., Rajpara, S.M., Reza, S.M., Lees, E., Shuman, S., Mathews, M.B., and Pe'ery, T. (2001). Three RNA polymerase II carboxyl-terminal domain kinases display distinct substrate preferences. J Biol Chem *276*, 10913-10920.

Ramirez-Carrozzi, V.R., Nazarian, A.A., Li, C.C., Gore, S.L., Sridharan, R., Imbalzano, A.N., and Smale, S.T. (2006). Selective and antagonistic functions of SWI/SNF and Mi-2beta

nucleosome remodeling complexes during an inflammatory response. Genes & development *20*, 282-296.

Ranjan, A., Mizuguchi, G., FitzGerald, P.C., Wei, D., Wang, F., Huang, Y., Luk, E., Woodcock, C.L., and Wu, C. (2013). Nucleosome-free region dominates histone acetylation in targeting SWR1 to promoters for H2A.Z replacement. Cell *154*, 1232-1245.

Raveh-Sadka, T., Levo, M., Shabi, U., Shany, B., Keren, L., Lotan-Pompan, M., Zeevi, D., Sharon, E., Weinberger, A., and Segal, E. (2012). Manipulating nucleosome disfavoring sequences allows fine-tune regulation of gene expression in yeast. Nat Genet *44*, 743-750.

Reynaud, D., Demarco, I.A., Reddy, K.L., Schjerven, H., Bertolino, E., Chen, Z., Smale, S.T., Winandy, S., and Singh, H. (2008). Regulation of B cell fate commitment and immunoglobulin heavy-chain gene rearrangements by Ikaros. Nat Immunol *9*, 927-936.

Reynolds, N., Latos, P., Hynes-Allen, A., Loos, R., Leaford, D., O'Shaughnessy, A., Mosaku, O., Signolet, J., Brennecke, P., Kalkan, T.*, et al.* (2012). NuRD suppresses pluripotency gene expression to promote transcriptional heterogeneity and lineage commitment. Cell stem cell *10*, 583-594.

Reynolds, N., O'Shaughnessy, A., and Hendrich, B. (2013). Transcriptional repressors: multifaceted regulators of gene expression. Development *140*, 505-512.

Rhee, H.S., Bataille, A.R., Zhang, L., and Pugh, B.F. (2014). Subnucleosomal Structures and Nucleosome Asymmetry across a Genome. Cell *159*, 1377-1388.

Rincon-Arano, H., Halow, J., Delrow, J.J., Parkhurst, S.M., and Groudine, M. (2012). UpSET Recruits HDAC Complexes and Restricts Chromatin Accessibility and Acetylation at Promoter Regions. Cell *151*, 1214-1228.

Roeder, R.G. (1996). The role of general initiation factors in transcription by RNA polymerase II. Trends in biochemical sciences *21*, 327-335.

Roeder, R.G., and Rutter, W.J. (1969). Multiple forms of DNA-dependent RNA polymerase in eukaryotic organisms. Nature *224*, 234-237.

Roeder, R.G., and Rutter, W.J. (1970). Specific nucleolar and nucleoplasmic RNA polymerases. Proceedings of the National Academy of Sciences of the United States of America *65*, 675-682.

Rougvie, A.E., and Lis, J.T. (1988). The RNA polymerase II molecule at the 5' end of the uninduced hsp70 gene of D. melanogaster is transcriptionally engaged. Cell *54*, 795-804.

Rufiange, A., Jacques, P.E., Bhat, W., Robert, F., and Nourani, A. (2007). Genome-wide replication-independent histone H3 exchange occurs predominantly at promoters and implicates H3 K56 acetylation and Asf1. Molecular cell *27*, 393-405.

Sabbattini, P., Lundgren, M., Georgiou, A., Chow, C., Warnes, G., and Dillon, N. (2001). Binding of Ikaros to the lambda5 promoter silences transcription through a mechanism that does not require heterochromatin formation. EMBO J *20*, 2812-2822.

Sainsbury, S., Niesser, J., and Cramer, P. (2013). Structure and function of the initially transcribing RNA polymerase II-TFIIB complex. Nature *493*, 437-440.

Saunders, A., Core, L.J., and Lis, J.T. (2006). Breaking barriers to transcription elongation. Nature reviews Molecular cell biology *7*, 557-567.

Schjerven, H., McLaughlin, J., Arenzana, T.L., Frietze, S., Cheng, D., Wadsworth, S.E., Lawson, G.W., Bensinger, S.J., Farnham, P.J., Witte, O.N*., et al.* (2013). Selective regulation of lymphopoiesis and leukemogenesis by individual zinc fingers of Ikaros. Nature immunology *14*, 1073-1083.

Schones, D.E., Cui, K., Cuddapah, S., Roh, T.Y., Barski, A., Wang, Z., Wei, G., and Zhao, K. (2008). Dynamic regulation of nucleosome positioning in the human genome. Cell *132*, 887-898.

Schubert, H.L., Wittmeyer, J., Kasten, M.M., Hinata, K., Rawling, D.C., Heroux, A., Cairns, B.R., and Hill, C.P. (2013). Structure of an actin-related subcomplex of the SWI/SNF chromatin remodeler. Proceedings of the National Academy of Sciences of the United States of America *110*, 3345-3350.

Schwickert, T.A., Tagoh, H., Gultekin, S., Dakic, A., Axelsson, E., Minnich, M., Ebert, A., Werner, B., Roth, M., Cimmino, L*., et al.* (2014). Stage-specific control of early B cell development by the transcription factor Ikaros. Nature immunology *15*, 283-293.

Scott, E.W., Simon, M.C., Anastasi, J., and Singh, H. (1994). Requirement of transcription factor PU.1 in the development of multiple hematopoietic lineages. Science *265*, 1573-1577.

Seet, C.S., Brumbaugh, R.L., and Kee, B.L. (2004). Early B cell factor promotes B lymphopoiesis with reduced interleukin 7 responsiveness in the absence of E2A. The Journal of experimental medicine *199*, 1689-1700.

Segal, E., Fondufe-Mittendorf, Y., Chen, L., Thastrom, A., Field, Y., Moore, I.K., Wang, J.P., and Widom, J. (2006). A genomic code for nucleosome positioning. Nature *442*, 772-778.

Shi, J., Whyte, W.A., Zepeda-Mendoza, C.J., Milazzo, J.P., Shen, C., Roe, J.S., Minder, J.L., Mercan, F., Wang, E., Eckersley-Maslin, M.A*., et al.* (2013). Role of SWI/SNF in acute leukemia maintenance and enhancer-mediated Myc regulation. Genes & development *27*, 2648-2662.

Shimizu, T., Mundt, C., Licence, S., Melchers, F., and Martensson, I.L. (2002). VpreB1/VpreB2/lambda 5 triple-deficient mice show impaired B cell development but functional allelic exclusion of the IgH locus. Journal of immunology *168*, 6286-6293.

Shimono, Y., Murakami, H., Kawai, K., Wade, P.A., Shimokata, K., and Takahashi, M. (2003). Mi-2 beta associates with BRG1 and RET finger protein at the distinct regions with transcriptional activating and repressing abilities. J Biol Chem *278*, 51638-51645.

Sigvardsson, M. (2000). Overlapping expression of early B-cell factor and basic helix-loop-helix proteins as a mechanism to dictate B-lineage-specific activity of the lambda5 promoter. Molecular and cellular biology *20*, 3640-3654.

Sigvardsson, M., O'Riordan, M., and Grosschedl, R. (1997). EBF and E47 collaborate to induce expression of the endogenous immunoglobulin surrogate light chain genes. Immunity *7*, 25-36.

Simon, M., North, J.A., Shimko, J.C., Forties, R.A., Ferdinand, M.B., Manohar, M., Zhang, M., Fishel, R., Ottesen, J.J., and Poirier, M.G. (2011). Histone fold modifications control nucleosome unwrapping and disassembly. Proceedings of the National Academy of Sciences of the United States of America *108*, 12711-12716.

Singh, J., and Padgett, R.A. (2009). Rates of in situ transcription and splicing in large human genes. Nature structural & molecular biology *16*, 1128-1133.

Smith, E., Lin, C., and Shilatifard, A. (2011). The super elongation complex (SEC) and MLL in development and disease. Genes Dev *25*, 661-672.

Soboleva, T.A., Nekrasov, M., Pahwa, A., Williams, R., Huttley, G.A., and Tremethick, D.J. (2012). A unique H2A histone variant occupies the transcriptional start site of active genes. Nature structural & molecular biology *19*, 25-30.

Sopta, M., Carthew, R.W., and Greenblatt, J. (1985). Isolation of three proteins that bind to mammalian RNA polymerase II. The Journal of biological chemistry *260*, 10353-10360.

Sridharan, R., and Smale, S.T. (2007). Predominant interaction of both Ikaros and Helios with the NuRD complex in immature thymocytes. J Biol Chem *282*, 30227-30238.

Straube, K., Blackwell, J.S., Jr., and Pemberton, L.F. (2010). Nap1 and Chz1 have separate Htz1 nuclear import and assembly functions. Traffic *11*, 185-197.

Struhl, K., and Segal, E. (2013). Determinants of nucleosome positioning. Nature structural & molecular biology *20*, 267-273.

Stumpf, M., Yue, X., Schmitz, S., Luche, H., Reddy, J.K., and Borggrefe, T. (2010). Specific erythroid-lineage defect in mice conditionally deficient for Mediator subunit Med1. Proc Natl Acad Sci U S A *107*, 21541-21546.

Su, Y.W., Flemming, A., Wossning, T., Hobeika, E., Reth, M., and Jumaa, H. (2003). Identification of a pre-BCR lacking surrogate light chain. J Exp Med *198*, 1699-1706.

Sun, L., Liu, A., and Georgopoulos, K. (1996). Zinc finger-mediated protein interactions modulate Ikaros activity, a molecular control of lymphocyte development. EMBO J *15*, 5358-5369.

Suto, R.K., Clarkson, M.J., Tremethick, D.J., and Luger, K. (2000). Crystal structure of a nucleosome core particle containing the variant histone H2A.Z. Nature structural biology *7*, 1121-1124.

Takahashi, H., Parmely, T.J., Sato, S., Tomomori-Sato, C., Banks, C.A., Kong, S.E., Szutorisz, H., Swanson, S.K., Martin-Brown, S., Washburn, M.P.*, et al.* (2011). Human mediator subunit MED26 functions as a docking site for transcription elongation factors. Cell *146*, 92-104.

Talbert, P.B., and Henikoff, S. (2010). Histone variants--ancient wrap artists of the epigenome. Nature reviews Molecular cell biology *11*, 264-275.

Tamrazi, A., Carlson, K.E., Daniels, J.R., Hurth, K.M., and Katzenellenbogen, J.A. (2002). Estrogen receptor dimerization: ligand binding regulates dimer affinity and dimer dissociation rate. Molecular endocrinology *16*, 2706-2719.

Tan, S., Hunziker, Y., Sargent, D.F., and Richmond, T.J. (1996). Crystal structure of a yeast TFIIA/TBP/DNA complex. Nature *381*, 127-151.

Tang, Z., Chen, W.Y., Shimada, M., Nguyen, U.T., Kim, J., Sun, X.J., Sengoku, T., McGinty, R.K., Fernandez, J.P., Muir, T.W.*, et al.* (2013). SET1 and p300 act synergistically, through coupled histone modifications, in transcriptional activation by p53. Cell *154*, 297-310.

Thakar, A., Gupta, P., Ishibashi, T., Finn, R., Silva-Moreno, B., Uchiyama, S., Fukui, K., Tomschik, M., Ausio, J., and Zlatanova, J. (2009). H2A.Z and H3.3 histone variants affect nucleosome structure: biochemical and biophysical studies. Biochemistry *48*, 10852-10857.

Thompson, E.C., Cobb, B.S., Sabbattini, P., Meixlsperger, S., Parelho, V., Liberg, D., Taylor, B., Dillon, N., Georgopoulos, K., Jumaa, H.*, et al.* (2007). Ikaros DNA-binding proteins as integral components of B cell developmental-stage-specific regulatory circuits. Immunity *26*, 335-344.

Tims, H.S., Gurunathan, K., Levitus, M., and Widom, J. (2011). Dynamics of nucleosome invasion by DNA binding proteins. Journal of molecular biology *411*, 430-448.

Titov, D.V., Gilman, B., He, Q.L., Bhat, S., Low, W.K., Dang, Y., Smeaton, M., Demain, A.L., Miller, P.S., Kugel, J.F.*, et al.* (2011). XPB, a subunit of TFIIH, is a target of the natural product triptolide. Nature chemical biology *7*, 182-188.

Tolstorukov, M.Y., Goldman, J.A., Gilbert, C., Ogryzko, V., Kingston, R.E., and Park, P.J. (2012). Histone variant H2A.Bbd is associated with active transcription and mRNA processing in human cells. Mol Cell *47*, 596-607.

Tolstorukov, M.Y., Kharchenko, P.V., Goldman, J.A., Kingston, R.E., and Park, P.J. (2009). Comparative analysis of H2A.Z nucleosome organization in the human and yeast genomes. Genome research *19*, 967-977.

Tolstorukov, M.Y., Sansam, C.G., Lu, P., Koellhoffer, E.C., Helming, K.C., Alver, B.H., Tillman, E.J., Evans, J.A., Wilson, B.G., Park, P.J.*, et al.* (2013). Swi/Snf chromatin remodeling/tumor suppressor complex establishes nucleosome occupancy at target promoters.

Proceedings of the National Academy of Sciences of the United States of America *110*, 10165-10170.

Tong, J.K., Hassig, C.A., Schnitzler, G.R., Kingston, R.E., and Schreiber, S.L. (1998). Chromatin deacetylation by an ATP-dependent nucleosome remodelling complex. Nature *395*, 917-921.

Tremethick, D.J. (2007). Higher-order structures of chromatin: the elusive 30 nm fiber. Cell *128*, 651-654.

Trinh, L.A., Ferrini, R., Cobb, B.S., Weinmann, A.S., Hahm, K., Ernst, P., Garraway, I.P., Merkenschlager, M., and Smale, S.T. (2001). Down-regulation of TDT transcription in CD4(+)CD8(+) thymocytes by Ikaros proteins in direct competition with an Ets activator. Genes & development *15*, 1817-1832.

Tropberger, P., Pott, S., Keller, C., Kamieniarz-Gdula, K., Caron, M., Richter, F., Li, G., Mittler, G., Liu, E.T., Buhler, M.*, et al.* (2013). Regulation of transcription through acetylation of H3K122 on the lateral surface of the histone octamer. Cell *152*, 859-872.

Uckun, F.M., Ma, H., Zhang, J., Ozer, Z., Dovat, S., Mao, C., Ishkhanian, R., Goodman, P., and Qazi, S. (2012). Serine phosphorylation by SYK is critical for nuclear localization and transcription factor function of Ikaros. Proceedings of the National Academy of Sciences of the United States of America *109*, 18072-18077.

Urbanek, P., Wang, Z.Q., Fetka, I., Wagner, E.F., and Busslinger, M. (1994). Complete block of early B cell differentiation and altered patterning of the posterior midbrain in mice lacking Pax5/BSAP. Cell *79*, 901-912.

Valdes-Mora, F., Song, J.Z., Statham, A.L., Strbenac, D., Robinson, M.D., Nair, S.S., Patterson, K.I., Tremethick, D.J., Stirzaker, C., and Clark, S.J. (2012). Acetylation of H2A.Z is a key epigenetic modification associated with gene deregulation and epigenetic remodeling in cancer. Genome research *22*, 307-321.

Valouev, A., Johnson, S.M., Boyd, S.D., Smith, C.L., Fire, A.Z., and Sidow, A. (2011). Determinants of nucleosome organization in primary human cells. Nature *474*, 516-520.

van Loo, P.F., Dingjan, G.M., Maas, A., and Hendriks, R.W. (2007). Surrogate-light-chain silencing is not critical for the limitation of pre-B cell expansion but is for the termination of constitutive signaling. Immunity *27*, 468-480.

Vermeulen, M., Eberl, H.C., Matarese, F., Marks, H., Denissov, S., Butter, F., Lee, K.K., Olsen, J.V., Hyman, A.A., Stunnenberg, H.G., *et al.* (2010). Quantitative interaction proteomics and genome-wide profiling of epigenetic histone marks and their readers. Cell *142*, 967-980.

Vermeulen, M., Mulder, K.W., Denissov, S., Pijnappel, W.W., van Schaik, F.M., Varier, R.A., Baltissen, M.P., Stunnenberg, H.G., Mann, M., and Timmers, H.T. (2007). Selective anchoring of TFIID to nucleosomes by trimethylation of histone H3 lysine 4. Cell *131*, 58-69.

Vispe, S., DeVries, L., Creancier, L., Besse, J., Breand, S., Hobson, D.J., Svejstrup, J.Q., Annereau, J.P., Cussac, D., Dumontet, C., *et al.* (2009). Triptolide is an inhibitor of RNA polymerase I and II-dependent transcription leading predominantly to down-regulation of short-lived mRNA. Molecular cancer therapeutics *8*, 2780-2790.

Wang, H.B., and Zhang, Y. (2001). Mi2, an auto-antigen for dermatomyositis, is an ATP-dependent nucleosome remodeling factor. Nucleic acids research *29*, 2517-2521.

Wang, J.H., Nichogiannopoulou, A., Wu, L., Sun, L., Sharpe, A.H., Bigby, M., and Georgopoulos, K. (1996). Selective defects in the development of the fetal and adult lymphoid system in mice with an Ikaros null mutation. Immunity *5*, 537-549.

Wang, Y., Lu, J.J., He, L., and Yu, Q. (2011). Triptolide (TPL) inhibits global transcription by inducing proteasome-dependent degradation of RNA polymerase II (Pol II). PloS one *6*, e23993.

Wang, Z., Zang, C., Cui, K., Schones, D.E., Barski, A., Peng, W., and Zhao, K. (2009). Genome-wide mapping of HATs and HDACs reveals distinct functions in active and inactive genes. Cell *138*, 1019-1031.

Wang, Z., Zang, C., Rosenfeld, J.A., Schones, D.E., Barski, A., Cuddapah, S., Cui, K., Roh, T.Y., Peng, W., Zhang, M.Q., *et al.* (2008). Combinatorial patterns of histone acetylations and methylations in the human genome. Nat Genet *40*, 897-903.

Watanabe, S., Radman-Livaja, M., Rando, O.J., and Peterson, C.L. (2013). A histone acetylation switch regulates H2A.Z deposition by the SWR-C remodeling enzyme. Science *340*, 195-199.

Weber, C.M., Henikoff, J.G., and Henikoff, S. (2010). H2A.Z nucleosomes enriched over active genes are homotypic. Nature structural & molecular biology *17*, 1500-1507.

Weber, C.M., and Henikoff, S. (2014). Histone variants: dynamic punctuation in transcription. Genes Dev *28*, 672-682.

Weber, C.M., Ramachandran, S., and Henikoff, S. (2014). Nucleosomes are context-specific, H2A.Z-modulated barriers to RNA polymerase. Mol Cell *53*, 819-830.

Weiner, A., Hughes, A., Yassour, M., Rando, O.J., and Friedman, N. (2010). High-resolution nucleosome mapping reveals transcription-dependent promoter packaging. Genome research *20*, 90-100.

Weinmann, R., Raskas, H.J., and Roeder, R.G. (1974). Role of DNA-dependent RNA polymerases II and III in transcription of the adenovirus genome late in productive infection. Proceedings of the National Academy of Sciences of the United States of America *71*, 3426-3439.

Weinmann, R., and Roeder, R.G. (1974). Role of DNA-dependent RNA polymerase 3 in the transcription of the tRNA and 5S RNA genes. Proceedings of the National Academy of Sciences of the United States of America *71*, 1790-1794.

Weiss, S., and Gladstone, L. (1959). A mammalian system for the incorporation of cytidine triphosphate into ribonucleic acid. J Am Chem Soc *81*, 4118-4119.

West, M.H., and Bonner, W.M. (1980). Histone 2A, a heteromorphous family of eight protein species. Biochemistry *19*, 3238-3245.

Whyte, W.A., Orlando, D.A., Hnisz, D., Abraham, B.J., Lin, C.Y., Kagey, M.H., Rahl, P.B., Lee, T.I., and Young, R.A. (2013). Master transcription factors and mediator establish super-enhancers at key cell identity genes. Cell *153*, 307-319.

Williams, C.J., Naito, T., Arco, P.G., Seavitt, J.R., Cashman, S.M., De Souza, B., Qi, X., Keables, P., Von Andrian, U.H., and Georgopoulos, K. (2004). The chromatin remodeler Mi-2beta is required for CD4 expression and T cell development. Immunity *20*, 719-733.

Winandy, S., Wu, P., and Georgopoulos, K. (1995). A dominant mutation in the Ikaros gene leads to rapid development of leukemia and lymphoma. Cell *83*, 289-299.

Wong, K.H., Jin, Y., and Struhl, K. (2014). TFIIH phosphorylation of the Pol II CTD stimulates mediator dissociation from the preinitiation complex and promoter escape. Molecular cell *54*, 601-612.

Woodage, T., Basrai, M.A., Baxevanis, A.D., Hieter, P., and Collins, F.S. (1997). Characterization of the CHD family of proteins. Proc Natl Acad Sci U S A *94*, 11472-11477.

Woodcock, C.L., Safer, J.P., and Stanchfield, J.E. (1976). Structural repeating units in chromatin. I. Evidence for their general occurrence. Exp Cell Res *97*, 101-110.

Wu, J.I., Lessard, J., and Crabtree, G.R. (2009). Understanding the words of chromatin regulation. Cell *136*, 200-206.

Xi, Y., Yao, J., Chen, R., Li, W., and He, X. (2011). Nucleosome fragility reveals novel functional states of chromatin and poises genes for activation. Genome research *21*, 718-724.

Xu, M., Long, C., Chen, X., Huang, C., Chen, S., and Zhu, B. (2010). Partitioning of histone H3-H4 tetramers during DNA replication-dependent chromatin assembly. Science *328*, 94-98.

Xue, Y., Wong, J., Moreno, G.T., Young, M.K., Cote, J., and Wang, W. (1998). NURD, a novel complex with both ATP-dependent chromatin-remodeling and histone deacetylase activities. Mol Cell *2*, 851-861.

Yagle, K., and Costa, L.G. (1999). Effects of alcohol on immediate-early gene expression in primary cultures of rat cortical astrocytes. Alcoholism, clinical and experimental research *23*, 446-455.

Yang, X., Zaurin, R., Beato, M., and Peterson, C.L. (2007). Swi3p controls SWI/SNF assembly and ATP-dependent H2A-H2B displacement. Nature structural & molecular biology *14*, 540-547.

Yang, Z., Yik, J.H., Chen, R., He, N., Jang, M.K., Ozato, K., and Zhou, Q. (2005). Recruitment of P-TEFb for stimulation of transcriptional elongation by the bromodomain protein Brd4. Molecular cell *19*, 535-545.

Yang, Z., Zhu, Q., Luo, K., and Zhou, Q. (2001). The 7SK small nuclear RNA inhibits the CDK9/cyclin T1 kinase to control transcription. Nature *414*, 317-322.

Yasuda, T., Sanjo, H., Pages, G., Kawano, Y., Karasuyama, H., Pouyssegur, J., Ogata, M., and Kurosaki, T. (2008). Erk kinases link pre-B cell receptor signaling to transcriptional events required for early B cell expansion. Immunity *28*, 499-508.

Yoshida, T., Hazan, I., Zhang, J., Ng, S.Y., Naito, T., Snippert, H.J., Heller, E.J., Qi, X., Lawton, L.N., Williams, C.J.*, et al.* (2008). The role of the chromatin remodeler Mi-2beta in

hematopoietic stem cell self-renewal and multilineage differentiation. Genes & development *22*, 1174-1189.

Yoshida, T., Ng, S.Y., Zuniga-Pflucker, J.C., and Georgopoulos, K. (2006). Early hematopoietic lineage restrictions directed by Ikaros. Nature immunology *7*, 382-391.

Young, R.A. (1991). RNA polymerase II. Annual review of biochemistry *60*, 689-715.

Yun, M., Wu, J., Workman, J.L., and Li, B. (2011). Readers of histone modifications. Cell research *21*, 564-578.

Zentner, G.E., and Henikoff, S. (2013). Regulation of nucleosome dynamics by histone modifications. Nature structural & molecular biology *20*, 259-266.

Zhang, H., Roberts, D.N., and Cairns, B.R. (2005a). Genome-wide dynamics of Htz1, a histone H2A variant that poises repressed/basal promoters for activation through histone loss. Cell *123*, 219-231.

Zhang, J., Jackson, A.F., Naito, T., Dose, M., Seavitt, J., Liu, F., Heller, E.J., Kashiwagi, M., Yoshida, T., Gounari, F.*, et al.* (2012). Harnessing of the nucleosome-remodeling-deacetylase complex controls lymphocyte development and prevents leukemogenesis. Nature immunology *13*, 86-94.

Zhang, R., Poustovoitov, M.V., Ye, X., Santos, H.A., Chen, W., Daganzo, S.M., Erzberger, J.P., Serebriiskii, I.G., Canutescu, A.A., Dunbrack, R.L.*, et al.* (2005b). Formation of MacroH2A-containing senescence-associated heterochromatin foci and senescence driven by ASF1a and HIRA. Dev Cell *8*, 19-30.

Zhang, Y., LeRoy, G., Seelig, H.P., Lane, W.S., and Reinberg, D. (1998). The dermatomyositis-specific autoantigen Mi2 is a component of a complex containing histone deacetylase and nucleosome remodeling activities. Cell *95*, 279-289.

Zhang, Y., Moqtaderi, Z., Rattner, B.P., Euskirchen, G., Snyder, M., Kadonaga, J.T., Liu, X.S., and Struhl, K. (2009). Intrinsic histone-DNA interactions are not the major determinant of nucleosome positions in vivo. Nature structural & molecular biology *16*, 847-852.

Zhang, Z., and Pugh, B.F. (2011). High-resolution genome-wide mapping of the primary structure of chromatin. Cell *144*, 175-186.

Zhang, Z., Wippo, C.J., Wal, M., Ward, E., Korber, P., and Pugh, B.F. (2011). A packing mechanism for nucleosome organization reconstituted across a eukaryotic genome. Science *332*, 977-980.

Zhou, Q., Li, T., and Price, D.H. (2012). RNA polymerase II elongation control. Annual review of biochemistry *81*, 119-143.

Zhuang, Y., Jackson, A., Pan, L., Shen, K., and Dai, M. (2004). Regulation of E2A gene expression in B-lymphocyte development. Molecular immunology *40*, 1165-1177.

Zhuang, Y., Soriano, P., and Weintraub, H. (1994). The helix-loop-helix gene E2A is required for B cell formation. Cell *79*, 875-884.

Appendix

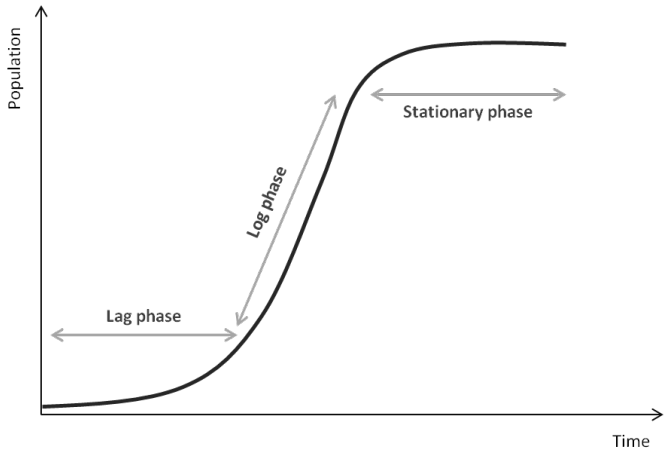

Figure S.1 Growth curve

Typical yeast growth curve contains lag phase, log phase and stationary phase. The shape of these phases were used to illustrate the trend in the kinetics of regulatory events during transcriptional regulation.

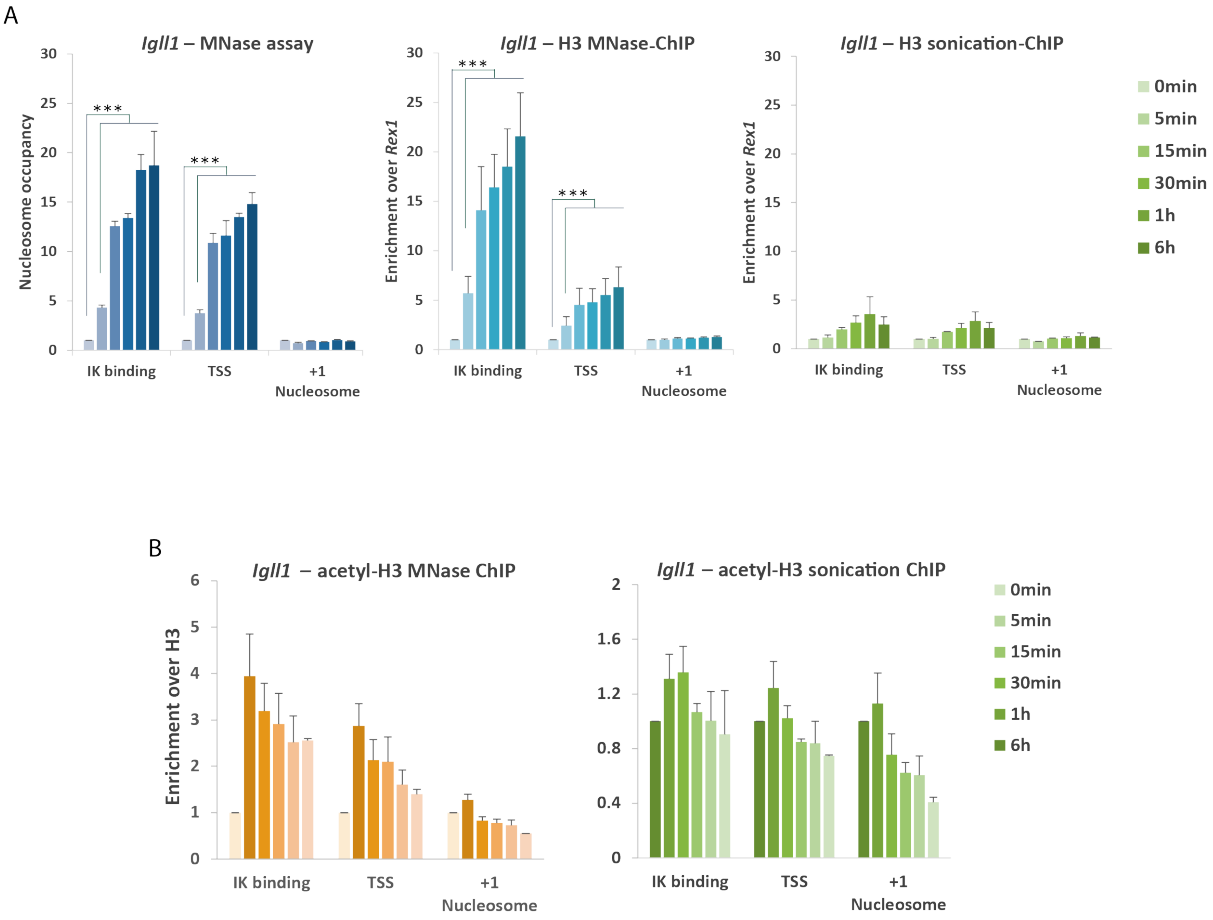

Figure S.2 Comparison of ChIP methods

A) shows different methods used to quantify nucleosome occupancy, namely MNase assay to directly quantify nucleosome protected DNA fragments (left), histone H3 ChIP using MNase digested chromatin (middle) and histone H3 ChIP using sonicated chromatin. (B) shows different methods used to quantify acetylated histone H3, namely acetyl-histone H3 ChIP using MNase digested chromatin (left) and acetyl-histone H3 ChIP using sonicated chromatin. Sonicated chromatin ChIP was an average of two biological replicates, the rest were three.

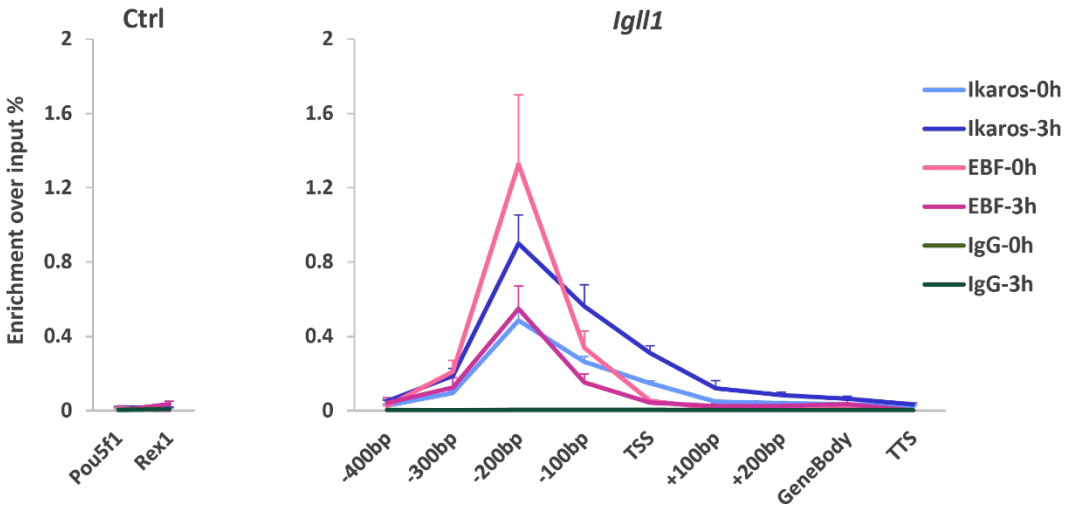

Figure S.3 Increased binding of Ikaros leads to a decrease of EBF binding at *Igll1* locus

Ikaros (blue shads) and EBF (pink shade) binding at the *Igll1* locus and negative control sites before (light) and after 3h (dark) of induction. IgG negative controls are shown in dark green. Data shown is an average of three biological replicates.

Table S.1 shRNA design

Oligos name	*Sequence*
H2AZ_sh1_F	**GATC**CCCCCTTATTATCTCAGGACTCTA**TTCAAGAGA**TAGAGTCCTGAGATAATAAGG**TTTTTGGAAC**
H2AZ_sh1_R	**TCGAG**TTCCAAAAACCTTATTATCTCAGGACTCTA**TCTCTTGAA**TAGAGTCCTGAGATAATAAGG**GGG**
H2AZ_sh2_F	**GATC**CCCCCGTATTCATCGACACCTGAA**TTCAAGAGA**TTCAGGTGTCGATGAATACGG**TTTTTGGAAC**
H2AZ_sh2_R	**TCGAG**TTCCAAAAACCGTATTCATCGACACCTGAA**TCTCTTGAA**TTCAGGTGTCGATGAATACGG**GGG**
H2AZ_sh3_F	**GATC**CCCCGACACCTGAAATCTAGGACA**TTCAAGAGA**TGTCCTAGATTTCAGGTGTCG**TTTTTGGAAC**
H2AZ_sh3_R	**TCGAG**TTCCAAAAACGACACCTGAAATCTAGGACA**TCTCTTGAA**TGTCCTAGATTTCAGGTGTCG**GGG**
Chd4_F	**GATC**CCCGACTACGACCTGTTCAAGCAG**TTCAAGAGA**CTGCTTGAACAGGTCGTAGTC**TTTTTGGAAC**
Chd4_R	**TCGAG**TTCCAAAAAGACTACGACCTGTTCAAGCAG**TCTCTTGAA**CTGCTTGAACAGGTCGTAGTC**GGG**
Brg1/Brm_F	**GATC**CCCCTGGAGAAGCAGCAGAAGATT**TTCAAGAGA**AATCTTCTGCTGCTTCTCCA**TTTTTGGAAC**
Brg1/Brm_R	**TCGAG**TTCCAAAAATGGAGAAGCAGCAGAAGATT**TCTCTTGAA**AATCTTCTGCTGCTTCTCCA**GGG**
Ikzf1_3UTR_3F	**GATC**CCCCCAGTGGTATTCAGAGATTAA**TTCAAGAGA**TTAATCTCTGAATACCACTGG**TTTTTGGAAC**
Ikzf1_3UTR_3R	**TCGAG**TTCCAAAAACCAGTGGTATTCAGAGATTAA**TCTCTTGAA**TTAATCTCTGAATACCACTGG**GGG**
Ikzf1_CDS_sh1_F	**GATC**CCCGGGCATGTACCCAGTCATTAA**TTCAAGAGA**TTAATGACTGGGTACATGCCC**TTTTTGGAAC**
Ikzf1_CDS_sh1_R	**TCGAG**TTCCAAAAAGGGCATGTACCCAGTCATTAA**TCTCTTGAA**TTAATGACTGGGTACATGCCC**GGG**
Ikzf1_CDS_sh2_F	**GATC**CCCGCAATGTCGCCAAACGTAA**TTCAAGAGA**TTACGTTTGGCGACATTGC**TTTTTGGAAC**
Ikzf1_CDS_sh2_R	**TCGAG**TTCCAAAAAGCAATGTCGCCAAACGTAA**TCTCTTGAA**TTACGTTTGGCGACATTGC**GGG**
Ikzf1_CDS_sh3_F	**GATC**CCCGCCCTATGACAGTGCCAACTA**TTCAAGAGA**TAGTTGGCACTGTCATAGGGC**TTTTTGGAAC**
Ikzf1_CDS_sh3_R	**TCGAG**TTCCAAAAAGCCCTATGACAGTGCCAACTA**TCTCTTGAA**TAGTTGGCACTGTCATAGGGC**GGG**
Ikzf1_CDS_sh4_F	**GATC**CCCGTGCCAACTATGAGAAGGA**TTCAAGAGA**TCCTTCTCATAGTTGGCAC**TTTTTGGAAC**
Ikzf1_CDS_sh4_R	**TCGAG**TTCCAAAAAGTGCCAACTATGAGAAGGA**TCTCTTGAA**TCCTTCTCATAGTTGGCAC**GGG**
Ikzf1_CDS_sh5_F	**GATC**CCCAGAAGGAGGATATGATGACAT**TTCAAGAGA**ATGTCATCATATCCTCCTTCT**TTTTTGGAAC**
Ikzf1_CDS_sh5_R	**TCGAG**TTCCAAAAAAGAAGGAGGATATGATGACAT**TCTCTTGAA**ATGTCATCATATCCTCCTTCT**GGG**

Ikzf1_CDS_sh6_F	**GATC**CCCACAGGACGCCGTGGATAACTT**TTCAAGAGA**AAGTTATCCACGGCGTCCTGT**TTTTTGGAAC**
Ikzf1_CDS_sh6_R	**TCGAG**TTCCAAAAAACAGGACGCCGTGGATAACTT**TCTCTTGAA**AAGTTATCCACGGCGTCCTGT**GGG**
Ikzf1_CDS_sh7_F	**GATC**CCCACTATGAGAAGGAGGATAT**TTCAAGAGA**ATATCCTCCTTCTCATAGT**TTTTTGGAAC**
Ikzf1_CDS_sh7_R	**TCGAG**TTCCAAAAAACTATGAGAAGGAGGATAT**TCTCTTGAA**ATATCCTCCTTCTCATAGT**GGG**

Table S.2 Primers for cloning

Primer name	***Sequence***
IRES_Forward	AAGCAGATCTCGCCCCTCTCCCTCCCCCCC
IRES_Reverse	**TGCTCACCATGGTGGCGACA**CCATGGTTGTGGCCATATTA
mCherry_Forward	**ATAATATGGCCACAACCATGG**TGTCGCCACCATGGTGAGCAA
mCherry_Reverse	AAGCGTCGACATCTACTTGTACAGCTCGTCC

Table S.3 Antibodies

Antibody	**Company**	**Catalogue #**	**IP (/10µl beads)**	**Western (/proteins)**
Histone H3	Abcam	AB1791	1.5µg	1:20000/5µg
Histone H2A	Abcam	AB18255	2.5µg	
Histone H2A.Z	Abcam	AB4174	2.5µg	
Histone H2B	Abcam	AB1790	2µg	
acetyl-Histone H3	Abcam	AB47915	2µl	1:2000/10µg
acetyl-Histone H4	Millipore	06-866	1µg	1:2000/10µg
H3K9Ac	Millipore	07-352	1µg	
H3K4Me3	Millipore	07-473	1µg	
H3K9Me3	Abcam	AB8898	2µg	
Mouse IgG	DakoCytomation	Z0259	1µg	
PolII-total	Santa Cruz	sc-899	20µl	
Chd4	Abcam	AB72418	7.5µl	1:2000/10µg
SNF2B/Brg1	Millipore	07-478		1:2000/10µg
Brm	BD Tranduction	610390		1:500/10µg
Ikaros-C	Stephen Smale's lab homemade		3µl	1:10000/5µg
HA.11	Covence	MMS-101R	3µl	1:5000/5µg
Tubulin	Sigma	T9026		1:2000/10µg

Table S.4 Primers for gene expression

Gene	Forward	Reverse
Chd4	ATCCGAAACCACAAGTACCG	CTTTCCTCGCCTTCACTGTC
H2afz	GGCACCCTAAAGCATTACCA	ACAGAAGGAGCCCATTTGTC
Igll1	CAGAGCGGAACATTCTCAGC	AAGGAAGGCAAGGGTCTCTC
Lig4	GCCGTATTCATCGACACCTG	AAGTGACGAGGGGTGATACG
Myc	TGGGCGTGCCTGTGAAATGA	ACGGAGTGCGTCCTCAGGTG
Smarca2(Brm)	CATGTCCCCTTTGCAGACTT	TTTCTGTTCTTATGAAGGGCATC
Smarca4(Brg1)	TTCTCACCTGTGCCCTAACC	GGTTTGCCTCTTCTCCACAG
Ubc	AGGAGGCTGATGAAGAGCTTGA	TGGTTTGAATGGATACTCTGCTGGA
Ywhaz	CGTTGTAGGAGCCCGTAGGTCAT	TCTGGTTGCGGAAGCATTGGG
Zfp36	GCTGGCTGGAAATGAGAGAG	CCCCCTACCTCAACCTTAGC

Table S.5 Primers for ChIP and MNase assay

Primer	Forward	Reverse	Size
Myc5	ACCCCAGCTCCTAAACCAGA	CCGGTCTACACCCCATACAC	121
Myc12	TCCAGGGTACATGGCGTATT	TCGGCTGAACTGTGTTCTTG	89
Myc14	TCATGCTGCGCTATTACTGTTT	CCTCTGCTTTGGGAACTCG	120
Myc17	CTCACTCAGCTCCCCTCCT	CTCCCCTCCCTTCTTTTTCC	75
Myc19	AGGGATCCTGAGTCGCAGT	CGCTCACTCCCTCTGTCTCT	92
Myc20	CAGCGAGAGACAGAGGGAGT	CACTCCAGAGCTGCCTTCTT	92
Myc21	CCTAAGAAGGCAGCTCTGGA	GCTGATGTTGGGTCAGTCG	88
Myc24	AACCAGAGGGAATCCTCACA	GAACCGCTCAGATCACGACT	100
Myc27	GAGTGCATTGACCCCTCAGT	GAATCGGACGAGGTACAGGA	80
Lig4_5	CAGCGTGCGGATACAACTAA	CTTTGTCCCAGCGTCACC	120
Lig4_7	GACAAAGCACGGGAAGGAC	CTGCTAAGCAAGTGGTGTGG	83
Lig4_9	CGCCTCCACTGTCTCTGC	CAGGCTCCAAGTTCCTCAAA	91
Lig4_11	CAGAAGAGAATCCTCCCACCT	CTGCACAGTGAAAAGGCTACC	101
Lig4_15	CTCTCTCAACTTCCCCCACA	CATTTTTATTTGCGGGCTCA	109
Zfp36_2	GCAGCTGTCTTTGAAGGGACT	AGGCACCTGCTAGGAATGAC	118
Zfp36_6	GGGGAGAGACAAGTTGGAAG	GCCGGAATCACAGTCCTAAA	112
Zfp36_13	TACGCGAGTGACAGCAGTGT	GCTGGCTGGAAATGAGAGAG	103
Zfp36_17	GGAAAAGGCTAAGGCAGGAT	GCCCCAAGTCTTCTGTTGTT	92
Zfp36_22	GAATGGCCTTGGTGAAGAGA	GCCCCATAAAAGGAGAAAGC	84
Zfp36_23	CGTGGCCACTAGAGCTTCC	TTTTGCATGCTAACCAGCAG	96
Zfp36_24	CATGCAAAATGTGCCTGAAC	CGCTACCATCACCTCCAGTT	99
Ccnd2_12	GAGAGAGAGAAGAGTGGAAGGTG	GAGAGAGGAGAGCGAGCTGA	109
Ccnd2_16	GCTAGGGGCCTCGGATAG	CTTTATGCCCCCATGGTATG	94
Igll1_9	TGTCTTAGTTTGTGATATGAGACCTACAGG	AGCAGAAGTATAGGCTCAGCAAAAA	110
Igll1_11	AGGATACCCCTGGCCCTACAT	GCCGTAGAGAGCAACTGAACACCT	107

Igll1_13	GGACCTGCTCCACAGACCCAG	CTGCCTGTCTTAACCCATCCC	92
Igll1_15	CTGTGAGTGAAAACAGTTAGGCTTGC	ACCAGCAGGCACACCCCAGTG	106
Igll1_17	GGTGGAAACTAGAGACAGCCTGG	CGGCAAAAGGATTGTTCCTCC	94
Igll1_19	GCAAGTGAGGCTAGAGTTGACTTTG	CAGCAGGAGGAGAACTTCACACTG	104
Igll1_21	TGCTGTTGGGTCTAGTGGATGG	GCCTGTTGCTTCCCACTGAAG	102
Igll1_31	CAGCCAGTATCCCGACAAGT	AGAATCTGCTGGGCCTGATA	93
Igll1_37	ACTGGGTTCCATGACTCCAC	TCACTGTCTTTCCTGTGCCTAA	117
HS17	GCTCACCCTGGAAACATCTGCTATTG	CGATGCTGCATGTGCTTCCACTTA	101
Rex1	TTTGCGGGAATCCAGCAGT	CGTCCCATCGCCACTCTAGAC	106
B-Actin	GCAGGCCTAGTAACCGAGACA	AGTTTTGGCGATGGGTGCT	101
Oct4-TSS	GGGTGAGAAGGCGAAGTCTGAA	GTGAGCCGTCTTTCCACCAGG	88